MAPPING AND CHARACTERIZATION OF YIELD COMPONENT TRAITS AND SEPTORIA NODORUM BLOTCH SUSCEPTIBILITY IN WHEAT

A Dissertation
Submitted to the Graduate Faculty
of the
North Dakota State University
of Agriculture and Applied Science

By

Amanda Rose Peters Haugrud

In Partial Fulfillment of the Requirements
for the Degree of
DOCTOR OF PHILOSOPHY

Major Program:
Genomics and Bioinformatics

October 2021

Fargo, North Dakota

North Dakota State University

Graduate School

Title

MAPPING AND CHARACTERIZATION OF YIELD COMPONENT TRAITS AND SEPTORIA NODORUM BLOTCH SUSCEPTIBILITY IN WHEAT

By

Amanda Peters Haugrud

The Supervisory Committee certifies that this ***disquisition*** complies with North Dakota State University's regulations and meets the accepted standards for the degree of

DOCTOR OF PHILOSOPHY

SUPERVISORY COMMITTEE:

Dr. Phillip E. McClean
Chair

Dr. Justin Faris

Dr. Timothy Friesen

Dr. Andrew Green

Dr. Zhaohui Liu

Approved:

11/04/2021
Date

Dr. Phillip E. McClean
Department Chair

ABSTRACT

Wheat, a major global economic crop and food source, is currently threatened by climate change and the cascading effects, including increased disease pressure. Additionally, wheat yields have not increased significantly for decades, which may impact future food supply. Compared to other crop species, relatively few genes related to wheat yield have been mapped and cloned, with the vast majority in bread, or hexaploid, wheat. In this dissertation, I used three tetraploid wheat populations, Ben × PI 41025 (BP025), Divide × PI 272527 (DP527), and Rusty × PI 193883 (RP883) which were derived from crossing durum cultivars with cultivated emmer accessions. These three populations were evaluated under field conditions in three seasons for 11 traits related to yield. Additionally, the DP527 population was evaluated under greenhouse conditions for these same 11 traits. The known genes *ELF3*, *Ppd-B1*, *Vrn-A1*, *Q*, *Vrn-B1*, *WAPO-A1*, *FT-1*, *GNI-A1*, *GRF4* and *Vrn2* were associated with numerous yield traits. For multiple QTL, the cultivated emmer parent contributed the increased effects. Findings from this study and the identified markers may be useful for breeders who are interested in introgressing the beneficial genes I identified into their germplasm. Here, I also report on the progress and markers developed for fine mapping of a kernels per spike gene that was first mapped in the BP025 population. The work I have done provides a foundation for the cloning of this kernels per spike gene. Lastly, in this dissertation, I screened a global winter wheat panel for genetic regions associated with susceptibility to the necrotrophic pathogen *Parastagonospora nodorum*, the causal agent of septoria nodorum blotch. I identified the previously cloned genes *Tsn1* and *Snn3-B1* to be associated with disease caused by the isolates Sn2000 and Sn4, respectively. I also report the first time a panel has been screened for sensitivity to the necrotrophic effectors SnTox267 and SnTox5, along with the prevalence of SnToxA, SnTox1, and SnTox3 sensitivity

in this panel. In conclusion, results obtained from these studies provides knowledge of genes/markers which are available to breeders that may provide useful in breeding programs and the overall goal of increasing wheat yield.

ACKNOWLEDGMENTS

I am eternally grateful to my advisor, Dr. Justin Faris, for taking a chance on a student six years ago who had minimal lab experience and welcoming her into his molecular genetics lab. His guidance has helped me to grow into the scientist I am today. He was always willing to answer my questions, correct my writing, and even applied for a grant to allow me to have a field component to my research. I am very grateful for having the opportunity to study in his lab and for the funding he provided for this research.

I would like to thank my academic advisor, Dr. Phillip McClean. His guidance throughout my PhD has been extremely helpful, especially in the classroom settings and the classes I took where he was the professor. I would like to especially thank Dr. Andrew Green for all his help with my field experiments and his guidance. I would also like to thank Dr. Timothy Friesen for all his assistance on the pathology side of my research and answering all my many questions on *Parastagonospora nodorum*. Lastly, I would like to thank Dr. Marion Harris, who served as my graduate school representative for the first three years, and Dr. Zhaohui Liu, who served in that position upon Dr. Harris' retirement.

I am extremely grateful to have worked with amazing lab mates throughout my graduate career. I want to especially thank Dr. Zengcui Zhang for being an awesome lab manager, always making time to answer my many questions and helping me navigate a working career with raising a family. I would also like to thank the other graduate students who I have worked with and I appreciate all the comradery we had: Dr. Jyoti Sharma, Dr. Sudeshi Seneviratne, Sapna Sharma, Katherine Running, and Gurminder Singh. I would like to also thank all the other lab personal over the years for all their help and support: Megan Overlander, Cayley Steen, Stephanie McCoy, Dr. Agnes Szabo-Hever, Dr. Aliya Momotaz, Samantha Steckler, Erika Shay

Bauer, Brianna Robinson, Libby Bateman, Ethan Kettner, Molly Holt, Jonathan Schwartz, and Marissa Condron.

This project could not have been made possible without funding from the WheatCAP project and Dr. Jorge Dubcovsky. I would like to thank all the grant members and the other students in the grant for all their support and the research community we have built over the last five years.

I would also like to thank the many members of the NDSU Plant Sciences department. Shannon Ueker in the office for all her help with setting up meetings and filling paperwork. I would like to thank the Durum wheat crew for planting part of my experiment in 2017. Also, I am very grateful and thankful for the Hard red spring wheat crew and Jesse Underdahl and all their help in planting in 2017, 2018, 2019, and 2020. Working with them has been a pleasure, especially when I got to take along for planting, and for all their help with spraying, plot maintenance, and answering my numerous questions. I would also like to thank the USDA-ARS Fargo genotyping lab for their assistance with genotyping for my projects, especially Mary Osenga.

I would like to thank all my family and friends. My parents, Charles and Diane Peters, have always supported my pursuit of my higher education degrees with the upmost support. For everything they have not only helped me with in graduate school but before, I am forever eternally grateful. I would not be in the place I am today without their love and support. I would also like to thank my twin sister Emmie Scheffler for all her love and support these past five years. She always believed I could achieve this goal.

Lastly, I would like to thank my husband Nathan and daughter Maria for all their love and support throughout working on my PhD. Although Maria is still young, God blessed me with

such a happy girl during these final stages of my schooling. And without the continual love, support, and encouragement from Nathan, I would not be where I am at today. He has always been the rock in our family, and without this foundation I would not have been able to finish this degree. He has always been there when Maria and I need him, taking care of her evenings and weekends when needed so I could pursue this dream. I cannot express how grateful I am for all his support and love.

DEDICATION

To Nathan and Maria and the life we are building together

TABLE OF CONTENTS

LIST OF TABLES

LIST OF FIGURES

LIST OF ABBREVIATIONS

BLAST.....basic local alignment search tool

bp.....base pairs

BP025.....Ben × PI 41025 population

CRD .....completely randomized design

DNA.....deoxyribonucleic acid

DP527 .....Divide × PI 272527 population

DTH .....days to heading

FDR.....false discovery rate

Gb.....giga bases

GLM.....general linear model

GWAS.....genome-wide association study

GWS.....grain weight per spike

GYS.....grain yield per spike

KA.....kernel area

KASP .....kompetitive allele specific PCR

KC.....kernel circularity

KL .....kernel length

KLW .....kernel length:width ratio

KPS .....kernels per spike

KW.....kernel width

LD .....linkage disequilibrium

LSD.....least significant difference

MAGIC .....multi-parent advanced generation inter cross

Mb.....mega bases

MLM.....mixed linear model

MSD.....mean square distance

MYA.....million years ago

NE.....necrotrophic effector

PCA.....principal component analysis

PCR.....polymerase chain reaction

PHT.....plant height

QTL.....quantitative trait locus

RCBD.....randomized complete block design

RIL.....recombinant inbred line

RNA.....ribonucleic acid

RP883.....Rusty × PI 193883 population

SNB.....septoria nodorum blotch

SNP.....single nucleotide polymorphism

SPS.....spikelets per spike

SSR.....simple sequence repeats/microsatellites

STARP.....semi-thermal asymmetric reverse PCR

TILLING.....targeting induced local lesions in genomes

TKW.....thousand kernel weight

WheatCAP.....wheat coordinated agriculture project

CHAPTER 1. GENERAL INTRODUCTION

The global human population is experiencing a rate of rapid growth and is expected to top nine billion people by 2050. Any increase in population results in an increased food demand. Wheat (*Triticum aestivum* and *T. durum*) is a major world food crop and supplies approximately 20% of the daily calories in the average human diet. In 2019, global wheat production was 766 million tonnes on 215 million hectares (http://www.fao.org/faostat/en/#data/QCL). To meet the expended demand in 2050 for wheat, the wheat research community has set goals of increasing wheat yield by approximately 60% of what it is currently at, breeding for increased disease resistance, breeding for adaptability to abiotic stresses and the changing climate, and growing wheat on less arable land (International Wheat Yield Partnership 2020).

One avenue of increased interest to the breeding community is mapping and cloning of wheat yield related traits. Much of the previous research in this area has been in bread, or common, wheat (*T. aestivum* L., $2n = 6x = 42$, AABBDD). However, another important but smaller class of wheat is durum wheat (*T. turgidum* ssp. *durum* L., $2n = 4x = 28$, AABB), which is grown for making pasta and other semolina products. Less research has been done to identify yield component traits in durum compared to bread wheat (Arriagada et al. 2020; Cao et al. 2020; Colasuonno et al. 2021), and compared to other major crops, relatively few yield component genes have been cloned in wheat (Cao et al. 2020). Identifying genomic regions and the underlying genes associated with yield will allow breeders to more fine-tune yield, along with giving the community a better understanding of the complex relationships between the different pathways that contribute to overall wheat yield.

Yield is comprised of three main subcomponents: the number of spikers per unit area, the number of kernels per spike and grain weight/size (Gegas et al. 2010; Brinton and Uauy 2018,

Cao et al. 2020). In this dissertation, I mapped 11 yield component traits (days to heading, plant height, spikelets per spike, kernels per spike, grain weight per spike, thousand kernel weight, kernel area, kernel width, kernel length, kernel circularity, and kernel length:width ratio) in three durum × cultivated emmer (*T. turgidum* ssp. *dicoccum* (Schrank) Schübl ($2n = 4x = 28$, AABB)) recombinant inbred populations under field conditions and one population under greenhouse conditions. Additionally, I began the fine-mapping and cloning process of a kernels per spike gene identified in tetraploid wheat.

Pathogens are a biotic stress of wheat and can result in yield loses and reduced quality (Singh et al. 2016). One such pathogen is *Parastagonospora nodorum*, the causal agent of septoria norodum blotch (SNB). *P. nodorum* is a necrotrophic pathogen that causes chlorotic and necrotic lesions of wheat leaves and glumes and cause up to 50% yield loss (Eyal et al. 1987). Wheat and *P. nodorum* interact in an inverse gene-for-gene manner (Friesen and Faris 2021) and to date, a total of nine interactions have been characterized in this pathosystem. These interactions are: *Tsn1*-SnToxA, *Snn1*-SnTox1, *Snn2*-SnTox267, *Snn3-B1*-SnTox3, *Snn3-D1*-SnTox3, *Snn4*-SnTox4, *Snn5*-SnTox5, *Snn6*-SnTox267, and *Snn7*-SnTox267 (see Chapter 3). Within this pathosystem, the host genes *Tsn1*, *Snn1*, and *Snn3-D1* have been cloned (Faris et al. 2010; Shi et al. 2016; Zhang et al. 2021) and the pathogen genes *SnToxA*, *SnTox1*, *SnTox267*, *SnTox3*, and *SnTox5* have been cloned (Friesen et al. 2006; Liu et al. 2009; Liu et al. 2012, Kariyawasam et al. 2021, Richards et al. 2021). Additionally, QTL associated with disease have been mapped to almost every chromosome. Many of the initial studies focused on using bi-parental populations, with more using association panels within the last decade (see Chapter 3). Most of the previous association mapping panels have been comprised of small regional lines or spring habit wheat. The purpose of my chapter mapping disease response to SNB was to fill this

material gap by using a global winter wheat panel to evaluate the prevalence of SnToxA, SnTox1, SnTox267, SnTox3, and SnTox5 sensitivity in a global panel, along with trying to identify if any new genomics regions are associated with SNB disease in this panel.

1.1. Literature Cited

Arriagada O, Marcotuil I, Gadaleta A, Schwember AR (2020) Molecular mapping and genomics of grain yield in durum wheat: a review. Int J Mol Sci 21:7021

Brinton J and Uauy C (2018) A reductionist approach to dissecting grain weight and yield in wheat. J Integr Plant Biol 61:337-358

Cao S, Xu D, Hanif M, Xia X, He Z (2020) Genetic architecture underpinning yield component traits in wheat. Theor Appl Genet 133:1811-1823

Colasuonno P, Marcotuli I, Gadaleta A, Soriano JM (2021) From genetic maps to QTL cloning: an overview for durum wheat. Plants 10:315

Eyal Z (1987) The Septoria diseases of wheat: concepts and methods of disease management. CIMMYT, Mexico

Faris JD, Zhang Z, Lu H, Lu Z, Reddy L, Cloutier S, Fellers JP, Meinhardt SW, Rasmussen JB, Xu SS, Oliver RP, Simons KJ, Friesen TL (2010) A unique wheat disease resistance-like gene governs effector-triggered susceptibility to necrotrophic pathogens. Proc Natl Acad Sci 107:13544-13549

Friesen TL, and Faris JD (2021) Characterization of effector-target interactions in necrotrophic pathosystems reveals trends and variation in host manipulation. Annu Rev Phytopathol 59:77-98

Friesen TL, Stukenbrock EH, Liu Z, Meinhardt S, Ling H, Faris JD, Rasmussen JB, Solomon PS, McDonald BA, Oliver RP (2006) Emergence of a new disease as a result of interspecific virulence gene transfer. Nat Genet 38:953-956

Gegas VC, Nazari A, Griffiths S, Simmonds J, Fish L, Orford S, Sayers L, Doonan JH, Snape JW (2010) A genetic framework for grain size and shape variation in wheat. Plant Cell 22:1046-1056

International Wheat Yield Partnership (2020) 2019/20 Annual Report. https://iwyp.org/wp-content/uploads/sites/34/2020/12/IWYP-Annual-Report-2019-20.pdf

Kariyawasam GK, Richards JK, Wyatt NA, Running KLD, Xu SS, Liu Z, Borowicz P, Faris JD, Friesen TL (2021) The *Parastagonospora nodorum* necrotrophic effector SnTox5 targets the wheat gene *Snn5* and facilitates entry into the leaf mesophyll. New Phytol https://doi.org/10.1111/nph.17602

Liu Z, Faris JD, Oliver RP, Tan KC, Solomon PS, McDonald MC, McDonald BA, Nunez A, Lu S, Rasmussen JB, Friesen TL (2009) SnTox3 acts in effector triggered susceptibility to induce disease on wheat carrying the *Snn3* gene. PLoS Pathog 5:e1000581

Liu Z, Zhang Z, Faris JD, Oliver RP, Syme R, McDonald MC, McDonald BA, Solomon PS, Lu S, Shelver WL, Xu S, Friesen TL (2012) The cysteine rich necrotrophic effector SnTox1 produced by *Stagonospora nodorum* triggers susceptibility of wheat lines harboring *Snn1*. PLoS Pathog 8:e1002467

Richards JK, Kariyawasam GK, Seneviratne S, Wyatt NA, Xu SS, Liu Z, Faris JD, Friesen TL (2021) A triple threat: the *Parastagonospora nodorum* SnTox267 effector exploits three distinct host genetic factors to cause disease in wheat. New Phytol https://doi.org/10.1111/nph.17601

Shi G, Zhang Z, Friesen TL, Raats D, Fahima T, Brueggeman RS, Lu S, Trick HN, Liu Z, Chao W, Frenkel Z, Xu SS, Rasmussen JB, Faris JD (2016) The hijacking of a receptor kinase-driven pathway by a wheat fungal pathogen leads to disease. Science Adv 2:e1600822

Singh RP, Singh PK, Rutkoski J, Hodson DP, He X, Jørgensen LN, Hovmøller MS, Huerta-Espino J (2016) Disease impact on wheat yield potential and prospects of genetic control. Annu Rev Phytopathol 54:303-322

Zhang Z, Running KLD, Seneviratne S, Peters Haugrud AR, Szabo-Hever A, Shi G, Brueggeman R, Xu SS, Friesen TL, Faris JD (2021) A protein kinase-major spem protein gene hijacked by a necrotrophic fungal pathogen triggers disease susceptibility in wheat. Plant J doi:10.1111/tpj.15194

CHAPTER 2. LITERATURE REVIEW

2.1. Introduction

Wheat (*Triticum* ssp.) is one of the major global food crops, supplying approximately 20% of calories and protein in the average human's diet. Currently, the world population is expanding at a rapid rate, with upwards of 9 billion people predicted by 2050. To meet the expected increase in food demand, wheat yields will need to increase by 50% of current production rates to meet this demand on the same, or less, amount of cultivable acreage used today (IWYP 2017). Additional challenges the agricultural industry faces are increased global temperatures and the effects of climate change, which can negatively impact crop yield and quality. Some factors that reduce yield are abiotic stresses, such as drought, flooding, extreme heat, and soil degradation, along with biotic stresses, including pathogens and insect pests (IWYP; Singh and Upadhyaya 2015). Along with climate change and land availability challenges, plant breeders and the agriculture community are working towards more sustainable systems along with working to preserve biodiversity (Colasuonno et al. 2021; Lyzenga et al. 2021).

The two main types of wheat grown worldwide are common, or bread, wheat (*Triticum aestivum* L.) and durum wheat (*T. turgidum* ssp. *durum* L.). Current global wheat production is approximately 763 million tons per year (Gupta et al. 2019). Bread wheat constitutes approximately 95% of the worldwide wheat production. Products made from bread wheat include bread, pastries, cookies and noodles. Durum wheat occupies most of the rest of the worldwide wheat production and is used to make pasta and other semolina products.

Bread wheat can be broken into multiple market classes, which are classified based on: winter or spring type, soft or hard kernels, and white or red kernels. Winter wheat requires a

vernalization period and is often grown in regions that experience periods of suitably low temperatures to meet this requirement without becoming cold enough to kill the plants. Within the US, bread wheat is grown from coast to coast, with the major production center in the Great Plains. Hard red winter wheat is the most abundantly grown market class, followed by hard red spring, soft red winter, and white wheat (https://www.ers.usda.gov/data-products/wheat data.aspx). Within the Great Plains, hard red winter wheat is grown in the southern portion and hard red spring wheat is primarily grown in the Dakotas, Minnesota and Montana.

Durum wheat is grown on 14 million hectares worldwide, producing ~38 million tons per year (Colasuonno et al. 2021). Most durum is planted in the Mediterranean basin, followed by North America. Within North America, durum is produced in Canada and a handful of regions in the United States, which includes North Dakota, South Dakota, Montana, Arizona, California, and Minnesota. North Dakota is the largest producer of durum within the US, growing roughly 60% of the total hectares (https://www.ag.ndsu.edu/plantsciences/research/durum/production). Approximately two-thirds of US durum is used within the country, with the rest being exported and the largest buyers from Italy and Algeria (https://www.ndwheat.com/buyers/NorthDakota WheatClasses/Durum/). Durum has a more limited growing range compared to bread wheat due to the need to be grown in a climate with cool summer nights and long warm days (http://www. ndwheat.com/buyers/?ID=295). Climate change and changing farmer preferences may push durum production out of North Dakota and the US within the coming decades. Understanding overall wheat yield and yield components in durum and deploying these traits may be essential for keeping production of this crop in this region and competitive on the worldwide market.

2.2. Wheat Domestication and Genome Reference Sequences

The *Triticum* genus contains three main domestication genes: *Q*, *Tg*, and *Br*. Without naturally occurring mutations in these genes, humans would not have been able to transition from a hunting and gathering lifestyle to the agrarian lifestyle we live in today. These three domestication genes allowed farmers to harvest and thresh more grain more easily, resulting in increased yields. Wheat domestication occurred approximately 10,000 years ago in the Fertile Crescent (Dubcovsky and Dvorak 2007; Faris 2014).

Wild wheat plants need a mechanism to disperse their seeds, which they do through having a brittle rachis, where abscission zones form along the base of the spike or spikelets making these parts prone to breakage. Mutations in the underlying gene, *Br*, and its homoeologs, led to the retention of the spikelets and the spike and allowed early farmers to harvest heads while still on the plant. Wild wheat has tough glumes that envelope wheat seeds to help protect them during dispersal but make extraction of the seed during threshing difficult. Wheat plants that have the wildtype *Tg* allele are non-free threshing partially due to this trait. Mutation of *Tg* led to plants with softer glumes, allowing for easier kernel extraction (Dubcovsky and Dvorak 2007; Faris 2014). Lastly, the domestication gene *q*, which encodes an *AP2*-like transcription factor, affects many domestication traits in wheat. The presence of the *Q* allele confers the free-threshing phenotype and affects many plant development components such as rachis fragility, glume toughness, spike architecture, flowering time and plant height, along with a square spike phenotype (Zhang et al. 2011a; Faris 2014, Zhang et al. 2020). For many years, *Q* had been the only wheat domestication gene that was cloned (Faris et al. 2003; Simons et al. 2006). Avni et al. (2017) cloned the brittle rachis gene *TtBtr1* using comparisons between the durum and wild emmer genome sequences. The mutation in both *TtBTR1* genes has a monophyletic origin, with

haplotype analysis indicating that the domestication of emmer, or loss of the brittle rachis trait, most likely occurred in the southern region of the Fertile Crescent (Nave et al. 2019).

Wheat evolution began approximately 3 million years ago (MYA) when a seven-chromosome ancestor gave rise to the two diploid progenitors of modern wheat: *Triticum* and *Aegilops* taxa (Faris 2014). The A genome donor, *T. urartu* Tumanian ex Gandylian ($2n = 2x = 14$, AA), evolved from the *Triticum* progenitor approximately 2.6 MYA. The *Aegilops* progenitor gave rise to *Ae. tauschii* Coss. ($2n = 2x = 14$, DD), the donor of the D genome lineage, and *Ae. speltoides* Tausch ($2n = 2x = 14$, SS), the progenitor of the B genome lineage. These groups all had the wild type alleles of *Br*, *Tg*, and *q* and were not free threshing (Dubcovsky and Dvorak 2007; Faris 2014).

The modern polyploid wheat lineage arose through the hybridization of a close relative of *Ae. speltoides* and *T. urartu* approximately 0.5 MYA (Huang et al. 2002; Chalupska et al. 2008). Controversy has surrounded the hypothesis that *Ae. speltoides* was the donor of the B-genome, with the current thought that it was indeed involved in the origin of the B genome, but may not have been the sole donor (Zhang et al. 2018). The resulting species from this hybridization was wild emmer wheat, *T. turgidum* ssp. *dicoccoides* (Körn.) Thell ($2n = 4x = 28$, AABB). Wild emmer has a brittle rachis, very thick glumes, and hulled seed. Wild emmer still grows today as a wild plant in the Fertile Crescent (Faris 2014).

Mutations in the *Br* gene in wild emmer led to the domesticated emmer species *T. turgidum* ssp. *dicoccum* (Schrank) Schübl ($2n = 4x = 28$, AABB). This event occurred approximately 10,000 BP in the Karacadag region of the northern Levant. Domesticated, or commonly called cultivated, emmer was widely grown in the Middle East during the Prepottery Neolithic B period and was the major cereal crop during this time. Distribution of cultivated

emmer spread throughout the Mediterranean basin and Northern Europe. It also spread south to Egypt and west into central Asia and India where it was widely grown until 3,000 BP (Dubcovsky and Dvorak 2007; Faris 2014). Today, cultivated emmer is grown in parts of the Middle East and south Asia as a niche crop used to make traditional foods. It has also been used in recent years in breeding programs as a source of disease resistance genes (Zaharieva et al. 2010).

The acquisition of the *Q* allele and mutations in *Tg* resulted in the free-threshing tetraploid species grown today, durum wheat, *T. turgidum* ssp. *durum* (Desf.) MacKey (2*n* = 4*x* = 28, AABB). Although the first evidence of durum was found at Can Hassan III (modern day Turkey) and originated approximately 7,000 years ago, durum was not widely grown until 2,300 BP since it was most likely intermixed with cultivated emmer (Faris 2014). *T. durum* is sexually compatible with both *T. dicoccoides* and *T. dicoccum*, providing researchers with ways to dissect differences in domestication, yield, disease, and additional traits between these species (Anvi et al. 2017).

The first hexaploid wheat was the result of a hybridization between an AB genome tetraploid with *Ae. tauschii* to form a hexaploid species similar to *T. aestivum* ssp. *spelta* (2*n*= 6*x* = 42, AABBDD). This early hexaploid wheat, had *Tg*, *br*, and *Q*. The acquisition of *tg* led to the fully free-threshing hexaploid wheat, *T. aestivum*, grown today (Faris 2014). Common wheat is grown throughout the world, and it spread further than durum wheat due to the presence of the D genome, which allows for increased genome plasticity and adaptability to broader environmental conditions and end uses (Dubcovsky and Dvorak 2007).

Knowledge of wheat evolution and the domestication lineage is important for unraveling the wheat genome and discovering economically important traits from wild and ancestral

species. Rapid advances in sequencing technologies within the last decade have allowed researchers to sequence the genomes of many species. The completion of a fully sequenced, high quality reference genome for wheat has been hindered by the high percentage of repetitive elements found throughout the wheat genome. This has not only affected the completion of a hexaploid wheat reference, but reference sequences for all three ploidy levels and tetraploid wheat (Marcussen et al. 2014). In addition to the presence of a high percent of repetitive elements, the tetraploid wheat genome is approximately 13.8 Gb/1C and the hexaploid genome is 17.3 Gb/1C (Bennett and Leitch 1995), making assembling this vast amount of data difficult.

The diploid wheat ancestors *T. urartu*, the A genome donor, and *Ae. tauschii*, the D genome donor, have been sequenced and are useful resources for understanding wheat evolution (Ling et al. 2013; Luo et al. 2013; Jia et al. 2013; Zhao et al. 2017). The wild emmer accession Zavitan (*T. turgidum* ssp. *dicoccoides*) was sequenced by Avni et al. (2017) and is being used to study the genetic differences between modern wheat and the common ancestor of both durum and bread wheat to unravel the genetic mechanisms of domestication.

The first durum genome to be sequenced was the Italian durum cultivar 'Svevo' (Maccaferri et al. 2019). The final assembly was 10.45 gigabases and is considered fully assembled and reference quality. Maccaferri et al. (2019) showed the importance and utilization of having a reference available through cloning the gene *TdHMA3-B1*, which encodes a metal transporter and is involved in high cadmium accumulation in grain. Additionally, the cultivars 'Cappelli' and 'Strongfield' have been sequenced (https://wheat-urgi.versailles.inra.fr/Seq-Repository/Assemblies) and are available for BLAST analysis.

In 2018, the first high quality reference sequence of the hexaploid wheat line Chinese Spring was released (IWGSC 2018). The annotated reference contains 21 chromosomes, 107,891

predicted high-confidence genes, and is 14.5 gigabases in length. Ramírez-González et al. (2018) used the reference to look at the transcriptional landscape and compare differences between the three subgenomes. It has also been useful in phylogenetic and diversity studies (Balfourier et al. 2019), along with cloning of wheat genes.

The next step in wheat genome sequencing is the development of pan-genomes. Walkowiak et al. (2020) released ten hexaploid genomes assembled as chromosome pseudomolecules and five as scaffold assemblies. These sequences, along with new ones as they become available, will provide a more complete picture of the gene repertoire of the wheat genome and will be an invaluable resource to the community for gene cloning, characterization, and breeding.

2.3. Yield and Yield Component Traits in Wheat

The most important trait that breeders strive to improve is yield. This is a difficult task because yield is a complex trait made up of many components. To add to the complexity of yield, each individual component is controlled by multiple genes scattered throughout the genome with each contributing to the final phenotype for that component. Grain yield is also strongly influenced by G × E interactions.

Grain yield is comprised of two main components, grain number and grain size/weight, and can be defined as the product of multiplying grain number per unit area of land by the grain size or thousand kernel weight (TKW) (Li and Yang 2017; Griffiths et al. 2015). Grain number is influenced by factors such as number of reproductive tillers, inflorescence architecture, spike initiation, elongation, branching, and spikelet formation. Grain weight and size is influenced by grain cell number, grain cell size, and sink capacity (Blanco et al. 2012; reviewed by Nadolska-Orczyk et al. 2017; Brinton et al. 2017). Often, a negative correlation is observed between

number of seeds and seed size, which is not only restricted to wheat but plant species in general (Sandras 2007). Breeders have bred for varieties that have minimized this trade off while favoring increased grain number; however, to greatly increase wheat yields, QTL that positively influence size without reducing grain number or vice versa could potentially lead to higher and more stable yields (Sehgal et al. 2017; Griffiths et al. 2015).

Increased seed size was an important trait selected for during crop domestication (Li and Li 2015). Modern wheat grains are wider and shorter than those of ancestral cultivars (Gegas et al. 2010). Increased grain size is still a trait that is positively selected for; however, grain shape is not a common trait that breeders select for because grain shape is not directly correlated with grain size (Gegas et al. 2010; Li and Yang 2017). Grain shape parameters such as length, width, and area are correlated with TKW, with increases in these and overall grain size leading to increased TKW (Simmonds et al. 2016). TKW, along with kernels per spike (KPS) are part of the larger yield component of grain yield per spike (GYS). Increases in either TKW or KPS usually lead to an increase in grain weight per spike (GWS) but are usually negatively correlated with one another (Mangini et al. 2018).

Mangini et al. (2018) proposed that the "negative relationship between grain number and grain weight is that the increase of grain number per unit area or per spike produced by a genotype results in a lower availability of photo-assimilates synthesized during grain filling for each grain, which leads to decrease in individual weight due to competition effects." Correlations between yield traits may be due to a variety of factors, such as genetic linkage, pleiotropy, environmental factors, and yield component compensations.

Additional yield determinants include the number of spikelets on an inflorescence and the number of fertile florets per spike. Very little is known about how these traits are genetically

controlled (Dixon et al. 2018). Optimizing floral fertility and improving wheat seed set may be another way to increase wheat yields. Mutants for the trait supernumerary spikelet have been developed and could be potentially used in future breeding efforts to enhance sink capacity and increase the number of grains per spike (Nadolska-Orczyk et al. 2017).

Genes that impact yield in cereal species can be classified into five functional groups: transcription factors, which play a role in spike development and impact grain number; metabolism, or signaling of growth regulators such as cytokinins, gibberellins, and brassinosteroids, which control plant architecture; cell division and proliferation genes, which impact grain size; floral regulators, which impact seed number; and carbohydrate metabolism genes, which impact architecture and yield (Li and Li 2015; Li and Yang 2017; Nadolska-Orczyk et al. 2017). Understanding how genes in these groups contribute to yield and how they interact with one another will be vital to achieving higher cereal yields using breeding and genetic approaches.

To breed for lines with superior yield traits, and to understand how these genes interact with one another, yield genes need to be first identified, mapped, and characterized. QTL for yield components such as spikelets per spike (SPS), KPS, GWS, TKW, and grain dimension components have been identified on every chromosome in tetraploid and hexaploid wheat (Kumar et al. 2016; Zhou et al. 2017; Mangini et al. 2018; Griffiths et al. 2015; Sehgal et al. 2017; Zhang et al. 2014a; Sukumaran et al. 2018a,b). The majority of wheat yield QTL studies have been done in hexaploid wheat, with the identification of yield QTL in tetraploid wheat lagging in comparison.

Studies on QTL analyses for yield components in durum has been done using RIL populations (Maccaferri et al. 2008; Blanco et al. 2012; Patil et al. 2013; Graziani et al. 2014;

Russo et al. 2014; Faris et al. 2014; Avni et al. 2018; Sharma et al. 2019; Jones et al. 2019; Giancaspro et al. 2019; Fariukha et al. 2020; Mo et al. 2021; Mangini et al. 2021), MAGIC populations (Milner et al. 2016), and association mapping panels (Maccaferri et al. 2011; Mengistu et al. 2016; Kidane et al. 2017; Sukumaran et al. 2018b; Mangini et al. 2018, Sun et al. 2020). To identify yield QTL that are present under specific conditions, multiple studies have been conducted under different moisture and climate regiments (Maccaferri et al. 2008; Maccaferri et al. 2011; Graziani et al. 2014; Sukumaran et al. 2018b).

Yield component QTL have been identified on all fourteen chromosomes in durum wheat in the mentioned studies. An important agronomic trait in durum is grain protein content. The study by Blanco et al. (2012) found that there is often a negative correlation between grain protein content and grain yield, which may hinder deploying genes underlying yield due to concomitant reductions in protein content. Several QTL were found that increased grain protein content while not affecting yield, which may be beneficial to breeders. The relationship between grain yield and grain protein QTL needs to be studied further to identify the best genotypes for increasing yield while providing growers with relatively high grain protein cultivars.

Mangini et al. (2018) studied the grain yield components GWS, KPS, and TKW in a tetraploid wheat population to dissect the genetic relationship among these traits. From their findings, they were able to split the QTL into four main classes. The first class consisted of QTL for KPS, which also led to a significant increase in GWS and had no effect on TKW. QTL in this category are most likely linked to spikelet fertility and may have a significant impact on increasing yield because an increase in KPS does not lead to a correlated decrease in grain weight. The second class was a QTL for KPS with a corresponding QTL observed for a decrease in TKW. Overall yield in this class does not change. The third class was QTL for TKW with a

significant increase in GWS and no change in KPS. The last class was QTL for TKW that had no effect on GWS. Knowledge on how different QTL interact with one another contributes to the overall knowledge of these complex traits and can give insight into which QTL may be deployed together to increase overall yield.

To my knowledge, only three studies have been performed mapping various yield components in a population derived from crossing durum wheat × cultivated emmer, which were published by Faris et al. (2014), Russo et al. (2014), Sharma et al. (2019). The Faris et al. (2014) findings will be discussed in the following section of this review. Russo et al. (2014) developed one of the first linkage maps based off such a population and used the maps to identify QTL for seed morphology traits under field conditions. Seed size and shape are important components of grain yield and are positively correlated with TKW. Cultivated emmer has thinner and longer seeds than durum since domestication led to selecting for plants with shorter seeds which are wider and overall larger, making populations developed from crossing these two species ideal for grain size studies. Russo et al. (2014) identified QTL for TKW on 3B and 4B, and QTL for kernel size and shape on 1B, 2B, 3A, 3B, 4B, and 7A. Additional work has been done with this population measuring root and shoot traits in seedlings (Iannucci et al. 2017). However, the population used was developed from crossing an Italian cultivar (Simeto) with a Mediterranean cultivated emmer variety (Molise Colli) and is not as transferable to North America.

To map genes/QTL governing yield components in North American durum lines, populations that contain a local durum variety as the durum parent are needed. Two such populations have been studied in the greenhouse by Faris et al. (2014) and Sharma et al. (2019). Both studies focused on threshability and other domestication traits; however, both measured SPS, with Faris et al. (2014) measuring grain weight and seed number. Neither study evaluated

seed size. Faris et al. (2014) used a RIL population derived from crossing the ND variety 'Ben' by the cultivated emmer accession PI 41025, which was collected in Russia. They identified QTL for grain weight components on 1A, 2B, 3B, 5B, and 7A; QTL for KPS on 2B, 5B, and 7A; and QTL for SPS on 1B, 3B, 7A, 7B. There was a positive correlation between SPS and KPS, SPS and GWS, KPS and GWS, KPS and TKW, and TKW and GWS. Interestingly, although there was a positive correlation between SPS and GWS, there was a negative correlation between SPS and TKW. Sharma et al. (2019) used a RIL population derived from crossing the ND germplasm line 'Rusty' by the cultivated emmer accession PI 193883, which was collected in Ethiopia. The only yield component trait they measured was SPS, which they identified QTL on 1B and 5A. Additional studies with these types of populations are needed that include additional yield component traits (grain number, size, and weight), along with more evaluations under field conditions.

Although many QTL have been identified for yield components in wheat, relatively few have been characterized and cloned compared to other traits, especially disease resistance. The lag is partially due to yield component genes having more minor effects on the overall phenotype compared to other traits. It has been suggested, with most groups taking this route, that a reductionist approach is taken when cloning and characterizing yield (Brinton and Uauy 2018). This can mainly be done through partitioning yield into its different components, such as spikelet architecture, kernel number, grain weight, and grain size. Within each of these groups, there are also various components that make up each. Additionally, a larger number replicates is required, compared to more qualitative traits, when phenotyping due to the small differences and environmental influences. To successfully deploy yield component traits, a deeper understanding

is required on how they influence grain yield individually (Li and Yang 2017; Brinton and Uauy 2018). Many of the genes cloned to date are involved with regulating grain size and weight.

Genes that influence grain size, both positively and negatively, are *TaGS5-3A* (Ma et al. 2016), *TaGW2* (Su et al. 2011; Wang et al. 2018), *TaGS-D1* (Zhang et al. 2014b), and *TaCYP78-A3* (Ma et al. 2015), and impact grain size differences through regulating cell division, the ubiquitin pathway, increasing cell length, and reducing cell number in the seed coat, respectively (Ma et al. 2016; Simmonds et al. 2016; Zhang et al. 2014b; Ma et al. 2015). Additional genes that have been found to be associated with grain size are: *TaGL3-5A*, which encodes a protein phosphatase with a Kelch-like repeat domain (Yang et al. 2019); *TaGW8-B1*, which encodes a squamosa promoter binding protein (Yan et al. 2019); *TaGS1a*, which encodes a glutamine synthetase (Guo et al. 2013), and *TaGRF4*, which encodes a growth-regulating factor 3 (Avni et al. 2018).

To date, sixteen genes that influence TKW have been cloned in wheat. These are: *TaSus1* and *TaSus2*, which encode for sucrose synthase genes (Hou et al. 2014, Jiang et al. 2011); *TaTGW-7A,* which encodes for an indole-3-glycerol-phosphate synthase (Hu et al. 2016); *TaCwi-A1* and *TaCWI-5D*, which encodes cell wall invertases (Ma et al. 2012; Jiang et al. 2015); *TaTGW6-A1*, which encodes an indole-3-aceticacid-glucose hydrolase (Hanif et al. 2016); *TaFlo2-A1*, which encodes for a floury endosperm2 (Sajjad et al. 2017); *TaAGP-S1*, which encodes for a ADP-glucose pyrophosphorylase (Hou et al. 2017); *TaTPP-6AL1*, which encodes for a protein that is part of the T6P metabolic pathway (Zhang et al. 2017a); *TaSnRK2.3* and *TaSnRK2.10*, which encode for sucrose non-fermenting 1-related protein kinases (Miao et al. 2017; Zhang et al. 2017b); *6-SFT-A2*, which encodes a sucrose-fructan 6-fructosyltransferase (Yue et al. 2015); *Tabas1-B1*, which encodes a 2-cys peroxiredoxin (Zhu et al. 2016); and

TaSPL16, *TaSPL20*, *TaSPL21*, which encode squamosa promoter binding protein like- proteins (Cao et al. 2019; Zhang et al. 2017c).

Three genes associated with grain number have been cloned. Two of these, *TaCKX2* and *TaCKX6-D1*, encode cytokinin oxidase/dehydrogenases (Zhang et al. 2012). The other gene is *TaSAP1-A1*, which encodes a stress association protein (Chang et al. 2013). Two other genes have been cloned that are related to grain yield; however, they are related to stressed environments and nitrogen availability. These genes are *TaTAR2.1-3A* and *TaNAC2-5A*, which encode a tryptophan amino transferase-related protein and a NAC transcription factor, respectively (Shao et al. 2017; He et al. 2015).

To date, only three genes that regulate spike development, other than *Q*, have been cloned. Boden et al. (2015) cloned *Ppd-1*, a member of the pseudo-response regulator genes and plays a role in regulating the formation of paired spikelets. Dixon et al. (2018) cloned and characterized *TB1*, a gene which increases number of paired spikelets and is a positive regulator of *FT-1*. The third gene is *TaAPO-A1*, which encodes a F-box protein, and increases the number of spikelets per spike through prolonging the maturation of inflorescence meristem proliferation, resulting in an increase in the number of spikelets (Kuzay et al. 2019; Voss-Fels et al. 2019; Muqaddasi et al. 2019). Mapping and cloning of genes regulating inflorescence development could be used to develop wheat spikes with increased number if spikelets per spike and other spike modifications that correlate with increased yield.

With the availability of new technologies, genes underlying yield traits in wheat are expected to be cloned and characterized at a faster pace than in the past. Although the gene has yet to be cloned and characterized, Brinton et al. (2017) identified a QTL on chromosome 5A that leads to increased pericarp cell length and grain weight in wheat. Later research using RNA-

sequencing revealed that ubiquitin-related genes are differentially expressed between lines with and without this QTL, further implying that this gene class is important for grain size and development (Brinton et al. 2018). New methods and technologies such as RNA-sequencing, TILLING populations, genome-wide association mapping, MutChromSeq, MutRenSeq, AgRenSeq, 'targeted chromosome-based cloning via long-range assembly', and cheaper and faster sequencing technologies will aid in the discovery and cloning on yield genes underlying economically important traits (Bettgenhaeuser and Krattinger 2019).

2.4. Septoria Nodorum Blotch in Wheat

Septoria nodorum blotch (SNB) is a foliar disease on wheat caused by the necrotrophic fungal pathogen *Parastagonospora nodorum* [syn. *Leptosphaeria nodorum* (Müll.), syn. *Septoria nodorum* (Berk.), syn. *Stagonospora nodorum* (Berk.)] *nodorum* (Berk.) Quaedvleig, Verkley & Crous. Wheat and *P. nodorum* interact in an inverse gene-for-gene manner (reviewed by Friesen and Faris 2010, Friesen and Faris 2021). *P. nodorum* produces necrotrophic effectors (NEs), which are recognized by host sensitivity/susceptibility genes.

An extensive and detailed review of the genetics of the wheat-*P. nodorum* pathosystem is included in Chapter 3. Therefore, this topic will not be reviewed further in this chapter. However, it is worthy to note that much of the previous research on wheat-*P. nodorum* interactions has been in spring wheat, durum, and other wheat species. The number of studies in winter wheat is lagging, especially within the US along with diverse, global panels. Within US germplasm pools, panel studies have been performed by Crook et al. (2012), Bertucci et al. (2014), and Cowger et al. (2020). As for global panels, to my knowledge there has never been a winter wheat global panel that has been evaluated for susceptibility to *P. nodorum* published, highlighting an area of research that is lacking within this pathosystem.

2.5. Literature Cited

Abeysekara NS, Faris JD, Chao S, McClean PE, Friesen TL (2012) Whole-genome analysis of Stagonospora nodorum blotch resistance and validation of the SnTox4-*Snn4* interaction in hexaploid wheat. Phytopathology 102:94-104

Abeysekara NS, Friesen TL, Keller B, Faris JD (2009) Identification and characterization of a novel host-toxin interaction in the wheat-*Stagonospora nodorum* pathosystem. Theor Appl Genet 120:117-126

Anvi R, Nave M, Barad O, Baruch K, Twardziok SO, Gundlach H, Hale I, Mascher M, Spannagl M, Wiebe K, Jordan KW, Golan G, et al. (2017) Wild emmer genome architecture and diversity elucidate wheat evolution and domestication. Science 357:93-97

Avni R, Oren L, Shabtay G, Assili S, Pozniak C, Hale I, Ben-David R, Peleg Z, Distelfeld A (2018) Genome based meta-QTL analysis of grain weight in tetraploid wheat identifies rare alleles of *GRF4* associated with larger grains. Genes 9:636

Balfourier F, Bouchet S, Robert S, De Oliveira R, Rimbert H, Kitt J, Choulet F, IWGSC, BreedWheat Consortium, Paux E (2019) Worldwide phylogeography and history of wheat genetic diversity. Science Advances 10.1126/sciadv.aav0536

Bennett MD and Leitch IJ (1995) Nuclear DNA amounts in angiosperms. Ann Bot-London 76:113-176

Bertucci M, Brown-Guedira G, Murphy JP, Cowger C (2014) Genes conferring sensitivity to *Stagonospora nodorum* necrotrophic effectors in Stagonospora nodorum blotch-susceptible U.S. wheat cultivars. Plant Dis 98:746-753

Bettgenhaeuser J and Krattinger SG (2019) Rapid gene cloning in cereals. Theor Appl Genet 132:699-711

Blanco A, Mangini G, Giancaspro A, Giove S, Colasuonno P, Simeone R, Signorile A, De Vita P, Mastrangelo AM, Cattivelli L, Gadaleta A (2012) Relationships between grain protein content and grain yield components through quantitative trait locus analyses in a recombinant inbred line population derived from two elite durum wheat cultivars. Mol Breeding 30:79-92

Boden SA, Cavanagh C, Cullis BR, Ramm K, Greenwood J, Finnegan EJ, Trevaskis B, Swain SM (2015) *Ppd-1* is a key regulator of inflorescence architecture and paired spikelet development in wheat. Nat Plants 1:14016

Brinton J, Simmonds J, Minter F, Leverington-Waite M, Snape J, Uauy C (2017) Increased pericarp cell length underlies a major quantitative trait locus for grain weight in hexaploid wheat. New Phytol 215:1026-1038

Brinton J, Simmonds J, Uauy C (2018) Ubiquitin-related genes are differentially expressed in isogenic lines contrasting for pericarp cell size and grain weight in hexaploid wheat. BMC Plant Biol 18:22 DOI 10.1186/s12870-018-1241-5

Brinton J and Uauy C (2018) A reductionist approach to dissecting grain weight and yield in wheat. J Integr Plant Biol 61:337-358

Cao R, Guo L, Ma M, Zhang W, Liu X, Zhao H (2019) Identification and functional characterization of *Squamosa* promoter binding protein-like gene *TaSPL16* in wheat (*Triticum aestivum* L.). Front Plant Sci https://doi.org/10.3389/fpls.2019.00212

Chalupska D, Lee HY, Faris JD, Evrard A, Chalhoub B, Haselkorn R, Gornicki P (2008) *Acc* homoeoloci and the evolution of wheat genomes. Proc Natl Acad Sci USA 105:9691-9696

Chang J, Zhang J, Mao X, Li A, Jia J, Jing R (2013) Polymorphism of *TaSAP1-A1* and its association with agronomic traits in wheat. Planta 237:1495-1508

Chapman JA, Mascher M, Buluc A, Barry K, Georganas E, Session A, Strnadova V, Jenkinds J, Sehgal S, Oliker L, et al. (2015) A whole-genome shotgun approach for assembling and anchoring the hexaploid bread wheat genome. Genome Biol 16:26

Clavijo BJ, Venturini L, Schudoma C, Accinelli GG, Kaithakottil G, Wright J, Borrill P, Kettleborough G, Heavens D, Chapman H, et al. (2017) An improved assembly and annotation of the allohexaploid wheat genome identifies complete families of agronomic genes and provides genomic evidence for chromosomal translocations. Genome Res 27:885-896

Colasuonno P, Marcotuli I, Gadeleta A, Soriano JM (2021). From genetic maps to QTL cloning: an overview for durum wheat. Plants 10:315

Cowger C, Ward B, Brown-Guedira G, Brown JKM (2020) Role of effector-sensitivity gene interactions and durability of quantitative resistance to Septoria Nodorum Blotch in Eastern U.S. Wheat. Front Plant Sci doi:10.3389/fpls.2020.00155

Crook AD, Friesen TL, Liu ZH, Ojimbo PS, Cowger C (2012) Novel necrotrophic effectors from *Stagonospora nodorum* and corresponding host sensitivities in winter wheat germplasm in the Southeastern United States. Phytopathology 102:498-505

Dixon LE, Greenwood JR, Bencivenga S, Zhang P, Cockram J, Mellers G, Ramm K, Cavanagh C, Swain SM, Boden SA (2018) TEOSINTE BRANCHED1 regulates inflorescence architecture and development in bread wheat (*Triticum aestivum* L.). Plant Cell DOI:10.1105/tpc.17.00961

Dubcovsky J and Dvorak J (2007) Genome plasticity a key factor in the success of polyploid wheat under domestication. Science 316:1862-1866

Faris JD (2014) Wheat domestication: key to agricultural revolutions past and future. Genomics and Plant Genetic Resources Volume 1. Managing, sequencing and mining genetic resources (pp. 439-464). Springer Netherlands.

Faris JD and Friesen TL (2009) Reevaluation of a tetraploid wheat population indicates that the *Tsn1*-ToxA interaction is the only factor governing Stagonospora nodorum blotch susceptibility. Phytopathology 99:906-912

Faris JD, Fellers JP, Brooks SA, Gill BS (2003) A bacterial artificial chromosome contig spanning the major domestication locus *Q* in wheat and identification of a candidate gene. Genetics 164:311-321

Faris JD, Zhang Z, Lu H, Lu Z, Reddy L, Cloutier S, Fellers JP, Meinhardt SW, Rasmussen JB, Xu SS, Oliver RP, Simons KJ, Friesen TL (2010) A unique wheat disease resistance-like gene governs effector-triggered susceptibility to necrotrophic pathogens. Proc Natl Acad Sci 107:13544-13549

Faris JD, Zhang Z, Rasmussen JB, Friesen TL (2011) Variable expression of the *Stagonospora nodorum* effector SnToxA among isolates correlated with levels of disease in wheat. Mol Plant Microbe In 24:1419-1426

Fatiukha A, Filler N, Lupo I, Lidzbarsky G, Klymiuk V, Korols AB, Pozniak C, Fahima T, Krugman T (2020) Grain protein content and thousand kernel weight QTLs identified in a durum × wild emmer wheat mapping population tested in five environments. Theor Appl Genet 133:119-131

Friesen TL and Faris JD (2010) Characterization of the wheat-*Stagonospora nodorum* system: what is the molecular basis of this quantitative necrotrophic disease interaction? Can J Plant Pathol 32:20-28

Friesen TL and Faris JD (2021) Characterization of effector-target interactions in necrotrophic pathosystems reveals trends and variation in host manipulation. Ann Rev Phytopathol 59

Friesen TL, Chu CG, Liu ZH, Xu SS, Halley S, Faris JD (2009) Host-selective toxins produced by Stagonospora nodorum confer disease susceptibility in adult wheat plants under field conditions. Theor Appl Genet 118:1489-1497

Friesen TL, Chu C, Xu SS, Faris JD (2012) SnTox5-*Snn5*: a novel *Stagonospora nodorum* effector-wheat gene interaction and its relationship with the SnToxA-*Tsn1* and SnTox3-*Snn3-B1* interactions. Mol Plant Pathol 13:1101-1109

Friesen TL, Meinhardt SW, Faris JD (2007) The *Stagonospora nodorum*-wheat pathosystem involves multiple proteinaceous host-selective toxins and corresponding host sensitivity genes that interact in an inverse gene-for-gene manner. Plant J 51:681-692

Friesen TL, Stukenbrock EH, Liu Z, Meinhardt S, Ling H, Faris JD, Rasmussen JB, Solomon PS, McDonald BA, Oliver RP (2006) Emergence of a new disease as a result of interspecific virulence gene transfer. Nat Genet 38:953-956

Friesen TL, Zhang Z, Solomon PS, Oliver RP, Faris JD (2008) Characterization of the interaction of a novel *Stagonospora nodorum* host-selective toxin with a wheat susceptibility gene. Plant Physiol 146:682-693

Gao Y, Faris JD, Liu Z, Kim YM, Syme RA, Oliver RP, Xu SS, Friesen TL (2015) Identification and characterization of the SnTox6-*Snn6* interaction in the *Parastagonospora nodorum*-wheat pathosystem. Mol Plant Microbe In 28:615-625

Gegas VC, Bazaru A, Griffiths S, Simmonds J, Lesley F, Orford S, Sayers L, Doonan JH, Snape JW(2010) A genetic framework for grain size and shape variation in wheat. Plant Cell 22:1046-1056

Giancaspro A, Giove SL, Zacheo SA, Blanco A, Gadaleta A (2019) Genetic variation for protin content and yield-related traits in a durum population derived from an inter-specific cross between hexaploid and tetraploid wheat cultivars. Front Plant Sci https://doi.org/10.3389/fpls.2019.01509

Graziani M, Maccaferri M, Royo C, Salvatorelli F, Tuberosa R (2014) QTL dissection of yield components and morpho-physiological traits in a durum wheat elite population tested in contrasting thermos-pluviometric conditions. Crop Pasture Sci 65:80-95

Griffiths S, Wingen L, Pietragalla J, Garcia G, Hasan A, Miralles D, Calderini DF, Bipinchandra Ankleshwaria J, Leverington Waite M, Simmonds J, Snape J, Reynolds M (2015) Genetic dissection of grain size and grain number trade-offs in CIMMYT wheat germplasm. PloS one 10(3):e0118847

Guo Y, Sun J, Zhang G, Wang Y, Kong F, Zhao Y, Li S (2013) Haplotype, molecular marker and phenotype effects associated with mineral nutrient and grain size traits of *TaGS1a* in wheat. Field Crop Res 154:119-125

Gupta PK, Balyan HS, Sharma S, Kumar R (2020) Genetics of yield, abiotic stress tolerance and biofortification in wheat (Triticum aestivum L.). Theor Appl Genet 133:1569-1602

Hanif M, Gao F, Liu J, Wen W, Zhang Y, Rasheed A, Xia X, He Z, Cao S (2016) *TaTGW6-A1*, an ortholog of rice TGW6, is associated with grain weight and yield in bread wheat. Mol Breeding 36:1

He X, Qu B, Li W, Zhao X, Teng W, Ma W, Ren Y, Li B, Li Z, Tong Y (2015) The nitrate-inducible NAC transcription factor TaNAC2-5A controls nitrate response and increases wheat yield. Plant Physiol 169:1991-2005

Hou J, Jiang Q, Hao C, Wang Y, Zhang H, Zhang X (2014) Global selection on sucrose synthase haplotypes during a century of wheat breeding. Plant Physiol 164:1918-1929

Hou J, Li T, Wang Y, Hao C, Liu H, Zhang X (2017) ADP-glucose pyrophosphorylase genes, associated with kernel weight, underwent selection during wheat domestication and breeding. Plant Biotechnol J https://doi.org/10.1111/pbi.12735

Hu M-J, Zhang, H-P, Liu K, Cao J-J, Wang S-X, Jiang H, Wu Z-Y, Lu J, Zhu XF, Xia X-C, Sun G-L, Ma C-X, Cheng C (2016) Cloning and characterization of *TaTGW-7A* gene associated with grain weight in wheat via SLAF-seq-BSA. Front Plant Sci 7:1902

Huang S, Sirikhachornkit A, Su X, Faris J, Gill B, Haselkorn R, Gornicki P (2002) Genes encoding plastid acetyl-CoA carboxylase and 3-phosphoglycerate kinase of the Triticum/Aegilops complex and the evolutionary history of polyploid wheat. Proc Natl Acad Sci USA 99:8133-8138

Iannucci A, Marone D, Russo MA, De Vita P, Miullo V, Ferragonio P, Blanco A, Gadaleta A, Mastrangelo AM (2017) Mapping QTL for root and shoot morphological traits in a durum wheat × *T. dicoccum* segregating population at seedling stage. Int J Genomics 2017:6876393

IWGSC, Appels R, Eversole K, Stein N, Feuillet C, Keller B, Rogers J, Pozniak CJ, Choulet F, Distelfeld A, et al. (2018) Shifting the limits in wheat research and breeding using a fully annotated reference genome. Science 10.1126/science.aar7191

International Wheat Yield Partnershup (2017) IWYP Strategic Plan 2017-2022. http://iwyp.org/wp-content/uploads/sites/34/2017/10/IWYP-Strategic-Plan-Full-Version-Published.pdf. Accessed 15 June 2021

Jia J, Zhao S, Kong X, Li Y, Zhao G, He W, Appels R, Pfeifer M, Tao Y, Zhang X, Jing R, Zhang C, Ma Y, et al. (2013) *Aegilops tauschii* draft genome sequence reveals a gene repertoire for wheat adaptation. Nature 496:91-95

Jiang Q, Hou J, Hao C, Wang L, Ge H, Dong Y, Zhang X (2011) The wheat (T. aestivum) sucrose synthase 2 gene (TaSus2) active in endosperm development is associated with yield traits. Funct Integr Genomic 11:49-61

Jiang Y, Jiang Q, Hao C, Hou J, Wang L, Zhang H, Zhang S, Chen X, Zhang X (2015) A yield-associated gene *TaCWI*, in wheat: its function, selection and evolution in global breeding revealed by haplotype analysis. Theor Appl Genet 128:131-143

Jones BH, Blake NK, Heo HY, Kalous JR, Martin JM, Torrion JA, Talbert LE (2019) Improving hexaploid spring wheat by introgression of alleles for yield component traits from durum wheat. Crop Sci https://doi.org/10.1002/csc2.20011

Kariyawasam GK, Richards JK, Wyatt NA, Running K, Xu SS, Liu Z, Borowicz P, Faris JD, Friesen TL (2021) The *Parastagonospora nodorum* necrotrophic effector SnTox5 targets the wheat gene *Snn5* and facilitates entry into the leaf mesophyll. New Phytol https://doi.org/10.1111/nph.17602

Kidane Y, Mancini C, Mengistu DK, Frascaroli E, Fadda C, Enrico Pè M, Matteo Dell'Acqua (2017) Genome wide association study to identify the genetic base of smallholder farmer preferences of durum wheat traits. Front Plant Sci 8:1230

Kumar A, Mantovani EE, Seetan R, Soltani A, Echeverry-Solarte M, Jain S, Simsek S, Doehlert D, Alamri MS, Elias EM, Kianian SF, Mergoum M (2016) Dissection of genetic factors underlying wheat kernel shape and size in an elite × nonadapted cross using a high density SNP linkage map. Plant Genome-US 9

Kuzay S, Xu Y, Zhang J, Katz A, Pearce S, Su Z, Fraser M, Anderson JA, Brown-Guedira G, DeWitt N, Peters Haugrud A, Faris JD, Akhunov E, Bai G, Dubcovsky J (2019) Identification of a candidate gene for a QTL for spikelet number per spike on wheat chromosome are 7AL by high-resolution genetic mapping. Theor Appl Genet 132:2689-2705

Li N and Li Y (2015) Maternal control of seed size in plants. J Exp Bot 66:1087-1097

Li W and B Yang (2017) Translational genomics of grain size regulation in wheat. Theor Appl Genet 130:1765-1771

Ling HQ, Zhao S, Liu D, Wang J, Sun H, Zhang C, Fan H, Li D, Dong L, Tao Y, et al. (2013) Draft genome of the wheat A-genome progenitor *Triticum urartu*. Nature 496:87-90

Liu ZH, Faris JD, Meinhardt SW, Ali S, Rasmussen JB, Friesen TL (2004b) Genetic and physical mapping of a gene conditioning sensitivity in wheat to a partially purified host-selective toxin produced by *Stagonospora nodorum*. Phytopathology 94:1056-1060

Liu Z, Faris JD, Oliver RP, Tan KC, Solomon PS, McDonald MC, McDonald BA, Nunez A, Lu S, Rasmussen JB, Friesen TL (2009) SnTox3 acts in effector triggered susceptibility to induce disease on wheat carrying the *Snn3* gene. PLoS Pathog 5:e1000581

Liu Z, Friesen TL, Ling H, Meinhardt SW, Oliver RP, Rasmussen JB, Faris JD (2006) The *Tsn1*-ToxA interaction in the wheat-*Stagonospora nodorum* pathosystem parallels that of the wheat-tan spot system. Genome 49:1265-1273

Liu ZH, Friesen TL, Rasmussen JB, Ali S, Meinhardt SW, Faris JD (2004a) Quantitative trait loci analysis and mapping of seedling resistance to *Stagonospora nodorum* leaf blotch in wheat. Phytopathology 94:1061-1067

Liu Z, Zhang Z, Faris JD, Oliver RP, Syme R, McDonald MC, McDonald BA, Solomon PS, Lu S, Shelver WL, Xu S, Friesen TL (2012) The cysteine rich necrotrophic effector SnTox1 produced by *Stagonospora nodorum* triggers susceptibility of wheat lines harboring *Snn1*. PLoS Pathog 8:e1002467

Luo MC, Gu YQ, You FM, Deal KR, Ma Y, Hu Y, Huo N, Wang Y, Wang J, Chen S, Jorgensen CM, Zhang Y, et al. (2013) A 4-gigabase physical map unlocks the structure and evolution of the complex genome of *Aegilops tauschii*, the wheat D-genome progenitor. Proc Natl Acad Sci USA 110:7940-7945

Lyzenga WJ, Pozniak CJ, Kagale S (2021) Advanced domestication: harnessing the precision of gene editing in crop breeding. Plant Biotechnol J 19:660-670

Ma L, Li T, Hao C, Wang Y, Chen X, Zhang X (2016) *TaGS5-3A*, a grain size gene selected during wheat improvement for larger kernel and yield. Plant Biotechnol 14:1269-1280

Ma M, Wang Q, Li Z, Cheng H, Li Z, Liu X, Song W, Appels R, Zhao H (2015) Expression of *TaCYP78A3*, a gene encoding cytochrome P450 CYP78A3 protein in wheat (*Triticum aestivum* L.), affects seed size. Plant J 83:312-325

Ma D, Jan J, He Z, Wu L, Xia X (2012) Characterization of a cell wall invertase gene *TaCwi-A1* on common wheat chromosome 2A and development of functional markers. Mol Breeding 29:43-52

Maccaferri M, Harris NS, Twardziok S, Pasam RK, Gundlach H, Spannagl M, Ormanbekova D, Lux T, Prade VM, Milner SG, et al. (2019) Durum wheat genome highlights past domestication signatures and future improvement targets. Nat Genet 51:885-895

Maccaferri M, Ricci A, Salvi S, Milner SG, Noli E, Martelli PL, Casadio R, Akhunov E, Scalabrin S, Vendramin V, Ammar K, Blanco A, et al. (2015) A high-density, SNP-based consensus map of tetraploid wheat as a bridge to integrate durum and bread wheat genomics and breeding. Plant Biotechnol 13:648-663

Maccaferri M, Sanguineti MC, Corneti S, Ortega JLA, Salem MB, Bort J, DeAmbrogio E, del Moral LFG, Demontis A, et al. (2008) Quantitative trait loci for grain yield and adaptation of durum wheat (*Triticum durum* Desf.) across a wide range of water availability. Genetics 178:489-511

Maccaferri M, Sanguineti MC, Demontis A, El-Ahmed A, del Moral LFG, Maalouf F, Nachit M, Nserallah N, Quabbou H, Rhouma S, et al. (2011) Association mapping in durum wheat grown across a broad range of water regimes. J Exp Bot 62:409-438

Mangini G, Blanco A, Nigro D, Signorile MA, Simeone R (2021) Candidate genes and quantitative trait loci for grain yield and seed size in durum wheat. Plants 10:312

Mangini G, Gadaleta A, Colasuonno P, Marcotuli I, Signorille AM, Simeone R, De Vita P, Mastrangelo AM, Laidò G, Pecchioni N, Blanco A (2018) Genetic dissection of the relationships between grain yield components by genome-wide association mapping in a collection of tetraploid wheats. PloS one 13:e0190162

Marcussen T, Sandve SR, Heier L, Spannagl M, Pfeifer M, IWGSC, Jakobsen KS, Wulff BBH, Steuernagel B, Mayer KFX, Olsen O-A (2014) Ancient hybridizations among the ancestral genomes of bread wheat. Science 345:125009. DOI:10.1126/science.1250092

Mengistu DK, Kidane YG, Catellani M, Frascaroli E, Fadda C, Enrico Pè, Dell'Acqua M (2016) High-density molecular characterization and association mapping in Ethiopian durum wheat landraces reveals high diversity and potential for wheat breeding. Plant Biotechnol 14:1800-1812

Miao L, Mao X, Wang J, Liu Z, Zhang B, Li W, Chang X, Reynolds M, Wang Z, Jing R (2017) Elite haplotypes of a protein kinase gene *TaSnRK2.3* associated with important agronomic traits in common wheat. Front Plant Sci https://doi.org/10.3389/fpls.2017.00368

Milner SG, Maccaferri M, Huang BE, Mantovani P, Massi A, Frascaroli E, Tuberosa R, Salvi S (2016) A multiparental cross population for mapping QTL for agronomic traits in durum wheat (Triticum turgidum ssp. durum). Plant Biotechnol 14:735-748

Mo Z, Zhu J, Wei J, Zhou J, Xu Q, Tang H, Mu Y, Jiang Q, Liu Y, Chen G, et al. (2021) The wheat 55K SNP-based exploration of loci for spikelet number per spike from a tetraploid wheat (*Triticum turgidum* L.) recombinant inbred line population derived from a Chinese landrace 'Ailanmai' and a wild emmer accession. bioRxiv https://doi.org/10.1101/2020.10.21.348227

Muqaddasi QH, Brassac J, Koppolu R, Plieske J, Ganal MW, Röder MS (2019) *TaAPO-A1*, an ortholog of rice *ABERRANT PANICLE ORGANIZATION 1*, is associated with total spikelet number per spike in elite European hexaploid winter wheat (*Triticum aestivum L.*) varieties. Sci Rep-UK 9:13853

Nadolska-Orczyk A, Rajchel IK, Orczyk W, Gasparis S (2017) Major genes determining yield-related traits in wheat and barley. Theor Appl Genet 130:1081-1098

Nave M, Avni R, Cakir E, Portnoy V, Sela H, Pourkheirandish M, Ozkan H, Hale I, Komatsuda T, Dvorak J, Distelfeld A (2019) Wheat domestication in light of haplotype analyses of the *Brittle rachis 1* genes (*BTR1-A* and *BTR1-B*). Plant Sci 285:193-199

Patil RM, Tamhankar SA, Oak MD, Raut AL, Honrao BK, Rao VS, Misra SC (2013) Mapping of QTL for agronomic traits and kernel characters in durum wheat (*Triticum durum* Desf.). Euphytica 190:117-129

Ramírez-González RH, Borril P, Lang D, Harrington SA, Brinton J, Venturini L, Davey M, Jacobs J, van Ex F, Pasha A, et al. (2018) The transcriptional landscape of polyploid wheat. Science 10.1126/science.aar6089

Reddy L, Friesen TL, Meinhardt SW, Chao S, Faris JD (2008) Genomic analysis of the *Snn1* locus on wheat chromosome arm 1BS and the identification of candidate genes. Plant Genome 1:55-66

Richards JK, Kariyawasam G, Seneviratne S, Wyatt NA, Xu SS, Liu Z, Faris JD, Friesen TL (2021) A triple threat: the *Parastagonospora nodorum* SnTox267 effector exploits three distinct host genetic factors to cause disease in wheat. New Phytol https://doi.org/10.1111/nph.17601

Russo MA, Ficco DBM, Laidò G, Marone D, Papa R, Blanco A, Gadaleta A, De Vita P, Mastrangelo AM (2014) A dense durum wheat × *T. dicoccum* linkage map based on SNP markers for the study of seed morphology. Mol Breeding 34:1579-1597

Sadras VO (2007) Evolutionary aspects of the trade-off between seed size and number in crops. Field Crop Res 100:125-138

Sajjad M, MaX, Khan SH, Shoaib M, Song Y, Yang W, Zhang A, Liu D (2017) *TaFlo2-A1*, an ortholog of rice *Flo2*, is associated with thousand grain weight in bread wheat (Triticum aestivum L.). BMC Plant Biol 17:164

Sehgal D, Autrque E, Singh R, Ellis M, Singh S, Dreisigacker S (2017) Identification of genomic regions for grain yield and yield stability and their epistatic interactions. Sci Rep-UK 7:41578 DOI:10.1038/srep41578

Shao A, Ma W, Zhao X, Hu M, He X, Teng W, Li H, Tong Y (2017) The auxin biosynthetic *TRYPTOPHAN AMINOTRANSFERASE RELATED TaTAR2.1-3A* increases grain yield of wheat. Plant Physiol 174:2274-2288

Sharma JS, Running KLD, Xu SS, Zhang Q, Peters Haugrud AR, Sharma S, McClean PE, Faris JD (2019) Genetic analysis of threshability and other spike traits in the evolution of cultivated emmer to fully domesticated durum wheat. Mol Genet Genomics 294:757-771

Shi G, Friesen TL, Saini J, Xu SS, Rasmussen JB, Faris JD (2015) The wheat *Snn7* gene confers susceptibility on recognition of the *Parastagonospora nodorum* necrotrophic effector SnTox7. Plant Genome 8

Shi G, Zhang Z, Friesen TL, Bansal U, Cloutier S, Wicker T, Rasmussen JB, Faris JD (2016a) Marker development, saturation mapping, and high-resolution mapping of the Septoria nodorum blotch susceptibility gene *Snn3-B1* in wheat. Molecular Genet Genomics 291:107-119

Shi G, Zhang Z, Friesen TL, Raats D, Fahima T, Brueggeman RS, Lu S, Trick HN, Liu Z, Chao W, Frenkel Z, Xu SS, Rasmussen JB, Faris JD (2016b) The hijacking of a receptor kinase-driven pathway by a wheat fungal pathogen leads to disease. Science Adv 2:e1600822

Simmonds J, Scott P, Brinton J, Mestre TC, Bush M, del Blanco A, Dubcovsky J, Uauy C (2016) A splice acceptor site mutation in TaGW2-A1 increases thousand grain weight in tetraploid and hexaploid wheat through wider and longer grains. Theor Appl Genet 129:1099-1112

Simons KJ, Fellers JP, Trick HN, Zhang Z, Tai Y-S, Gill BS, Faris JD (2006) Molecular characterization of the major wheat domestication gene *Q*. Genetics 172:547-555

Singh M, Upadhyaya HD (2015) *Genetic and Genomic Resources for Grain Cereals Improvement.* Academic Press.

Su Z, Hao C, Wang L, Dong Y, Zhang X (2011) Identification and development of a functional marker of *TaGW2* associated with grain weight in bread wheat (*Triticum aestivum* L.). Theor Appl Genet 122:211-223

Sukumaran S, Lopes M, Dreisigacker S, Reynolds M (2018a) Genetic analysis of multi-environmental spring wheat trials identifies genomic regions for locus-specific trade-offs for grain weight and grain number. Theor Appl Genet 131:985-998

Sukumaran S, Reynolds MP, Sansaloni C (2018b) Genome-wide association analyses identify QTL hotspots for yield and component traits in durum wheat grown under yield potential, drought, and heat stress environments. Front Plant Sci 9:81 doi:10.3389/fpls.2018.00081

Sun L, Huang S, Sun G, Zhang Y, Hu X, Nevo E, Peng J, Sun D (2020) SNP-based association study of kernel architecture in a worldwide collection of durum wheat germplasm. PloS one 15:e0229159

Voss-Fels KP, Keeble-Gagnere G, Hickey LT, Tibbits J, Nagornyy S, Hayden MJ, Pasam RK, Kant S, Friedt W, Snowden RJ, Appels R, Wittkop B (2019) High-resolution mapping of

rachis nodes per rachis, a critical determinant of grain yield components in wheat. Theor Appl Genet 132:2707-2719

Walkowiak S, Gao L, Monat C, Haberer G, Kassa MT, Brinton J, Ramirez-Gonzalez RH, Kolodziej MC, Delorean E, Thambugala D (2020) Multiple wheat genomes reveal global variation in modern breeding. Nature 588:277-283

Wang W, Simmonds J, Pan Q, Davidson D, He F, Battal A, Akhunova A, Trick HN, Uauy C, Akhunov E (2018) Gene editing and mutagenesis reveal inter-cultivare differences and additivity in the contribution of *TaGW2* homoeologues to grain size and weight in wheat. Theor Appl Genet 131:2463-2475

Yan X, Zhao L, Ren Y, Dong Z, Cui D, Chen F (2019) Genome-wide association study revealed that the TaGW8 gene was associated with kernel size in Chinese bread wheat. Sci Rep-UK 9:2702

Yang J, Zhou Y, Wu Q, Chen Y, Zhang P, Zhang Y, Hu W, Wang X, Zhao H, Dong L, Han J, Liu Z, Cao T (2019) Molecular characterization of a novel *TaGL3-5A* allele and its association with grain length in wheat (Triticum aestivum L.). Theor Appl Genet 132:1799-1814

Yue A, Li A, Mao X, Chang X, Li R, Jing R (2015) Identification and development of a functional marker from *6-SFT-A2* associated with grain weight in wheat. Mol Breeding 35:63

Zaharieva M, Ayana NG, Hakimi AA, Misra SC, Monneveux P (2010) Cultivated emmer wheat (*Triticum dicoccon* Shrank), an old crop with promising future: a review. Genet Resour Crop Ev 57:937-962

Zhang B. Xu W, Liu X, Mao X, Li A, Wang J, Chang X, Zhang X, Jing R (2017c) Functional conservation and divergence among homoeologs of *TaSPL20* and *TaSPL21*, two SBP-box genes governing yield-related traits in hexaploid wheat. Plant Physiol 174:1177-1191

Zhang J, Chen J, Chu C, Zhao W, Wheeler J, Souza EJ, Zemetra RS (2014a) Genetic dissection of QTL associated with grain yield in diverse environments. Agronomy 4:556-578

Zhang L, Zhao YL, Gao LF, Zhao GY, Zhou RH, Zhang BS, Jia JZ (2012) *TaCK6-D1*, the ortholog of rice *OsCKX2*, is association with grain weight in hexaploid wheat. New Phytol 195:574-584

Zhang P, He Z, Tian X, Gao F, Xu D, Liu J, Wen W, Fu L, Li G, Sui X, Xia X, Wang C, Cao S (2017a) Cloning of *TaTPP-6AL1* associated with grain weight in bread wheat and development of functional marker. Mol Breeding 37:78

Zhang W, Zhang M, Zhu X, Cao Y, Sun Q, Ma G, Chao S, Yan C, Xu SS, Cai X (2018) Molecular cytogenetic and genomic analyses reveal new insights into the origin of the wheat B genome. Theor Appl Genet 131:365-375

Zhang Y, Liu J, Xia X, He Z (2014b) *TaGS-D1*, an ortholog of rice OsGS3 is associated with grain weight and grain length in common wheat. Mol Breeding 34:1097-1107

Zhang Z, Blecram H, Gornicki P, Charles M, Just J, Huneau C, Magdelenat G, Couloux A, SamAIN s, Gill BK, Rasmussen JB, Barbe V, Faris JD, Chalhoub B (2011a) Duplication and partitioning in evolution and function of homoeologous *Q* loci governing domestication characters in wheat. Proc Natl Acad Sci USA 108:18737-18742

Zhang Z, Li Aili, Song G, Geng S, Gill BS, Faris JD, Mao L (2020) Comprehensive analysis of *Q* gene near-isogenic lines reveals key molecular pathways for wheat domestication and improvement. Plant J 102:299-310

Zhang Z, Friesen TL, Simons KJ, Xu SS, Faris JD (2009) Development, identification, and validation of markers for marker-assisted selection against the *Stagonospora nodorum* toxin sensitivity genes *Tsn1* and *Snn2* in wheat. Mol Breeding 23:35-49

Zhang Z, Friesen TL, Xu SS, Shi G, Liu Z, Rasmussen JB, Faris JD (2011b) Two putatively homoeologous wheat genes mediate recognition of SnTox3 to confer effector-triggered susceptibility to *Stagnonospora nodorum*. Plant J 65:27-38

Zhang Z, Running KLD, Seneviratne S, Peters Haugrud AR, Szabo-Hever A, Shi G, Brueggeman R, Xu SS, Friesen TL, Faris JD (2021) A protein kinase-major sperm protein gene hijacked by a necrotrophic fungal pathogen triggers disease susceptibility in wheat. Plant J doi:10.1111/tpj.15194

Zhang ZG, Lv G, Li B, Wang JJ, Zhao Y, Kong FM, Guo Y, Li SS (2017b) Isolation and characterization of the *TaSnRK2.10* gene and its association with agronomic traits in wheat (*Triticum aestivum* L.). PloS one https://doi.org/10.1371/journal.pone.0174425

Zhao G, Zou C, Li K, Wang K, Li T, Gao L, Zhang X, Wang H, Yang Z, Liu X, Jiang W, Mao L, Kong X, Jiao Y, Jia J (2017) The *Aegilops tauschii* genome reveals multiple impacts of transposons. Nat Plants 3:946-955

Zhou Y, Conway B, Miller D, Marshall D, Cooper A, Murphy P, Chao S, Brown-Guedira G, Costa J (2017) Quantitative trait loci mapping for spike characteristics in hexaploid wheat. Plant Genome-US 10.doi:10.3835/plantgenome2016.10.0101

Zhu XF, Zhang HP, Hu MJ, Wu ZY, Jiang H, Cao JJ, Xia XC, Ma CX, Chang C (2016) Cloning and characterization of Tabas1-B1 gene associated with flag leaf chlorophyll content and thousand-grain weight and development of a gene-specific marker in wheat. Mol Breeding 36:142

Zimin V, Puiu D, Hall R, Kingan S, Clavijo BJ, Salzberg SL (2017) The first near-complete assembly of the hexaploid bread wheat genome, *Triticum aestivum*. GigaScience 6:1-7

CHAPTER 3. GENETICS OF RESISTANCE TO SEPTORIA NODORUM BLOTCH IN WHEAT[1]

3.1. Abstract

Septoria nodorum blotch (SNB) is a foliar disease of wheat caused by the necrotrophic fungal pathogen *Parastagonospora nodorum*. Research over the last two decades has shown that the wheat-*P. nodorum* pathosystem mostly follows an inverse gene-for-gene model. The fungus produces necrotrophic effectors (NEs) that interact with specific host gene products encoded by dominant sensitivity (S) genes. When a compatible interaction occurs, a 'defense response' in the host leads to programmed cell death thereby provided dead/dying cells from which the pathogen, being a necrotroph, can acquire nutrients allowing it to grow and sporulate. To date, nine S gene-NE interactions have been characterized in this pathosystem. Five NE-encoding genes, *SnTox1*, *SnTox3*, *SnToxA, SnTox5,* and *SnTox267*, have been cloned along with three host S genes, *Tsn1*, *Snn1,* and *Snn3-D1*. Studies have shown that *P. nodorum* hijacks multiple and diverse host targets to cause disease. SNB resistance is often quantitative in nature because multiple compatible interactions usually occur concomitantly. NE gene expression plays a key role in disease severity, and the effect of each compatible interaction can vary depending on the other existing compatible interactions. Numerous SNB-resistance QTL have been identified in addition to the known S genes, and more research is needed to understand the nature of these resistance loci. Marker-assisted elimination of S genes through conventional breeding practices and disruption of S genes using gene editing techniques are both effective strategies for the

[1] The material in this chapter was co-authored by Amanda R. Peters Haugrud, Zengcui Zhang, Timothy L. Friesen, and Justin D. Faris. Amanda R. Peters Haugrud had primary responsibility for performing the literature search along with writing the initial draft. Amanda R. Peters Haugrud also drafted and revised all versions of this chapter. Amanda R. Peters Haugrud, Zengcui Zhang, Timothy L. Friesen, and Justin D. Faris proofread made edits, and added content to this chapter. [Publication has been submitted to the journal Theoretical and Applied Genetics].

development of SNB-resistant wheat cultivars, which will become necessary as the global demand for sustenance grows.

3.2. Introduction

By the year 2050, the world population is expected to increase to approximately nine billion people, and this will lead to an increase in demand for common wheat (*Triticum aestivum* L., $2n = 6x = 42$, AABBDD genomes), which provides 20% of the calories consumed by humans. Current wheat production is ~730 million tons annually and production need is predicted to increase to greater than 900 million tons annually by 2050 (Marcussen et al. 2014; Singh and Upadhyaya 2015). To meet increased food demand, wheat yields will need to increase by approximately 60% along with the additional constraint of less arable land available to farmers (International Wheat Yield Partnership 2017). Some major factors that influence yield are abiotic stresses (drought, soil degradation, floods, temperature increases, increased CO_2), biotic stresses (viral, bacterial and fungal pathogens and insect pests), and agronomic practices (Singh et al. 2016; Singh and Upadhyaya 2015; International Wheat Yield Partnership 2017).

Necrotrophic pathogens are biotic stress contributors of common wheat and durum wheat (*T. turgidum* (Desf.) Husnot., $2n = 4x = 28$, AABB genomes). One such pathogen is *Parastagonospora* (syn. *Stagonospora nodorum* (Berk.) *nodorum* (Berk.) Quaedvleig, Verkley & Crous, the causal agent of septoria nodorum blotch (SNB). *P. nodorum* affects wheat leaves and glumes, decreasing wheat quality and yield by up to 50% (Eyal 1987). SNB can cause severe economic losses in wheat-growing regions where it is prevalent including North America, Australia, and Europe (Ficke et al. 2018).

Genetically, wheat and *P. nodorum* interact in an inverse gene-for-gene manner (reviewed by Friesen and Faris 2010, 2021; Faris and Friesen 2020). The mechanisms underlying

interactions associated with the inverse gene-for-gene model are essentially the same as those associated with the classical gene-for-gene model (Flor 1955, 1956), which involves biotrophic pathogens, except that the outcomes of the interactions are susceptibility as opposed to resistance due to differing pathogen lifestyles (Figure 3.1). In both models, host recognition of a foreign invader, often through secreted pathogen proteins known as effectors, results in a host defense response involving an increase in reactive oxygen species (ROS), cell-to-cell signaling, DNA laddering, electrolyte leakage, up-regulation of defense response genes, and ultimately programmed cell death (PCD) (reviewed by Jones and Dangl 2006; Day et al. 2011; van Schie and Takken 2014). The activation of this response when a host resistance (R) gene product recognizes an effector produced by a biotrophic pathogen leads to effector-triggered immunity (ETI). In this case, the outcome is resistance because the PCD is in the form of a hypersensitive response (HR), which prohibits the biotroph from acquiring nutrients from living tissue, and other host defense responses contribute to the suppression of pathogen growth and fitness. Essentially the same response occurs when a plant 'sensitivity' gene recognizes an effector produced by a necrotrophic pathogen, or necrotrophic effector (NE, formerly referred to as host-selective toxins). NEs directly or indirectly interact with host targets to induce PCD (Friesen and Faris 2021). In this case the outcome is susceptibility because the pathogen, being a necrotroph, is equipped to acquire nutrients from the dead/dying tissue as a result of the PCD and tolerate the other plant-induced suppression mechanisms (Friesen and Faris 2021 for review). Thus, this outcome is referred to as necrotrophic effector-triggered susceptibility (NETS).

In this model, the host gene involved in the recognition of the NE is considered a sensitivity (S) gene when direct infiltration of the NE into the leaf results in cell death (Figure 3.2). In most cases, recognition of the pathogen-produced NE by the host S gene also leads to the

development of SNB disease, in which case the host gene is also considered a susceptibility gene (Friesen and Faris 2010, 2021; Oliver et al. 2012). However, sensitivity to an NE does not always lead to disease susceptibility because the effects of S gene-NE interactions can sometimes be masked or suppressed due to epistasis among interactions (see below) or variability in different genetic backgrounds (Virdi et al. 2016). Also, host genes that condition susceptibility do not always recognize NEs (see van Schie and Takken 2014 for review). Therefore, the terms 'sensitivity' and 'susceptibility' for describing genes are not interchangeable.

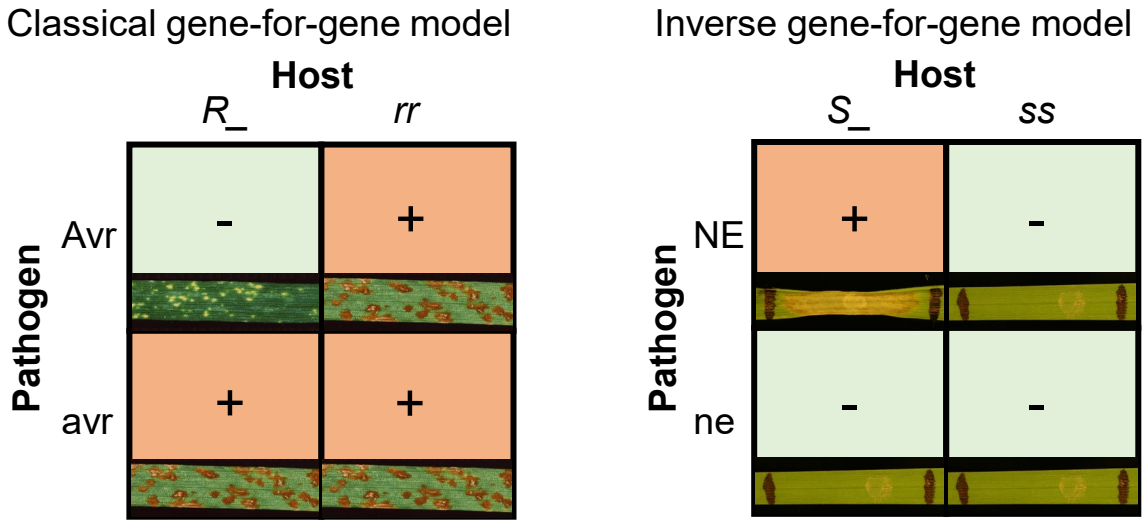

Figure 3.1. Left: Classical gene-for-gene model often found in biotrophic plant-pathogen interactions where the interaction between the host and pathogen components leads to disease resistance. Reactions to stem rust of wheat are used as an example. Right: Inverse gene-for-gene model found in wheat-Parastagonospora nodorum interactions where the interaction between the host and pathogen leads to necrotrophic effector-triggered susceptibility. Plus signs (+) represent compatible (sensitive/susceptible) interactions, minus signs (-) represent incompatible (insensitive/resistant) interactions.

Figure 3.2. Wheat leaves inoculated (A, C) with *P. nodorum* spores and infiltrated (B, D) with NE-containing cultures derived from *P. nodorum.* Plants A and B are susceptible and sensitive, and C and D are resistance and insensitive.

3.3. Septoria Nodorum Blotch

Parastagonospora nodorum is a necrotrophic pathogen belonging to the Dothideomycetes class of fungi and causes SNB (reviewed by Oliver et al. 2012; Friesen and Faris 2010, 2021). *P. nodorum* can infect both wheat leaves (Figure 3.3) and glumes. The genetic relationship between wheat and *P. nodorum* in the glumes and leaves appear to be under different genetic control (Shatalina et al. 2014). The genetic mechanisms underlying resistance to glume blotch has not been studied as intensely as the mechanisms associated with leaf blotch. The focus of this review article will be on the genetics of resistance/susceptibility to the leaf blotch component of SNB caused by *P. nodorum*.

SNB symptoms begin as small chlorotic lesions, gradually turning into a brownish tan and eventually into lens-shaped lesions that are ashen gray/brown in the center. A key indicator that the lesions are from *P. nodorum* and not *P. tritici-repentis* is the presence of pycnidia in the

lesions (Friskop and Liu 2016) however, the pycnidia are not always visible and can lead to a misdiagnosis of the causal pathogen. Current control methods for SNB include fungicide applications and genetic resistance in the host (reviewed by Oliver et al. 2012).

Figure 3.3. Septoria nodorum blotch on leaves of susceptible wheat plants in the field.

3.4. Inverse Gene-For-Gene Interactions in the Wheat-*P. nodorum* Pathosystem

To date, a total of nine interactions have been characterized in the wheat-*P. nodorum* pathosystem: *Tsn1*-SnToxA (Friesen et al. 2006, 2009; Liu et al. 2006; Zhang et al. 2009; Faris et al. 2010, 2011; Faris and Friesen 2009), *Snn1*-SnTox1 (Liu et al. 2004a, b, 2012; Reddy et al. 2008; Shi et al. 2016b), *Snn2*-SnTox267 (Friesen et al. 2007, 2009; Zhang et al. 2009; Richards et al. 2021), *Snn3-B1*-SnTox3 (Friesen et al. 2008; Liu et al. 2009; Shi et al. 2016a), *Snn3-D1*-SnTox3 (Friesen et al. 2008; Liu et al. 2009; Zhang et al. 2011), *Snn4*-SnTox4 (Abeysekara et al. 2009, 2012), *Snn5*-SnTox5 (Friesen et al. 2012; Sharma 2019; Kariyawasam et al. 2021), *Snn6*-SnTox267 (Gao et al. 2015; Richards et al. 2021), and *Snn7*-SnTox267 (Shi et al. 2015; Richards et al. 2021). Thus far, the cloning of three host S genes including *Tsn1* (Faris et al. 2010), *Snn1* (Shi et al. 2016b), and *Snn3-D1* (Zhang et al. 2021), along with the NE genes *SnToxA* (Friesen et

al. 2006), *SnTox3* (Liu et al. 2009), *SnTox1* (Liu et al. 2012), *SnTox5* (Kariyawasam et al. 2021), and *SnTox267* (Richards et al. 2021), has been reported (Table 3.1).

Table 3.1. Characterized wheat sensitivity gene-necrotrophic effector interactions in the wheat-*P. nodorum* pathosystem.

Host gene(s)	Necrotrophic effector	Host gene chromosome arm location	Host gene status	NE cloned	Maximum disease explained	Differential Line	Markers	Reference
Tsn1	SnToxA	5BL	Cloned	Yes	95%	BG261	*Xfcp620* and *Xfcp394* (Zhang et al. 2009) *fcp791*, *fcp792* (Running and Faris, unpublished)	Friesen et al. (2006) Liu et al. (2006) Faris and Friesen (2009) Faris et al. (2010)
Snn1	SnTox1	1BS	Cloned	Yes	58%	Chinese Spring, W-7984	*B500093078_5* (Cockram et al. 2015); *Xfcp624, Xfcp618, Xfcp667* (Shi et al. 2016b),	Liu et al. (2004a) Liu et al. (2004b) Liu et al. (2012) Shi et al. (2016b)
Snn2	SnTox2	2DS	Fine mapped	Yes	47%	BG223	*XTC253803*, *Xcfd56*; *Xcfd51*	Friesen et al. (2007) Zhang et al. (2009) Richards et al. (2021)
Snn3-B1	SnTox3	5BS	Cloned but unpublished	Yes	35%	BG220	*Xfcp654*, *Xfcp665*, *Xmag705*	Friesen et al. (2008) Liu et al. (2009) Shi et al. (2016a)
Snn3-B2	SnTox3	5BS	Cloned but unpublished	Yes	NA	NA	NA	NA
Snn3-D1	SnTox3	5DS	Cloned	Yes	100%	LDN2377	*Xcfd18*, *Xhbg337, fcp783-fcp787*	Zhang et al. (2011) Zhang et al. (2021)
Snn4	SnTox4	1AS	Mapped	No	41%	AF89	*XBG262267*, *XBG262975*, *Xcfd58*	Abeysekara et al. (2009)
Snn5	SnTox5	4BL	Cloned but unpublished	Yes	63%	LP29	*Xwmc349*, *Xcfd22*	Friesen et al. (2012); Sharma 2019; Kariyawasam et al. (2021)
Snn6	SnTox6	6AL	Mapped	Yes	27%	ITMI37	*XBE424987*, *XBE403326*	Gao et al. (2015) Richards et al. (2021)
Snn7	SnTox7	2DL	Mapped	Yes	33%	CTm208	*Xcfd44*, *Xgwm349*	Shi et al. (2015) Richards et al. (2021)

3.4.1. *Snn1*-SnTox1

The first host S gene-NE interaction identified in the wheat-*P. nodorum* pathosystem was *Snn1*-SnTox1 (Liu et al. 2004a). Liu et al. (2004a) used the International Triticeae Mapping Initiative (ITMI) population and the *P. nodorum* isolate Sn2000 to first characterize this interaction. This work led to the conclusion that one gene in the host was responsible for susceptibility to a NE produced by the pathogen. A dominant S gene was mapped to the short arm of wheat chromosome 1B and designated *Snn1*. SnTox1 was found to be proteinaceous and between 10 and 30 kDa in size. A compatible *Snn1*-SnTox1 interaction has explained from up to 58% of the disease variation depending on the isolate and host genetic background (Liu et al. 2004a; Friesen et al. 2007; Chu et al. 2010; Phan et al. 2016; Peters Haugrud et al. 2019) (Table 3.1).

The *Snn1* gene and the gene encoding SnTox1 (designated *SnTox1*) have both been cloned and characterized (Liu et al. 2012; Shi et al. 2016b). *SnTox1* was cloned using the *P. nodorum* reference genome to find candidate genes that matched previously known characteristics of SnTox1, along with similar characteristics of *SnToxA* and *SnTox3* (Liu et al. 2012). The predicted gene *SNOG_20078* fit the criteria, and through yeast expression studies on different plant lines with and without *Snn1*, it was confirmed to encode SnTox1. Liu et al. (2012) demonstrated that SnTox1 was a highly stable protein containing 117 amino acids, with the mature protein consisting of 100 amino acids and a predicted size of 10.33 kDa. The mature protein had a cleaved signal peptide domain and was cysteine rich. SnTox1 also contained a C-terminal conserved chitin-binding (CB) motif (Liu et al. 2012, 2016). The CB motif was more similar to those found in plants than those found in other fungal pathogens. This domain was predicted to play an important role in protecting the fungus during the initial penetration of the

host leaf (Liu et al. 2016). SnTox1 was shown to bind chitin and not only protect *P. nodorum*, but it also protected other fungal species from multiple wheat chitinases upregulated during defense (Figure 3.4).

In planta transcription analysis of *SnTox1* revealed that expression increased at 3 hours post infection (hpi) and then decreased at 6 hpi (Liu et al. 2012). After the 6 hpi point, expression slowly increased and peaked at 72 hpi, which corresponded to the onset of necrotic lesion development. After 72 hpi, expression of *SnTox1* decreased until 7 days post inoculation where it reached levels similar to those observed at 6 hpi. The high levels of *SnTox1* transcripts at early post-inoculation time points suggested SnTox1 is important in the early stages of infection (Liu et al. 2012). A compatible *Snn1*-SnTox1 interaction differs phenotypically from the other compatible interactions in this system in that small white flecks appear on leaves around 2 days post inoculation (Liu et al. 2004a; Liu et al. 2012). It was hypothesized that the necrotic and chlorotic lesions develop from these flecks and were related to the early expression of *SnTox1* (Liu et al. 2012).

SnTox1 differed from the other cloned *P. nodorum* NEs in that direct application of the SnTox1 protein to the leaf surface in the absence of the fungus resulted in necrotic flecks (Liu et al. 2016). When SnTox1 was co-inoculated with fungal spores of an avirulent isolate onto *Snn1* lines, disease symptoms developed indicating SnTox1 assisted fungal penetration of the host leaf tissue allowing infection to occur. This also demonstrated SnTox1 was sufficient to transform an avirulent isolate into a virulent isolate.

Fluorescent labeling of SnTox1 *in planta* during infection indicated it remained on the cell surface and was not internalized into the mesophyll or epidermal cells (Liu et al. 2016). This suggested the SnTox1 receptor was located on the cell surface, which was later confirmed by Shi

et al. (2016b) (Figure 3.4). During infection and penetration, SnTox1 was localized to the outer surface of the mycelium, indicating SnTox1 protects the fungal cell wall during penetration allowing *P. nodorum* to successfully penetrate and colonize (Liu et al. 2016). Liu et al. (2016) concluded not only does SnTox1 elicit cell death, but it also protects the fungal cells from degradation by wheat chitinases. The group also hypothesized that recognition of SnTox1 by *Snn1* wheat lines occurs on the epidermal cell and triggers cell-to-cell signaling throughout the leaf, with PCD occurring in both epidermal and mesophyll cells within 48 h of infection.

A compatible *Snn1*-SnTox1 interaction induces an oxidative burst, which is a plant cell biochemical response associated with defense (Liu et al. 2012). The *Snn1*-SnTox1 interaction also induces multiple pathogenesis-related (PR) genes typically associated with plant defense in response to biotrophic pathogens (Liu et al. 2012) (Figure 3.4). Liu et al. (2012) evaluated the expression of 28 wheat genes in *Snn1* lines post infection and found that PR-1-A1, a thaumatin-like protein gene, and a chitinase gene were all up-regulated with maximum expression at 36 hpi. DNA laddering was also observed, which is a response that has been associated with ETI and PCD (Dickman et al. 2001; Ryerson et al. 1996).

A survey of a worldwide collection of 1000 *P. nodorum* isolates for the presence of *SnTox1* indicated the gene was present in 84% of the isolates evaluated (McDonald et al. 2013). The dual function of SnTox1 in both eliciting PCD and binding chitin may be the driving factor behind the high frequency of *SnTox1* in *P. nodorum* (Liu et al. 2016). Liu et al. (2012) sequenced *SnTox1* in 159 global *P. nodorum* isolates and found 11 haplotypes. Remaining unchanged in all the isoforms of SnTox1 were the cysteine residues, providing evidence the disulfide bridges are important structural features of the protein.

Reddy et al. (2008) used a population of F_2 plants derived from the common wheat line Chinese Spring (CS) and a genetic stock of CS that had its native chromosome 1B substituted by 1B chromosome from the wild emmer [*T. turgidum* ssp. *dicoccoides* (Körn. Ex Asch. & Graebner) Aarons ($2n = 4x = 28$, AABB genomes)] accession TA106 (CS-DIC 1B) to develop high-density and high-resolution genetic linkage maps of the *Snn1* region and to assess colinearity with the rice genome. High-resolution mapping using markers developed from wheat expressed-sequence tags (ESTs) delineated the *Snn1* locus to a 0.46 cM interval, and two markers cosegregated with *Snn1* in 8,510 recombinant gametes. However, subsequent BAC-based chromosome walking attempts revealed that the CS-DIC 1B line contained a large deletion within the *Snn1* region that severely suppressed recombination (J.D. Faris, unpublished). Therefore, a new mapping population was developed by crossing CS with a line where chromosome 1B from the common wheat variety Hope was substituted for the native CS 1B chromosomes (CS-Hope 1B). High-resolution mapping in over 17,000 recombinant gametes using the markers developed by Reddy et al. (2008) and new markers developed from a CS BAC-based physical map delineated the *Snn1* locus to a genomic region that contained a single candidate gene, which was predicted to be a member of the wall-associated kinase (WAK) class of plant receptor kinases (Shi et al. 2016b).

Snn1 is 3,045 bp in size and contains three exons with a coding sequence of 2,145 bp (Shi et al. 2016b) (Figure 3.5). The mature protein contains an N-terminal signal sequence, and a conserved wall-associated receptor kinase galacturonan binding domain (GUB_WAK) and an epidermal growth factor-calcium binding domain (EGF_CA) are predicted to be extracellular. A transmembrane domain is predicted to span the cellular membrane, and a serine/threonine protein kinase (S/TPK) domain is located intracellularly. *Snn1* is a member of a group of WAK

genes that are specific to monocots. Through mutagenesis, the GUB_WAK, EGF_CA, and S/TPK domains were shown to be essential for a compatible *Snn1*-SnTox1 interaction.

Snn1 was specifically expressed in wheat leaves and not in stems, spikes, or roots (Shi et al. 2016b). The transcription level of *Snn1* in leaf tissues peaked at subjective dawn and then decreased throughout the day and was lowest at subjective dusk before increasing again until subjective dawn. The rhythmic expression oscillations were not present when plants were placed under continuous darkness, indicating *Snn1* expression is regulated by light signals but not the circadian clock. Interestingly, *Snn1* was down regulated after exposure to SnTox1, which differs from the expression pattern of *SnTox1* in the fungus (Shi et al. 2016b, Liu et al. 2012).

Shi et al. (2016b) found that once SnTox1 was recognized by *Snn1*, TaMAPK3 was activated within 15 minutes. Receptor kinase activation of MAPK genes is usually associated with the so-called PAMP-triggered immunity (PTI) pathway (Jones and Dangl 2006; Couto and Zipfel 2016; Shi et al. 2016b). Shi et al. (2016b) also provided evidence that the Snn1 and SnTox1 proteins interact directly, which was not surprising given the previous finding that SnTox1 does not enter the cell (Liu et al. 2012) and that Snn1 is a membrane-spanning protein with extra-cellular domains typically involved in interactions (Figure 3.4). Yeast-two hybrid analysis indicated SnTox1 directly bound to a 140-amino acid residue region between the GUB_WAK and EGF_CA domains.

Multiple groups have reported SnTox1 sensitivity in differing germplasm groups. Shi et al. (2016b) reported out of 826 wheat lines evaluated, 73% of the durum lines were sensitive whereas only 16% of the common wheat lines were sensitive to SnTox1. Other studies have reported a large range based on germplasm, with 0, 12.1, 32.9, 35.1, 71.7, and 75.9 % sensitivity reported for collections of Southeastern US, Norwegian, Canadian, Vavilov wheat collection,

Australian, and European germplasm, respectively (Bertucci et al. 2014; Ruud et al. 2018; Downie et al. 2018; Hafez et al. 2020; Phan et al. 2018; Tan et al. 2014) (Table 3.2). This data indicates that depending on the germplasm base, some programs may need to focus on eliminating *Snn1* from their germplasm if SNB occurrence is high, whereas it may not be as important in other programs.

With many breeding programs moving towards marker-assisted selection (MAS), two groups have published marker sequences for the *Snn1* locus that are more user-friendly and closely linked than the previously published flanking markers. The first is a KASP marker, based off the SNP BS00093078_5, which was designed using a MAGIC population by Cockram et al. (2015) (Table 3.1). Shi et al. (2016b) developed several simple sequence repeat (SSR) and gene-based markers upon cloning *Snn1*, but these markers are not as amenable to high-throughput genotyping platforms as KASP markers. In related work to characterized *Snn1* diversity in global panels of common and durum wheat, we have identified several causal SNPs for SnTox1 sensitivity and have developed KASP markers for each. These markers are available upon request.

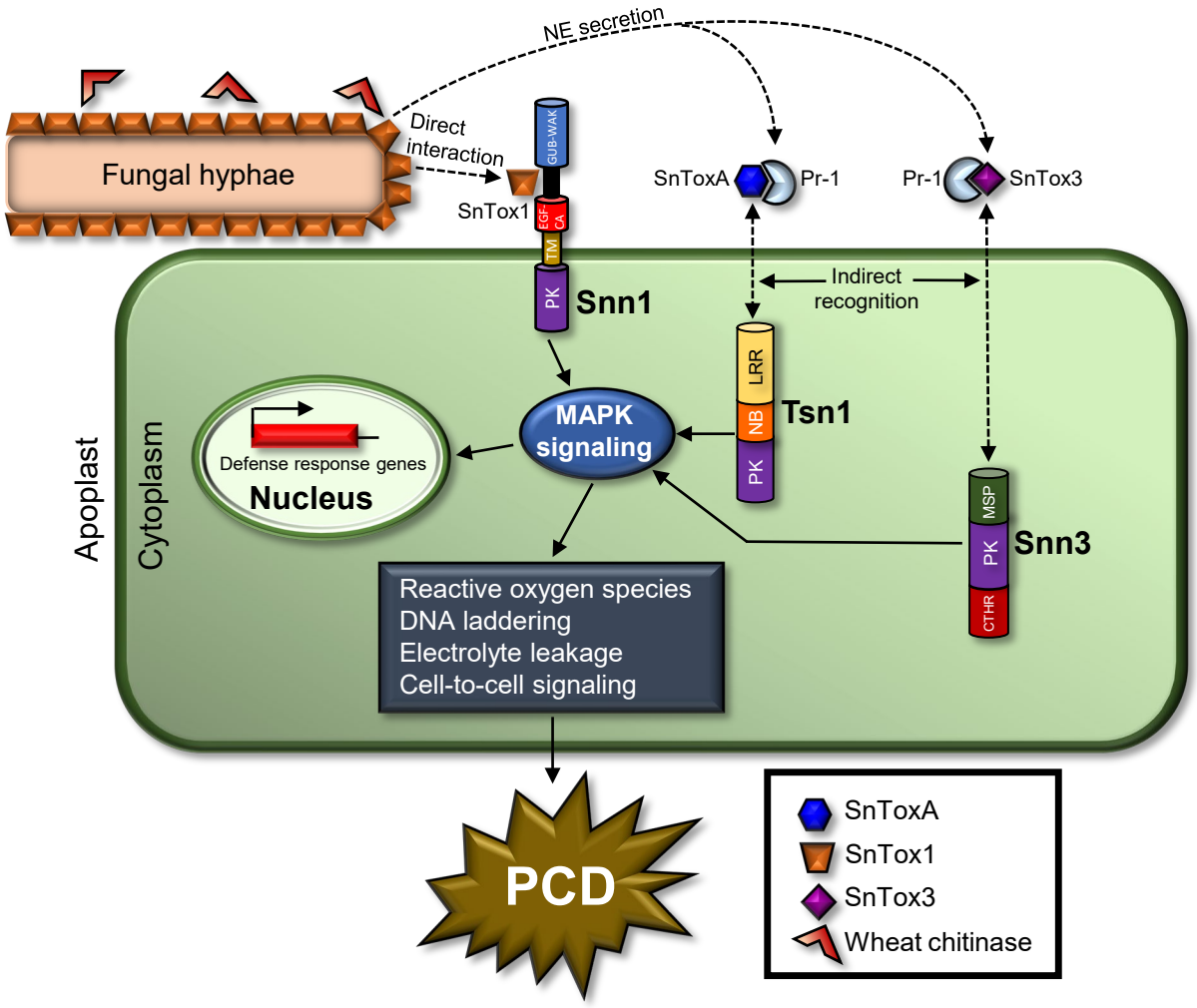

Figure 3.4. Overview of the *Snn1*-SnTox1, *Snn3*-SnTox3, and *Tsn1*-SnToxA interactions and known downstream events that result in necrotrophic effector-triggered susceptibility (NETS) in the wheat-*P. nodorum* pathosystem. The NE SnTox1, SnTox3, and SnToxA are secreted by the fungus. SnTox1 interacts directly with Snn1, and SnTox1 binds chitin to protect the fungal hyphae from wheat chitinases. SnToxA and SnTox3 interact with PR1 proteins, likely in the apoplast. Tsn1 and Snn3-D1 are hypothesized to be a guards of other host proteins that may interact directly with SnToxA and SnTox3, respectively. Upon these recognition events of SnTox1, SnTox3, and SnToxA by Snn1, Snn3-D1, and Tsn1, respectively, signaling is initiated via the MAPK signaling pathway leading to an up-regulation of defense response pathways, an increase in reactive oxygen species, DNA laddering, electrolyte leakage, cell-to-cell signaling, and ultimately programmed cell death which provides nutrients for the pathogen to survive and reproduce.

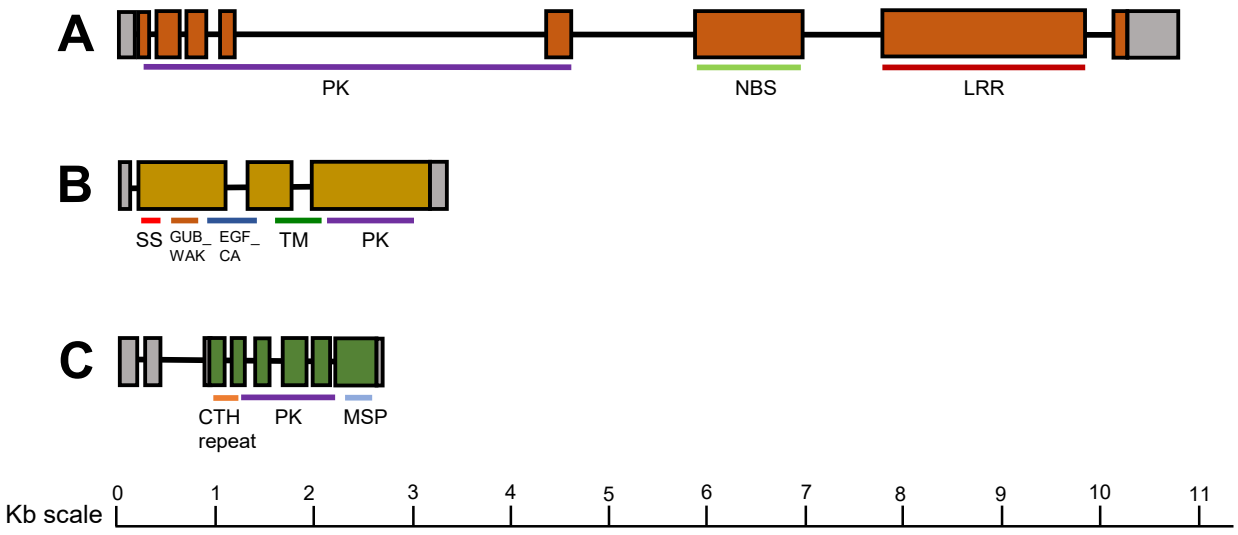

Figure 3.5. Structure of cloned *P. nodorum* sensitivity genes in wheat. A kilobase scale is indicated along the bottom. Colored boxes represent exons and grey boxes represent untranslated regions. **A:** The structure of the *Tsn1* gene from Faris et al. (2010). Colored lines indicate the serine/threonine protein kinase (PK) domain, nucleotide binding site (NBS) domain, and leucine-rich repeat (LRR) domain. **B:** The structure of the *Snn1* gene from Shi et al. (2016b). Colored lines indicate the signal sequence (SS), the wall-associated receptor kinase galacturonan binding (GUB_WAK) domain, epidermal growth factor-calcium binding (EGF_CA) domain, transmembrane (TM) domain, and the serine/threonine protein kinase (PK) domain. **C:** The structure of the *Snn3-D1* gene from Zhang et al. (2021). Colored lines indicate the collagen triple helix (CTH) repeat, serine/threonine protein kinase (PK) domain and the major sperm protein (MSP) domain.

Table 3.2. Reports of sensitivity to the necrotrophic effectors SnToxA, SnTox1, and SnTox3 in wheat collections and panels.

Reference	Germplasm panel	Total number of lines	% sensitive SnToxA	% sensitive SnTox1	% sensitive SnTox3
Bertucci et al. 2014	US winter wheat cultivars	26	31	0	62
Downie et al. 2018	European lines	461[1]	26.5	75.9	75
Hafez et al. 2020	Canadian cultivars	79	59[2*]	32.9	56.9
Liu et al. 2015	North American hard red winter wheat cultivars	120	69.2	5	35
Phan et al. 2018	Vavilov collection	259	49.4	35.1	63
Ruud et al. 2018	Norwegian and international Spring wheat cultivars	157	45.2	12.1	55
Ruud et al. 2019	Nordic spring wheat panel	121	46	14	58.5
Tan et al. 2014	Western Australian cultivars	46	63	71.7	91.3
Waters et al. 2011	Australian cultivars	60	55.9	NA	86.7

*Denotes studies where % sensitivity was found screening with diagnostic marker and is % of lines with sensitivity gene.

[1]61 cultivars used for PCR testing

[2]457 lines for SnTox3, 460 lines for SnToxA, 461 lines for SnTox1

3.4.2. *Tsn1*-SnToxA

The *Tsn1*-SnToxA interaction differs from other interactions characterized in this pathosystem in that *ToxA* has been discovered in three different fungal species thus far (Friesen and Faris 2021 for review). ToxA was first discovered in *Pyrenophora tritici-repentis*, the causal agent of tan spot in wheat, and was designated Ptr ToxA (Tomás and Bockus 1987; Ballance et al. 1989). Like *P. nodorum*, *P. tritici-repentis* is a member of the Dothideomycete class and a necrotrophic fungal pathogen. The *ToxA* gene and the *Tsn1*-Ptr ToxA interaction, as they pertain to the wheat-*P. tritici-repentis* pathosystem, have been reviewed elsewhere (Ciuffetti et al. 2010; Singh et al. 2010; Faris et al. 2013) and will not be revisited in this review.

After the *P. nodorum* genome was sequenced, a homolog with 99.7% similarity to *Ptr ToxA* was identified (Friesen et al. 2006). When Friesen et al. (2006) evaluated the diversity of *ToxA* in the two pathogens, they found that only one haplotype was present for *P. tritici-repentis* whereas *P. nodorum* had 11 haplotypes and therefore a higher level of nucleotide diversity. From this, it was concluded that *ToxA* likely originated in *P. nodorum* and was horizontally transferred to *P. tritici-repentis* prior to 1940, upon which it rendered *P. tritici-repentis* an economically significant disease of wheat.

Liu et al. (2006) found that Ptr ToxA and SnToxA were functionally identical and both interacted with the same host gene, *Tsn1*, and both elicited necrosis in susceptible genotypes. More recently, *ToxA* was identified in *Bipolaris sorokiniana* (McDonald et al. 2017; Friesen et al. 2018; Navathe et al. 2020), the causal agent of spot blotch and common root rot in wheat and barley. As with Ptr ToxA and SnToxA, recognition of BsToxA by *Tsn1* leads to disease (Friesen et al. 2018).

QTL mapping studies have revealed the *Tsn1*-SnToxA interaction accounts for 25- 95% of the disease variation to SNB in both tetraploid and hexaploid wheat (Friesen et al. 2006; Liu et al. 2006; Friesen et al. 2008; Faris and Friesen 2009; Chu et al. 2010; Faris et al. 2011; Virdi et al. 2016) (Table 3.1). In the absence of the *Tsn1*-SnToxA interaction, disease levels decreased, even in the presence of other wheat S gene-NE interactions (Virdi et al. 2016; Faris and Friesen 2009; Friesen et al. 2012).

The mature ToxA protein is 13.2 kDa (reviewed by Ciufetti and Touri 1999). The pre-pro-protein is 19.7 kDa, 178 amino acids, and contains a signal peptide that is required for secretion (Ballance et al. 1989, 1996; reviewed by Manning and Ciuffetti 2005; Friesen and Faris 2010, 2021; Oliver et al. 2012). The mature ToxA protein contains multiple domains and structural motifs, such as N-terminal pyroglutamate, C domain, two myristoylation sites, six phosphorylation sites, and an RGD cell attachment motif (Tuori et al. 1995; Tuori et al. 2000; Ciuffetti et al. 1997; Zhang et al. 1997, Meinhardt et al. 2002). Mutation of any of these motifs/domains decreased or halted ToxA activity in wheat lines containing *Tsn1* (Manning et al. 2004).

Tsn1 was mapped to the long arm of chromosome 5B using *P. tritici-repentis* culture filtrates (Faris et al. 1996). Subsequent genomic targeting, marker development, and fine mapping (Haen et al. 2004), comparative analysis of colinearity with rice (Lu and Faris 2006), and BAC-based physical mapping (Lu et al. 2006) eventually led to the positional cloning of *Tsn1* by Faris et al. (2010) using a traditional map-based chromosome walking strategy (see Faris et al. 2013 for review). The candidate region was delineated to a 351 kb segment that accounted for 0.9 cM and contained six candidate genes. Comparative sequence analysis of the candidate genes among sixteen ToxA-insensitive mutant lines and the corresponding wild type

revealed *Tsn1* had C-terminal nucleotide binding (NB) and leucine-rich repeat (LRR) domains (Figure 3.5), which are domains typically associated with resistance to biotrophic pathogens (Kourelis and van der Hoom 2018). However, it also had an additional N-terminal serine/threonine protein kinase (S/TPK) domain. The only other gene known to date to contain all three domains in a single open reading frame is the barley stem rust resistance gene *Rpg5* (Brueggeman et al. 2008), with the difference being the S/TPK domains are positioned at opposite terminals. *Tsn1* and *Rpg5* do not share a recent ancestry and probably both evolved through independent gene-fusion events (Faris et al. 2010).

Tsn1 is 10,581 bp in length from start to stop codon, containing eight exons, and the coding sequence is 4,473 bp in length (Faris et al. 2010) (Figure 3.5). The predicted protein product is 1,490 amino acids and all three domains are required for ToxA sensitivity. *Tsn1* was expressed in leaves, stems, and immature spikes, but not roots. Transcriptional analysis of *Tsn1* indicated that it was regulated by light and followed the same oscillation patterns as were observed for *Snn1* described above (Faris et al. 2010; Shi et al. 2016b).

Unlike the *Snn1*-SnTox1 interaction, which was a direct interaction, yeast two-hybrid analysis suggested that the Tsn1 protein, which does not contain a transmembrane domain and was predicted to be located intracellular, did not interact directly with ToxA (Faris et al. 2010). Although *Tsn1* was essential for ToxA recognition and sensitivity, *Tsn1* was suspected to be a guard for ToxA recognition (Figure 3.4). Early work into un-raveling this interaction at the molecular level indicated that ToxA was internalized and located to chloroplasts within wheat cells in lines that contained *Tsn1*, but not in lines that lacked *Tsn1*. Manning et al. (2007) screened a yeast two-hybrid library of chloroplast specific proteins to find the potential target of ToxA, and they identified ToxA binding protein 1 (ToxABP1).

Successful recognition of ToxA in lines harboring *Tsn1* led to photosystem changes and an accumulation of reactive oxygen species (ROS), which was associated with ETI and PCD (Manning et al. 2009) (Figure 3.4). The presence of ROS decreased in the absence of light, providing further evidence towards this being a light dependent interaction. The concentration of ROS present in chloroplast cells corresponded to the amount of necrosis visible on the leaf, which suggested that ROS accumulation led to cell death and therefore an increase in disease (Manning et al. 2009). This accumulation of ROS cascaded to disruption of the thylakoids, decreased photosystem II activity (Manning et al. 2004), and chlorophyll loss (Manning et al. 2007), which contributed to eventual cell death and necrosis.

Tai et al. (2007) used a similar yeast two-hybrid analysis technique and found another host target of ToxA, a wheat plastocyanin, which is a part of the electron transport chain of photosynthesis. During this study, they discovered that G141, located in the RGD motif, was required for plastocyanin interaction. Mutations at E145 and D149 also resulted in a loss of ToxA-ToxA oligomerization, resulting in a loss of ToxA activity and necrosis (Tai et al. 2007).

A third potential target of ToxA is a PR-1-type pathogenesis-related (PR) protein, PR-1-5 (Lu et al. 2014) (Figure 3.4), which is often involved in HR/defense pathways ending in cell death. Using similar methods as the two other groups, PR-1-5 physically interacted with ToxA and was further validated using co-immunoprecipitation assays (Lu et al. 2014). N102 and N141, both surface-exposed asparagine residues on turning loops, were essential for ToxA-PR-1-5 binding. Differing from ToxABP1 and the plastocyanin interactions, *PR-1-5* was upregulated in wheat lines post ToxA infiltration, however the expression was not significantly different between sensitive and insensitive lines, and it was concluded that the upregulation may not contribute to necrosis (Lu et al. 2014).

The frequency of SnToxA sensitivity (presence of *Tsn1*) in various wheat germplasm collections has varied from 26.5% of lines in a panel of European lines evaluated by Downie et al. (2018) to about 86% of wheat cultivars planted in Australia up to 2008 (Oliver et al. 2008) (Table 3.2). Screening of different geographical panels from Canada, Australia, the southeastern US, and Norway have indicated the frequency of *Tsn1* was around 50% (Hafez et al. 2020; Waters et al. 2011; Phan et al. 2018; Bertucci et al. 2014; Tan et al. 2014; Ruud et al. 2018). In areas where SNB can be a major problem, focusing on the elimination of *Tsn1* from breeding program materials would likely be beneficial.

Codominant SSR markers *fcp394* and *fcp620*, which flank *Tsn1* within a physical segment of about 300 kb, were developed by Zhang et al. (2009), and a PCR-based marker (*fcp623*) for *Tsn1* itself was developed by Faris et al. (2010). Because ToxA-insensitive plants are typically null for *Tsn1* due to the absence of a large segment encompassing the gene (Faris et al. 2010, 2013), *fcp623* is dominant and not suitable for high-throughput genotyping platforms. Although *fcp394* and *fcp620* are codominant, SSRs are not optimal for modern high-throughput platforms either. In an effort to develop new and better markers for *Tsn1*, we developed codominant KASP markers that delineate *Tsn1* to a physical segment of about 40 kb and are highly robust (K.L.D. Running and J.D. Faris, unpublished) (Table 3.1). These markers, designated *fcp791* and *fcp792*, are available upon request from J. Faris.

3.4.3. *Snn2*-SnTox267, *Snn6*-SnTox267, and *Snn7*-SnTox267

Earlier research indicated the *Snn2*-SnTox2, *Snn6*-SnTox6, and *Snn7*-SnTox7 interactions were independent of one another, and SnTox2, SnTox6 and SnTox7 were three different NEs (Friesen et al. 2007; Gao et al. 2015; Shi et al. 2015). However, through gene cloning experiments, Richards et al. (2021) recently showed that NEs SnTox2, SnTox6, and

SnTox7 were the same protein, and therefore the NE was redesignated SnTox267. In this section, we first discuss each interaction separately and then conclude with the new findings by Richards et al. (2021).

The first report of the *Snn2*-SnTox2 interaction was by Friesen et al. (2007). Analysis of a population of RI lines derived from the two hard red spring wheat cultivars BR34 and Grandin (BG population) revealed that it segregated in a 3:1 ratio (sensitive: insensitive) when infiltrated with *P. nodorum* isolate Sn6 culture filtrates, indicating two genes in the host were interacting with NEs in the culture filtrate. Further analysis determined that one of the NEs was SnToxA and the other was a novel NE designated SnTox2. After partial purification of Sn6 culture filtrate to eliminate SnToxA, a single dominant host gene located at the distal end of the short arm of chromosome 2D was identified that conferred sensitivity to SnTox2. This gene was designated as *Snn2*. Like the previous S gene-NE interactions identified in this system, a compatible *Snn2*-SnTox2 interaction resulted in the development of necrosis.

Phenotypic evaluation of the BG population using the *P. nodorum* isolate Sn6 showed the *Snn2*-SnTox2 interaction explained 47% of the disease variation and the *Tsn1*-SnToxA interaction explained 20% of the disease variation (Table 3.1). The two interactions were generally additive with plants containing both *Snn2* and *Tsn1* having higher disease severity than those with a single S gene. This was the first study to show the inverse gene-for-gene model differed from the classical gene-for-gene model in that multiple interactions led to a higher amount of disease in affected plants (Friesen et al. 2007). A high-density genetic linkage map was developed for the region of chromosome 2D harboring *Snn2*, which narrowed the *Snn2* gene to a 4.0 cM region and was useful in discovering markers for MAS and to begin the positional cloning process of the *Snn2* gene (Zhang et al. 2009).

The *Snn6*-SnTox6 interaction was characterized by Gao et al. (2015) using the ITMI population, which was also used to initially characterize the *Snn1*-SnTox1 interaction (Liu et al. 2004a). Culture filtrates of *P. nodorum* isolates Sn6 and Sn6KOTox3 were used to initially characterize this interaction and to identify and map the wheat S gene, *Snn6,* to the distal region of the long arm of chromosome 6A. Characterization of SnTox6 indicated it was likely a protein approximately 12 kDa in size.

When the ITMI population was inoculated with the isolate Sn6, the *Snn6*-SnTox6 interaction explained 27% of the disease variation (Table 3.1). The ITMI population segregated not only for *Snn6*, but the S genes *Snn1* and *Snn3-B1* as well. Interestingly, although both SnTox1 and SnTox3 were produced by *P. nodorum* isolate Sn6, the *Snn1*-SnTox1 and *Snn3-B1*-SnTox3 interactions did not contribute significantly to SNB caused by Sn6 (Gao et al. 2015). Follow up experiments indicated the *SnTox1* gene was not expressed in isolate Sn6 providing an explanation for why *Snn1*-SnTox1 did not contribute to disease. Related work, discussed above and below, indicated some wheat-*P. nodorum* interactions are epistatic to the *Snn3-B1*-SnTox3 interaction thus providing an explanation for the lack of association of the *Snn3-B1*-SnTox3 interaction with SNB development in the work by Gao et al. (2015) (Friesen et al. 2008; Peters Haugrud et al. 2019).

Screening of the complete set of 21 Chinese Spring (CS)-Timstein (CS-Tm) disomic chromosome substitution lines with culture filtrates of *P. nodorum* isolate Sn6 revealed the CS-Tm2D and CS-Tm5B substitution lines were sensitive and harbored S genes (Shi et al. 2015). The sensitivity was due to the presence of *Snn3-B1* on the Tm5B chromosome and the presence of SnTox3 but not SnToxA in the culture filtrate. Evaluations of differential lines indicated the sensitivity of Tm2D was not due to *Snn2*, but rather a new S gene. This gene was designated as

Snn7, and it was presumed that *Snn7* conferred sensitivity to a new NE, which was designated SnTox7. Genetic analysis and mapping in an F_2 population derived from CS × CS-Tm 2D revealed the location of *Snn7* on the long arm of chromosome 2D, approximately 170 cM from *Snn2*.

When the population was inoculated with isolate Sn6, the *Snn7*-SnTox7 interaction explained 33% of the disease variation (Table 3.1). Evaluation of 52 diverse hexaploid wheat lines indicated that the *Snn7* allele is rare and the only identified cultivar containing it was Timstein (Shi et al. 2015).

Using GWAS, Richards et al. (2021) identified the *P. nodorum* gene *CJJ_13380* to be a strong candidate for both *SnTox2* and *SnTox6*. SnTox7 was previously found to have similar characteristics to SnTox2 and SnTox6, therefore Richards et al. (2021) infiltrated the NE encoded by *CJJ_13380* on the CS × CS-Tm 2D population. QTL mapping indicated that CJJ_13380 interacted with *Snn7*, which led them to conclude that *CJJ_13380* encodes SnTox7. Therefore, what was originally thought to be three separate NEs (SnTox2, SnTox6, and SnTox7) was confirmed to be one NE, now redesignated as SnTox267 (Richards et al. 2021; Friesen and Faris 2021 for review).

SnTox267 consists of a single 798 bp exon and encodes a secreted protein consisting of 265 amino acids including 10 cysteine residues (Richards et al. 2021). SnTox267 has structural similarity to SnTox3 and SnTox5, and diversity analysis showed that it was present in 95.43% of the sequenced isolates collected throughout the US; however, there is a high level of nucleotide diversity with 22 polymorphic nucleotides identified thus far in the coding region and a total of 32 nucleotide haplotypes.

Richards et al. (2021) showed that *Snn2* and *Snn6* are both required for SnTox267 sensitivity and are therefore complementary genes. The genetic relationship of *Snn7* to *Snn2* and *Snn6* is not yet resolved, and related research has indicated at least several additional genes in the wheat genome function as S genes for SnTox267 (J. Faris, unpublished data). Therefore, it appears the wheat-*P. nodorum* interactions involving SnTox267 is genetically complex compared to the other interactions.

Expression of *SnTox267* was highest at 24 hpi in infected wheat leaves and tapered off until 120 hpi, suggesting that SnTox267 was involved in the early infection process (Richards et al. 2021). Whether the only role of SnTox267 is pathogen recognition or if it has secondary effector function remains unknown. The exact role SnTox267 plays in eliciting disease has yet to be uncovered, along with the pathways SnTox267 targets and whether it directly interacts with the protein products of *Snn2*, *Snn6*, *Snn7*, or other targets. Cloning of the host S genes will help unravel this complex relationship between SnTox267 and its targets.

3.4.4. *Snn3* -SnTox3

The *Snn3*-SnTox3 interaction was first identified using the BG population and several *P. nodorum* isolates that produced various combinations of NEs (Friesen et al. 2008). A compatible interaction played a significant role in the development of disease explaining from 13-35% of the phenotypic variation in SNB (Table 3.1), but the *Snn3*-SnTox3 interaction was not always significant in the presence of other compatible interactions. Infiltrations with partially purified cultures containing only SnTox3 indicated a dominant *Snn3* gene conferred sensitivity to SnTox3, and the *Snn3-B1*-SnTox3 interaction fit the inverse gene-for-gene model.

Friesen et al. (2008) showed that SnTox3 was a protein between 10 and 30 kDa in size. In follow up work to clone the SnTox3-encoding gene, *SnTox3*, Liu et al. (2009) analyzed proteins

of avirulent and virulent isolates containing SnTox3 and identified the gene *SNOG_08981* from the *P. nodorum* reference genome as the best candidate. Gene disruption and heterologous expression of *SNOG_08981* demonstrated that it was *SnTox3*. *SnTox3* encoded a pre-pro protein consisting of 230 amino acids. SnTox3 was 25.85 kDa, contained a 20 amino acid signal peptide, and six cysteine residues that were predicted to form disulfide bonds and help stabilize the mature protein and in protein activity. *SnTox3* expression was highest during the first few days post infection and then decreases once the host tissue had been colonized (Liu et al. 2009).

The frequency of *SnTox3* in global *P. nodorum* populations varied among regions (Liu et al. 2009; McDonald et al. 2013). It was proposed that unless a NE has a dual function, like SnTox1, they were under positive selection and frequency of the NE corresponded with frequency of the corresponding S gene in that region (Liu et al. 2009, Liu et al. 2012). Liu et al. (2012) found that *SnTox3* was present in 60% of the 923 worldwide isolates screened and was an important virulence factor. Recently, Sung et al. (2020) demonstrated SnTox3 does have a dual function in that it not only mediates *Snn3*-induced necrosis, but it also independently interacts with TaPR1 proteins to suppress host defense responses.

Friesen et al. (2008) mapped the *Snn3* gene to the distal end of chromosome arm 5BS in the BG population (Table 3.1). The marker *Xcfd20* was located 1.4 cM proximal to *Snn3*, and no marker on the distal side of *Snn3* was identified. Subsequent saturation and fine mapping of *Snn3* on 5BS using 5,600 gametes derived from the hard red spring wheat lines BR34 and Sumai3 by Shi et al. (2016a) led to the identification and development of additional markers that delineated the locus to a 1.5 cM interval. The study by Shi et al. (2016a) also suggested that different *Snn3* alleles can underlie differences in levels of SnTox3 sensitivity. However, our ongoing research

has recently revealed a second *Snn3* gene exists on chromosome arm 5BS that is responsible for the higher level of sensitivity to SnTox3 in some wheat lines (see below).

A survey of *Ae. tauschii* accessions for sensitivity to SnTox3 revealed several sensitive accessions. Subsequent genetic analysis by Zhang et al. (2011) led to the identification of a gene on the short arm of chromosome 5D that conferred sensitivity to SnTox3 in the *Ae. tauschii* accession TA2377 (Table 3.1). Comparative mapping analysis indicated this locus was likely homoeologous to the *Snn3* locus on 5B in polyploid wheat, and the 5B and 5D genes were subsequently named *Snn3-B1* and *Snn3-D1*, respectively. Zhang et al. (2011) tested 180 *Ae. tauschii* accessions and found that 11.7% were sensitive to SnTox3 and therefore likely harbored functional *Snn3-D1* alleles. They also tested 93 common wheat lines and found that 38.7% were sensitive to SnTox3. When evaluating hexaploid wheat populations segregating for SnTox3 sensitivity, they discovered all had *Snn3-B1* and none had *Snn3-D1* suggesting the D-genome donor of hexaploid wheat did not have *Snn3-D1*.

Fine-mapping of the *Snn3-D1* locus in *Ae. tauschii* by Zhang et al. (2011) using a population consisting of 1,726 recombinant gametes delineated the gene to a 1.38 cM interval by markers *Xhbg337* and *Xcfd18*. In an effort to clone *Snn3-D1* using a map-based approach, these two flanking markers were used to screen 7,700 recombinant gametes derived from an *Ae. tauschii* population and 9,200 gametes derived from a cross between the hard red spring wheat line BR34 and a synthetic hexaploid wheat line developed from the durum wheat variety Langdon and the *Ae. tauschii* accession TA2377 (LDN2377) (Zhang et al. 2021). This strategy narrowed the *Snn3-D1* candidate region to a 362 kb segment in TA2377 containing 11 putative genes. Comparative sequence analysis of EMS-induced SnTox3-insensitive mutants

demonstrated that a gene containing protein kinase (PK) and major sperm protein (MSP) domains was *Snn3-D1*.

The genomic sequence of *Snn3-D1* was 1,977 bp from start to stop codon, and the coding region was 1,476 bp and contained six exons (Figure 3.5) (Zhang et al. 2021). Mutagenesis confirmed the PK and MSP domains were both critical for *Snn3-D1* gene function. *Snn3-D1* was expressed in various tissues including leaves, stems, and roots, and it showed a diurnal rhythm but with the opposite peak and valley times as *Tsn1* and *Snn1*. The expression of *Snn3-D1* gradually increased during the day and reached its peak around midnight, then gradually decreased to the lowest level in the morning.

A survey of 105 *Ae. tauschii* accessions indicated *Snn3-D1* was present in 42 of them (Zhang et al. 2021). Subsequent sequence analysis of the *Snn3-D1* gene from 17 sensitive accessions revealed almost 100% identity among them, which suggested a relatively recent origin of the gene. Genomic analysis and tracking the geographic origins of SnTox3-sensitive and -insensitive accessions suggested a genomic insertion harboring the functional *Snn3-D1* allele likely took place along the west bank of the Caspian Sea.

The cloning of *Snn3-D1* led to the identification of the homoeologous candidate gene for *Snn3-B1* (Zhang et al. 2021). We continue to characterize *Snn3-B1*, and in doing so, we identified a second SnTox3-S gene on wheat chromosome arm 5BS that we refer to as *Snn3-B2*. We are in the process of characterizing both genes, and preliminary results indicate the two genes lie approximately 1 Mb apart. As mentioned above, *Snn3-B2* appears to confer a higher level of sensitivity to SnTox3 than does *Snn3-B1*.

Multiple panels have been screened for SnTox3 sensitivity; however, not all have not differentiated between whether sensitivity is due to *Snn3-B1/B2* or *Snn3-D1*. Zhang et al. (2011)

showed that *Snn3-D1* was not likely present in hexaploid wheat or was extremely rare. Phan et al. (2021) recently reported the presence of *Snn3-D1* in a few hexaploid wheat lines, some of which were synthetic hexaploid wheats indicating the *Snn3-D1* gene had been introduced from the *Ae. tauschii* accessions used to create them. This finding emphasizes the importance of being cautious when using synthetic hexaploids in breeding programs to not inadvertently introgress *Snn3-D1* or other S genes.

Percent sensitivity has been reported ranging from 55% in a European spring wheat panel (Ruud et al. 2018) to 91.3% in Australian cultivars (Tan et al. 2014) (Table 3.2). This high prevalence in different panels from multiple global locations indicates that, where there is SnTox3 in the local pathogen population, having *Snn3-B1/B2* or *Snn3-D1* in local cultivars may contribute to the SNB disease severity in that region.

A few studies have been conducted to gain understanding of the molecular mechanisms underlying a compatible *Snn3*-SnTox3 interaction. Plant cell death around the site of infection occurred at about 72 hpi (Winterberg et al. 2014), and 24 to 48 hpi before this, there was an upregulation of plant defense genes such as PR proteins, jasmonic acid pathway proteins and phenylpropanoid pathway proteins. There was also an increase in expression of receptor-like kinase genes, suggesting an increased cell-to-cell signaling that was associated with an ETI response (Day et al. 2011; Winterberg et al. 2014). Several MAP kinases were induced in plants post SnTox3 infiltration. One of the kinases, TaMPK3, was also shown to be upregulated by SnToxA and SnTox1 (Winterberg et al. 2014; Shi et al. 2016b). Multiple microarray and proteomic studies have been performed on wheat leaves post infection with NEs, such as SnTox3, SnToxA and Ptr ToxA, and offer insights into the possible cellular mechanisms that lead to PCD and NETS (Pandelova et al. 2009; Vincent et al. 2012; Winterberg et al. 2014).

Preliminary experiments indicated that Snn3 does not interact directly with SnTox3 (Zhang et al. 2021) (Figure 3.4). Breen et al. (2016) used a yeast-two-hybrid approach to show SnTox3 directly interacts with TaPR-1-1 and with additional wheat PR-1 proteins; however, the latter were not as strong as the SnTox3-TaPR-1-1 interaction. As mentioned above, SnToxA was also shown to interact with a PR-1 protein (Lu et al. 2014). Therefore, it is possible that PR proteins may be common targets for NE effectors leading to the upregulation of defense genes and ultimately NETS (Breen et al. 2016).

3.4.5. *Snn4*-SnTox4

The *Snn4*-SnTox4 interaction was described by Abeysekara et al. (2009). An RI population developed from crossing Arina and Forno (Paillard et al. 2003), which are both Swiss winter wheat cultivars, was used to map *Snn4* using culture filtrates of the Swiss *P. nodorum* isolate Sn99CH 1A7a (Sn99). When differential wheat lines were infiltrated with Sn99 culture filtrate, it was discovered the filtrate contained a novel NE designated SnTox4 (Abeysekara et al. 2009). The *Snn4*-SnTox4 interaction fit the inverse gene-for-gene model, with one dominant S gene conferring sensitivity to one NE.

The gene, designated *Snn4*, was located on the short arm of chromosome 1A and delineated to a 2.5 cM interval (Abeysekara et al. 2009). The NE SnTox4 is most likely a small protein, approximately 10 to 30 kDa in size. A compatible *Snn4*-SnTox4 interaction explained 41% of the disease variation with additional minor QTLs contributing to disease in an additive manner (Table 3.1).

A population derived from Katepwa × Salamouni was evaluated using the same *P. nodorum* isolate, Sn99 (Abeysekara et al. 2012). In this population, the *Snn4*-SnTox4 interaction explained 23% of the disease variation, with an additional uncharacterized QTL on 7AS

explaining 16% of the disease variation. These two interactions were additive and accounted for 35.7% of the total disease variation. The difference in disease explained may be due to the background or the presence of the minor genes. Therefore, depending on the wheat background and the NE susceptibility genes present, the *Snn4*-SnTox4 interaction explained 23-41% of the disease variation when plants were infected with the *P. nodorum* isolate Sn99. In both populations, the phenotype associated with this interaction was unique in that it was a mottled necrotic reaction and not as severe in appearance as the necrosis seen with many of the other interactions (Abeysekara et al. 2009).

3.4.6. *Snn5*-SnTox5

Culture filtrates of *P. nodorum* isolate Sn2000 were used to screen a doubled haploid (DH) population derived from crossing Lebsock, a North Dakota durum wheat variety, with *T. turgidum* ssp. *carthlicum* accession PI 94749 (LP749 population) (Friesen et al. 2012). QTL analysis revealed significant associations with markers on the long arm of chromosome 5B that represented the *Tsn1* locus and with markers on the long arm of chromosome 4B. The 4BL locus was determined to be associated with a new host S gene-NE interaction and was designated *Snn5*-SnTox5 (Table 3.1).

Recently, *SnTox5* was cloned by Kariyawasam et al. (2021) and found to be 654 bp and intron-free. To validate their candidate gene as encoding SnTox5, Kariyawasam et al. (2021) used a combination of GWAS, QTL analysis, CRISPR/Cas9-based gene disruption, and gain-of-function transformation. *SnTox5* encoded a small, secreted protein consisting of 217 amino acids with a secretion signal and a 45 amino acid pro-sequence cleaved at a Kex2 protease cleavage site. SnTox5 also contained six cysteine residues and had structural similarity to SnTox3. *SnTox5* expression was highest at 24 hpi, and then gradually decreased and leveled off by 120 hpi. Using

laser confocal microscopy, Kariyawasam et al. (2021) found the *Snn5*-SnTox5 interaction resulted in PCD but that SnTox5 also facilitated mesophyll colonization even in the absence of *Snn5*. The exact mechanism of how SnTox5 facilitates colonization of the mesophyll remains unknown, however, it is likely that in addition to inducing PCD, SnTox5 has a secondary function that facilitates mesophyll colonization. A total of 22 nucleotide haplotypes were identified from isolates collected across the US and analysis indicated that *SnTox5* had high levels of diversification within the US, and the type of selection differed based on region. From the 22 nucleotide haplotypes, there were 20 different SnTox5 isoforms, which were also under region-specific selection pressure.

The LP749 population was inoculated with multiple *P. nodorum* isolates to characterize the role the *Snn5*-SnTox5 interaction played in disease development and severity. The population segregated for the NE susceptibility genes *Snn5*, *Tsn1*, and *Snn3-B1*. When the isolate Sn2000, which produces both SnTox5 and SnToxA, was inoculated onto the population, the *Snn5*-SnTox5 interaction explained 37% of the disease variation and *Tsn1*-SnToxA explained 31% (Table 3.1). When the population was inoculated with Sn2000KO6-1, which lacks SnToxA, the *Snn5*-SnTox5 interaction explained 63% of the disease variation; however, the average disease scores for the population as a whole and for each genotypic class decreased. These experiments showed when both the *Snn5*-SnTox5 and *Tsn1*-SnToxA interactions were present, the disease level was greater than when only one was present and therefore, the effects of the two interactions were additive.

The authors also used Sn1501, which produces SnTox5 and SnTox3, and isolate Sn1501ΔTox3, which lacks SnTox3 but still produces SnTox5 (Friesen et al. 2012). The *Snn5*-SnTox5 interaction explained 53% of the disease variation caused by Sn1501, but the *Snn3-B1*-

SnTox3 interaction explained only 3% of the variation. When inoculated with Sn1501ΔTox3, the *Snn5*-SnTox5 interaction explained 51% of the disease variation, indicating that, depending on the host and pathogen genetic backgrounds, the *Snn5*-SnTox5 interaction can play a major role in SNB development.

Recently, Sharma (2019) reported the development of a saturated map of the *Snn5* region to initiate the gene cloning process. The *Snn5* locus was delineated to 2.8 cM, which corresponded to a physical distance of 1.38 Mb and contained 16 putative genes flanked by markers *Xfcp762* and *Xfcp763*. Recent work in our labs using various wheat genomic resources have led to the cloning of *Snn5*, and we are currently in the process of characterizing the gene and the interaction. This work will provide additional insights into this complex pathosystem and tools to breed for genetic resistance.

3.5. Studies on Multiple Interactions and NE Expression

Multiple studies have been performed evaluating disease using isolates that produce multiple NEs and populations that segregate for two or more NE susceptibility genes (Liu et al. 2004a; Liu et al. 2012; Liu et al. 2009; Zhang et al. 2011; Friesen et al. 2008; Virdi et al. 2016; Liu et al. 2006; Friesen et al. 2007; Abeysekara et al. 2009; Abeysekara et al. 2012; Friesen et al. 2012; Gao et al. 2015; Faris et al. 2011; Phan et al. 2016; Peters Haugrud et al. 2019). In many of these studies, multiple compatible interactions were additive, with wheat genotypes containing multiple NE susceptibility genes exhibiting a greater level of disease than systems where only one interaction occurred. Thus, SNB development in systems involving multiple interactions appears to be controlled quantitatively.

Although past research has determined which NEs are produced in cultures of specific isolates, few studies have examined the expression of NEs *in planta* and how this corresponds to

the interactions observed and the amount of disease on infected plants. Gao et al. (2015) observed that although *P. nodorum* isolate Sn6 had previously been shown to produce SnTox1 and SnTox3, the *Snn1*-SnTox1 and *Snn3-B1*-SnTox3 interactions were not significantly associated with disease in the population under study. Expression levels were tested at 3 days post infection in sensitive wheat lines. No transcripts of *SnTox1* were observed, providing an explanation for the lack of significance of the *Snn1*-SnTox1 interaction, however, high levels of *SnTox3* transcripts were observed. One explanation was that the *Snn3-B1*-SnTox3 interaction was relatively weak compared to other wheat-*P. nodorum* interactions and may therefore be masked in some backgrounds (Gao et al. 2015).

Faris et al. (2011) examined the *Tsn1*-SnToxA and *Snn2*-SnTox2 interactions in a segregating RI population to determine the effects of each interaction on disease using multiple *P. nodorum* isolates. For isolate Sn4, *Snn2*-SnTox267 explained 26% of the variation in SNB development and *Tsn1*-SnToxA explained 25%. When the same population was inoculated with isolate Sn5, *Snn2*-SnTox267 explained only 6% of the disease variation and *Tsn1*-SnToxA explained 56%. Expression of *SnToxA* in parental lines was studied using quantitative PCR with samples collected at multiple time points post infection. Expression of *SnToxA* was highest in both Sn4 and Sn5 at 26 hpi, and higher levels of transcription were observed in both the resistant and susceptible line inoculated with Sn5 compared to the same lines inoculated with Sn4. This corresponded to the disease level difference observed for the *Tsn1*-SnToxA interaction between the two isolates. Because the same host population was used for both isolates, Faris et al. (2011) suggested that the difference was not due to host background differences, but rather pathogen genetic factors that influence NE gene expression.

Virdi et al. (2016) used a tetraploid wheat population to show the level of disease attributed to the *Tsn1*-ToxA interaction differed between *P. nodorum* and *P. tritici-repentis* isolates. When plants were inoculated with isolates of each pathogen, the level of *ToxA* expression differed substantially with the *P. nodorum* isolate Sn2000 transcribing *ToxA* at much higher levels than the *P. tritici-repentis* isolate 86-124. This corresponded to the disease evaluation findings and provided further evidence that pathogen genetic factors influence NE gene expression and therefore the significance of a particular interaction in causing disease.

Phan et al. (2016) evaluated the expression of *SnTox1* and *SnTox3* in *P. nodorum* isolate SN15 on a wheat population that segregated for *Snn1* and *Snn3-B1*. In seedlings inoculated with SN15, the *Snn1*-SnTox1 interaction explained 18% of the disease variation, and the *Snn3-B1*-SnTox3 interaction was not significant. Expression of *SnTox1* and *SnTox3* was studied *in planta* at 48 hpi in all four genotypic combinations (*snn1/snn3-B1*; *snn1/Snn3-B1*; *Snn1/snn3-B1*; *Snn1/Snn3-B1*). No significant difference was observed in expression of *SnTox1* and *SnTox3* among the four genotypic classes, indicating that the presence of the corresponding NE susceptibility gene did not influence NE expression. *SnTox3* expression differences between SN15 and SN15tox1-6, which lacks *SnTox1,* were also evaluated. Here, transcriptional expression of *SnTox3* was significantly higher in the SN15tox1-6 isolate compared to the wildtype SN15. This led Phan et al. (2016) to conclude that *SnTox3* expression may be suppressed by *SnTox1*.

Some research indicates NE genes are positively regulated by transcription factors that are global regulators. *PnPf2*, which encodes a GAL4-like Zn_2Cys_6 transcription factor, was found to be a positive regulator of *SnToxA* and *SnTox3* expression (Rybak et al. 2017). Lin et al. (2018) found that *PnCon7*, a zinc finger transcription factor, also positively regulates *SnTox3*.

The PnCon7 protein directly interacts with the cis-regulatory element in the *SnTox3* promoter region. Interestingly, *SnToxA* and *SnTox1* expression was reduced in isolates with *PnCon7* silenced; however, the authors speculated that PnCon7 acted upstream of the regulatory elements for these genes and did not directly regulate *SnToxA* or *SnTox1*. These findings indicate NE genes may be regulated by similar transcription factors. To date, no regulatory factors of *SnTox1* have been discovered.

Peters Haugrud et al. (2019) evaluated a wheat RI population that segregated for *Snn1*, *Snn3-B1*, and *Tsn1*, with several *P. nodorum* isolates that produced various combinations of the NEs SnTox1, SnTox3, and SnToxA. For isolates that produced all three NEs, only the *Tsn1*-SnToxA and *Snn3-B1*-SnTox3 interactions contributed to disease, but the relative effects of these interactions ranged from additive to epistatic depending on the pathogen isolate. The *Snn1*-SnTox1 interaction contributed very little to disease development except when an isolate with a disrupted *SnToxA* gene (Sn2000KO6-1) was used. In this case, the *Snn1*-SnTox1 interaction played a much more significant role in SNB development compared to when the wild type isolate (Sn2000) was used. Transcription experiments indicated that the enhanced role of the *Snn1*-SnTox1 interaction was due to a significance increase in the expression level of the *SnTox1* gene when *SnToxA* was eliminated. This suggests *SnToxA* may downregulate *SnTox1* expression. Overall, the experiments by Faris et al. (2011), Phan et al. (2016), and Peters Haugrud et al. (2019) demonstrated that differences in the genetic background of both the pathogen and host, along with inter-NE gene regulation leading to complex interplay among the interactions, all play roles in determining the significance of individual interactions and ultimately, overall disease severity.

Further research into how multiple wheat-*P. nodorum* interactions interact with one another to confer disease is needed. As previously stated, the disease-severity potential of individual isolates appears to be governed by the expression levels of pathogen NE genes. It is possible that there is a fitness cost to the pathogen for NE gene expression, which would explain why all NE genes possessed by a given isolate are not all expressed at high levels. Perhaps the pathogen acquires feedback from the host as to the S genes it carries and then upregulates those that would cause the host to induce PCD most efficiently. This might explain why an NE gene is upregulated when another is rendered nonfunctional as seen in the case with *SnTox1* and *SnToxA* in the wild type isolate Sn2000 and the corresponding *SnToxA*-knockout isolate Sn2000KO6-1 (Peters Haugrud et al. 2019). These findings were corroborated by Richards et al. (2021), who demonstrated that a deletion of *SnTox267* resulted in increased expression of *SnToxA*, *SnTox1*, and *SnTox3*. Studies examining not only pathogen expression but also host S gene expression are needed to further characterize this pathosystem at the molecular level as are studies to determine if epistasis occurs between NE genes and how these genes are regulated in the pathogen. Research in these areas will provide a broader understanding of this system, which will be useful for devising novel control strategies.

3.6. Additional QTLs Associated with a Compatible Wheat-*P. nodorum* Interaction

In addition to the S gene-NE interactions, multiple QTL have been reported in the wheat-*P. nodorum* pathosystem for susceptibility to SNB on leaves (Figure 3.6, Table 3.3). QTLs that explain over 10% of the SNB variation in biparental studies have been reported on chromosomes 1A (Ruud et al. 2017; Singh et al. 2019), 1B (Francki et al. 2011), 2A (Francki et al. 2011; Phan et al. 2016), 2B (Czembor et al. 2003), 2D (Aguilar et al. 2005; Shanker et al. 2008; Phan et al. 2016; Ruud et al. 2017), 3B (Czembor et al. 2003; Lu and Lillemo 2014), 4B (; Liu et al. 2004,

2012; Aguilar et al. 2005); 5A (Friesen et al. 2007, 2009; Shankar et al. 2008; Hu et al. 2019; Singh et al. 2019), 5B (Czembor et al. 2003; Shankar et al. 2008; Francki et al. 2011); 5D (Czembor et al. 2003), 6A (Arseniuk et al. 2004), 6B (Phan et al. 2016), 7A (Abeysekara et al. 2012), and 7B (Aguilar et al. 2005; Ruud et al. 2017).

In MAGIC panels, significant marker trait associations that explain over 10% of the SNB variation have been reported on chromosomes 2A (Lin et al. 2021), 2D (Lin et al. 2021), 3A (Lin et al. 2021), and 5A (Cockram et al. 2015). In association mapping panels, significant marker trait associations that explain over 10% of the SNB variation have been reported on chromosomes 1A (Ruud et al. 2019), 1B (Ruud et al. 2019; Francki et al. 2020), 2B (Ruud et al. 2019), 2D (Ruud et al. 2019), 3A (Phan et al. 2018; Ruud et al. 2019), 3B (Ruud et al. 2019), 4A (Phan et al. 2018; Ruud et al. 2019), 4B (Phan et al. 2018; Ballini et al. 2020), 5A (Liu et al. 2015; Phan et al. 2018; Hu et al. 2019; Ruud et al. 2019), 5D (Ruud et al. 2019), 6A (Francki et al. 2020); 6B (Ruud et al. 2019), 7A (Adhikari et al. 2011; Phan et al. 2018; Ruud et al. 2019), 7B (Ruud et al. 2019; Ballini et al. 2020), and 7D (Phan et al. 2018; Ruud et al. 2019). Whether the active genes underlying these QTLs confer susceptibility or resistance to *P. nodorum* has yet to be determined. Recently, Zhang et al. (2019) identified genes for resistance to both SNB and tan spot on chromosome 2S of *Aegilops speltoides*, but the nature of the resistance mechanism has yet to be identified. Additionally, Friesen et al. (2007) hypothesized that some QTLs may be due to general non-pathogen specific resistance or susceptibility mechanisms and may not follow the inverse gene-for-gene model commonly observed in this pathosystem. Studies examining host populations that segregate for the genes underlying these QTLs are needed to determine the type of resistance each provides against *P. nodorum*.

Table 3.3. Studies reporting QTL associated with SNB on wheat leaves that explain 10% or more of the disease variation.

Reference	Population Type	Total number of QTL	Variation explained (%)	Chromosomes with QTL	Field or Greenhouse	Sensitivity gene potentially associated with SNB QTLs
Czembor et al. 2003	Bi-parental	4	14-37%	2B, 3B, 5B, 5D	Greenhouse	None
Arseniuk et al. 2004	Bi-parental	1	36%	6A	Greenhouse	*Snn6*
Liu et al. 2004, 2012	Bi-parental	1	50%	4B	Greenhouse	*Snn5*
Aguilar et al. 2005	Bi-parental	3	13-21%	2D, 4B, 7B	Field	*Snn7*
Friesen et al. 2006	Bi-parental	2	10-62%	1B, 5B	Greenhouse	*Tsn1, Snn1*
Liu et al. 2006	Bi-parental	2	10-62%	1B, 5B	Greenhouse	*Tsn1, Snn1*
Friesen et al. 2007	Bi-parental	4	10-47%	1B, 2D, 5A, 5B	Greenhouse	*Tsn1*, *Snn1*, *Snn2*
Shankar et al. 2008	Bi-parental	3	13-21%	2D, 5A, 5B	Field/Greenhouse	*Tsn1*
Friesen et al. 2008	Bi-parental	3	13-37%	2D, 5B (2)	Greenhouse	*Tsn1*, *Snn2*, *Snn3-B1*
Liu et al. 2009	Bi-parental	2	10-64%	2D, 5B	Greenhouse	*Snn2, Snn3-B1*
Abeysekara et al. 2009	Bi-parental	1	41%	1A	Greenhouse	*Snn4*
Friesen et al. 2009	Bi-parental	4	10-37%	1B, 2D, 4B, 5A, 5B	Field/Greenhouse	*Tsn1*, *Snn1*, *Snn2*, *Snn5*
Chu et al. 2010	Bi-parental	2	22-50%	1B, 5B	Greenhouse	*Tsn1*, *Snn1*
Adhikari et al. 2011	AM panel	2	10-12%	7A, 2D	Greenhouse	*Snn2*
Francki et al. 2011	Bi-parental	3	14-22%	1B, 2A, 5B	Field	*Snn1*
Zhang et al. 2011	Bi-parental	2	25-56%	2D, 5B	Greenhouse	*Tsn1*, *Snn2*
Abeysekara et al. 2012	Bi-parental	2	16-24%	1A,7A	Greenhouse	*Snn4*
Friesen et al. 2012	Bi-parental	2	31-63%	4B, 5B	Greenhouse	*Tsn1*, *Snn5*
Gurung et al. 2014	AM panel	2	12-15%	2D, 5B	Greenhouse	*Snn2*, *Tsn1*
Lu and Lillemo 2014	Bi-parental	2	12%	3B(2)	Field	None
Cockram et al. 2015	MAGIC	2	NA	1B, 5A	Greenhouse	*Snn1*
Liu et al. 2015	AM panel	2	10%	5A, 5B	Greenhouse	*Tsn1*
Gao et al. 2015	Bi-parental	1	27%	6A	Greenhouse	*Snn6*
Shi et al. 2015	Bi-parental	1	33%	2D	Greenhouse	*Snn7*
Phan et al. 2016	Bi-parental	3	10-29%	2A, 2D, 6B	Field/Greenhouse	*Snn2*
Virdi et al. 2016	Bi-parental	1	38%	5B	Greenhouse	*Tsn1*
Ruud et al. 2017	Bi-parental	3	11-16%	1A, 2D, 7B	Field	*Snn2, Snn4*
Phan et al. 2018	AM panel	10	NA	1B, 2D (2), 3A, 4A, 4B, 5A, 5B, 7A, 7D	Greenhouse	*Snn1, Snn3-B1, Snn2, Snn7*
Hu et al. 2019	Bi-parental	1	17%	5A	Greenhouse	None
Ruud et al. 2019	AM panel	18	NA	1A(2), 1B, 2B, 2D, 3A, 3B(2), 4A, 4B, 5A, 5B(2), 5D, 6B, 7A, 7B, 7D	Field/Greenhouse	*Snn3-B1, Snn7*, *Tsn1*, *Snn5*
Singh et al. 2019	Bi-parental	3	11-21%	1A, 5A, 5B	Greenhouse	*Tsn1*
Peters Haugrud et al. 2019	Bi-parental	4	10-34%	1B, 4B, 5B(2)	Greenhouse	*Tsn1*, *Snn1, Snn3-B1*, *Snn5*
Ballini et al. 2020	AM panel	2	9-18%	4B, 7B	Greenhouse	None
Francki et al. 2020	AM panel	3	10-11%	1B, 6A(2)	Field	None
Lin et al. 2021	MAGIC	5	10-16%	2A, 2D, 3A, 5B(2)	Field/Greenhouse	*Snn3-B1*, *Tsn1*
Kariyawasam et al. 2021	Bi-parental	2	10-66%	4B, 5B	Greenhouse	*Tsn1*, *Snn5*

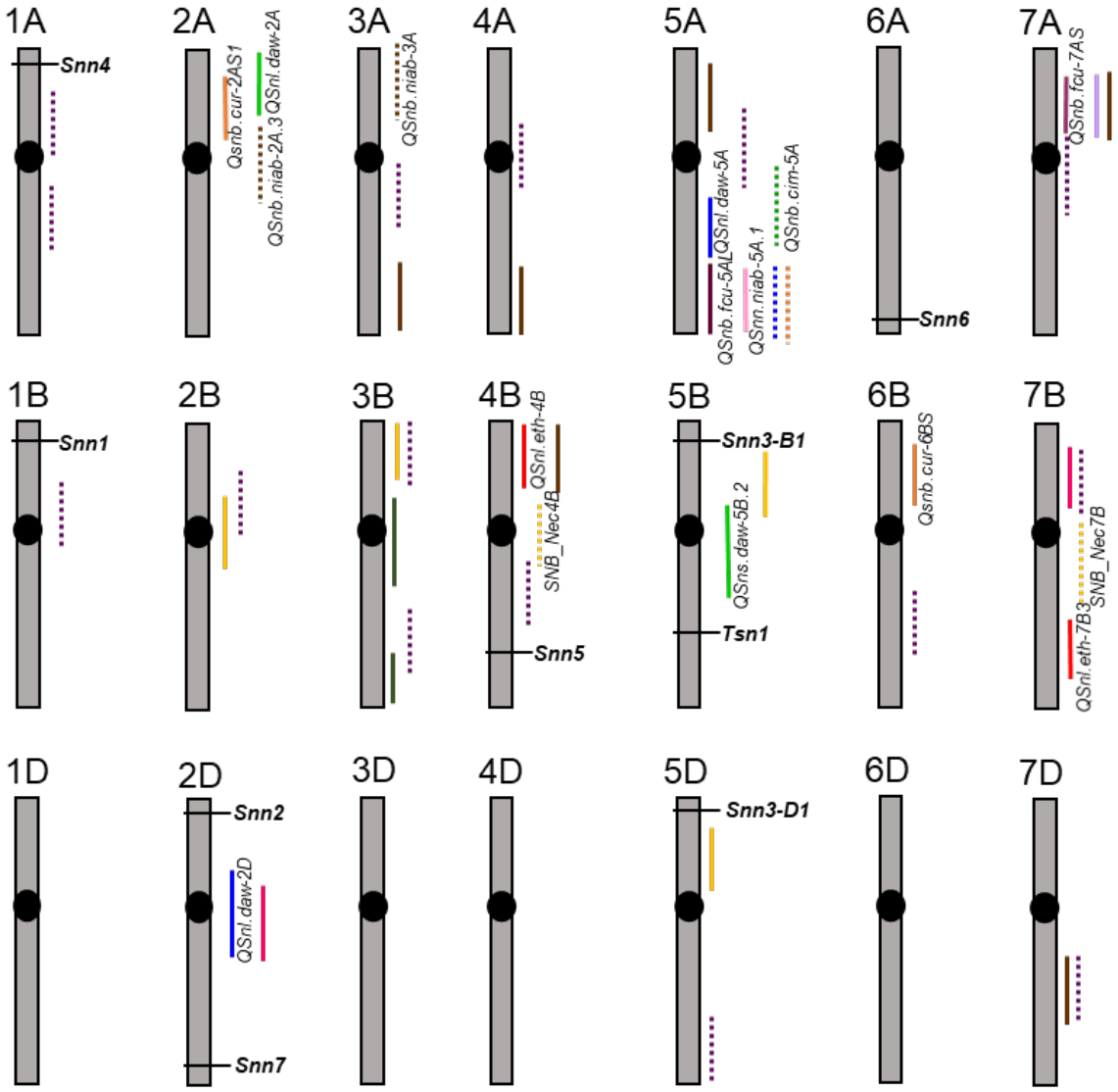

Figure 3.6. QTLs associated with septoria nodorum blotch disease that explain over 10% of the disease variation and are not associated with characterized NE sensitivity genes. The genomic positions of the known septoria nodorum blotch NE sensitivity genes *Tsn1*, *Snn1*, *Snn2*, *Snn3-B1*, *Snn3-D1*, *Snn4*, *Snn5*, *Snn6*, and *Snn7* are shown for reference. Table 3.3 contains a summary of the results illustrated here, along with studies that have identified QTLs associated with known sensitivity genes. Colored bars next to QTL designations indicates the approximate locations of the QTLs, and the different colors indicate QTLs identified from different studies. *dark blue* Shanker et al. (2008); *light blue* Arseniuk et al. (2004); *orange* Phan et al. (2016); *light green* Francki et al. (2011); *dark green* Lu and Lillemo (2014); *dark pink* Ruud et al. (2017); *gold* Czembor et al. (2003); *light purple* Adhikari et al. (2011); *brown* Phan et al. (2018); *light pink* Cockram et al. (2015); *hatched blue* Hu et al. (2019); *red* Aguilar et al. (2005); *hatched orange* Liu et al. (2015); *hatched purple* Ruud et al. (2019); *hatched green* Singh et al. (2019); *hatched brown* Lin et al. (2021); *hatched pink* Gurung et al. (2014); *hatched yellow* Ballini et al. (2020); *maroon* Friesen et al. (2009), Abeysekara et al. (2012).

3.7. Breeding and Marker-Assisted Selection for SNB Resistance

Because SNB susceptibility is typically quantitative due to the presence of multiple S genes that all play roles in conferring susceptibility, all the host S genes should be eliminated to achieve genetic resistance. A lack of understanding or awareness of the genetic control of SNB resistance is the main reason that breeders have been hindered in their efforts to develop SNB-resistant germplasm. With the knowledge that wheat possesses susceptibility genes as opposed to resistance genes and the availability of molecular markers linked to those genes, breeders now have the tools available to effectively select against multiple S genes at once (Table 3.1).

Gene-based markers have been developed for *Tsn1* and *Snn1* (Faris et al. 2010; Shi et al. 2016b), but even though markers have been developed based on the gene sequences themselves, they are not perfect. *Tsn1* lies on an inserted segment in the genome, and ToxA-insensitive lines are in the null state (Faris et al. 2010). Therefore, the *Tsn1* gene-based marker is dominant making it less than ideal for MAS platforms. Flanking codominant KASP markers suitable for high-throughput platforms that predict the *Tsn1* allelic state with high accuracy have recently been developed and are available upon request from the corresponding author (K.L.D. Running and J.D. Faris, personal communication). Ongoing work to characterize *Snn1* allelic diversity has revealed that recessive alleles exist, but there are at least four functional SNPs (S. Seneviratne and J.D. Faris, personal communication). Work is ongoing to develop markers specific to each SNP and to determine the frequency of each SNP across global collections. Cloning of additional S genes or high-resolution mapping will provide more accurate and precise markers for selecting against these genes.

Another method breeders and geneticists may use to detect S genes is to infiltrate plants with cultures of the yeast *Pichia pastoris* expressing a cloned NE gene. To date, *SnToxA*,

SnTox1, *SnTox3,* and *SnTox267* have been cloned into *P. pastoris* for culture production (Liu et al. 2006; Liu et al. 2012; Liu et al. 2009; Richards et al. 2021). This method is more accurate in showing which plants are truly insensitive or sensitive to a particular NE, however this method is typically not as user friendly for large plant breeding programs compared to high-throughput genotyping. Infiltrations are more laborious and require expertise working with fungal and yeast cultures. Another disadvantage of plant infiltrations using NE-containing cultures is the inability to detect heterozygotes in the F_2 generation and beyond. Because host S genes are dominant, culture infiltrations will not distinguish between homozygous dominant and heterozygous plants because both will be sensitive. For use in breeding, MAS is the recommended method for detecting the genotypes for these genes whereas when working with RI or DH populations for genetic studies, *P. pastoris* culture filtrates work just as well as markers.

A set of S gene differential lines for the known wheat-*P. nodorum* interactions involving cloned NEs have been established (Figure 3.7). If using crude culture filtrates of *P. nodorum* or *P. pastoris* cultures to evaluate wheat lines or accessions for the presence of known S genes, it is important to include the differentials as controls. It is important to note that not all compatible S gene-NE interactions result in the same type of reaction or level of cell death. As Figure 3.7 shows, some reactions yield strong and fast-occurring necrosis whereas others occur more slowly or simply do not lead to the same level of cell death.

Figure 3.7. Wheat NE sensitivity gene differentials infiltrated with the different NEs. BR34 is a universally insensitive line and was infiltrated with SnToxA to show the lack of a reaction. The corresponding reaction for each is shown on the right. All images were taken at 3 days post infiltration, except BG223, which was taken at 6 days post infiltration. Infiltration borders were marked with a permanent marker. SnToxA, SnTox1, and SnTox3 expressed in *Pichia pastoris* were used for infiltrations, and SnTox5 and SnTox267 were concentrated from *P. nodorum* grown in Fries media. SnTox4 was not infiltrated in its respective differential (AF89) due to not being cloned.

3.8. Future Work

Modern genetic research methods and resources can help to expedite research progress and advance our understanding of the wheat-*P. nodorum* pathosystem. GWAS employs large panels of lines and takes advantage of historical recombination events to detect multiple QTL at

once and are often more powerful than bi-parental studies (i.e., traditional QTL studies). Currently, research is being conducted on both wheat and *P. nodorum* to detect additional susceptibility genes and pathogen virulence genes using GWAS. Hopefully, this will help facilitate more rapid cloning of host and pathogen genes, providing tools for geneticists and breeders alike.

Winter wheat is currently lagging in the number of studies identifying SNB susceptibility genes compared to durum and spring wheat in the United States. Crook et al. (2012) studied a panel of southeastern United States winter wheat cultivars for SNB caused by winter wheat isolates, along with known S genes. Crook et al. (2012) found that very few of the cultivars contained *Snn1*, *Snn3-B1*, or *Tsn1*; however, they were still sensitive to components of culture filtrates. Another study performed in the same region with another winter wheat panel found that some cultivars contained *Tsn1* and *Snn3-B1,* but many contained unknown S genes (Bertucci et al. 2014). Recently, Cowger et al. (2020) published a perspective article discussing preliminary evidence indicating within the eastern region of the U.S., there is durable quantitative resistance to SNB and none of the previously characterized S gene-NE interactions play substantial roles in SNB disease severity within this region. These studies show that U.S. winter wheat germplasm may contain different S loci than those observed thus far in spring and durum wheat and provides an area of future research.

Additionally, the number of studies dissecting S gene-NE interactions under field conditions is lagging compared to the amount of greenhouse studies performed to date, although a few have been performed. The *Tsn1*-SnToxA, *Snn1*-SnTox1, *Snn2*-SnTox267, *Snn3-B1*-SnTox3, and likely *Snn6*-SnTox267 interactions have each been shown to be important for the development of SNB under field conditions as well as in the greenhouse (Friesen et al. 2009;

Phan et al. 2016; Ruud et al. 2017; Ruud et al. 2018; Ruud et al. 2019; Lin et al. 2021; Francki et al. 2020). These results provide evidence that results of greenhouse studies on this pathosystem are generally transferable to what is observed in the field. However, field studies provide a more accurate depiction of what is occurring in a farmer's field due to the presence of multiple isolates infecting wheat at the same time, whereas greenhouse studies usually focus on single-isolate infections. Field studies allow researchers to determine what interactions are important for causing disease from a variety of isolates in a geographic region. Additional field studies will provide breeders with the information on which S genes are most important in their region, and therefore should be considered highest priority for removal from their germplasm.

Now that more S genes and their corresponding NE genes have been cloned, future work should focus on the characterization of these interactions at the molecular level. As previously stated, only Snn1 and SnTox1 have been shown to directly interact (Shi et al. 2016), and the relationship between recognition of SnToxA and SnTox3 and the Tsn1 and Snn3 proteins, respectively, remains unknown. Once these relationships are known, further work can include identifying the genetic pathways and networks associated with the host response post pathogen recognition. Within the host, the fate of the NEs remains unknown, along with how the pathogen is able to tolerate the host defense response and how the wheat-*P. nodorum* relationship changes as disease progresses. Lastly, dominant S genes are ideal candidates for disruption via CRISPR/cas9, especially when developing elite germplasm. By "turning off" the S gene, the plant is no longer able to recognize the pathogen, PCD does not occur, and the outcome is a resistance response. To use CRISPR/cas9 on S genes, the genes must be cloned. This tool could be used to expedite the disruption of S genes from breeding lines leading to an increase in genetic resistance to SNB and therefore less disease. One caveat to eliminating S genes is they

could provide resistance to biotrophic and/or hemibiotrophic pathogens. However, to date, none of the S genes within the wheat-*P. nodorum* have been found to confer resistance to other pathogens.

Overall, there are still many aspects of the wheat-*P. nodorum* pathosystem that warrant further study. Progress over the last twenty years has shown that the interaction mimics that which occurs between plants and biotrophic pathogens; however, recognition leads to susceptibility rather than resistance due to the ability of the necrotrophs to feed and thrive on dead/dying tissue and to tolerate the plant's defense response. This finding has shed light not only on this pathosystem, but on how other crop plants and necrotrophic pathogens interact with one another.

3.9. Literature Cited

Abeysekara NS, Faris JD, Chao S, McClean PE, Friesen TL (2012) Whole-genome analysis of Stagonospora nodorum blotch resistance and validation of the SnTox4-*Snn4* interaction in hexaploid wheat. Phytopathology 102:94-104

Abeysekara NS, Friesen TL, Keller B, Faris JD (2009) Identification and characterization of a novel host-toxin interaction in the wheat-*Stagonospora nodorum* pathosystem. Theor Appl Genet 120:117-126

Adhikari TB, Jackson EW, Gurung S, Hansen JM, Bonman JM (2011) Association mapping of quantitative resistance to *Phaeosphaeria nodorum* in spring wheat landraces from the USDA National Small Grains Collection. Phytopathology 101:1301-1310

Aguilar V, Stamp P, Winzeler M, Winzeler H, Schachermayr G, Keller B, Zanetti S, Messmer MM (2005) Inheritance of field resistance to *Stagonospora nodorum* leaf and glume

blotch and correlations with other morphological traits in hexaploid wheat (*Triticum aestivum* L.). Theor Appl Genet 111:325-336

Arseniuk E, Czembor PC, Czaplicki A, Song Q, Cregan PB, Hoffman DL, Ueng PP (2004) QTL controlling partial resistance to *Stagonospora nodorum* leaf blotch in winter wheat cultivar Alba. Euphytica 137:225-231

Balance GM, Lamari L, Bernier CC (1989) Purification and characterization of a host selective toxin from *Pyrenophora tritici-repentis*. Physiol Mol Plant P 35:203-213

Balance GM, Lamari L, Kowatsch R, Bernier CC (1996) Cloning, expression and occurrence of the gene encoding the Ptr necrosis toxin from *Pyrenophora tritici-repentis*. Mol Plant Pathol http://w.bspp.org.uk/mppol/1996/1209ballance/

Ballini E, Tavaud M, Ducasse A, Sanchez D, Paux E, Kitt J, Charmet G, Audigeos D, Roumet P, David J, Morel J (2020) Genome wide association mapping for resistance to multiple fungal pathogens in a panel issued from a broad composite cross-population of tetraploid wheat *Triticum turgidum*. Euphytica 216:92

Bertucci M, Brown-Guedira G, Murphy JP, Cowger C (2014) Genes conferring sensitivity to *Stagonospora nodorum* necrotrophic effectors in Stagonospora nodorum blotch-susceptible U.S. wheat cultivars. Plant Dis 98:746-753

Breen S, Williams SJ, Winterberg B, Kobe B, Solomon PS (2016) Wheat PR-1 proteins are targeted by necrotrophic pathogen effector proteins. Plant J 88:13-25

Brueggeman R, Druka A, Nirmala J, Cavileer T, Drader T, Rostoks N, Mirlohi A, Beenypaul H, Gill U, Kudrna D, Whitelaw C, Killian A, Han F, Sun Y, Gill K, Steffenson B, Kleinhofs A (2008) The stem rust resistance gene *Rpg5* encodes a protein with nucleotide-binding-site, leucine-rich, and protein kinase domains. Proc Natl Acad Sci 105:14970-14975

Ciuffetti LM, Manning VA, Pandelova I, Betts MF, Martinez JP (2010) Host-selective toxins, Ptr ToxA and Ptr ToxB, as necrotrophic effectors in the *Pyrenophora tritici-repentis*-wheat interaction. New Phytol 187:911-919

Ciuffetti LM, Tuori RP, Gaventa JM (1997) A single gene encodes a selective toxin causal to the development of tan spot of wheat. Plant Cell 9:135-144

Chu CG, Faris JD, Xu SS, Friesen TL (2010) Genetic analysis of disease susceptibility contributed by the compatible *Tsn1*-SnToxA and *Snn1*-SnTox1 interactions in the wheat-Stagonospora nodorum pathosystem. Theor Appl Genet 120:1451-1459

Cockram J, Scuderi A, Barber T, Furuki E, Gardner KA, Gosman N, Kowalczyk R, Phan HP, Rose GA, Tan KC, Oliver RP, Mackay IJ (2015) Fine-mapping the wheat *Snn1* locus conferring sensitivity to the *Parastagonospora nodorum* necrotrophic effector SnTox1 using an eight founder multiparent advanced generation inter-cross population. G3-Genes Genom Genet 5:2257-2266

Couto D and Zipfel C (2016) Regulation of pattern recognition receptor signalling in plants. Nat Rev Immunol 16:537-552

Cowger C, Ward B, Brown-Guedira G, Brown JKM (2020) Role of effector-sensitivity gene interactions and durability of quantitative resistance to Septoria Nodorum Blotch in Eastern U.S. Wheat. Front Plant Sci doi: 10.3389/fpls.2020.00155

Crook AD, Friesen TL, Liu ZH, Ojimbo PS, Cowger C (2012) Novel necrotrophic effectors from *Stagonospora nodorum* and corresponding host sensitivities in winter wheat germplasm in the Southeastern United States. Phytopathology 102:498-505

Czembor PC, Arseniuk E, Czaplicki A, Song Q, Cregan PB, Ueng PP (2003) QTL mapping of partial resistance in winter wheat to *Stagonospora nodorum* blotch. Genome 46:546-554

Day B, Henty JL, Porter KJ, Staiger CJ (2011) The pathogen-actin connection: a platform for defense signaling in plants. Annu Rev Phytopathol 49:483-506

Dickman MB, Park YK, Oltersdorf T, Li W, Clemente T, French R (2001) Abrogation of disease development in plants expressing animals antiapoptotic genes. Proc Natl Acad Sci USA 98:6957-6962

Downie RC, Bouvet L, Furuki E, Gosman N, Gardner KA, Mackay IJ, Mantello CC, Mellers G, Phan HTT, Rose GA, Tan KC, Oliver RP, Cackram J (2018) Assessing European wheat sensitivities to *Parastagonospora nodorum* necrotrophic effectors and fine-mapping the *Snn3-B1* locus conferring sensitivity to the effector SnTox3. Front Plant Sci 9:881

Eyal Z (1987) The Septoria diseases of wheat: concepts and methods of disease management. CIMMYT, Mexico

Faris JD and Friesen TL (2009) Reevaluation of a tetraploid wheat population indicates that the *Tsn1*-ToxA interaction is the only factor governing Stagonospora nodorum blotch susceptibility. Phytopathology 99:906-912

Faris JD and Friesen TL (2020) Plant genes hijacked by necrotrophic fungal pathogens. Curr Opin Plant Biol 56:74-80

Faris JD, Anderson JA, Francl LJ, Jordahl JG (1996) Chromosomal location of a gene conditioning insensitivity in wheat to a necrosis-inducing culture filtrate from *Pyrenophora tritici-repentis*. Phytopathology 86:459-463

Faris JD, Liu Z, Xu SS (2013) Genetics of tan spot resistance in wheat. Theor Appl Genet 126:2197-2217

Faris JD, Zhang Z, Lu H, Lu Z, Reddy L, Cloutier S, Fellers JP, Meinhardt SW, Rasmussen JB, Xu SS, Oliver RP, Simons KJ, Friesen TL (2010) A unique wheat disease resistance-like

gene governs effector-triggered susceptibility to necrotrophic pathogens. Proc Natl Acad Sci 107:13544-13549

Faris JD, Zhang Z, Rasmussen JB, Friesen TL (2011) Variable expression of the *Stagonospora nodorum* effector SnToxA among isolates correlated with levels of disease in wheat. Mol Plant Microbe In 24:1419-1426

Ficke A, Cowger C, Bergstrom G, Brodal G (2018) Understanding yield loss and pathogen biology to improve disease management: Septoria nodorum blotch-a case study in wheat. Plant Dis 102:696-707

Flor HH (1955) Host-parasite interaction in flax-rust-its genetics and other implications. Phytopathology 45:680-685

Flor HH (1956) Complementary genetic systems in flax and flax rust. Advanced Genetics 8:29-54

Francki MG, Shankar M, Walker E, Loughman R, Golzar H, Ohm H (2011) New quantitative trait loci in wheat for flag leaf resistance to Stagonospora nodorum blotch. Phytopathology 101:1278-1284

Francki MG, Walker E, McMullan CJ, Morris WG (2020) Multi-location evaluation of global wheat lines reveal multiple QTL for adult plant resistance to Septoria nodorum blotch (SNB) detected in specific environments and in response to different isolates. Front Plant Sci 11:771

Friesen TL and Faris JD (2010) Characterization of the wheat-*Stagonospora nodorum* system: what is the molecular basis of this quantitative necrotrophic disease interaction? Can J Plant Pathol 32:20-28

Friesen TL and Faris JD (2021) Characterization of effector-target interactions in necrotrophic pathosystems reveals trends and variation in host manipulation. Ann Rev Phytopathol 59:77-98

Friesen TL, Chu CG, Liu ZH, Xu SS, Halley S, Faris JD (2009) Host-selective toxins produced by *Stagonospora nodorum* confer disease susceptibility in adult wheat plants under field conditions. Theor Appl Genet 118:1489-1497

Friesen TL, Chu C, Xu SS, Faris JD (2012) SnTox5-*Snn5*: a novel *Stagonospora nodorum* effector-wheat gene interaction and its relationship with the SnToxA-*Tsn1* and SnTox3-*Snn3-B1* interactions. Mol Plant Pathol 13:1101-1109

Friesen TL, Holmes DJ, Bowden RL, Faris JD (2018) *ToxA* is present in U.S. *Bipolaris sorokiniana* population and is a significant virulence factor on wheat harboring *Tsn1*. Plant Dis 102:2446

Friesen TL, Meinhardt SW, Faris JD (2007) The *Stagonospora nodorum*-wheat pathosystem involves multiple proteinaceous host-selective toxins and corresponding host sensitivity genes that interact in an inverse gene-for-gene manner. Plant J 51:681-692

Friesen TL, Stukenbrock EH, Liu Z, Meinhardt S, Ling H, Faris JD, Rasmussen JB, Solomon PS, McDonald BA, Oliver RP (2006) Emergence of a new disease as a result of interspecific virulence gene transfer. Nat Genet 38:953-956

Friesen TL, Zhang Z, Solomon PS, Oliver RP, Faris JD (2008) Characterization of the interaction of a novel *Stagonospora nodorum* host-selective toxin with a wheat susceptibility gene. Plant Physiol 146:682-693

Friskop A, Liu Z (2016) Fungal leaf spot diseases of wheat: tan spot, Septoria/Stagonospora nodorum blotch and Septoria tritici blotch. NDSU Extension Service, North Dakota State University

Gao Y, Faris JD, Liu Z, Kim YM, Syme RA, Oliver RP, Xu SS, Friesen TL (2015) Identification and characterization of the SnTox6-*Snn6* interaction in the *Parastagonospora nodorum*-wheat pathosystem. Mol Plant Microbe In 28:615-625

Ghaderi F, Sharifnabi B, Javan-Nikkhah M, Brunner PC, McDonald BA (2020) *SnToxA*, *SnTox1*, and *SnTox3* originated in *Parastagonospora nodorum* in the Fertile Crescent. Plant Path 69:1482-1491

Gurung S, Mamidi S, Bonman JM, Xiong M, Brown-Guedira G, Adhikari TB (2014) Genome-wide association study reveals novel quantitative loci associated with resistance to multiple leaf spot diseases of spring wheat. PLoS ONE 9:e108179

Haen KM, Lu HJ, Friesen TL, Faris JD (2004) Genomic targeting and high-resolution mapping of the *Tsn1* gene in wheat. Crop Sci 44:951-962

Hafez M, Gourlie R, Despins T, Turkington TK, Friesen TL, Aboukhaddour R (2020) *Parastagonospora nodorum* and related species in Western Canada: genetic variability and effector genes. Phytopath 110:1946-1958

Hane JK, Lowe RGT, Solomon PS, Tan KC, Schoch CL, Spatafora JW, Crous PW, Kodira C, Birren BW, Galagan JE, Torriani SFF, McDonald BA, Oliver RP (2007) Dothideomycete-plant interactions illuminated by genome sequencing and EST analysis of the wheat pathogen *Stagonospora nodorum*. Plant Cell 19:3347-3368

Hu W, He X, Dreisigacker S, Sansaloni CP, Juliana P, Singh PK (2019) A wheat chromosome 5AL region confers seedling resistance to both tan spot and Septoria nodorum blotch in two mapping populations. Crop J 7:809-818

International Wheat Yield Partnership (2017) Strategic Plan 2017-2022. http://iwyp.org/wp-content/uploads/sites/34/2017/10/IWYP-Strategic-Plan-Full-Version-Published.pdf Accessed 4 April 2018

Jones JDG and Dangl JL (2006) The plant immune system. Nature 444:323-329

Kariyawasam GK, Richards JK, Wyatt NA, Running K, Xu SS, Liu Z, Borowicz P, Faris JD, Friesen TL (2021) The *Parastagonospora nodorum* necrotrophic effector SnTox5 targets the wheat gene *Snn5* and facilitates entry into the leaf mesophyll. New Phytol https://doi.org/10.1111/nph.17602

Kourelis J and van der Hoom RAL (2018) Defended to the nines: 25 years of resistance gene cloning identifies nine mechanisms for R protein function. Plant Cell 30:285-299

Lin M, Corsi B, Ficke A, Tan KC, Cockram J, Lillemo M (2020) Genetic mapping using a wheat multi-founder population reveals a locus on chromosome 2A controlling resistance to both lead and glume blotch caused by the necrotrophic fungal pathogen *Parastagonospora nodorum*. Theor Appl Genet 133:785-808

Lin M, Stadlmeier M, Mohler V, Tan KC, Ficke A, Cockram J, Lillemo M (2021) Identification and cross-validation of genetic loci conferring resistance to Septoria nodorum blotch using a German multi-founder winter wheat population. Theor Appl Genet 134:125-142

Lin SY, Chooi YH, Solomon PS (2018) The global regulator of pathogenesis PnCon7 positively regulates *Tox3* effector gene expression through direct interaction in the wheat pathogen *Parastagonospora nodorum*. Mol Microbiol 109:78-90

Liu Z, El-Basyoni I, Kariyawasam G, Zhang G, Fritz A, Hansen J, Marais F, Friskop A, Chao S, Akhunov E, Baenziger PS (2015) Evaluation and association mapping of resistance to tan spot and stagonospora nodorum blotch in adapted winter wheat germplasm. Plant Dis 99:1333-1341

Liu ZH, Faris JD, Meinhardt SW, Ali S, Rasmussen JB, Friesen TL (2004b) Genetic and physical mapping of a gene conditioning sensitivity in wheat to a partially purified host-selective toxin produced by *Stagonospora nodorum*. Phytopathology 94:1056-1060

Liu Z, Faris JD, Oliver RP, Tan KC, Solomon PS, McDonald MC, McDonald BA, Nunez A, Lu S, Rasmussen JB, Friesen TL (2009) SnTox3 acts in effector triggered susceptibility to induce disease on wheat carrying the *Snn3* gene. PLoS Pathog 5:e1000581

Liu Z, Friesen TL, Ling H, Meinhardt SW, Oliver RP, Rasmussen JB, Faris JD (2006) The *Tsn1*-ToxA interaction in the wheat-*Stagonospora nodorum* pathosystem parallels that of the wheat-tan spot system. Genome 49:1265-1273

Liu ZH, Friesen TL, Rasmussen JB, Ali S, Meinhardt SW, Faris JD (2004a) Quantitative trait loci analysis and mapping of seedling resistance to Stagonospora nodorum leaf blotch in wheat. Phytopathology 94:1061-1067

Liu Z, Gao Y, Kim YM, Faris JD, Shelver WL, de Wit PJGM, Xu SS, Friesen TL (2016) SnTox1, a *Parastagonospora nodorum* necrotrophic effector, is a dual-function protein that facilitates infection while protecting from wheat-produced chitinases. New Phytol 211:1052-1064

Liu Z, Zhang Z, Faris JD, Oliver RP, Syme R, McDonald MC, McDonald BA, Solomon PS, Lu S, Shelver WL, Xu S, Friesen TL (2012) The cysteine rich necrotrophic effector SnTox1

produced by *Stagonospora nodorum* triggers susceptibility of wheat lines harboring *Snn1*. PLoS Pathog 8:e1002467

Lu H and Faris JD (2006) Macro- and microcolinearity between the genomic region of wheat chromosome 5B containing the *Tsn1* gene and the rice genome. Funct Integr Gneomic 6:90-103

Lu HJ, Fellers JP, Friesen TL, Meinhardt SW, Faris JD (2006) Genomic analysis and marker development for the *Tsn1* locus in wheat using bin-mapped ESTs and flanking BAC contigs. Theor Appl Genet 112:1132-1142

Lu Q and Lillemo M (2014) Molecular mapping of adult plant resistance to *Parastagonospora nodorum* leaf blotch in bread wheat lines 'Shanghai-3/Catbird' and 'Naxos'. Theor Appl Genet 127:2635-2644

Lu S, Faris JD, Sherwood R, Friesen TL, Edwards MC (2014) A dimeric PR-1-type pathogenesis-related protein interacts with ToxA and potentially mediates ToxA-induced necrosis in sensitive wheat. Mol Plant Pathol 15:650-663

Manning VA, Andrie RM, Trippe AF, Ciuffetti LM (2004) Ptr ToxA requires multiple motifs for complete activity. Mol Plant Microbe In 17:491-501

Manning VA and Ciufetti LM (2005) Localization of Ptr ToxA produced by *Pyrenophora tritici-repentis* reveals protein import into wheat mesophyll cells. Plant Cell 17:3203-3212

Manning VA, Chu AL, Steeves JE, Wolpert TJ, Ciufetti LM (2009) A host-selective toxin of *Pyrenophora* tritici-repentis, Ptr ToxA, induces photosystem changes and reactive oxygen species accumulation in sensitive wheat. Mol Plant Microbe In 22:665-676

Manning VA, Hardison LK, Ciufetti LM (2007) Ptr ToxA interacts with a chloroplast-localized protein. Mol Plant Microbe In 20:168-177

Marcussen T, Sandve SR, Heier L, Spannagl M, Pfeifer M, The International Wheat Genome Sequencing Consortium, Jakobsen KS, Wulff BBH, Steuernagel B, Mayer KFX, Olsen OA (2014) Ancient hybridizations among the ancestral genomes of bread wheat. Science 345:1250092

McDonald MC, Ahren D, Simpfendorfer S, Milgate A, Solomon PS (2017) The discovery of the virulence gene *ToxA* in the wheat and barley pathogen *Bipolaris sorokiniana*. Mol Plant Pathol. 19:432-439

McDonald MC, Oliver RP, Friesen TL, Brunner PC, McDonald BA (2013) Global diversity and distribution of three necrotrophic effectors in *Phaeosphaeria nodorum* and related species. New Phytol 199:241-251

Meinhardt SW, Cheng W, Kwon CY, Donohue CM, Rasmussen JB (2002) Role of the arginyl-glycyl-aspartic motif in the action of the Ptr ToxA produced by *Pyrenophora tritici-repentis.* Plant Physiol 130:1545-1551

Navathe S, Yadav PS, Chand R, Mishra VK, Vasistha NK, Meher PK, Joshi AK, Gupta PK (2020) *ToxA-Tsn1* interaction for spot blotch susceptibility in Indian wheat: an example of inverse gene-for-gene relationship. Plant Dis 104:71

Oliver RP, Friesen TL, Faris JD, Solomon PS (2012) *Stagonospora nodorum*: from pathology to genomics and host resistance. Ann Rev Phytopathol 50:23-43

Oliver RP, Lord M, Rybak K, Faris JD, Solomon PS (2008) Emergence of Tan Spot disease caused by toxigenic *Pyrenophora tritici-repentis* in Australia is not associated with increased deployment of toxin-sensitive cultures. Phytopathol doi:10.1094/PHYTO-98-5-0488

Pandelova I, Betts MF, Manning VA, Wilhelm LJ, Mockler TC, Ciuffetti LM (2009) Analysis of transcriptome changes induced by Ptr ToxA in wheat provides insights into the mechanisms of plant susceptibility. Molecular Plant 2:1067-1083

Peters Haugrud AR, Zhang Z, Richards JK, Friesen TL, Faris JD (2019) Genetics of variable disease expression conferred by inverse gene-for-gene interactions in the wheat-*Parastagonospora nodorum* pathosystem. Plant Physiology 180:420-434

Phan HTT, Furuki E, Hunziker L, Rybak K, Tan KC (2021) GWAS analysis reveals distinct pathogenicity profiles of Australian *Parastagonospora nodorum* isolates and identification of marker-trait-associations to Septoria nodorum blotch. Sci Rep-UK 11:10085

Phan HTT, Rybak K, Bertazzoni S, Furuki E, Dinglasan E, Hickey LT, Oliver RP, Tan KC (2018) Novel sources of resistance to Septoria nodorum blotch in the Vavilov wheat collection identified by genome-wide association studies. Theor Appl Genet 131:1223-1238

Phan HTT, Rybak K, Furuki E, Breen S, Solomon PS, Oliver RP, Tan KC (2016) Differential effector gene expression underpins epistasis in a plant fungal disease. Plant J 87:343-354

Paillard P, Schurbusch T, Winzeler M, Messmer M, Sourdille P, Abderhalden O, Keller B, Schachermayr G (2003) An integrative genetic linkage map of winter wheat (*Triticum aestivum* L.). Theor Appl Genet 115:313-323

Reddy L, Friesen TL, Meinhardt SW, Chao S, Faris JD (2008) Genomic analysis of the *Snn1* locus on wheat chromosome arm 1BS and the identification of candidate genes. Plant Genome 1:55-66

Richards JK, Kariyawasam G, Seneviratne S, Wyatt NA, Xu SS, Liu Z, Faris JD, Friesen TL (2021) A triple threat: the *Parastagonospora nodorum* SnTox267 effector exploits three distinct host genetic factors to cause disease in wheat. New Phytol https://doi.org/10.1111/nph.17601

Richards JK, Stukenbrock EH, Carpenter J, Liu Z, Cowger C, Faris JD, Friesen TL (2019) Local adaptation drives the diversification of effectors in the fungal wheat pathogen *Parastagonospora nodorum* in the United States. PLoS Genet 15:e1008223

Richards JK, Wyatt NA, Liu Z, Faris JD, Friesen TL (2018) Reference quality genome assemblies of three *Parastagonospora nodorum* isolates differing in virulence on wheat. G3-Genes Genom Genet 8:393-399

Ruud AK, Dieseth JA, Ficke A, Furuki E, Phan HTT, Oliver RP, Tan KC, Lillemo M (2019) Genome-wide association mapping of resistance to Septoria nodorum leaf blotch in a Nordic spring wheat collection. Plant Genome 12:180105

Ruud AK, Dieseth JA, Lillemo M (2018) Effects of three *Parastagonospora nodorum* necrotrophic effectors on spring wheat under Norwegian field conditions. Crop Sci 58:159-168

Ruud AK, Windju S, Belova T, Friesen TL, Lillemo M (2017) Mapping of SnTox3-*Snn3* as a major determinant of field susceptibility to Septoria nodorum blotch in the SHA3/CBRD × Navos population. Theor Appl Genet 130:1361-1374

Rybak K, See PT, Phan HTT, Syme RA, Moffat CS, Oliver RP, Tan KC (2017) A functionally conserved Zn_2Cys_6 binuclear cluster transcription factor class regulates necrotrophic effector gene expression and host-specific virulence of two major Pleopsporales fungal pathogens of wheat. Mol Plant Pathol 18:420-434

Ryerson DE, Heath MC (1996) Cleavage of nuclear DNA into oligonucleosomal fragments during cell death induced by fungal infection or by abiotic treatments. Plant Cell 8:393-402

Sarris PF, Cevik V, Dagdas G, Jones JDG, Krasileva KV (2016) Comparative analysis of plant immune receptor architectures uncovers host proteins likely targeted by pathogens. BMC Biol 14:8

Senevirantne SL (2019) Genomic analysis of Septoria nodorum blotch susceptibility genes *Snn1* and *Snn2* in wheat. Doctorial dissertation, North Dakota State University

Shankar M, Walker E, Golzar H, Loughman R, Wilson RE, Francki MG (2008) Quantitative trait loci for seedling and adult plant resistance to *Stagonospora nodorum* in Wheat. Phytopathology 98:886-893

Sharma S (2019) Genetics of wheat domestication and Septoria nodorum blotch susceptibility in wheat. Masters thesis, North Dakota State University

Shatalina M, Messmer M, Feuillet C, Mascher F, Paux E, Choulet F, Wicker T, Keller B (2014) High-resolution analysis of a QTL for resistance to Stagonospora nodorum glume blotch in wheat reveals presence of two distinct resistance loci in the target interval. Theor Appl Genet 127:573-586

Shi G, Friesen TL, Saini J, Xu SS, Rasmussen JB, Faris JD (2015) The wheat *Snn7* gene confers susceptibility on recognition of the *Parastagonospora nodorum* necrotrophic effector SnTox7. Plant Genome 8

Shi G, Zhang Z, Friesen TL, Bansal U, Cloutier S, Wicker T, Rasmussen JB, Faris JD (2016a) Marker development, saturation mapping, and high-resolution mapping of the Septoria

nodorum blotch susceptibility gene *Snn3-B1* in wheat. Molecular Genet Genomics 291:107-119

Shi G, Zhang Z, Friesen TL, Raats D, Fahima T, Brueggeman RS, Lu S, Trick HN, Liu Z, Chao W, Frenkel Z, Xu SS, Rasmussen JB, Faris JD (2016b) The hijacking of a receptor kinase-driven pathway by a wheat fungal pathogen leads to disease. Science Adv 2:e1600822

Singh M, Upadhyaya HD (2015) *Genetic and Genomic Resources for Grain Cereals Improvement*. Academic Press.

Singh PK, Singh S, Deng Z, He X, Kehel Z, Singh RP (2019) Characterization of QTLs for seedling resistance to Tan spot and Septoria nodorum blotch in the PBW343/Kenya Nyangumi wheat recombinant inbred lines population. Int J Mol Sci 20:5432

Singh PK, Singh RP, Duveiller E, Mergoum M, Adhiikari TB, Elias EM (2010) Genetics of wheat-*Pyrenophora tritici-repentis* interactions. Euphytica 171:1-13

Singh RP, Singh PK, Rutkoski J, Hodson DP, He X, Jørgensen LN, Hovmøller MS, Huerta-Espino J (2016) Disease impact on wheat yield potential and prospects of genetic control. Ann Rev Phytopathol 54:303-322

Solomon PS, Lee RC, Greer Wilson TJ, Oliver RP (2004) Pathogenicity of Stagonospora nodorum requires malate synthase. Mol Micro 53:1065-1073

Solomon PS, Lowe RGT, Tan K-C, Waters ODC, Oliver RP (2006) *Stagonospora nodorum*: cause of stagonospora nodorum blotch of wheat. Mol Plant Pathol 7:147-156

Stukenbrock EH, Banke S, McDonald BA (2006) Global migration patterns in the fungal wheat pathogen *Phaeosphaeria nodorum*. Mol Ecol 15:2895-2904

Sung YC, Outram MA, Breen S, Wang C, Dagvadorj B, Winterberg B, Kobe B, Williams SJ, Solomon PS (2020) PR1-mediated defence via C-terminal peptide release is targeted by a fungal pathogen effector. New Phytol 229:3467-3480

Syme RA, Hane JK, Friesen TL, Oliver RP (2013) Resequencing and comparative genomics of *Stagonospora nodorum*: sectional gene absence and effector discovery. G3-Genes Genom Genet 3:959-969

Syme RA, Tan K-C, Hane JK, Dodhia K, Stoll T, Hastie M, Furuki E, Ellwood SR, Williams AH, Tan Y-F, Testa AC, Gorman JJ, Oliver RP (2016) Comprehensive annotation of the *Parastagonospora nodorum* reference genome using next-generation genomics, transcriptomics and proteogenomics. PLoS ONE 11:e0147221

Tan KC, Waters ODC, Rybak K, Antoni E, Furuki E, Oliver RP (2014) Sensitivity to three *Parastagonospora nodorum* necrotrophic effects in current Australian wheat cultivars and the presence of further fungal effectors. Crop Pasture Sci 65:150-158

Tomás A and Bockus WW (1987) Cultivar specific toxicity of culture filtrate of *Pyrenophora tritici-repentis*. Phytopathology 77:1337-1366

Tuori RP, Wolpert TJ, and Ciuffetti LM (1995) Purification and immunological characterization of toxic components from cultures of *Pyrenophora tritici-repentis*. Mol Plant Microbe In 8:41-48

Tuori RP, Wolpert TJ, and Ciuffetti LM (2000) Heterologous expression of functional Ptr ToxA. Mol Plant Microbe In 13:456-464

van Schie CCN and Takken FLW (2014) Susceptibility genes 101: how to be a good host. Ann Rev Phytopathol 52:551-581

Vincent D, Du Fall LA, Livk A, Mathesius U, Lipscombe RJ, Oliver RP, Friesen TL, Solomon PS (2012) A functional genomics approach to dissect the mode of action of the *Stagonospora nodorum* effector protein SnToxA in wheat. Mol Plant Pathol 13:467-482

Virdi SK, Liu Z, Overlander ME, Zhang Z, Xu SS, Friesen TL, Faris JD (2016) New insights into the roles of host gene-necrotrophic effector interactions in governing susceptibility of durum wheat to tan spot and spetoria nodorum blotch. G3-Genes Genom Genet 6:4139-4150

Waters ODC, Lichtenzveig J. Rybak K, Friesen TL, Oliver RP (2011) Prevalence and importance of sensitivity to the *Stagonospora nodorum* necrotrophic effector SnTox3 in current Western Australian wheat cultivars. Crop Pasture Sci 62:556-562

Winterberg B, Du Fall LA, Song X, Pascovici D, Care N, Molloy M, Ohms S, Solomon PS (2014) The necrotrophic effector protein SnTox3 re-programs metabolism and elicits a strong defence response in susceptible wheat leaves. BMC Plant Biol 14:215

Zhang H, Francl LJ, Jordahl JG, Meinhardt SW (1997) Structural and physical properties of a necrosis-inducing toxin from *Pyrenophora tritici-repentis*. Phytopathology 87:154-160

Zhang Z, Friesen TL, Simons KJ, Xu SS, Faris JD (2009) Development, identification, and validation of markers for marker-assisted selection against the *Stagonospora nodorum* toxin sensitivity genes *Tsn1* and *Snn2* in wheat. Mol Breeding 23:35-49

Zhang Z, Friesen TL, Xu SS, Shi G, Liu Z, Rasmussen JB, Faris JD (2011) Two putatively homoeologous wheat genes mediate recognition of SnTox3 to confer effector-triggered susceptibility to *Stagnonospora nodorum*. Plant J 65:27-38

Zhang Z, Running KLD, Seneviratne S, Peters Haugrud AR, Szabo-Hever A, Shi G, Brueggeman R, Xu SS, Friesen TL, Faris JD (2021) A protein kinase-major sperm

protein gene hijacked by a necrotrophic fungal pathogen triggers disease susceptibility in wheat. Plant J doi:10.1111/tpj.15194

Zhang W, Zhu X, Zhang M, Shi G, Liu Z, Cai X (2019) Chromosome engineering-mediated introgression and molecular mapping of novel *Aegilops speltoides*-derived resistance genes for tan spot and Septoria nodorum blotch diseases in wheat. Theor Appl Genet 132:2605-2614

CHAPTER 4. GENETIC ANALYSIS OF YIELD RELATED TRAITS IN A DURUM × CULTIVATED EMMER WHEAT POPULATION UNDER FIELD AND GREENHOUSE CONDITIONS

4.1. Abstract

Wheat (*Triticum* ssp.) yields will need to increase by at least 60% by 2050 to meet the expected demands. Numerous studies have identified yield component genes in hexaploid wheat; however, fewer studies have been performed in tetraploid wheat. Additionally, no studies in tetraploid wheat have evaluated the same population for kernel dimension traits under field and greenhouse growing conditions. Here, I evaluated a tetraploid recombinant inbred line population derived from a cross between the North Dakota durum wheat variety Divide and the cultivated emmer wheat accession PI 272527, or the DP527 population. Plants were grown in the summers of 2017 and 2019 in Prosper, ND and 2020 in Casselton, ND in a randomized complete block design in hill plots under non-irrigated conditions. Additionally, the population was grown in two trials under greenhouse conditions and the same eleven traits were evaluated. QTL analysis identified 108 QTL under field conditions, 67 under greenhouse conditions, 27 QTL observed in two or more field environments, and 17 QTL that were present under greenhouse conditions and multiple field environments. PI 27527 contributed to increased days to heading, plant height, spikelets per spike, thousand kernel weight, kernel area, kernel width, kernel length, kernel circularity, and kernel length:width ratio. The findings from this study provides insights into the traits that differ between the two tetraploid wheat subspecies and are consistent between greenhouse and field conditions, along with tools breeders can use to introgress these traits into their breeding lines.

4.2. Introduction

Wheat (*Triticum* ssp.) is one of the major global food crops, supplying approximately 20% of the calories in the average human's diet. About 95% of wheat grown is hexaploid common (bread) wheat (*Triticum aestivum* L., $2n = 6x = 42$, AABBDD genomes), and tetraploid durum wheat (*T. turgidum* ssp. *durum* L., $2n = 4x = 28$, AABB genomes) accounts for about 5%. Durum wheat is grown on approximately 16 million hectares worldwide and is used to make pasta and other semolina-based products (Arriagada et al. 2020). Due to the rapidly rising global population, wheat production and yields need to increase by upwards of 50% of current production by 2050 to meet expected increased demands (IWYP 2017).

Rapid increases in wheat yields were observed in the mid to late 1900s during the green revolution (Hedden 2003). In the latter part of the 20th century, the increase in wheat yield per year due to genetic improvements was slight, with changing agronomic practices contributing more to yield gains. Genetic advancements in wheat partially lagged due to the complexity of the wheat genome and the ability of researchers to identify genes underlying wheat yield components (Brinton and Uauy 2018; Taagen et al. 2021).

Grain yield is a complex trait controlled by a multitude of genes and pathways (Cao et al. 2020). Final grain yield is determined by three main subcomponents: the number of spikes per unit area, the number of kernels per spike and grain weight/size and shape (Gegas et al. 2010; Brinton and Uauy 2018; Cao et al. 2020). Each component can be further split into numerous subcomponents, adding to the overall complexity of wheat yield, and many yield genes are present as homoeologs, which can also influence the phenotypic variation explained by one locus (Borrill et al. 2018). Additionally, the wheat genome is an allopolyploid and is comparably larger

in size than most cultivated crop genomes (IWGSC 2018), requiring a larger number of markers to adequately cover the genome.

Grain morphology has traditionally been an understudied yield component due to the difficulty in measuring this trait (Gegas et al. 2010), and the few studies that have been conducted have been in hexaploid wheat populations (Russo et al. 2014; Sun et al. 2020). Grain yield and grain size/shape components have been reported to be significantly correlated (Gegas et al. 2010; Russo et al. 2014; Sun et al. 2020; Corsi et al. 2021), therefore breeding for increased grain size may increase grain yield.

Recently, multiple reviews have been published on QTLs present in durum wheat (Colasuonno et al. 2021; Arriagada et al. 2020) along with reviews on yield component traits and pathways in tetraploid and hexaploid wheat (Nadolska-Orczyk et al. 2017; Brinton and Uauy 2018; Gauley and Boden 2018; Cao et al. 2020). However, the majority of the work done to identify mechanisms governing wheat yield components has been in hexaploid wheat (Cao et al. 2020). In durum wheat, various quality, abiotic, and biotic stress QTL studies have been published, whereas relatively few have been published on mapping yield components (Arriagada et al. 2020, Colasuonno et al. 2021).

Cultivated emmer, *T. turgidum* ssp. *dicoccum* (Schrank) Schübl ($2n = 4x = 28$, AABB), is the direct progenitor of durum wheat and is considered a minor crop globally (Zaharieva et al. 2010, Scott et al. 2019). Cultivated emmer was first domesticated in the Fertile Crescent (Faris 2014; Scott et al. 2019) from wild emmer (*T. turgidum* ssp. *dicoccoides* (Körn.) Thell ($2n = 4x = 28$, AABB) due to mutations in the *Br* loci, resulting in cultivated emmer having a non-brittle rachis, but it remained non free-threshing with hulled seed (Faris 2014). Subsequently, durum arose from cultivated emmer through the acquisition of mutations in *Q*, the major wheat

domestication gene, and the tenacious glume gene *Tg*, resulting in free-threshing plants (Faris et al. 2014).

Historically, genes from cultivated emmer have been introgressed for disease resistance, stress tolerance, and quality traits (Ellis et al. 2014; Sun et al. 2004, Guzmán et al. 2011; Mohler et al. 2013; reviewed by Zaharieva et al. 2010). A few studies have been published using bi-parental populations and mapping spike and agronomic related traits. Previously, durum × cultivated emmer populations were grown under greenhouse conditions by Faris et al. (2014) and Sharma et al. (2019), and under field conditions by Russo et al. (2014). Findings from these studies have identified QTL for yield traits with the cultivated emmer parents contributing the desired phenotype. Cultivated emmer has been shown to be a promising resource for improving durum genetic diversity.

To date, most QTL mapping studies in tetraploid wheat have been durum × durum or durum × wild emmer. Recombinant inbred line (RIL) populations with closely related parents often lack the power to detect QTL due to reduced diversity in the germplasm pool. Durum × wild emmer crosses are highly diverse and useful for identifying a larger number of QTL; however, introgressing traits from wild emmer into the durum germplasm pool is often associated with increased linkage drag of deleterious traits (Yu et al. 2019). Durum × cultivated emmer crosses are useful for not only identifying genes in both durum and cultivated emmer but cultivated emmer has been cultivated for centuries and may be a source of beneficial yield genes (Zaharieva et al. 2010).

In this study, I phenotyped a durum × cultivated emmer population derived from Divide × PI 272527, referred to as the DP527 population, under field and greenhouse conditions. My two primary objectives were 1) to identify QTLs associated with 11 yield component traits in the

DP527 population under field and greenhouse conditions and 2) determine which QTLs are stable over multiple environments and suitable for deployment in breeding programs in durum improvement.

4.3. Materials and Methods

4.3.1. Plant Material

The durum × cultivated emmer RIL population DP527 was evaluated for grain yield components under greenhouse and field conditions in North Dakota, USA. The DP527 population was developed by crossing Divide (PI 642021), a North Dakota hard amber durum variety (Elias and Manthey 2007), with PI 27527, a cultivated emmer accession collected near Pest, Hungary. The DP527 population consists of 219 RILs, which were developed using the single-seed descent method by Dr. Steven Xu, Cereal Crops Research Unit, USDA-ARS, Fargo, ND.

4.3.2. Phenotyping

The population and parental lines were evaluated under field conditions for a total of three seasons and were grown in a randomized complete block design (RCBD) with three replicates each season. Plants were grown in hill plots, with each plot consisting of 10-15 seeds and considered an experimental unit. The 2017 and 2019 plots were grown at the North Dakota State University (NDSU) field site near Prosper, ND (47.002, -97.115). The 2020 plots were grown at the NDSU agronomy seed farm in Casselton, ND (46.880, -97.243).

The DP527 population and parental lines were phenotyped for eleven traits: days to heading (DTH), plant height (PHT), total number of spikelets per spike (SPS), kernels per spike (KPS), grain weight per spike (GWS), thousand kernel weight (TKW), kernel area (KA), kernel width (KW), kernel length (KL), kernel circularity (KC), and kernel length:width ratio (KLW).

DTH was measured as the number of days from planting until 50% of the spikes were beyond the flag leaf. PHT was measured from the base of the hill plot to the tip of the highest spike (excluding awns) in the plot in centimeters. Fifteen main heads per plot were hand harvested, and eight heads were used for phenotypic evaluations. SPS was counted as the total number of spikelets per head. KPS, GWS, TKW, KA, KW, KL, KC, and KLW data was obtained using a MARVIN grain analyzer (GAT Sensorik GMBH, Neubrandenburg, Germany). KPS and GWS data from the MARVIN was divided by the number of heads in the sample to obtain an average per wheat head. For the 2019 growing season, planting occurred in late May, and by early September about one third of the lines were not mature. Therefore, for the 2019 season only DTH, PHT, and SPS were evaluated.

The DP527 population and parents were evaluated under greenhouse conditions in two greenhouse seasons (2018 and 2019) with two replicates per season. Plants were grown in 6-in pots in a greenhouse with 16-h photoperiod and a temperature of 21 °C. All plants were grown in a completely randomized design (CRD) with one plant per pot, which was one experimental unit. DTH was measured as the number of days from planting until the emergence of the first spike beyond the flag leaf, and PHT was measured from the base of the plant to the tip of the highest spike in centimeters. Plants were hand harvested and four heads per plant were used for the rest of the phenotypic evaluations, which were measured the same as the field trials.

4.3.3. Genotyping and Linkage Mapping

DNA extraction, genotyping, linkage analysis, and map construction were done by the USDA-ARS small grains genotyping lab at Fargo, ND, Megan Overlander, and Dr. Justin Faris. Briefly, DNA of the DP527 population along with the parental lines was extracted using the methods described in Sharma et al. (2019a). The DP527 population along with the parental lines

was genotyped using the iSelect 90k wheat SNP array (Wang et al. 2014). The genotyping assay was carried out using Illumina's Infinium assay following the manufacture's protocols. SNP clustering and genotyping calling were performed using Illumina's GenomeStudio software v.2011.1. The genotype callings were manually inspected to correct cluster shifts due to copy number differences and to ensure call accuracy for every SNP.

The *Q* gene functional marker *Xfcp650(Q)*, a simple sequence repeat (SSR) marker designed by Simons et al. (2006), was used to map the *Q* gene on chromosome 5A. The primer sequences for the FCP650 set are 5' GCACTAGCTAATTCAGTGGTTAGATTTGCTCA 3' and 5' ATTCAGTGGTAGCAACAGTTTCAGTAAGCTGG 3' and an annealing temperature of 65 °C was used.

Linkage maps were assembled using MapDisto 1.7.7.0.1.1 (Lorieux et al. 2012). Markers were first organized into groups using the 'find groups' command with a minimum LOD = 3.0 and a maximum theta of 0.30. The 'order' sequence command was used to establish the initial order of markers within a linkage group. Subsequent interrogation of the sequence using the 'check inversions', 'ripple order', and 'drop locus' commands was conducted to determine the best map. Map distances were calculated using the Kosambi mapping function (Kosambi 1943).

4.3.4. Statistical Analysis and QTL Mapping

Statistical analysis was performed using the PROC GLM procedure in SAS 9.4 (SAS institute). Fisher's Least Significant Difference (LSD) test was used to determine significant differences among the RILs at the 0.05 level of probability. For each season (field and greenhouse), Bartlett's Chi squared test for homogeneity of error variances (Snedecor and Cochran 1989) was used to determine if replicates within the same environment could be combined. For those traits that were not normally distributed, Levene's test (Levene 1960) was

used instead. For those that could be combined, the scores of each replicate for those traits were used to calculate the overall mean, which was used in further analyses and QTL mapping. For field data, TKW 2020 replicates were not homogeneous using both Bartlett's and Levene's, and DTH and GWS could not be combined across years in the GH; therefore, each replicate for these traits was analyzed separately. Trait mean, max, min, and correlations were calculated in R v4.0.3, with Pearson correlation coefficients calculated using the R command *cor* (R Development Core Team) and plotted using R/corrplot (Wei and Simko 2017).

QTL analysis was performed using R/qtl (Broman et al. 2003). For simple interval mapping, significant QTL were identified using the function 'scanone' with the extended Haley-Knott method (Haley and Knott 1992). An LOD significance threshold was determined using a permutation test with 1000 interactions. 'Scantwo' with the extended Haley-Knott method was used to identify QTL × QTL interactions and a LOD significance threshold was determined using a permutation test with 1000 interactions. Multiple QTL mapping was performed using the stepwiseqtl command (Manichaikul et al. 2009) using method=imp (Sen and Churchill 2001). A forward/backward search method was used, with a maximum of 12 QTL allowed. The initial model was given based on the 'scanone' QTL results. An approximate Bayesian credible interval was calculated using 'Bayesint' with a probability of 0.99 (Broman et al. 2003). QTL names include the trait abbreviation followed by "fcu", which stands for Fargo Cereals Unit.

Markers that were significantly associated with each QTL were subjected to BLASTn searches against Svevo RefSeq Rel. 1.0 pseudomolecules (Maccaferri et al. 2019), Zavitan WEWSeq v2.0 pseudomolecules (Zhu et al. 2019), and the Chinese Spring IWGSC RefSeq v2.1 genome assembly (Zhu et al. 2021) using the Graingenes website (https://wheat.pw.usda.gov/GG3/) to obtain the physical positions for comparing QTL between environments, along with

identifying previously reported genes that may reside within each QTL region. The sequence for reported genes were obtained from Genbank or the gene cloning papers.

4.4. Results

4.4.1. Map Construction

The DP527 population map was constructed using the 90K iSelect polymorphic SNP results and the SSR marker *Xfcp650(Q)* (Table 4.1). The final map consisted of 10,486 markers and was assembled into 14 linkage groups representing each of the 14 durum wheat chromosomes (Supplementary File 1). The average number of markers per chromosome was 749, with a range from 466 markers on chromosome 5A to 1,188 markers on chromosome 1B (Table 4.1). The average chromosome map length was 174.31 cM, with chromosome 6A being the shortest at 129.23 cM in length and chromosome 5A was the longest at 226.73 cM. Density ranged from 2.06 to 6.79 markers/cM among linkage groups, with a genome-wide density of 4.30 markers/cM. The B genome had a higher marker density than the A genome. A total of 3,519 (33.56%) markers had segregation ratios that significantly ($P < 0.05$) deviated from the expected 1:1 ratio. The percentage of markers with distorted segregations varied, ranging from 0.19% on chromosome 4B to 79.04% on chromosome 1B.

Table 4.1. Chromosome assignment and distribution of markers, length of chromosome linkage groups, and marker density of maps generated in the Divide × PI 272527 (DP527) recombinant inbred population.

Chromosome	SSR	SNP	Total markers	Loci	Length	Markers/cM	% distorted markers
1A	0	658	658	137	163.68	4.02	27.20
1B	0	1,188	1,188	181	166.03	7.16	79.04
2A	0	699	699	120	187.95	3.72	46.49
2B	0	1,107	1,107	220	188.00	5.89	56.37
3A	0	637	637	163	196.38	3.24	7.38
3B	0	923	923	215	169.11	5.46	17.01
4A	0	554	554	126	173.57	3.19	55.78
4B	0	523	523	118	141.72	3.69	0.19
5A	1	465	466	144	226.73	2.06	41.20
5B	0	771	771	173	192.16	4.01	9.60
6A	0	621	621	133	129.23	4.81	43.00
6B	0	964	964	170	141.94	6.79	17.22
7A	0	680	680	176	195.50	3.48	7.94
7B	0	695	695	137	168.29	4.13	26.62
A genome	1	4,314	4,315	999	1273.04	3.39	31.82
B genome	0	6,171	6,171	1,214	1167.25	5.29	34.78
Total	1	10,485	10,486	2,213	2440.29	4.30	33.56

4.4.2. Trait Evaluations Under Greenhouse Conditions

In the greenhouse, DTH and GWS were not homogeneous across years (Table 4.2), therefore, the data for each year, consisting of two replicates each, were analyzed separately. Mature spikes and seeds of Divide and PI 272527 are presented in Figure 4.1. In the 2019 greenhouse environment, the population mean, range, and the two parental lines headed ~10 days earlier than in the 2018 environment (Table 4.3, Figure 4.2a). The 2019 environment was planted in mid-October whereas the 2018 environment was planted in late September. PI 272527 headed 24.50 days later in 2018 than Divide and 30.50 days later in 2019; however, the population range was 54.50 to 95.50 days in 2018 and 39.00 to 83.00 days in 2019, indicating the two parental lines possess different genes for DTH. For PHT, a population range of 56.25 to 154.00 cm was observed, with a mean of 112.98 cm (Table 4.3, Figure 4.2b). PI 272527 had a mean PHT of 152.5 cm, indicating that it most likely contributes all the alleles for increased PHT.

For SPS, PI 272527 had a mean of 31.00 SPS, whereas Divide was 17.06 and the population range was 14.75 to 28.56 (Table 4.3, Figure 4.2c), suggesting that PI 262527 was the main contributor to increased SPS. Average KPS for the parents differed by 0.13 KPS, with Divide and PI 272527 having values of 33.38 and 33.25 (Table 4.3), respectively, and were not significantly different. However, the population mean was 30.19 and the range was 4.19 to 45.81 KPS (Table 4.3, Figure 4.2d), indicating that the two parents possess different genes for KPS, and transgressive segregation was observed.

For GWS, the two seasons were analyzed separately. In 2018, Divide had greater GWS at 2.25 g than PI 272527 at 1.78 g; however, in 2019, Divide had lower GWS at 0.71 g than PI 272527 at 1.20 g (Table 4.3). The population mean and range was also lower in 2018, at 1.00 g and 0.06 g to 1.96 g, respectively, compared to the 2019 season (Table 4.3, Figure 4.2e). For TKW, the two parental lines did not significantly differ with 40.89 g and 44.53 g for Divide and PI 272527, respectively (Table 4.3). The population mean was 43.90 g, which was not significantly different than the parental lines; however, the population range was 27.01 g to 60.46 g for TKW (Table 4.3, Figure 4.2f), suggesting the two parental lines possess different genes for kernel weight.

For kernel dimension traits, the parental lines significantly differed for KA, KL, KC, and KLW (Table 4.3). The two parental lines were not significantly different for KW, with a KW of 3.39 mm and 3.44 mm for Divide and PI 272527, respectively. However, the population mean was 2.31 mm, with a range of 1.49 mm to 3.80 mm for KW, indicating that the two parental lines differ in their genes for KW (Table 4.3, Figure 4.2h). For KA, KL, KC, and KLW, PI 272572 had a higher value for all of these than Divide, and the PI 272527 value was near the maximum value observed in the population, suggesting PI 272527 was the main contributor of genetic

factors for increased KA, KL, KC, and KLW in the DP527 population (Table 4.3, Figures 4.2g, i, j, k).

Table 4.2. Homogeneity test values for the DP527 population when grown under greenhouse environments.

Trait	Bartlett's	*P*-value	Levene's	*P*-value
DTH*	10.03	<0.05	3.64	<0.05
DTH2018	0.05	0.83	<0.05	0.87
DTH2019	<0.05	0.90	0.10	0.75
PHT	0.33	0.95	0.98	0.40
SPS	12.05	<0.05	2.05	0.11
KPS	1.37	0.71	0.17	0.92
GWS*	24.95	<0.05	5.73	<0.05
GWS2018	<0.05	0.97	<0.05	0.98
GWS2019	<0.05	0.94	0.06	0.80
TKW	3.62	0.31	1.49	0.22
KA	7.12	0.07	0.50	0.68
KW	22.46	<0.05	0.80	0.49
KL	7.50	0.06	0.50	0.68
KC	5.39	0.15	2.40	0.07
KLW	1.72	0.63	0.56	0.64

*year/trait combinations that could not be combined based on both the Bartlett's and Levene's test

Table 4.3. Parental and population means, ranges, and least significant differences (LSD) at the 0.05 level of probability (P<0.05) for the DP527 population grown under greenhouse conditions.

Trait[A]	Mean				LSD
	Divide	PI 272527	DP527 population	DP527 population range	(0.05)
DTH18[B]	62.50	87.00	70.31	54.50-95.50	9.85
DTH19[B]	52.00	82.50	59.63	39.00-83.00	14.06
PHT	87.25	152.5	112.98	56.25-154.00	27.40
SPS	17.06	31.00	22.89	14.75-28.56	4.25
KPS	33.38	33.25	30.19	4.19-45.81	12.67
GWS18[B]	2.25	1.78	1.74	0.10-2.57	0.75
GWS19[B]	0.71	1.20	1.00	0.06-1.96	0.71
TKW	40.89	44.53	43.90	27.01-60.46	11.85
KA	18.07	21.16	19.49	15.22-23.82	2.96
KW	3.39	3.44	2.31	1.49-3.80	0.31
KL	7.32	9.01	8.05	6.87-9.55	0.66
KC	1.46	1.72	1.56	1.40-1.76	0.07
KLW	2.18	2.64	2.40	2.03-2.82	0.14

[A]Trait abbreviations are: days to heading (DTH), plant height (PHT), spikelets per spike (SPS), kernels per spike (KPS), grain weight per spike (GWS), thousand kernel weight (TKW), kernel area (KA), kernel width (KW), kernel length (KL), kernel circularity (KC), and kernel length:width ratio (KLW).

[B]Replicates were not statistically homogeneous and therefore analyzed separately.

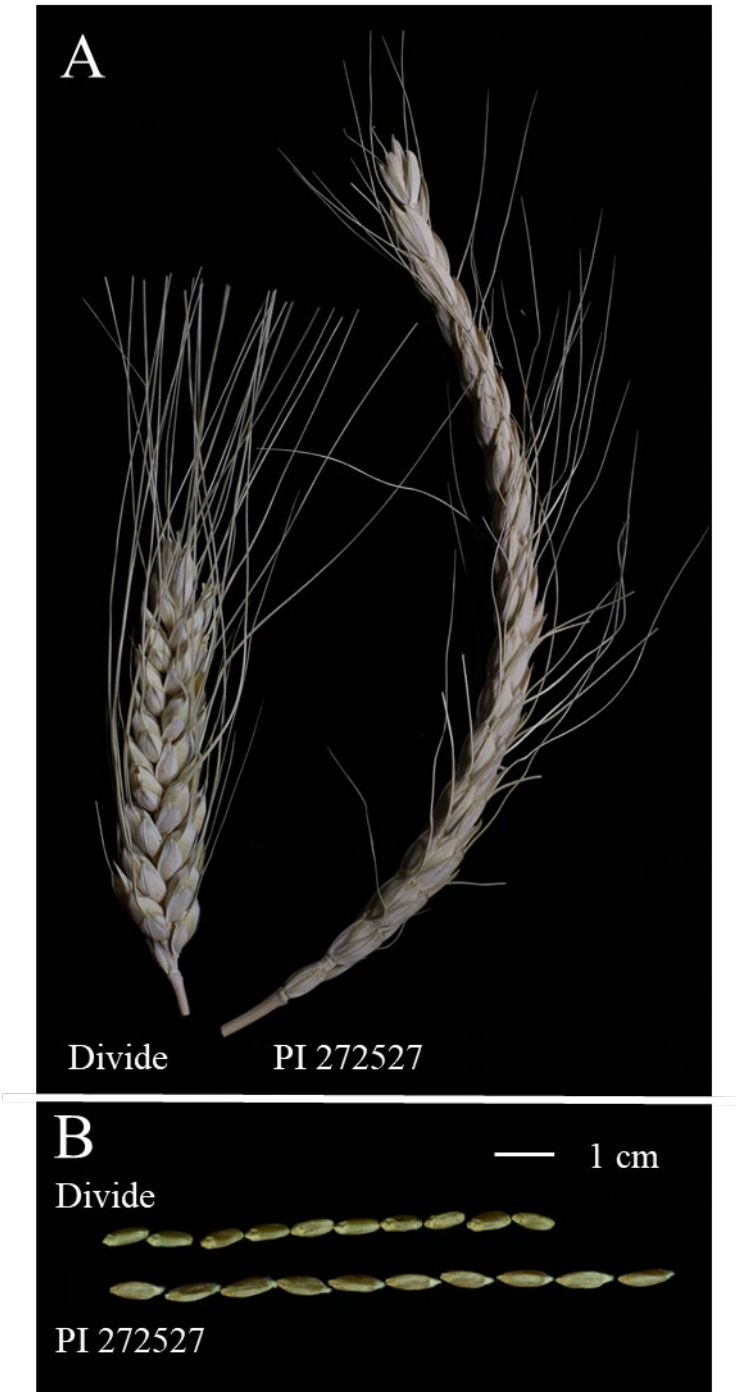

Figure 4.1. Spike and seed morphology of Divide and PI 272527, the two parental lines of the DP527 population. (a) Mature spikes of Divide (left) and PI 272527 (right). (b) seed of the durum variety Divide (top) and the cultivated emmer wheat accession PI 272527 (bottom).

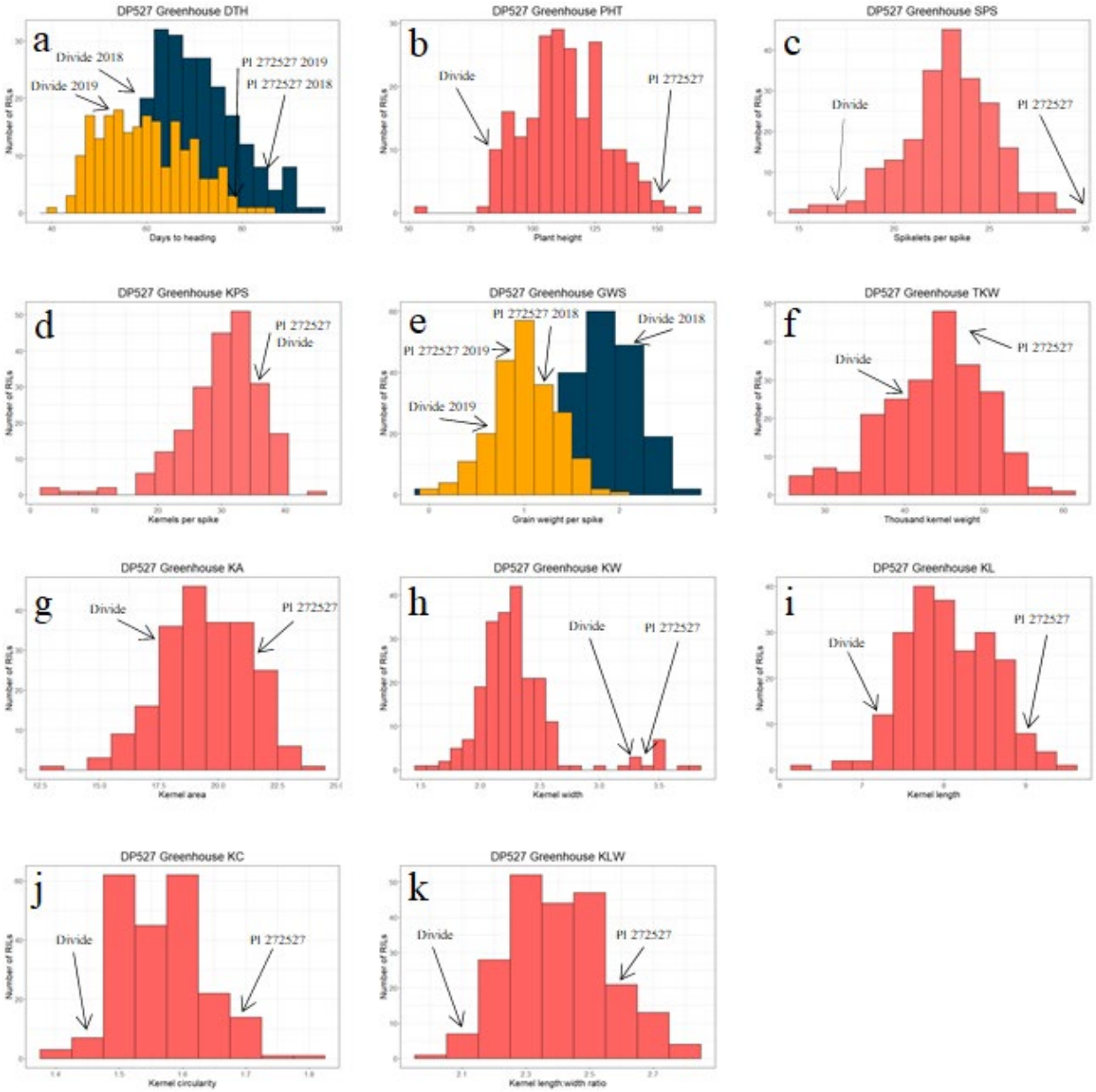

Figure 4.2. Histograms of the DP527 population under greenhouse conditions for the traits a) days to heading (DTH), b) plant height (PHT), c) spikelets per spike (SPS), d) kernels per spike (KPS), e) grain weight per spike (GWS), f) thousand kernel weight (TKW), g) kernel area (KA), h) kernel weight (KW), i) kernel length (KL), j) kernel circularity (KC), k) kernel length:width ratio (KLW). The values in pink are those replicates that were homogenous and combined across trials. For panels a and e, those in blue are from the 2018 replicate and yellow from the 2019 replicate.

4.4.3. Correlations Under Greenhouse Conditions

Correlations between all the traits under greenhouse conditions are shown in Figure 4.3, along with the correlation coefficient values given in Table 4.4. DTH had a positive correlation with SPS in environments. DTH had a negative correlation with KPS in 2018, GWS18, GWS19, TKW, KA, KW, and KL. PHT was positively correlated with SPS, KPS, GWS18, GWS19, TKW, KA, KW, and KL. SPS was positively correlated with KPS, GWS18, and GWS19, whereas KPS was positively correlated with GWS18, GWS19, TKW, and KW. Both GWS18 and GWS19 had a strong positive correlation with TKW, KA, KW, and KL, but not KC or KLW. Similar to GWS, TKW had a strong positive correlation with KA, KW, and KL, but not KC or KLW. KA was positively correlated with the other kernel dimension traits, KW, KL, KC, KLW; whereas KW other had a positive correlation with KL. KL, KC, and KLW all had a strong positive correlation with one another.

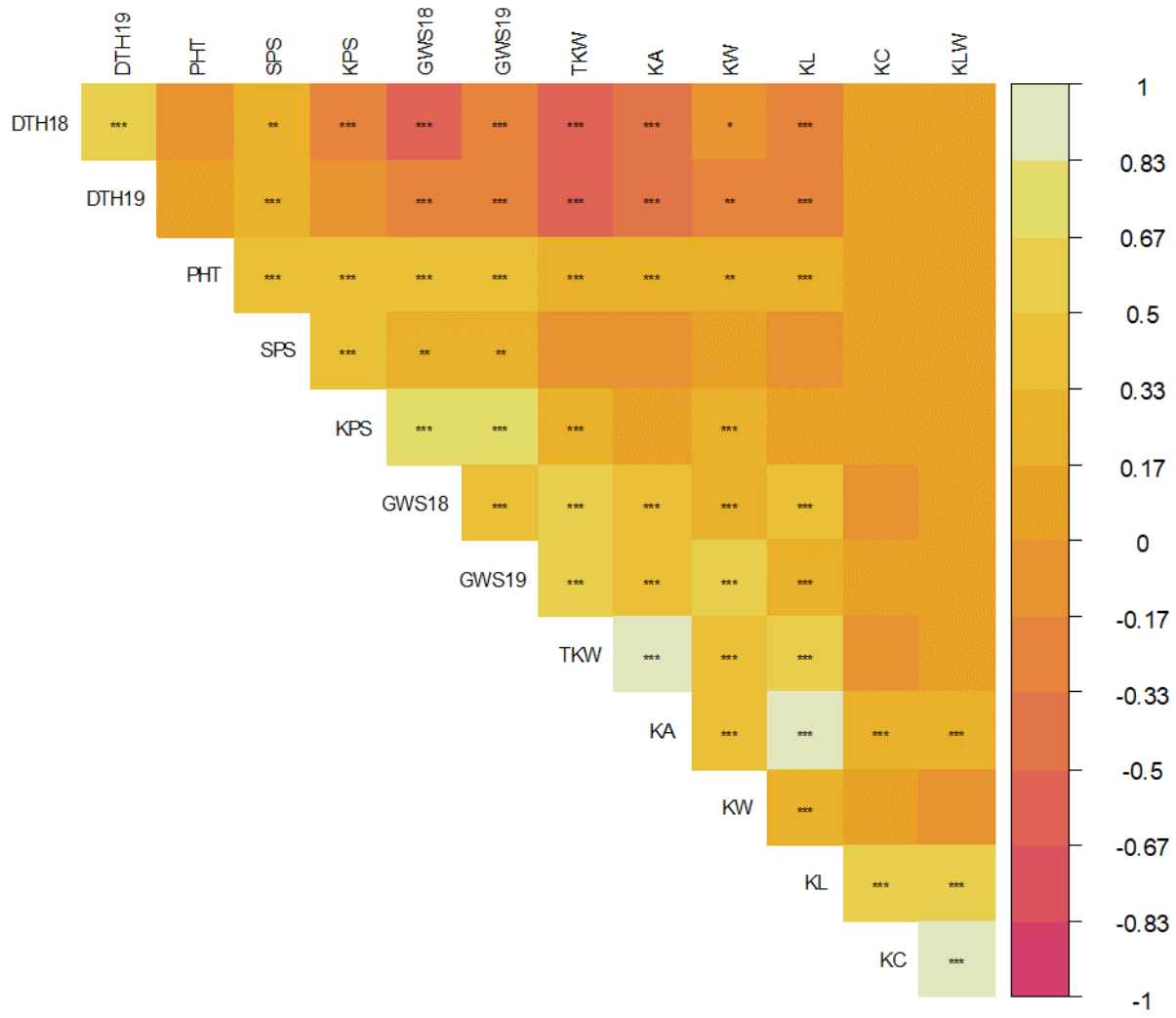

Figure 4.3. Pearson correlation coefficients between the 11 traits measured in the DP527 population grown under greenhouse conditions. Trait abbreviations are: days to heading (DTH), plant height (PHT), spikelets per spike (SPS), kernels per spike (KPS), grain weight per spike (GWS), thousand kernel weight (TKW), kernel area (KA), kernel width (KW), kernel length (KL), kernel circularity (KC), and kernel leght:width ratio (KLW). For DTH and GWS, the replicates were not statistically homogeneous and therefore were analyzed separately. Along the right is a color scale for the correlation values. Blocks that are orange to pink have a negative correlation, with dark pink being a correlation close to -1. Blocks that are orange to light yellow have a positive correlation, with light yellow being a correlation close to 1. Significance values are denoted as *P<0.05, **P<0.01, ***P<0.001.

Table 4.4. Correlation coefficients for the DP527 population grown under greenhouse conditions between the mean values of the traits days to heading (DTH), plant height (PHT), spikelets per spike (SPS), kernels per spike (KPS), grain weight per spike (GWS), thousand kernel weight (TKW), kernel area (KA), kernel width (KW), kernel length (KL), kernel circularity (KC), and kernel length:width ratio (KLW).

	DTH18[A]	DTH19[A]	PHT	SPS	KPS	GWS18[A]	GWS19[A]	TKW	KA	KW	KL	KC	KLW
DTH18[A]	1.00												
DTH19[A]	0.64***	1.00											
PHT	-0.01	0.07	1.00										
SPS	0.19**	0.24***	0.43***	1.00									
KPS	-0.25***	-0.11	0.42***	0.39***	1.00								
GWS18[A]	-0.56***	-0.32***	0.40***	0.22**	0.71***	1.00							
GWS19[A]	-0.23***	-0.31***	0.35***	0.22**	0.73***	0.43***	1.00						
TKW	-0.59***	-0.56***	0.30***	-0.02	0.26***	0.65***	0.51***	1.00					
KA	-0.45***	-0.43***	0.24***	-0.04	0.10	0.47***	0.39***	0.88***	1.00				
KW	-0.16*	-0.22**	0.19**	0.01	0.33***	0.23***	0.51***	0.42***	0.43***	1.00			
KL	-0.31***	-0.26***	0.26***	-0.02	0.11	0.36***	0.33***	0.66***	0.87***	0.33***	1.00		
KC	0.09	0.13	0.12	0.04	0.05	-0.03	0.06	-0.02	0.22***	0.01	0.65***	1.00	
KLW	0.04	0.10	0.12	0.03	0.05	0.00	0.09	0.02	0.25***	-0.04	0.67***	0.96***	1.00

*P<0.05
**P<0.01
***P<0.001
[A]Replicates were not statistically homogeneous and therefore analyzed separately.

4.4.4. Trait Evaluations Under Field Conditions

Replicates for TKW in the 2020 field experiment were not homogeneous (Table 4.5), so each replicate was evaluated separately in QTL analysis and correlations, but the overall mean of the three replicates was used for population mean and range (Table 4.6). For DTH, PI 272527 had a mean of 69.67 and 71.33 days in 2017 and 2019, respectively, which was close to the population maximum in those years (Table 4.6, Figure 4.4a). In 2019, PI 272527 headed at 94.50 days, which was greater than the population maximum of 91.00, suggesting that PI 272527 was the main genetic contributor of increased DTH. Additionally, PI 272527 was taller than Divide in all three environments and was the same as the population maximum in 2020 with a PHT of 138.00 cm (Table 4.6, Figure 4.4b), suggesting that PI 272527 was also the main genetic contributor for increased plant height.

Transgressive segregation was observed for SPS (Table 4.6, Figure 4.4c), with some individuals having fewer SPS than Divide and others having greater than PI 272527. Divide and PI 272527 had average SPS values of 17.67 and 24.47 over the three years, respectively. The DP527 population had a range of 13.50 in 2017 to 27.29 in 2020, with a mean of 20.86 across the three years, suggesting that both parents contributed some genetic factors for increased SPS. Interestingly, although PI 272527 had a greater number of SPS than Divide, Divide had an average of 39.88 KPS across the two years whereas PI 272527 had 29.10 KPS. This suggests that Divide had more fertile florets per spike than PI 272527. The DP527 population range was 15.92 to 52.75 KPS and 15.67 to 43.54 KPS in 2017 and 2020, respectively (Table 4.6, Figure 4.4d), suggesting that both Divide and PI 272527 contain genes that contribute to increased KPS, but the genes differ between the two lines.

As for GWS and TKW, although PI 272527 had fewer KPS, it had greater GWS than Divide in 2017 and higher TKW in both years (Table 4.6). For both GWS and TKW, transgressive segregation was observed, with the population maximum being higher than the average of either parents (Table 4.6, Figures 4.4e, f), suggesting that for GWS and TKW, the two parental lines harbor different genes that confer increases in these traits.

Typically, cultivated emmer has longer but more narrow kernels than durum. I observed that PI 272527 had a significantly higher value for KA, KW, KC, and KL traits measured across the two years than Divide (Table 4.6). For KA, Divide averaged 18.10 mm^2 whereas PI 272527 averaged 21.95 mm^2. The population mean was between the two parental lines at 20.53 mm^2, and the population range both years had a minimum and maximum below and above the two parental lines (Table 4.6, Figure 4.4g), indicating both parents contributed genetic factors towards increased KA. Although the two parental lines were not significantly different for KW in 2020, they were in 2017 with Divide having a KW of 3.24 mm and PI 272527 of 3.48 mm (Table 4.6). As with KA, the population had a population mean that was between the two parental lines in both environments, and the population range in 2020 was 2.85 to 3.76 mm (Table 4.6, Figure 4h), indicating both parents contributed genetic factors towards increased KW. For the other kernel dimension traits (KL, KC, KLW), the population mean was between the two parental lines in each environment, along with the population range falling lower than Divide and greater than PI 272527 for KL, KC, KLW (Table 4.6, Figures 4.4i, j, k), indicating that both parents contributed genetic factors governing these traits.

Table 4.5. Bartlett Chi-Square values for the DP527 population when grown under field environments.

Trait	Year	Bartlett's	*P*-value	Levene's[A]	*P*-value
SPS	2017	3.74	0.15		
KPS	2017	4.93	0.09		
GWS	2017	5.56	0.06		
TKW	2017	4.57	0.10		
DTH	2017	4.77	0.09		
PHT	2017	0.53	0.77		
KA	2017	0.90	0.64		
KW	2017	1.19	0.55		
KL	2017	0.12	0.94		
KC	2017	0.44	0.80		
KLW	2017	0.65	0.72		
SPS	2019	0.49	0.78		
DTH	2019	0.79	0.67		
PHT	2019	3.30	0.19		
SPS	2020	11.58	<0.05	0.71	0.49
KPS	2020	1.99	0.37		
GWS	2020	1.00	0.61		
TKW*	2020	15.76	<0.05	4.01	<0.05
DTH	2020	11.64	<0.05	2.88	0.06
PHT	2020	1.71	0.43		
KA	2020	1.76	0.41		
KW	2020	1.79	0.41		
KL	2020	1.61	0.45		
KC	2020	0.31	0.86		
KLW	2020	0.45	0.80		

*year/trait combinations that could not be combined based on both the Bartlett's and Levene's test

[A]Those which could not be combined were tested using Levene's, with those values shown for those traits.

Table 4.6. Parental and population means, ranges, and least significant differences (LSD) at the 0.05 level of probability (P<0.05) for the DP527 population grown under field conditions.

Trait[A]	Year[B]	Mean			DP527 population	LSD
		Divide	PI 272527	DP527 population	range	(0.05)
DTH	2017	57.00	69.67	62.56	55.33-71.67	3.38
DTH	2019	63.33	94.50	65.98	49.33-91.00	6.86
DTH	2020	53.00	71.33	57.09	47.33-75.00	4.33
PHT	2017	90.67	129.00	110.36	73.33-150.33	7.41
PHT	2019	119.33	144.00	122.32	88.00-157.33	14.83
PHT	2020	82.00	138.00	105.88	70.00-138.00	11.23
SPS	2017	15.38	24.04	19.04	13.50-25.83	2.63
SPS	2019	18.92	24.13	21.31	16.71-25.63	2.02
SPS	2020	18.71	25.23	22.22	17.25-27.29	2.09
KPS	2017	40.67	34.63	33.44	15.92-52.75	6.01
KPS	2020	39.08	23.56	31.02	15.67-43.54	5.95
GWS	2017	1.77	2.00	1.70	0.73-2.49	0.32
GWS	2020	1.36	1.02	1.20	0.58-1.83	0.34
TKW	2017	45.31	59.72	51.12	40.23-70.36	5.87
TKW	2020	34.82	43.52	38.39	13.28-53.47	7.60
KA	2017	18.65	24.06	21.94	18.30-25.40	1.16
KA	2020	17.54	19.83	19.11	15.65-22.70	1.59
KW	2017	3.24	3.48	3.45	3.00-3.80	0.12
KW	2020	3.17	3.26	3.23	2.85-3.76	0.17
KL	2017	7.82	9.82	8.79	7.70-9.90	0.22
KL	2020	7.61	8.66	8.27	7.36-9.44	0.33
KC	2017	1.54	1.75	1.61	1.50-1.80	0.05
KC	2020	1.57	1.70	1.65	1.45-1.85	0.06
KLW	2017	2.43	2.83	2.57	2.20-3.00	0.08
KLW	2020	2.42	2.67	2.58	2.10-3.04	0.10

[A]Trait abbreviations are: days to heading (DTH), plant height (PHT), spikelets per spike (SPS), kernels per spike (KPS), grain weight per spike (GWS), thousand kernel weight (TKW), kernel area (KA), kernel width (KW), kernel length (KL), kernel circularity (KC), and kernel length:width ratio (KLW).

[B]Each field environment was analyzed separately.

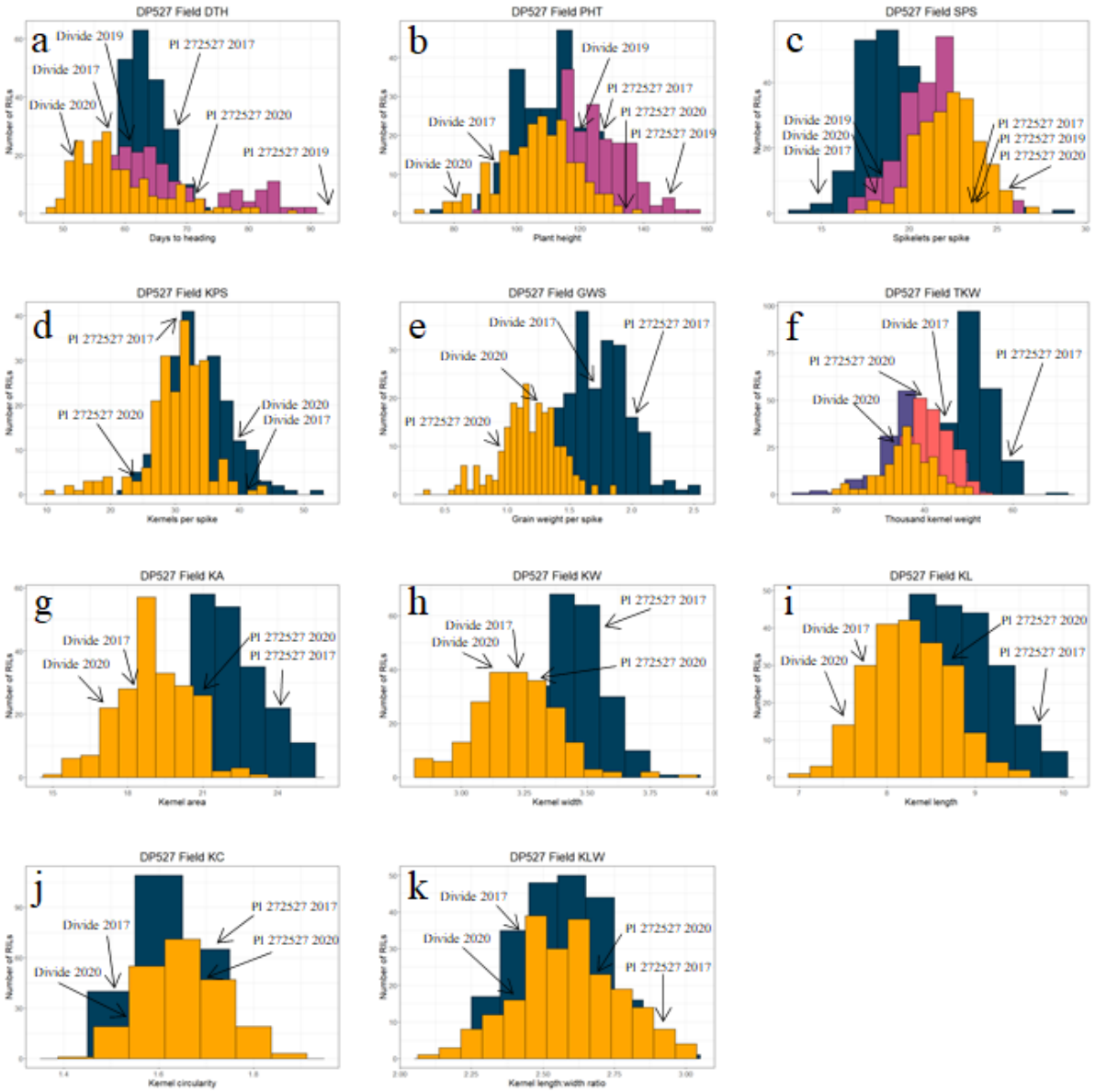

Figure 4.4. Histograms of the DP527 population under field conditions for the traits a) days to heading (DTH), b) plant height (PHT), c) spikelets per spike (SPS), d) kernels per spike (KPS), e) grain weight per spike (GWS), f) thousand kernel weight (TKW), g) kernel area (KA), h) kernel weight (KW), i) kernel length (KL), j) kernel circularity (KC), k) kernel length:width ratio (KLW). The values in blue are from the 2017 environment, pink from 2019, and yellow from 2020. For panel d, dark blue was 2017 and purple, coral, and yellow were 2020 replicates.

4.4.5. Correlations Under Field Conditions

Correlations between all the traits under field conditions are shown in Figure 4.5, along with the correlation coefficient values given in Tables 4.7, 4.8, and 4.9. For each trait, there was

a strong, significant positive correlation across environments within each trait. The general trend was that when correlations were significant, they tended to be in the positive direction. Traits that had strong, negative correlations were KW with KC and KLW, and DTH with KPS, GWS, and TKW; which were trends observed in both 2017 and 2020 (Tables 4.7, 4.9, Figure 4.5). In 2017, KPS had a strong positive correlation (near one) with GWS. Additional traits that had strong positive correlations near one in 2017 were TKW and KA, KA with KL, and KLW with KL and KC.

In 2019, only three traits were measured. SPS had a significant positive correlation with DTH and PHT, whereas DTH and PHT were negatively correlated (Table 4.8, Figure 4.5). In 2020, traits that had a strong positive correlation were KPS with GWS, GWS with TKW, TKW with KA and KW, KA with KW and KL, and KL with KC and KLW (Table 4.9, Figure 4.5). The kernel weight traits GWS and TKW were significantly correlated with the kernel dimension traits KA, KW, and KL in 2017 and 2020, along with TKW being correlated with KC and KLW in 2017 and 2020 (Tables 4.7, 4.9, Figure 4.5). Interestingly, in 2017 all the kernel dimension traits were significantly correlated; however, in 2020, KA was not correlated with KC and KLW, and KW and KL were not correlated.

Table 4.7. Correlation coefficients for the DP527 population grown under field conditions in 2017 between the mean values of the traits days to heading (DTH), plant height (PHT), spikelets per spike (SPS), kernels per spike (KPS), grain weight per spike (GWS), thousand kernel weight (TKW), kernel area (KA), kernel width (KW), kernel length (KL), kernel circularity (KC), and kernel length:width ratio (KLW).

	SPSavg	KPSavg	GWSavg	TKWavg	DTHavg	PHTavg	KAavg	KWavg	KLavg	KCavg	KLWavg
SPSavg	1.00										
KPSavg	0.46***	1.00									
GWSavg	0.46***	0.85***	1.00								
TKWavg	0.07	-0.11	0.43***	1.00							
DTHavg	0.51***	0.28***	0.18**	-0.17*	1.00						
PHTavg	0.36***	0.13	0.31***	0.37***	0.24***	1.00					
KAavg	0.08	-0.16*	0.34***	0.88***	-0.09	0.32***	1.00				
KWavg	-0.01	-0.12	0.24***	0.66***	-0.04	0.29***	0.61***	1.00			
KLavg	0.17*	-0.12	0.27***	0.67***	-0.05	0.27***	0.86***	0.19**	1.00		
KCavg	0.19**	-0.08	0.06	0.21**	-0.01	0.12	0.42***	-0.28***	0.77***	1.00	
KLWavg	0.16*	-0.05	0.09	0.21**	-0.02	0.03	0.42***	-0.40***	0.79***	0.87***	1.00

*P<0.05
**P<0.01
***P<0.001

Table 4.8. Correlation coefficients for the DP527 population grown under field conditions in 2019 between the mean values of the traits days to heading (DTH), plant height (PHT), and spikelets per spike (SPS).

	SPSavg	DTHavg	PHTavg
SPSavg	1.00		
DTHavg	0.17*	1.00	
PHTavg	0.18**	-0.21**	1.00

*P<0.05
**P<0.01
***P<0.001

Table 4.9. Correlation coefficients for the DP527 population grown under field conditions in 2020 between the mean values of the traits days to heading (DTH), plant height (PHT), spikelets per spike (SPS), kernels per spike (KPS), grain weight per spike (GWS), thousand kernel weight (TKW), kernel area (KA), kernel width (KW), kernel length (KL), kernel circularity (KC), and kernel length:width ratio (KLW).

	SPSavg	KPSavg	GWSavg	TKWrep1[A]	TKWrep2[A]	TKWrep3[A]	DTHavg	PHTavg	KAavg	KWavg	KLavg	KCavg	KLWavg
SPSavg	1.00												
KPSavg	0.30***	1.00											
GWSavg	0.14*	0.73***	1.00										
TKWrep1[A]	-0.08	0.08	0.59***	1.00									
TKWrep2[A]	-0.09	0.13	0.61***	0.55***	1.00								
TKWrep3[A]	-0.11	0.12	0.62***	0.56***	0.59***	1.00							
DTHavg	0.14*	-0.37***	-0.40***	-0.47***	-0.36***	-0.36***	1.00						
PHTavg	0.37***	0.18**	0.29***	0.12	0.19**	0.20**	0.21**	1.00					
KAavg	-0.19**	-0.14*	0.40***	0.66***	0.67***	0.71***	-0.25***	0.11	1.00				
KWavg	-0.12	-0.06	0.39***	0.60***	0.54***	0.64***	-0.14*	0.14*	0.72***	1.00			
KLavg	-0.11	-0.10	0.22**	0.37***	0.43***	0.41***	-0.20**	0.09	0.75***	0.12	1.00		
KCavg	0.02	-0.06	-0.19**	-0.24***	-0.13	-0.22**	0.04	-0.01	0.07	-0.56***	0.70***	1.00	
KLWavg	0.00	-0.05	-0.13	-0.15*	-0.07	-0.13	-0.04	-0.03	0.07	-0.62***	0.70***	0.96***	1.00

*P<0.05
**P<0.01
***P<0.001
[A]For TKW, replicates were not statistically homogeneous and therefore were analyzed separately.

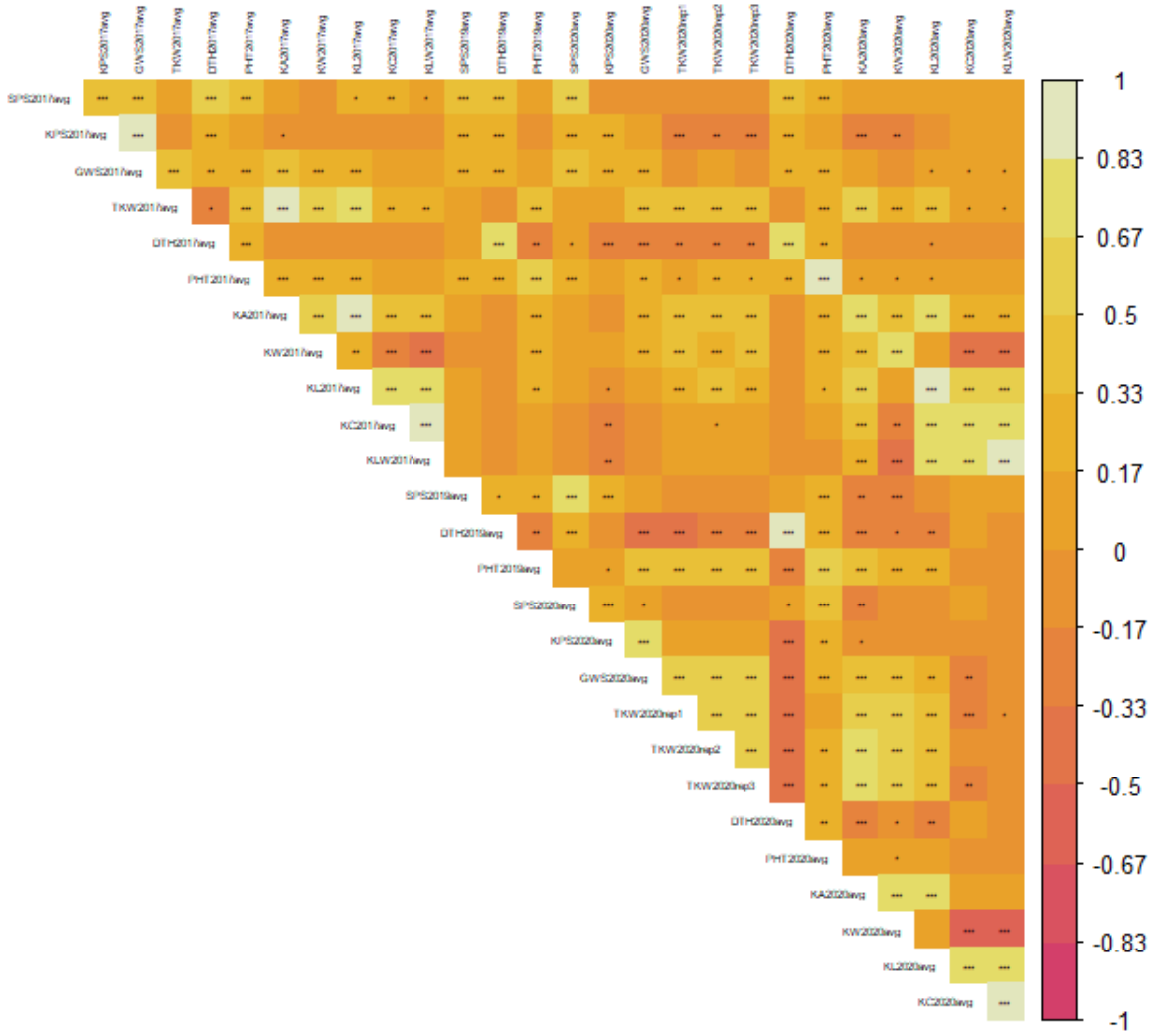

Figure 4.5. Pearson correlation coefficients between the 11 traits measured in the DP527 population grown under field conditions in 2017, 2019, and 2020. Trait abbreviations are: days to heading (DTH), plant height (PHT), spikelets per spike (SPS), kernels per spike (KPS), grain weight per spike (GWS), thousand kernel weight (TKW), kernel area (KA), kernel width (KW), kernel length (KL), kernel circularity (KC), and kernel leght:width ratio (KLW). For TKW 2020 the replicates were not combines because they were not statistically homogeneous. For 2019, only the traits SPS, DTH and PHT were evaluated. Along the right is a color scale for the correlation values. Blocks that are orange to pink have a negative correlation, with dark pink being a correlation close to -1. Blocks that are orange to light yellow have a positive correlation, with light yellow being a correlation close to 1. Significance values are denoted as *P<0.05, **P<0.01, ***P<0.001.

4.4.6. QTL Analysis Under Greenhouse and Field Conditions

In the greenhouse experiments, I identified 67 significant QTL and QTL×QTL interactions using forward/backward selection to identify the QTL model with the highest LOD

score. DTH and GWS were not homogeneous between 2018 and 2019 (Table 4.2) and were therefore analyzed separately. The 67 QTL and their statistics are presented in Supplementary File 2. The main purpose of this study was to identify QTL that were consistent between both greenhouse and field environments. Therefore, the greenhouse QTL discussed in this section were present under both greenhouse and field environments (Table 4.10, Figure 4.6). Of the 67 QTL identified under greenhouse conditions, 17 were also identified under two or more field environments.

Among the three field seasons for the DP527 population, I identified 108 significant QTL and QTL×QTL interactions using forward/backward selection to identify the QTL model with the highest LOD score. Within individual field seasons, 54, 10, and 44 QTL were identified in 2017, 2019, and 2020, respectively (Supplementary File 2). Fewer QTL were observed in the 2019 field season due to only measuring SPS, DTH, and PHT.

A total of 24 QTL were observed to be present in two field environments, and three were observed in all three field environments (Table 4.11, Figure 4.6, Supplementary File 2). A total of 11 genomic regions were associated with the 27 QTL that were observed in multiple field environments. Of these 27 QTL, 17 were for kernel dimension traits. No QTL for KPS and GWS were observed under multiple environments, therefore these traits will not be discussed below. Additionally, no QTL × QTL interactions were observed across multiple environments and therefore will not be discussed.

Only one QTL for SPS was observed in multiple field seasons. *QSpn.fcu-7B*, which mapped on chromosome 7B, was also observed under greenhouse conditions (Tables 4.10, 4.11, Figure 4.6). *QSpn.fcu-7B* is within the *FT-1* region. The maximum LOD was 14.20 and 5.19, and *QSpn.fcu-7B* explained up to 19.58 and 9.34% of the variation in SPS under greenhouse and field

conditions, respectively. PI 272527 was the donor of the increased effects in SPS at *QSpn.fcu-7B*.

For TKW, three stable QTL were identified under field conditions. These QTL, designated *QTkw.fcu-3A*, *QTkw.fcu-6A*, and *QTkw.fcu-7B* mapped on chromosomes 3A, 6A, and 7B (Tables 4.10, 4.11, Figure 4.6). *QTkw.fcu-7B* was also associated with TKW under greenhouse conditions, but not *QTkw.fcu-3A* and *QTkw.fcu-6A. QTkw.fcu-6A* is within the *GRF4* region and *QTkw.fcu-7B* mapped near *FT-1*. *QTkw.fcu-3A* and *QTkw.fcu-6A* had maximum LOD values of 7.33 and 4.73 and explained as much as 13.49 and 7.75% of the variation in TKW, respectively. *QTkw.fcu-7B* had a maximum LOD of 6.29 and 3.92 and explained up to 11.45 and 7.30% of the variation in TKW under field and greenhouse conditions, respectively. PI 272527 contributed the alleles for increased effects at *QTkw.fcu-3A* and *QTkw.fcu-6A* and Divide was the donor parent at *QTkw.fcu-7B*.

As with SPS and TKW, a QTL within the *FT-1* region on chromosome 7B was associated with DTH (Tables 4.10, 4.11, Figure 4.6). This QTL, designated *QEet.fcu-7B*, was present under three field environments and the greenhouse environment and had a maximum LOD value of 34.93 and 20.65 and explained up to 49.64 and 27.37% of the variation in DTH, respectively. PI 272527 was the donor of increased effects at *QEet.fcu-7B*.

A total of five stable QTL were identified to be associated with PHT in the DP527 population. These QTL, designated *QHt.fcu-3A.1*, *QHt.fcu-3A.2*, *QHt.fcu-5A.1*, *QHt.fcu-5A.2*, and *QHt.fcu-7B* were mapped to chromosomes 3A, 5A, and 7B (Table 4.11, Figure 4.6). Three of these QTL, *QHt.fcu-3A.1*, *QHt.fcu-3A.2*, and *QHt.fcu-5A.2* were also observed under greenhouse conditions (Table 4.10, Figure 4.6). *QHt.fcu-3A.1* and *QHt.fcu-5A*.2 were observed in three field environments, whereas the others in only two environments. *QHt.fcu-5A.2* and

QHt.fcu-7B are near the known genes *Q* and *FT-1*. Under field conditions, *QHt.fcu-3A.1*, *QHt.fcu-3A.2*, *QHt.fcu-5A.1*, *QHt.fcu-5A.2*, and *QHt.fcu-7B* had maximum LOD values of 23.43, 6.14, 7.36, 11.25, and 7.73 and explained up to 26.09, 4.85, 5.90, 10.68, and 6.22% of the variation in PHT, respectively. As for those QTL under greenhouse conditions, *QHt.fcu-3A.1*, *QHt.fcu-3A.2*, and *QHt.fcu-5A.2* had maximum LOD values of 20.25, 6.69, and 22.53 and explained up to 22.20, 6.31, and 25.36% of the variation in PHT, respectively. PI 272527 was the donor of the increased effects at each QTL.

Three QTL were identified for KA in two or more environments. These QTL were mapped to chromosomes 3A, 3B, and 6A and designated *QKa.fcu-3A*, *QKa.fcu-3B*, and *QKa.fcu-6A* (Table 4.11, Figure 4.6). *QKa.fcu-6A* was also observed under greenhouse conditions and had a maximum LOD of 5.23 and explained 8.42% of the variation in KA (Table 4.10, Figure 4.6). Under field conditions, *QKa.fcu-3A*, *QKa.fcu-3B*, and *QKa.fcu-6A* had maximum LOD values of 8.44, 4.58, and 11.88 and explained up to 10.33, 6.08, and 15.10% of the variation in KA, respectively. Divide contributed the increased effects at *QKa.fcu-3B* whereas PI 272527 was the donor parent for increased effects at *QKa.fcu-3A* and *QKa.fcu-6A*.

For KW, four stable QTL were identified on chromosomes 2A, 3A, 3B, and 6A (Table 4.11, Figure 4.6). None of these four QTL were observed under greenhouse conditions. These QTL, designated *QKw.fcu-2A*, *QKw.fcu-3A*, *QKw.fcu-3B*, and *QKw.fcu-6A* had maximum LOD values of 6.11, 4.12, 11.86, and 6.44 and explained up to 8.52, 5.61, 14.58, and 9.01% of the variation in KW, respectively. PI 272526 contributed to increased effects at all four QTL.

Five stable QTL were identified for KL, with all five also being observed under greenhouse conditions (Tables 4.10, 4.11, Figure 4.6). Under greenhouse conditions, these QTL, designated *QKl.fcu-1B*, *QKl.fcu-2A.2*, *QKl.fcu-2B*, *QKl.fcu-3A.1*, and *QKl.fcu-6A* had maximum

LOD values of 5.02, 10.86, 12.47, 4.99, and 7.51 and explained 4.37, 10.06, 11.76, 4.34, and 6.70% of the variation in KL, respectively (Table 4.10). Under field conditions, these QTL were *QKl.fcu-1B*, *QKl.fcu-2A*, *QKl.fcu-2B*, *QKl.fcu-3A*, and *QKl.fcu-6A* and had maximum LOD values of 9.58, 5.58, 12.42, 7.27, and 11.41 and explained up to 10.21, 5.76, 13.65, 8.64, and 12.40% of the variation in KL, respectively (Table 4.11). At all five QTL, PI 272527 was the contributor of increased effects.

As with KL, all the stable QTL for KC identified under field conditions were also present under greenhouse conditions (Tables 4.10, 4.11, Figure 4.6). These two QTL are designated *QKc.fcu-1B* and *QKc.fcu-2B* under field conditions (Table 4.11) and *QKc.fcu-1B* and *QKc.fcu-2B.1* under greenhouse conditions (Table 4.10). *QKc.fcu-1B* had a maximum LOD value of 10.17 and 10.20 and explained up to 16.93 and 10.55% of the variation in KL under field and greenhouse conditions, respectively. *QKc.fcu-2B* and *QKc.fcu-2B.1* had maximum LOD values of 10.11 and 7.16 and explained up to 11.93 and 7.16% of the variation in KL, respectively. All these QTL had PI 272527 as the donor of the positive alleles.

The three QTL that were observed across multiple environments for KLW were also identified under greenhouse conditions (Tables 4.10, 4.11, Figure 4.6). These QTL were mapped to chromosomes 1B, 2A, and 2B. Under field conditions, they are *QKlw.fcu-1B*, *QKlw.fcu-2A*, and *QKlw.fcu-2B* and under greenhouse conditions they are *QKlw.fcu-1B*, *QKlw.fcu-2A.1*, and *QKlw.fcu-2B.1*. Under field conditions, *QKlw.fcu-1B*, *QKlw.fcu-2A*, and *QKlw.fcu-2B* had maximum LOD values of 10.36, 11.45, and 9.56 and explained as much as 13.48, 14.15, and 11.58% of the variation in KLW, respectively. As for greenhouse QTL, *QKlw.fcu-1B*, *QKlw.fcu-2A.1*, and *QKlw.fcu-2B.1* had LOD values of 10.47, 13.79, and 7.24 and explained 13.20, 18.03,

and 8.81% of the variation in KLW, respectively. Divide contributed the increased effects at *QKlw.fcu-2A* and *QKlw.fcu-2A.1*, whereas PI 272527 was the donor parents at the other QTL.

Table 4.10. Quantitative trait loci associated with the traits evaluated in the Divide × PI 272527 (DP527) recombinant inbred population grown under greenhouse conditions and were present in two or more environments in the field.

Trait	QTL	Chromosome	Position (cM)	Peak marker	LOD	$R^2 \times 100$	Donor parent	Putative gene
SPS	*QSpn.fcu-7B*	7B	10.58	IWB3164	14.20	19.58	PI 272527	*FT-1*
TKW	*QTkw.fcu-7B*	7B	12.49	*IWB11170*	3.92	7.30	Divide	*FT-1*
DTH	*QEet.fcu-7B*	7B	10.58-12.49	*IWB3164-IWB11170*	15.25-20.65	23.08-27.37	PI 272527	*FT-1*
PHT	*QHt.fcu-3A.1*	3A	89.85	*IWB65564*	20.25	22.20	PI 272527	
PHT	*QHt.fcu-3A.2*	3A	151.61	*IWB16621*	6.69	6.31	PI 272527	
PHT	*QHt.fcu-5A.2*	5A	180.22	*Xfcp650*	22.53	25.36	PI 272527	*Q*
KA	*QKa.fcu-6A*	6A	70.25	*IWB8079*	5.23	8.42	PI 272527	
KL	*QKl.fcu-1B*	1B	30.78	*IWB27824*	5.02	4.37	PI 272527	
KL	*QKl.fcu-2A.2*	2A	114.04	IWB72154	10.86	10.06	PI 272527	
KL	*QKl.fcu-2B*	2B	45.91	*IWB2317*	12.47	11.76	PI 272527	
KL	*QKl.fcu-3A.1*	3A	87.98	*IWB74967*	4.99	4.34	PI 272527	
KL	*QKl.fcu-6A*	6A	74.06	*IWB7281*	7.51	6.70	PI 272527	
KC	*QKc.fcu-1B*	1B	32.87	*IWB7813*	10.20	10.55	PI 272527	
KC	*QKc.fcu-2B.1*	2B	48.25	*IWB8355*	7.16	7.16	PI 272527	
KLW	*QKlw.fcu-1B*	1B	31.48	*IWB60559*	10.47	13.20	PI 272527	
KLW	*QKlw.fcu-2A.1*	2A	87.16	*IWB62849*	13.79	18.03	Divide	
KLW	*QKlw.fcu-2B.1*	2B	48.25	*IWB8355*	7.24	8.81	PI 272527	

Table 4.11. Quantitative trait loci associated with the traits evaluated in the Divide × PI 272527 (DP527) recombinant inbred population grown under field conditions and were present in two or more environments.

Trait	QTL	Chromosome	Position (cM)	Peak marker	LOD	$R^2 \times 100$	Donor parent	Putative gene
SPS	*QSpn.fcu-7B*	7B	10.58	*IWB3164*	4.62-5.19	8.37-9.34	PI 272527	*FT-1*
TKW	*QTkw.fcu-3A*	3A	78.66-87.98	*IWB49380-IWB74967*	4.35-7.33	7.51-13.49	PI 272527	
TKW	*QTkw.fcu-6A*	6A	67.10-72.65	*IWB30925-IWB9600*	3.52-4.73	7.24-7.75	PI 272527	*GRF4*
TKW	*QTkw.fcu-7B*	7B	4.89-12.49	*IWB70086-IWB11170*	4.39-6.29	7.58-11.45	Divide	*FT-1*
DTH	*QEet.fcu-7B*	7B	10.58	*IWB3164*	21.32-34.93	23.79-49.64	PI 272527	*FT-1*
PHT	*QHt.fcu-3A.1*	3A	89.39-89.85	*IWB2704-IWB65564*	10.30-23.43	18.30-26.09	PI 272527	
PHT	*QHt.fcu-3A.2*	3A	142.50-145.68	*IWB64845-IWB41859*	3.71-6.14	3.38-4.85	PI 272527	
PHT	*QHt.fcu-5A.1*	5A	76.49-82.04	*IWB66908-IWB6959*	4.76-7.36	4.39-5.90	PI 272527	
PHT	*QHt.fcu-5A.2*	5A	180.22	*Xfcp650*	5.04-11.25	8.44-10.68	PI 272527	*Q*
PHT	*QHt.fcu-7B*	7B	10.58	*IWB3164*	3.68-7.73	3.36-6.22	PI 272527	*FT-1*
KA	*QKa.fcu-3A*	3A	87.98-89.39	*IWB74967-IWB2704*	7.24-8.44	9.91-10.33	PI 272527	
KA	*QKa.fcu-3B*	3B	62.78-63.95	*IWB76128-IWB13416*	4.24-4.58	4.95-6.08	Divide	
KA	*QKa.fcu-6A*	6A	67.34-68.06	*IWB33567-IWB81565*	7.51-11.88	10.30-15.10	PI 272527	
KW	*QKw.fcu-2A*	2A	87.16	*IWB62849*	3.81-6.11	4.29-8.52	PI 272527	
KW	*QKw.fcu-3A*	3A	8.43-9.13	*IWB63094-IWB46311*	3.66-4.12	4.11-5.61	PI 272527	
KW	*QKw.fcu-3B*	3B	62.78	*IWB76128*	9.62-11.86	13.92-14.58	PI 272527	
KW	*QKw.fcu-6A*	6A	65.45	*IWB66345*	5.68-6.44	6.52-9.01	PI 272527	
KL	*QKl.fcu-1B*	1B	23.44-25.36	*IWB72705-IWB21571*	6.03-9.58	7.72-10.21	PI 272527	
KL	*QKl.fcu-2A*	2A	105.86-114.04	*IWB35671-IWB72154*	4.54-5.58	4.57-5.76	PI 272527	
KL	*QKl.fcu-2B*	2B	47.09-48.02	*IWB77048-IWB76653*	7.39-12.42	9.59-13.65	PI 272527	
KL	*QKl.fcu-3A*	3A	80.73-87.98	*IWB38468-IWB74967*	6.70-7.27	7.55-8.64	PI 272527	
KL	*QKl.fcu-6A*	6A	73.83-76.68	*IWB6286-IWB78960*	5.61-11.41	7.15-12.40	PI 272527	
KC	*QKc.fcu-1B*	1B	25.36-28.44	*IWB21571-IWB16228*	8.22-10.17	9.50-16.93	PI 272527	
KC	*QKc.fcu-2B*	2B	47.55	*IWB70916*	5.02-10.11	7.90-11.93	PI 272527	
KLW	*QKlw.fcu-1B*	1B	25.36-31.48	*IWB21571-IWB60559*	7.81-10.36	9.27-13.48	PI 272527	
KLW	*QKlw.fcu-2A*	2A	87.16	*IWB62849*	7.24-11.45	9.09-14.15	Divide	
KLW	*QKlw.fcu-2B*	2B	47.09-48.02	*IWB77048-IWB76653*	7.88-9.56	9.98-11.58	PI 272527	

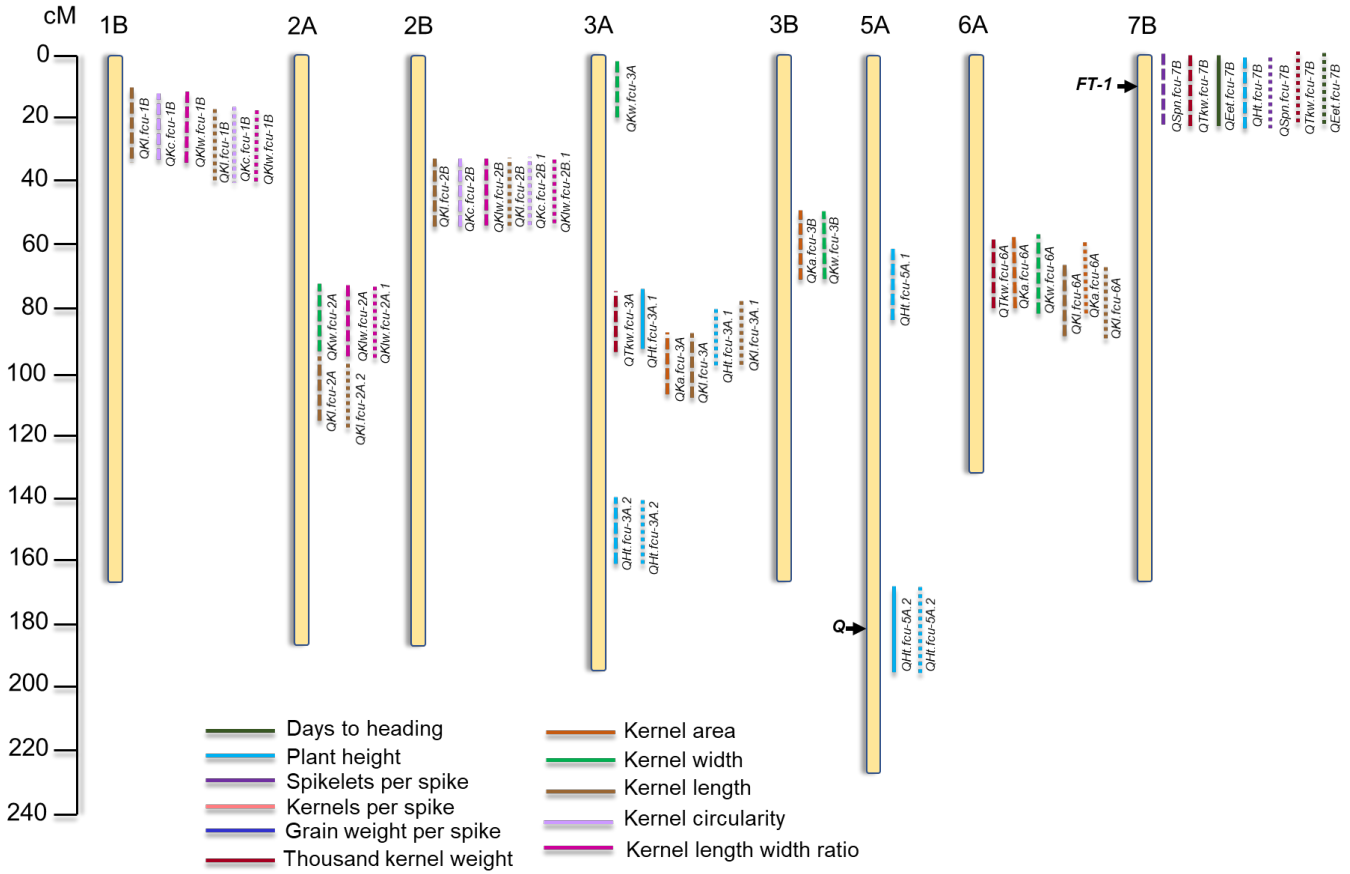

Figure 4.6. Illustration of the chromosomal locations of the quantitative trait loci (QTL) associated with the eleven traits evaluated in the Divide × PI 272527 (DP527) recombinant inbred line population under field and greenhouse conditions. Under field conditions, only those QTL which were present in two or more are shown and for those identified under greenhouse conditions, only those which were also present in the field are illustrated. A total of 27 QTL are shown which were identified under field conditions. Those observed in two environments are illustrated with dashed lines and those in three with solid lines. A total of 17 QTL associated with greenhouse conditions are illustrated with dotted lines. The known positions of the *Q* and *FT-1* loci are indicated in black. Chromosomes 1A, 4A, 4B, 5B, 6B, and 7A are not shown because not stable QTL were detected on them in this research.

4.5. Discussion

4.5.1. Trade-offs Between Yield Component Traits

In this study, I analyzed the correlations between all the traits measured. The correlations given between yield components and PHT and DTH may be of interest in breeding and the selection process; however, our interest lie with how the different yield components measured were correlated and trade-offs between them.

Increased SPS was positively correlated with the number of KPS and GWS. Plants that have more spikelets have increased capacity to produce more kernels, which influences the grain weight per spike (Gauley and Boden 2018). However, the number of kernels per spike is often negatively correlated with kernel weight and size due to limitations in nutrient availability and trade-offs in the size-shape relationship (Sandras 2007; Mangini et al. 2018). Surprisingly, KPS had a significant positive correlation with TKW and KW under greenhouse conditions, but not under field conditions. The reasoning behind this may be due to increased water and nutrient availability for plants under greenhouse conditions compared to the field, therefore, the competition for resources wasn't as intense as under field conditions.

Generally, studies to evaluate different yield component interactions in wheat have shown negative correlations between the number of kernels per spike and kernel size/weight (Li and Yang 2017; Brinton and Uauy 2018; Corsi et al. 2021). In this study, KA was the only kernel dimension trait that was negatively associated with KPS under the field environments. KPS had a correlation value near zero for the other kernel dimension traits. These findings were interesting because increasing kernel size in this population does not lead to a significant reduction in the number of KPS, indicating that the genes that control these pathways may be beneficial for breeders who are interested in increasing the number of KPS without significantly reducing

kernel size or vice versa. Additional trials under varying environmental conditions are needed to determine if this lack of a negative correlation is due to environmental factors or has high heritability, and the utility of this population for breeding programs.

As expected, GWS and TKW were positively correlated with KA, KW, and KL, i.e., increased kernel size, in all environments. However, KC and KLW were only correlated with increased TKW in the 2017 field environment and there was a negative correlation between KC and KLW in the 2020 field season. These findings are similar to those by Corsi et al. (2021), with KA, KW, and KL being positively associated with kernel weight, whereas KLW is not a significant indicator of increased kernel weight. Sun et al. (2020) found using a durum panel of 150 lines that TKW was significantly correlated with KA, KW, KL, and KC, but not KLW, indicating our results are consistent with those of previous studies. Using KA, KW, and KL may be useful for breeders when selecting lines for increased kernel weight, especially in situations in which kernel weight is difficult to accurately measure.

Interestingly, when comparing trade-offs between the kernel dimension traits, the results varied depending on the environment. Increases in KW and KL consistently resulted in increased KA and therefore larger kernels. These findings were identical to those of Corsi et al. (2021) and Sun et al. (2020). Under field conditions, both studies also observed KW to be negatively correlated with KLW, and KL to be positively correlated with KLW. These same results were observed in two other durum × cultivated emmer populations, BP025 and RP883 (Chapter 5). KL must have a larger influence on the KLW ratio than KW. Additionally, Gegas et al. (2010) found that kernel shape and size are independent traits and most likely under the influence of different pathways and genes. KL and KLW, along with KC, are often described as kernel shape traits, whereas KA and KW are kernel size traits. The results seen in this study are consistent

with those of Gegas et al. (2010) and further support their hypothesis. Further research elucidating the interaction between the different kernel size components and how they interact to determine kernel size is needed at the molecular and physiological level to untangle these relationships.

4.5.2. QTL Associated with Multiple Traits in Multiple Environments

4.5.2.1. Chromosome 1B

I identified a multi-trait QTL on the short arm of chromosome 1B involved in the control of multiple kernel dimension traits under greenhouse and field conditions. Within this region, QTL for KL, KC, and KLW were identified. Interestingly, no stable QTL for KW was observed although a significant KLW QTL was present. However, there was a QTL at this location for KW in 2020, indicating that KL, KC, KLW may be less influenced by environmental factors then KW. Few studies have been published on kernel dimension traits in tetraploid wheat. Russo et al. (2014) identified QTL near this physical region for multiple kernel dimension traits in a durum × tetraploid wheat population. To my knowledge, there have been no other QTL reported in this region in either durum or hexaploid wheat. Li et al. (2018) reported a QTL for KPS near this region in hexaploid wheat. PI 272527 may be a source of increasing KL, KC, and KLW in durum wheat if breeders are interested in changing kernel shape.

4.5.2.2. Chromosome 2A

A region on chromosome 2A from 87.16 cM to 114.04 cM harbored three QTL. A QTL for KW was observed under field conditions, and QTL for KLW and KL were observed under both greenhouse and field conditions. Corsi et al. (2021) also identified QTL for KL, KW, and KLW within this region in a European hexaploid MAGIC population. To my knowledge, no other studies have identified kernel size QTL within this region. QTL for KPS and TKW have

been identified near this region (McCartney et al. 2005; Würschum et al. 2018), which are often associated with kernel size. Although the underlying gene(s) within this region for these traits remains unknown, an increase in kernel size is due to cell size and rate of grain filling (Brinton and Uauy 2018). Also, located less than 100 Mb from the peak markers is *GNI1-A1*, which is a gene associated with kernel weight and size (Sakuma et al. 2019). In this study, I observed that PI 272527 alleles resulted in an increase in KW, whereas at the same peak marker, Divide alleles resulted in increased KLW. It remains unclear if there is a trade-off occurring at this locus, and if so, the mechanism behind it.

4.5.2.3. Chromosome 2B

A multi-trait QTL was identified on chromosome 2B to be associated with KL, KC, and KLW under greenhouse and field conditions. The increased effects at this locus were contributed by PI 272527 for each trait, indicating that PI 272527 alleles within this region may be useful for breeding for increased kernel size. To my knowledge, no QTL for grain kernel traits have been identified within this region. Russo et al. (2014) and Corsi et al. (2021) identified QTL for kernel size on chromosome 2B, but not within the same region. The gene *Ppd-B1*, which is part of the photoperiod regulatory flowering pathway (Beales et al. 2007; Nishida et al. 2013) is located within 20 Mb of the peak markers and could potentially be a candidate gene for these QTL. My peak markers may have shifted due to environmental effects and/or my QTL analysis method. Further studies under diverse environments or additional GH replicates would be required to determine if this is the case or an uncharacterized gene for KL, KC, and KLW is within this region.

4.5.2.4. Chromosome 3A

A region spanning 40.52 Mb on chromosome 3A was associated with QTL for TKW, PHT, KA, and KL. QTL near this region for yield component traits have been identified by Blanco et al. (2012), Russo et al. (2014), and Son et al. (2020). Within two other durum × cultivated emmer populations, I have observed QTL for PHT and TKW at the same locus Chapter 5). The physiological relationship between these two traits remains unclear. Often, either TKW or PHT is associated with DTH; however, I did not observe a DTH QTL in this region under field or greenhouse conditions. Previously, it was shown that increased kernel size is correlated with increased kernel weight (Brinton and Uauy 2018). Depending on the magnitude of the height increase that having PI 272527 alleles within this region confers, if it is slight this region may be useful for introgressing into current durum breeding programs who are looking to increase kernel size and weight.

4.5.2.5. Chromosome 3B

A multi-trait QTL was identified on chromosome 3B to be associated with KA and KW. Russo et al. (2014) identified QTL on chromosome 3B that were near this region and Li et al. (2018) identified a QTL for TKW within this physical region. The gene *TaCKX2* is within 35 Mb of our peak marker (Supplementary File 2). *TaCKX2* plays a role in the regulation of cytokinin and has been previously been shown to influence yield related traits (Zhang et al. 2012; Jablonski et al. 2021). Although introgressing this QTL may increase kernel size, one caveat is that Divide alleles within this region resulted in increased KA whereas PI 272527 alleles resulted in wider kernels. Because no kernel weight QTL was associated with this region under both greenhouse and field conditions, this QTL region may not be of interest to breeders.

4.5.2.6. Chromosome 6A

QTL for TKW, KA, KW, and KL co-located on the long arm of chromosome 6A. The presence of the TKW QTL at this locus is mostly likely due to increased kernel size having a pleiotropic effect and influencing kernel weight (Gegas et al. 2010; Brinton and Uauy 2018). Within this QTL region is the previously identified gene *TtGRF4* (Anvi et al. 2018). *TtGRF4* is an ortholog of *OsGRF*4 from rice, which encodes the transcription factor GROWTH-REGULATING FACTOR, and is negatively regulated by OsmiR396 (Sun et al. 2016; Duan et al. 2016). Duan et al. (2016) found in rice that *OsGRF4* is involved in chromatin-remodeling in rice panicles, with mutations in the miR396 cleavage location having larger and longer hulls and grains (Duan et al. 2016; Sun et al. 2016). Studies are still needed to determine the relationship between *TtGRF4* and increased TKW, however, it can be hypothesized that the most likely scenario is that mutations in *TtGRF4* result in decreased binding of a transcription factor resulting in longer and wider kernels, aka larger kernels, which lead to an increased in grain weight. Interestingly, PI 272527 was the donor parent of the positive allele at this QTL, indicating that potentially the allele of *TtGRF4* is not present or is an alternative allele in North Dakota durum germplasm. Breeding this QTL into local germplasm may prove beneficial to breeders for increasing kernel weight.

4.5.2.7. Chromosome 7B

A multi-trait QTL was identified on the distal end of the short arm of chromosome 7B. QTL for SPS, TKW, DTH, and PHT co-segregated at this locus, with the wheat gene *FT1* physically located within this region. *FT1* was cloned by Yan et al. (2006) and is involved in flowering time regulation and the transition from vegetative to reproductive growth (reviewed by Gauley and Boden 2018). Dixon et al. (2018) found that the different alleles of *FT1* perform

different under varying environmental conditions, and *FT1* plays a role in promoting inflorescence development. Interestingly, QTL associated with PHT and TKW have not been reported at the *FT1* locus. Potentially, because *FT1* is part of the regulation of the vegetative to reproductive growth transition, an earlier transition to reproductive growth may result in shorter plants. Additionally, the donor parent of increased TKW at this locus was Divide, whereas the other QTL had PI 272527 as the positive parent. Potentially, the Divide *FT1* allele may result in reduced number of SPS, which may result in fewer kernels but increased grain weight. Further investigation is needed to determine the molecular and physiological mechanisms behind these relationships and if *FT1* is indeed the gene underlying these QTL. If this is the case, although selecting for the PI 272527 allele at *FT1* would result in increased number of SPS, it may lead to an increase in DTH and PHT, which are not desirable traits in most situations. Therefore, the PI 272527 allele at *FT1* would not be a strong candidate to introgress into most breeding programs.

4.5.3. Beneficial Traits from PI 272527

Genes transferred from cultivated emmer into the durum germplasm pool have traditionally been related to disease and stress tolerance (reviewed in Zaharieva et al. 2010, Sharma et al. 2019b). Here, I identified nine robust multi-trait QTL, for which many had the agronomically desired phenotype contributed by PI 272527. As discussed above, some of these may be resources for improving yield component traits in durum wheat. PI 272527 had a greater number of SPS, TKW, and grain size compared to the durum parent, Divide. In 2020, Divide was grown on 20% of the acres in North Dakota (https://www.ag.ndsu.edu/publications/crops/north-dakota-durum-wheat-variety-trial-results-for-2020-and-selection-guide) and is considered to have a high test weight. Therefore, because PI 272527 had a higher TKW in this study than

Divide, it may be useful for improvement of durum varieties in the USA and potentially other regions of the world.

4.5.4. Future Directions/Conclusion

Previously, the vast majority of yield component studies in wheat have been under greenhouse or field conditions. In this study, I evaluated the DP527 population under both field and greenhouse conditions for the same 11 traits. My results illustrate that many of the QTL identified in two or more environments were also observed under greenhouse conditions. Therefore, these QTL can be considered robust and stable, and the genes underlying these QTL are ideal candidates for implementing into durum breeding programs. Recently, it has been shown that in winter wheat that using SNP associated with large effect or stable QTL as fixed effects may improve genomic selection models (Lozada et al. 2019; Sarinelli et al. 2019). Therefore, QTL identified in this study, along with their associated markers, may provide useful tools for improving yield in durum breeding programs to increase grain yield and change kernel morphological traits to meet consumer demands.

4.6. Literature Cited

Arriagada O, Marcotuli I, Gadaleta A, Schwember AR (2020) Molecular mapping and genomics of grain yield in durum wheat: a review. Int J Mol Sci 21:7021

Avni R, Oren L, Shabtay G, Assili S, Pozniak C, Hale I, Ben-David R, Peleg Z, Distelfeld A (2018) Genome based meta-QTL analysis of grain weight in tetraploid wheat identifies rare alleles of *GRF4* associated with larger grains. Genes 9:636

Beales J, Turner A, Griffiths S, Snape JW, Laurie DA (2007) A *Pseudo-Response Regulator* is misexpressed in the photoperiod insensitive *Ppd-D1a* mutant of wheat (*Triticum aestivum* L.). Theor Apple Genet 115:721-733

Blanco A, ManginiG, Giancaspro A, Giove S, Colasuonno P, Simeone R, Signorile A, De Vita P, Mastrangelo AM, Cattivelli L, Gadaleta A (2012) Relationships between grain protein content and grain yield components through quantitative trait locus analyses in a recombinant inbred line population derived from two elite durum wheat cultivars. Mol Breeding 30:79-92

Borrill P, Harrington SA, Uauy C (2018) Applying the latest advances in genomics and phenomics for trait discovery in polyploid wheat. Plant J 97:56-72

Brinton J and Uauy C (2018) A reductionist approach to dissecting grain weight and yield in wheat. J Integr Plant Biol 61:337-358

Broman KW, Wu H, Sen S, Churchill GA (2003) R/qtl: QTL mapping in experimental crosses. Bioinformatics 19:889-890

Cao S, Xu D, Hanif M, Xia X, He Z (2020) Genetic architecture underpinning yield component traits in wheat. Theor Appl Genet 133:1811-1823

Cavanagh CR, Chao S, Wang S, Huang BE, Stephen S, Kiani S, Forrest K, Saintenac C, Brown-Guedira GL, Akhunova A, See D, Bai G, et al. (2013) Genome-wide comparative diversity uncovers multiple targets of selection for improvement in hexaploid wheat landraces and cultivars. Proc Natl Acad Sci 110:8057-8062

Colasuonno P, Marcotuli I, Gadaleta A, Soriano JM (2021) From genetic maps to QTL cloning: an overview for durum wheat. Plants 10:315

Corsi B, Obinu L, Zanella CM, Cutrupi S, Day R, Geyer M, Lillemo M, Lin M, Mazza L, Percival-Alwyn L, Stadlmeier M, Mohler V, Hartl L, Cockram J (2021) Identification of eight QTL controlling multiple yield components in a German multi-parental wheat

population, including *Rht24, WAPO-A1, WAPO-B1* and genetic loci on chromosome 5A and 6A. Theor Apple Genet 134:1435-1454

Dixon LE, Farré A, Finnegan EJ, Orford S, Griffiths S, Boden SA (2018) Developmental responses of bread wheat to changes in ambient temperature following deletion of a locus that includes *FLOWERING LOCUS T1*. Plant Cell Environ 41:1715-1725

Duan P, Ni S, Wang J, Zhang B, Xu R, Wang Y, Chen H, Zhu X, Li Y (2016) Regulation of *OsGRF4* by OsmiR396 controls grain size and yield in rice. Nat Plants 2:15203

Elias EM and Manthey FA (2007) Registration of 'Divide' durum wheat. J Plant Regist 1:7-8

Ellis JG, Lagudah ES, Spielmeyer W, Dodds PN (2014) The past, present and future of breeding rust resistant wheat. Front Plant Sci https://doi.org/10.3389/fpls.2014.00641

Faris JD, Zhang Q, Chao S, Zhang Z, Xu SS (2014) Analysis of agronomic and domestication traits in a durum × cultivated emmer wheat populations using a high-density single nucleotide polymorphism-based linkage map. Theor Appl Genet 127:2333-2348

Farré A, Sayers L, Leverington-Waite M, Goram R, Orford S, Wingen L, Mumford C, Griffiths S (2016) Application of a library of near isogenic lines to understand context dependent expression of QTL for grain yield and adaptive traits in bread wheat. BMC Plant Biol 16:161

Gauley A and Boden SA (2018) Genetic pathways controlling inflorescence architecture and development in wheat and barley. J Integr Plant Biol 61:296-309

Gegas VC, Nazari A, Griffiths S, Simmonds J, Fish L, Orford S, Sayers L, Doonan JH, Snape JW (2010) A genetic framework for grain size and shape variation in wheat. Plant Cell 22:1046-1056

Golan G, Ayalon I, Perry A, Zimran G, Ade-Ajayi T, Mosquna A, Distelfeld A, Peleg Z (2019) *GNI-A1* meditates trade-off between grain number and grain weight in tetraploid wheat. Theor Appl Genet 132:2353-2365

Guzmán C, Caballero L, Alvarez JB (2011) Molecular characterization of the *Wx-B1* allelic variants identified in cultivated emmer wheat and comparison with those of durum wheat. Mol Breeding 28:403-411

Haley CS and Knott SA (1992) A simple regression method for mapping quantitative trait loci in line crosses using flanking markers. Heredity 69:315-324

Hedden P (2003) The genes of the green revolution. Trends in Genetics 19:5-9

International Wheat Genome Sequencing Consortium (2018) Shifting the limits in wheat research and breeding using a fully annotated reference genome. Science 361:6403

Jablonski B, Szala K, Przyborowski M, Bajguz A, Chmur M, Gasparis S, Orczyk W, Nadolska-Orczyk A (2021) *TaCKX2.2* genes coordinate expression of other *TaCKX* family members, regulate phytohormone content and yield-related traits of wheat. Int J Mol Sci 22:4142

Kosambi DD (1944) The estimation of map distances from recombination values. Ann Eugen 12:172-175

Levene H (1960) Robust tests for equality of variances. In: Olkin I, Hotelling H et al (eds) Contributions to probability and statistics: essays in honor of harold hoteling. Stanford University Press, Stanford, CA, pp 278-292

Li F, Wen W, He Z, Liu J, Jin H, Cao S, Geng H, Yan J, Zhang P, Wan Y, Xia X (2018) Genome-wide linkage mapping of yield-related traits in three Chinese bread wheat populations using high-density SNP markers. Theor Appl Genet 131:1903-1924

Lorieux M (2012) MapDisto: fast and efficient computation of genetic linkage maps. Mol Breeding 30:1231-1235

Lozada D, Mason RE, Sarinelli JM, Brown-Guedira G (2019) Accuracy of genomic selection for grain yield and agronomic traits in soft red winter wheat. BMC Genet 20:82

Maccaferri M, Harris NS, Twardziok SO, Pasam RK, Gundlach H, Spannagl M, Ormanbekova D, Lux T, Prade VM, Milner SG, et al. (2019) Durum wheat genome highlights past domestication signatures and future improvement targets. Nat Genet 51:885-895

Manichaikul A, Moon JY, Sen Ś, Yandell BS, Broman KW (2009) A model selection approach for the identification of quantitative trait loci in experimental crosses, allowing epistasis. Genetics 181:1077-1086

McCartney CA, Somers DJ, Humphreys DG, Lukow O, Ames N, Noll J, Cloutier S, McCallum BD (2005) Mapping quantitative trait loci controlling agronomic traits in spring wheat cross RL4452 × 'AC Domain'. Genome 48:870-883

Mohler V, Bauer C, Schweizer G, Kempf H, Hartl L (2013) *Pm50*: a new powdery mildew resistance gene in common wheat derived from cultivated emmer. J Appl Genetics 54:259-263

Nadolska-Orczyk A, Rajchel IK, Orczyk W, Gasparis S (2017) Major genes determining yield-related traits in wheat and barley. Theor Appl Genet 130:1081-1098

Nishida H, Yoshida T, Kawakami K, Fujita M, Long B, Akashi Y, Laurie DA, Kato K (2013) Structural variation in the 5' upstream region of photoperiod-insensitive alleles *Ppd-A1a* and *Ppd-B1a* identified in hexaploid wheat (*Triticum aestivum* L.), and their effect on heading time. Mol Breeding 31:27-37

Russo MA, Ficco DBM, Laidò G, Marone D, Papa R, Blanco A, Gadaleta A, De Vita P, Mastrangelo AM (2014) A dense durum wheat × *T. dicoccum* linkage map based on SNP markers for the study of seed morphology. Mol Breeding 34:1579-1597

Sakuma S, Golan G, Guo Z, Ogawa T, Tagiri A, Sugimoto K, Bernhardt N, Brassac J, Mascher M, Hensel G, et al. (2019) Unleashing floret fertility in wheat through the mutation of a homeobox gene. Proc Natl Acad Sci 116:5182-5187

Sarinelli JM, Murphy JP, Tyagi P, Holland JB, Johnson JW, Mergoum M, Mason RE, Babar A, Harrison S, Sutton R, Griffey CA, Brown-Guedira G (2019) Training population selection and use of fixed effects to optimize genomic predictions in a historical USA winter wheat panel. Theor Appl Genet 132:1247-1261

Scott MF, Botigué LR, Brace S, Stevens CJ, Mullin VE, Stevenson A, Thomas MG, Fuller DQ, Mott R (2019) A 3,000-year-old Egyptian emmer wheat genome reveals dispersal and domestication history. Nat Plants 5:1120-1128

Sen Ś and Churchill GA (2001) A statistical framework for quantitative trait mapping. Genetics 159:371-387

Sharma JS, Running KLD, Xu SS, Zhang Q, Peters Haugrud AR, Sharma S, McClean PE, Faris JD (2019a) Genetic analysis of threshability and other spike traits in the evolution of cultivated emmer to fully domesticated durum wheat. Mol Genet and Genomics 294:757-771

Sharma JS, Zhang Q, Rouse MN, Klindworth DL, Friesen TL, Long Y, Olivera PD, Jin Y, McClean PE, Xu SS, Faris JD (2019b) Mapping a characterization of two stem rust resistance genes derived from cultivated emmer wheat accession PI 193883. Theor Appl Genet 132:3177-3189

Simons KJ, Fellers JP, Trick HN, Zhang Z, Tai YS, Gill BS, Faris JD (2006) Molecular characterization of the major wheat domestication gene *Q*. Genetics 172:547-555

Snedecor GW and Cochran WG (1989) Statistical methods, Eighth Edition. Iowa State University Press, Ames

Sun L, Huang S, Sun G, Zhang Y, Hu X, Nevo E, Peng J, Sun D (2020) SNP-based association study of kernel architecture in a worldwide collection of durum wheat germplasm. PLoS ONE 15:e0229159

Sun M, Yan Y, Jiang Y, Xiao Y, Hu Y, Cai M, Li Y, Hsam SLK, Zeller FJ (2004) Molecular cloning and comparative analysis of a y-type inactive HMW glutenin subunit gene from cultivated emmer wheat (*Triticum dicoccum* L.). Hereditas 141:46-54

Sun P, Zhang W, Wang Y, He Q, Shu F, Liu H, Wang J, Wang J, Yuan L, Deng H (2016) *OsGRF4* controls grain shape, panicle length and seed shattering in rice. J Integr Plant Biol 58:836-847

Taagen E, Tanaka J, Gul A, Sorrells ME (2021) Positional-based cloning 'fail-safe' approach is overpowered by wheat chromosome structural variation. Plant Genome-US 14:e20106

Wang S, Wong D, Forrest K, Allen A, Chao S, Huang BE, Maccaferri M, Salvi S, Milner SG, Cattivelli L, et al. (2014) Characterization of polyploidy wheat genomic diversity using a high-density 90,000 single nucleotide polymorphism array. Plant Biotechnol J 12:787-796

Wei T and Simko V (2017) R package "corrplot":visualization of a correlation matrix (version 0.90). https://github.com/taiyun/corrplot

Würschum T, Leiser WL, Langer SM, Tucker MR, Longin CFH (2018) Phenotypic and genetic analysis of spike and kernel characteristics in wheat reveals long-term genetic trends of grain yield components. Theor Appl Genet 131:2071-2084

Yan L, Fu D, Li C, Blechl A, Tranquilli G, Bonafede M, Sanchez A, Valarik M, Yasuda S, Dubcovsky J (2006) The wheat and barley vernalization gene *VRN3* is an orthologue of *FT*. Proc Natl Acad Sci 103:19581-19586

Yu J, Zhao Y, Ding M, Yu Z, Jiang Y, Ma W, Rong J (2019) Wild emmer chromosome arm substitution lines: useful resources for wheat genetic study and breeding. Crop Sci 60:1761-1769

Zaharieva M, Ayana NG, Hakimi AA, Misra SC, Monneveux P (2010) Cultivated emmer wheat (*Triticum dicoccon* Schrank), an old crop with promising future: a review. Genet Resour Crop Ev 57:937-962

Zhang L, Zhao YL, Gao LF, Zhao GY, Zhou RH, Zhang BS, Jia JZ (2012) *TaCK6-D1*, the ortholog of rice *OsCKX2*, is association with grain weight in hexaploid wheat. New Phytol 195:574-584

Zhu T, Wang L, Rimbert H, Rodrigues JC, Deal KR, De Oliveira R, Choulet F, Keeble-Gagnere G, Tibbits J, Rogers J, et al. (2021) Optical maps refine the bread wheat *Triticum aesiticum* cv. Chinese Spring genome assembly. Plant J https://doi.org/10.1111/tpj.15289

Zhu T, Wang L, Rodriguez JC, Deal KR, Avni R, Distelfeld A, McGuire PE, Dvorak J, Luo MC (2019) Improved genome sequence of wild emmer wheat Zavitan with the aid of optical maps. G3-Genes Genom Genet 9:619-624

CHAPTER 5. GENETIC ANALYSIS OF YIELD RELATED TRAITS IN TWO DURUM × CULTIVATED EMMER WHEAT POPULATIONS UNDER FIELD CONDITIONS

5.1. Abstract

Wheat (*Triticum* ssp.) is a major world food crop, and with the projected increases in world population, wheat yields will need to increase by at least 60% by 2050 to meet the increased expected demands. Numerous studies have identified yield component QTL in hexaploid wheat; however, fewer yield evaluation studies have been performed in tetraploid wheat grown under field conditions. A potential source for allelic variation for wheat improvement is cultivated emmer (*T. turgidum* ssp. *dicoccum*). Here, I evaluated two populations of tetraploid recombinant inbred lines derived from crosses between North Dakota durum wheat varieties and cultivated emmer wheat accessions under field conditions to identify quantitative trait loci for eleven yield component and seed morphological traits. The two populations were developed from the following crosses: Ben × PI 41025 (BP025) and Rusty × PI 193883 (RP883). Plants were grown in the summers of 2017, 2018, and 2019 in Prosper, ND and in 2020 in Casselton, ND in a randomized complete block design in hill plots under non-irrigated conditions. QTL associated with each of these traits were identified on every chromosome in these populations. A total of 164 QTL were identified in the BP025 population, with 44 QTL observed in two or more environments. For the RP883 population, 149 QTL were identified, with 34 observed in multiple environments. The findings from this study provide insights into the traits that differ between the two tetraploid wheat subspecies, along with tools breeders can use to introgress these traits into their breeding lines.

5.2. Introduction

Wheat (*Triticum* ssp.) is one of the major global food crops, supplying approximately 20% of the calories in the average human's diet. Approximately 95% of wheat grown is hexaploid common (bread) wheat (*Triticum aestivum* L., $2n = 6x = 42$, AABBDD genomes), and 5% is tetraploid durum wheat (*T. turgidum* ssp. *durum* L., $2n = 4x = 28$, AABB genomes). Durum wheat is grown on approximately 16 million hectares worldwide and is used to make pasta and other semolina-based products (Arriagada et al. 2020). Within the United States, North Dakota is the largest durum wheat producer (https://www.ndwheat.com/buyers/NorthDakota WheatClasses/Durum/). With the growing world population, wheat production and yields need to increase by 50% to meet increased demands (IWYP 2017).

Grain yield is a quantitative trait controlled by a multitude of genes and pathways, many which have a complex interplay with one another (Cao et al. 2020). Final grain yield is determined by three main components: kernel weight/size and shape, the number of kernels per spike, and the number of spikes per unit area (Gegas et al. 2010; Brinton and Uauy 2018; Cao et al. 2020). Each component can be further split into numerous subcomponents, adding to the overall complexity of wheat yield. Additionally, the wheat genome is an allopolyploid and is comparably larger in size than most cultivated crop genomes (IWGSC 2018), and the presence of multiple homoeologs of yield associated genes confounds the effects of the individual loci and ability to map the gene regions (Borrill et al. 2018).

Recently, a review was published on characterized yield component traits in both tetraploid and hexaploid wheat (Cao et al. 2020), along with two reviews on the various QTL identified in durum wheat relating to yield component traits (Arriagada et al. 2020; Colasuonno et al. 2021). However, the majority of the work done on identifying and unraveling wheat yield

has been in hexaploid wheat (Cao et al. 2020). In durum wheat, more quality, abiotic, and biotic stress studies have been published compared to studies on yield components (Arriagada et al. 2020, Colasuonno et al. 2021).

According to Arriagada et al. (2020), over 665 QTL for yield component traits have been identified in durum wheat, with 264 of these being kernel weight QTLs. The majority of these studies under field conditions have been in the Mediterranean region, which is the largest durum production region globally. To my knowledge, the only study mapping yield component traits in tetraploid wheat in North Dakota under field conditions is Salsman et al. (2021). Due to the complexity of grain yield and the relatedness of the lines in their GWAS panel, no yield component gene regions were identified.

Cultivated emmer, *T. turgidum* ssp. *dicoccum* (Schrank) Schübl ($2n = 4x = 28$, AABB), is the progenitor of durum and hexaploid wheat and currently is grown in isolated areas for local use (Zaharieva et al. 2010). Cultivated emmer arose through mutations in the *Br* loci in wild emmer, *T. turgidum* ssp. *dicoccoides* (Körn.) Thell ($2n = 4x = 28$, AABB), resulting in cultivated emmer having a non-brittle rachis and non free-threshing, or hulled, seed (Faris 2014). Acquisition of mutations in *q* and *Tg* resulted in free-threshing durum wheat.

Previously, two durum × cultivated emmer recombinant inbred line (RIL) populations, one derived from crossing the durum cultivar Ben with the cultivated emmer accession PI 41025 (referred to as BP025) and the other derived from crossing the durum germplasm line Rusty with the cultivated emmer accession PI 193883 (referred to as RP883), have been evaluated in the greenhouse for various spike and domestication traits (Sharma et al. 2019a; Faris et al. 2014), and the BP025 population was also evaluated for multiple agronomic traits (Faris et al. 2014). Additionally, the BP025 population has been used to map QTL for Fusarium head blight

resistance, resistance to tan spot, and to validate the spikelet per spike gene *WAPO-A1* (Zhang et al. 2014; Kuzay et al. 2019; Liu et al. 2020; Guo et al. 2020). The RP883 population has also been evaluated for resistance to tan spot (Liu et al. 2020) and stem rust resistance (Sharma et al. 2019b).

To date, most QTL mapping studies in tetraploid wheat have been durum × durum or durum × wild emmer populations. RIL populations with closely related parents often lack the power to detect QTL due to the genetic similarities between the two parents and the population size is often too small to detect minor effect QTL. Durum × wild emmer crosses are diversely related and useful for identifying a larger number of QTL; however, introgressing traits from wild emmer into the durum germplasm pool is often associated with deleterious linkage drag (Yu et al. 2019). To overcome this, durum × cultivated emmer crosses are useful for not only identifying genes in both durum and cultivated emmer but cultivated emmer has been cultivated for centuries and may be a source of beneficial yield genes (Zaharieva et al. 2010).

Previously, the BP025 population was evaluated in the greenhouse but kernel shape/size traits were not measured (Faris et al. 2014). Additionally, although the RP883 population was evaluated in the greenhouse by Sharma et al. (2019a), the focus of their analysis was on threshability and domestication, therefore kernel size/shape traits were not evaluated. In this study, my two primary objectives were 1) to identify QTLs associated with various yield component traits in the BP025 and RP883 populations grown under field conditions and 2) determine which QTLs were stable over multiple environments and across populations and suitable for deployment in breeding programs for durum improvement.

5.3. Materials and Methods

5.3.1. Plant Material

Two durum × cultivated emmer RIL populations were evaluated for grain yield components under field conditions in North Dakota, US. The two RIL populations were developed using single-seed descent. The BP025 population was developed by Steven Xu at the USDA-ARS in Fargo, ND from crossing Ben (PI 596557), a North Dakota hard amber durum variety (Elias and Miller 1998), with PI 41025, a cultivated emmer accession collected near Samara, Russia. The BP025 population consists of 200 RILs, was genotyped using the 9k iSelect SNP array (Cavanagh et al. 2013), and the map was published by Faris et al. (2014). The RP883 population was developed by Steven Xu at the USDA-ARS in Fargo, ND from crossing Rusty (PI 639869), a North Dakota durum germplasm line (Klindworth et al. 2006), with PI 193883, a cultivated emmer wheat accession collected near Shewa, Ethiopia. The RP883 population consists of 190 RILs, was genotyped using the 90k iSelect SNP array (Wang et al. 2014), and the map was published by Sharma et al. (2019a).

5.3.2. Phenotyping

The BP025 and RP883 populations and parental lines were phenotyped for eleven traits: days to heading (DTH), plant height (PHT), total number of spikelets per spike (SPS), kernels per spike (KPS), grain weight per spike (GWS), thousand kernel weight (TKW), kernel area (KA), kernel width (KW), kernel length (KL), kernel circularity (KC), and kernel length:width ratio (KLW).

The two populations and parental lines were evaluated under field conditions for a total of three seasons each and were grown in a randomized complete block design (RCBD) with three replicates each season. Plants were grown in hill plots, with each plot consisting of 10-15

seeds and considered an experimental unit. The 2017, 2018, and 2019 plots were grown at the North Dakota State University (NDSU) field site near Prosper, ND (47.002, -97.115). The 2020 plots were grown at the NDSU agronomy seed farm in Casselton, ND (46.880, -97.243). The BP025 population was planted and evaluated in 2017, 2018, and 2019. The RP883 population was evaluated in 2018, 2019, and 2020. DTH was measured as the number of days from planting until 50% of the spikes were beyond the flag leaf. PH was measured in centimeters from the base of the plot to the tip of the tallest spike (excluding awns). Fifteen main heads per plot were hand harvested and eight heads were used for phenotypic evaluations. SPS was counted as the total number of spikelets per head. KPS, GWS, TKW, KA, KW, KL, KC, and KLW were obtained using a MARVIN grain analyzer (GAT Sensorik GMBH, Neubrandenburg, Germany). For KPS and GWS, the value given by MARVIN for each sample was divided by the number of spikes in that sample to obtain KPS and GWS for data analysis.

5.3.3. Statistical Analysis and QTL Mapping

Statistical analysis was performed using the PROC GLM procedure in SAS 9.4 (SAS institute). Fisher's Least Significant Difference (LSD) test was used to determine significant differences among the RILs at the 0.05 level of probability. For each field season, Bartlett's Chi squared test for homogeneity of error variances (Snedecor and Cochran 1989) was used to determine if replicates within the same environment could be combined (Tables 5.1, 5.2). For those traits that were not normally distributed, Levene's test (Levene 1960) was used instead. For those that could be combined, the scores of each replicate for those traits were used to calculate the overall average, which was used in further analyses and QTL mapping. For field data, RP883 TKW 2018, RP883 KW 2018, and RP883 PHT 2020 replicates were not homogeneous using both Bartlett's and Levene's; therefore, each replicate for these traits was analyzed separately.

Trait mean, maximum, minimum, and correlations were calculated in R v4.0.3, with Pearson correlation coefficients calculated using the R command *cor* (R Development Core Team) and plotted using R/corrplot (Wei and Simko 2017).

Table 5.1. Bartlett Chi-Square values for the BP025 population.

Trait	Year	Bartlett's	*P*-value
SPS	2017	4.71	0.09
KPS	2017	0.32	0.85
GWS	2017	0.06	0.97
TKW	2017	1.30	0.52
DTH	2017	3.14	0.21
PHT	2017	3.19	0.20
KA	2017	0.94	0.63
KW	2017	2.01	0.37
KL	2017	0.16	0.93
KC	2017	1.68	0.43
KLW	2017	1.62	0.45
SPS	2018	0.05	0.98
KPS	2018	2.96	0.23
GWS	2018	4.03	0.13
TKW	2018	4.10	0.13
DTH	2018	0.18	0.92
PHT	2018	0.37	0.83
KA	2018	2.14	0.34
KW	2018	4.69	0.10
KL	2018	2.24	0.33
KC	2018	5.13	0.08
KLW	2018	2.62	0.27
SPS	2019	0.34	0.84
KPS	2019	1.13	0.57
GWS	2019	0.33	0.85
TKW	2019	0.26	0.88
DTH	2019	3.90	0.14
PHT	2019	0.51	0.78
KA	2019	0.52	0.77
KW	2019	0.35	0.84
KL	2019	0.68	0.71
KC	2019	0.25	0.88
KLW	2019	0.10	0.95

Table 5.2. Bartlett Chi-Square values for the RP883 population when grown under field environments.

Trait	Year	Bartlett's	*P*-value	Levene's[A]	*P*-value
SPS	2018	0.09	0.96		
KPS	2018	0.46	0.80		
GWS	2018	5.31	0.07		
TKW*	2018	17.73	<0.05	8.19	<0.05
DTH	2018	0.56	0.76		
PHT	2018	0.98	0.61		
KA	2018	7.02	<0.05	2.35	0.10
KW*	2018	20.07	<0.05	9.9	<0.05
KL	2018	0.08	0.96		
KC	2018	4.66	0.10		
KLW	2018	2.49	0.29		
SPS	2019	0.76	0.68		
KPS	2019	0.82	0.66		
GWS	2019	2.68	0.26		
TKW	2019	1.87	0.39		
DTH	2019	3.33	0.19		
PHT	2019	9.83	<0.05	0.56	0.57
KA	2019	0.30	0.86		
KW	2019	1.46	0.48		
KL	2019	0.34	0.84		
KC	2019	0.40	0.82		
KLW	2019	0.45	0.80		
SPS	2020	4.82	0.09		
KPS	2020	9.64	<0.05	2.87	0.06
GWS	2020	3.22	0.20		
TKW	2020	3.58	0.17		
DTH	2020	1.45	0.48		
PHT*	2020	26.69	<0.05	10.76	<0.05
KA	2020	0.97	0.62		
KW	2020	1.25	0.54		
KL	2020	0.43	0.81		
KC	2020	0.96	0.62		
KLW	2020	0.57	0.75		

*year/trait combinations that could not be combined based on both the Bartlett's and Levene's test

[A]Those which could not be combined were tested using Levene's, with those values shown for those traits.

QTL analysis was performed using R/qtl (Broman et al. 2003). For simple interval mapping, significant QTL were identified using the function 'scanone' with the extended Haley-Knott method (Haley and Knott 1992). An LOD significance threshold was determined using a permutation test with 1000 interactions. 'Scantwo' with the extended Haley-Knott method was used to identify QTL × QTL interactions and an LOD significance threshold was determined using a permutation test with 1000 interactions. Multiple QTL mapping was performed using the stepwiseqtl command (Manichaikul et al. 2009) using method=imp (Sen and Churchill 2001). A forward/backward search method was used, with a maximum of 12 QTL allowed. The initial model was given based on the 'scanone' QTL results. An approximate Bayesian credible interval was calculated using 'Bayesint' with a probability of 0.99 (Broman et al. 2003). QTL names include the trait abbreviation followed by "fcu", which stands for Fargo Cereals Unit.

Markers most significantly associated with each QTL were subjected to BLASTn searches against Svevo RefSeq Rel. 1.0 pseudomolecules, Zavitan WEWSeq v2.0 pseudomolecules, and Chinese Spring IWGSC RefSeq v2.1 genome assembly to obtain the physical positions for comparing QTL between environments, along with identifying known genes within each QTL region. Markers that were the most significantly associated with each QTL were subjected to BLASTn searches against Svevo RefSeq Rel. 1.0 pseudomolecules (Maccaferri et al. 2019), Zavitan WEWSeq v2.0 pseudomolecules (Zhu et al. 2019), and Chinese Spring IWGSC RefSeq v2.1 genome assembly (Zhu et al. 2021) using the Graingenes website (https://wheat.pw.usda.gov/GG3/) to obtain the physical positions for comparing QTL between environments, along with identifying previously reported genes within each QTL region. The sequences for reported genes were obtained from Genbank or the published articles.

5.4. Results

5.4.1. Trait Evaluations in BP025

For DTH, the two parental lines differed significantly in 2017, with Ben and PI 41205 having values of 55.67 and 64.00, respectively (Table 5.3). However, in 2018, Ben and PI 41025 differed only by one day for DTH and in 2019 by three days, which were not significantly different. The population mean was 59.06 days in 2017, which was between the two parental means, with a population range of 48.33 to 68.00 (Table 5.3, Figure 5.1a). However, in 2018 and 2019 the population mean was lower than the two parental lines at 52.02 and 52.42 DTH, respectively. In 2018 the population range was 42.67 to 74.33 DTH, and in 2019 it was 43.50 to 80.67 DTH, indicating that the two parents possess different genes governing heading date.

For PHT, the two parental means were significantly different with Ben averaging 100.22 cm and PI 41025 averaging 117.89 cm across the three field seasons (Table 5.3). The population mean each season was between the two parental lines; however, the value was closer to Ben at 105.76 cm than PI 41025. The population range fell below Ben each season and greater than PI 41025, indicating that both parental lines are contributing genetic factors to increased PHT (Table 5.3, Figure 5.1b).

Mature spikes and seed of Ben and PI 40125 are presented in Figure 5.2. PI 41025 had significantly more SPS than Ben in all three environments (Table 5.3). PI 41025 averaged 23.13, 24.71, and 24.79 SPS in 2017, 2018, and 2019, respectively. Between the three summers, PI 41025 averaged 6.79 more SPS than Ben. The maximum values for the population in 2017, 2018, and 2019 were 22.79, 25.58, and 26.54, respectively, suggesting that PI 41025 is most likely contributing most or all of the genetic factors for increased SPS (Table 5.3, Figure 5.1c). Interestingly, Ben averaged 39.65 KPS whereas PI 41025 averaged 36.00 KPS. Although the two

parental lines were not significantly different, it suggested that PI 41025 had fewer fertile spikelets per spike than Ben. The BP025 population mean fell between that of the two parents at 34.27 KPS, with a population range of 12.17 to 45.75 KPS in 2017, 24.46 to 47.50 KPS in 2018, and 16.04 to 51.42 KPS in 2019, suggesting that both Ben and PI 41025 are contributing to increased KPS; however, both harbor different genes for the number of KPS (Table 5.3, Figure 5.1d).

For the kernel weight components, Ben had significantly higher values than PI 41025 in all three environments. On average, Ben had 1.73 g per spike whereas PI 41025 was 1.00 g per spike (Table 5.3). The BP025 population mean was 1.17 g, with a population range of 0.43 to 1.91 g, 0.73 to 2.08 g, and 0.29 to 1.73 g in 2017, 2018, and 2019, respectively (Table 5.3, Figure 5.1e). As for TKW, Ben averaged 43.92 g across the three environments, with PI 41025 averaging 28.90 g (Table 5.3). The BP025 population average was between the two parents at 34.13 g, with a population range of 27.50 to 49.65 g, 24.96 to 49.02 g, and 12.23 to 38.96 g in 2017, 2018 and 2019, respectively (Table 5.3, Figure 5.1f). Interestingly, for both GWS and TKW, the population range was near the value for Ben in most years. This suggests that Ben most likely harbors genes that confer increased GWS and TKW; however, these genes may be highly influenced by environmental factors.

For kernel morphology traits, Ben had a significantly higher KA and KW than PI 41025, whereas PI 41025 had significantly higher KC and KLW than Ben (Table 5.3). The two parental lines did not differ at the significance level for KL; however, Ben had a longer KL in all three environments. Ben averaged 18.50 mm^2, 3.29 mm, 7.64 mm, 1.51 mm, and 2.33 mm for KA, KW, KL, KC, and KLW, respectively. PI 41025 averaged 14.43 mm^2, 2.77 mm, 7.48 mm, 1.73 mm, and 2.73 mm for KA, KW, KL, KC, and KLW, respectively. The BP025 population mean

was between the two parental averages, with population means of 16.51 mm^2, 3.02 mm, 7.62 mm, 1.62 mm, and 2.55 mm for KA, KW, KL, KC, and KLW, respectively (Table 5.3, Figures 5.1g,h,i,j,k). For KA, the BP025 population range was 14.48 to 20.89 mm^2 in 2017, 13.90 to 20.80 mm^2 in 2018, and 10.59 to 18.64 mm^2 in 2019 (Figure 5.1g), suggesting that both Ben and PI 41025 contribute genetic factors to KA. For KW, the population range was 2.74 to 3.51 mm in 2017, 2.70 to 3.50 mm in 2018, and 2.30 to 3.40 mm in 2019 (Figure 5.1h), suggesting that both Ben and PI 41025 contribute genetic factors to KW. As was observed for KA and KW, the BP025 population range fell below and above both parental lines for KL and KLW (Figures 5.1i,k), suggesting that both parents are contributing genetic factors for increases in these traits. However, for KC, PI 41025 had an average of 1.77 mm in 2017, which was the same as the population maximum (Figure 5.1j). In 2018 and 2019, the population maximum was above the PI 41205 value at 1.80 and 1.85, respectively. This suggest that PI41025 most likely harbors most of the genetic factors that confer increased KC; however, these factors may be highly influenced by the environment.

Table 5.3. Parental and population means, ranges, and least significant differences (LSD) at the 0.05 level of probability (P<0.05) for the BP025 population grown under field conditions.

Trait[A]	Year[B]	Mean			BP025 population	LSD
		Ben	PI 41025	BP025 population	range	(0.05)
DTH	2017	55.67	64.00	59.06	48.33-68.00	2.71
DTH	2018	58.00	57.00	52.02	42.67-74.33	2.24
DTH	2019	58.00	55.00	52.42	43.50-80.67	3.44
PHT	2017	90.33	111.67	101.59	74.00-128.33	7.54
PHT	2018	101.67	119.00	106.00	82.83-139.00	8.14
PHT	2019	108.67	123.00	109.70	88.00-136.00	8.87
SPS	2017	14.67	23.13	17.71	11.75-22.79	1.81
SPS	2018	18.13	24.71	19.87	14.25-25.58	1.07
SPS	2019	19.46	24.79	20.28	15.25-26.54	1.20
KPS	2017	34.25	31.58	32.96	12.17-45.75	5.67
KPS	2018	40.17	37.79	34.54	24.46-47.50	4.09
KPS	2019	44.54	38.63	35.32	16.04-51.42	6.36
GWS	2017	1.61	0.87	1.28	0.43-1.91	0.25
GWS	2018	2.00	1.19	1.27	0.73-2.08	0.27
GWS	2019	1.57	0.94	0.95	0.29-1.73	0.28
TKW	2017	47.16	30.72	38.97	27.50-49.65	4.02
TKW	2018	49.82	31.49	36.73	24.96-49.02	5.56
TKW	2019	34.79	24.49	26.68	12.23-38.96	5.08
KA	2017	19.00	14.03	17.68	14.48-20.89	0.97
KA	2018	19.73	15.43	17.01	13.90-20.80	2.36
KA	2019	16.77	13.83	14.83	10.59-18.64	1.28
KW	2017	3.30	2.70	3.12	2.74-3.51	0.11
KW	2018	3.43	2.90	3.08	2.70-3.50	0.15
KW	2019	3.13	2.70	2.86	2.30-3.40	0.16
KL	2017	7.73	7.47	7.90	6.93-8.76	0.20
KL	2018	7.80	7.67	7.71	6.60-8.70	0.31
KL	2019	7.40	7.30	7.26	6.38-8.06	0.29
KC	2017	1.50	1.77	1.61	1.44-1.77	0.04
KC	2018	1.50	1.70	1.61	1.40-1.80	0.06
KC	2019	1.53	1.73	1.65	1.42-1.85	0.06
KLW	2017	2.30	2.80	2.56	2.15-2.91	0.08
KLW	2018	2.30	2.67	2.53	2.10-2.90	0.10
KLW	2019	2.40	2.73	2.57	2.08-2.99	0.10

[A]Trait abbreviations are: days to heading (DTH), plant height (PHT), spikelets per spike (SPS), kernels per spike (KPS), grain weight per spike (GWS), thousand kernel weight (TKW), kernel area (KA), kernel width (KW), kernel length (KL), kernel circularity (KC), and kernel length:width ratio (KLW).
[B]Each field environment was analyzed separately.

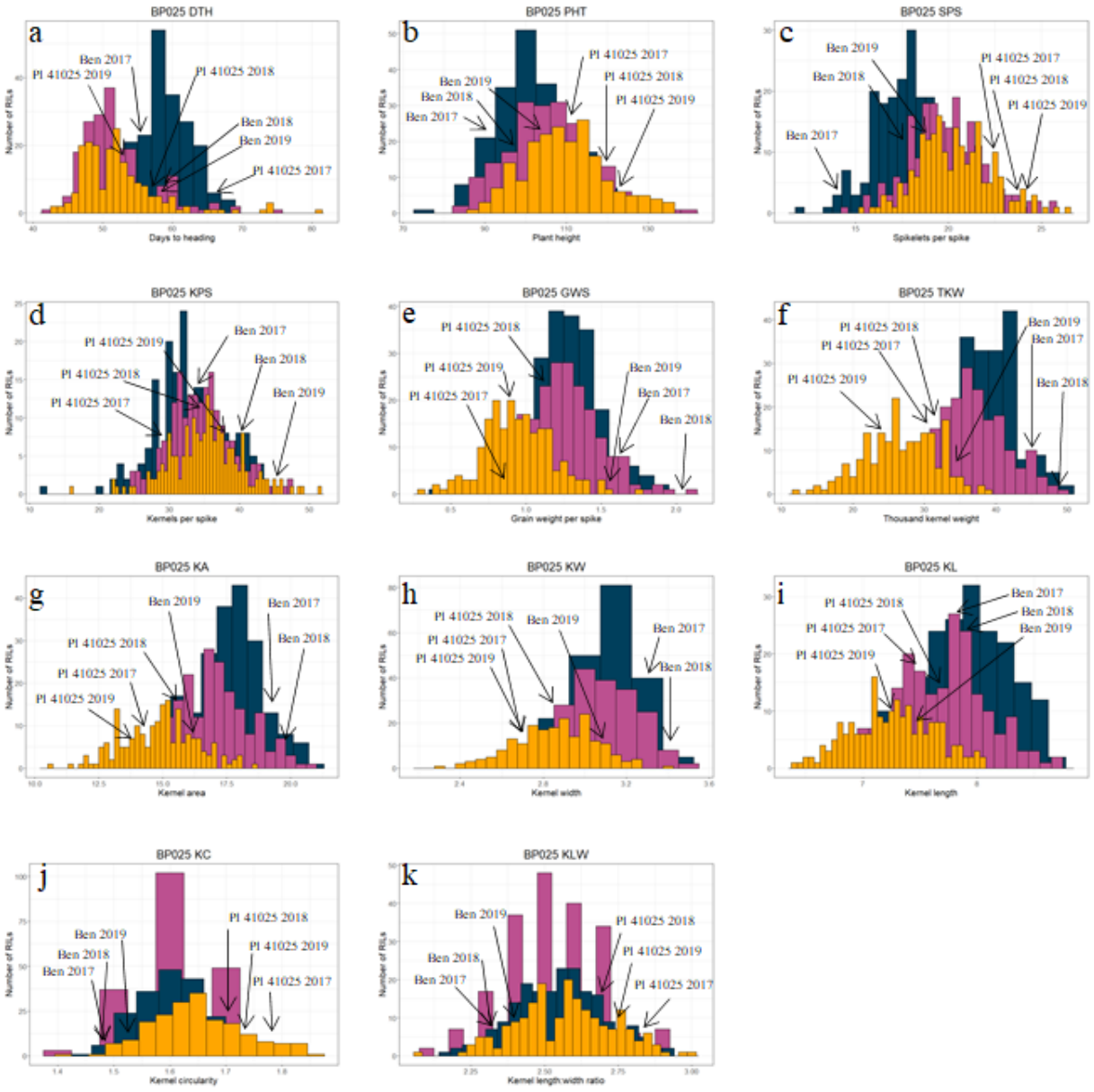

Figure 5.1. Histograms of the BP025 population for the traits a) days to heading (DTH), b) plant height (PHT), c) spikelets per spike (SPS), d) kernels per spike (KPS), e) grain weight per spike (GWS), f) thousand kernel weight (TKW), g) kernel area (KA), h) kernel weight (KW), i) kernel length (KL), j) kernel circularity (KC), k) kernel length:width ratio (KLW). The blue, pink, and yellow bars represent the 2017, 2018, and 2019 environments, respectively.

Figure 5.2. Spike and seed morphology of Ben and PI 41025, the two parental lines of the BP025 population. (a) Mature spikes of Ben (left) and PI 41025 (right). (b) seed of the durum variety Ben (top) and the cultivated emmer wheat accession PI 41025 (bottom).

5.4.2. Correlations in BP025

Correlations for the BP025 population between all the traits are shown in Figure 5.3, along with the correlation coefficient values given in Tables 5.4, 5.5, 5.6. For each trait, there was a strong positive correlation across environments, suggesting that these traits are stable across environments. Within the 2017 season, SPS was strongly positively correlated with KPS, GWS, DTH, and PHT (Table 5.4, Figure 5.3). In 2018, SPS was strongly correlated with those traits, along with KW (Table 5.5, Figure 5.3). However, in 2019, SPS was only positively correlated with DTH, PHT, and GWS, not KPS and GWS (Table 5.6, Figure 5.3). SPS had a weak, but significant negative correlation with KL in 2017 (Table 5.4), KLW in all three environments (Figure 5.3), with the strong correlation in 2018, and KC in 2018 (Table 5.5). KPS and GWS had a consistent, strong positive correlation in all three environments (Figure 5.3), along with GWS and TKW having a significant, positive correlation in all three environments. GWS and TKW had strong positive correlations with PHT, KA, KW, and KL in 2017, 2018, and 2019 (Tables 5.4, 5.5, 5.6, Figure 5.3), except for GWS and KL in 2017 (Table 5.4, Figure 5.3). Significant negative correlations were observed for GWS and TKW with KC and KLW in all three environments (Tables 5.4, 5.5, 5.6, Figure 5.3).

As for the kernel dimension traits, KA was significantly correlated with KW, KL, KC, and KLW in 2019 (Table 5.6, Figure 5.3). A strong positive correlation was observed for KA with KW and KL in 2019, along with 2017 and 2018 (Tables 5.4, 5.5, 5.6, Figure 5.3). However, a strong negative correlation was observed for KA with KC and KLW in 2019 (Table 5.6, Figure 5.3), but in 2017 and 2018 there was no significant correlations between these traits (Tables 5.4, 5.5, Figure 5.3). As for the other kernel dimension traits with one another, KW with KL, KL with KC, KL with KLW, and KC with KLW in 2017, 2018, and 2019 all had strong positive

correlations (Tables 5.4, 5.5, 5.6, Figure 5.3). The only negative correlations between kernel dimension traits were KW with KC and KW with KLW in all three environments (Figure 5.3).

Table 5.4. Correlation coefficients for the BP025 population grown under field conditions in 2017 between the mean values of the traits days to heading (DTH), plant height (PHT), spikelets per spike (SPS), kernels per spike (KPS), grain weight per spike (GWS), thousand kernel weight (TKW), kernel area (KA), kernel width (KW), kernel length (KL), kernel circularity (KC), and kernel length:width ratio (KLW).

	SPSavg	KPSavg	GWSavg	TKWavg	DTHavg	PHTavg	KAavg	KWavg	KLavg	KCavg	KLWavg
SPSavg	1.00										
KPSavg	0.58***	1.00									
GWSavg	0.44***	0.81***	1.00								
TKWavg	-0.12	-0.16*	0.45***	1.00							
DTHavg	0.23***	0.14	0.03	-0.18**	1.00						
PHTavg	0.40***	0.12	0.23**	0.22**	0.26***	1.00					
KAavg	-0.11	-0.21**	0.36***	0.93***	-0.15*	0.13	1.00				
KWavg	0.04	-0.01	0.49***	0.83***	-0.02	0.26***	0.78***	1.00			
KLavg	-0.18*	-0.34***	0.04	0.57***	-0.15*	-0.03	0.76***	0.21**	1.00		
KCavg	-0.09	-0.23**	-0.31***	-0.18*	-0.02	-0.20**	0.03	-0.53***	0.67***	1.00	
KLWavg	-0.17*	-0.27***	-0.35***	-0.17*	-0.10	-0.22**	0.02	-0.59***	0.66***	0.97***	1.00

*P<0.05
**P<0.01
***P<0.001

Table 5.5. Correlation coefficients for the BP025 population grown under field conditions in 2018 between the mean values of the traits days to heading (DTH), plant height (PHT), spikelets per spike (SPS), kernels per spike (KPS), grain weight per spike (GWS), thousand kernel weight (TKW), kernel area (KA), kernel width (KW), kernel length (KL), kernel circularity (KC), and kernel length:width ratio (KLW).

	SPSavg	KPSavg	GWSavg	TKWavg	DTHavg	PHTavg	KAavg	KWavg	KLavg	KCavg	KLWavg
SPSavg	1.00										
KPSavg	0.26***	1.00									
GWSavg	0.26***	0.68***	1.00								
TKWavg	0.10	-0.07	0.67***	1.00							
DTHavg	0.43***	-0.12	0.08	0.23***	1.00						
PHTavg	0.55***	-0.09	0.26***	0.46***	0.52***	1.00					
KAavg	0.11	-0.10	0.61***	0.95***	0.28***	0.41***	1.00				
KWavg	0.29***	-0.03	0.58***	0.83***	0.37***	0.51***	0.81***	1.00			
KLavg	-0.06	-0.15	0.33***	0.61***	0.08	0.15*	0.75***	0.27***	1.00		
KCavg	-0.23**	-0.07*	-0.25***	-0.29***	-0.25***	-0.32***	-0.14	-0.57***	0.50***	1.00	
KLWavg	-0.27***	-0.09	-0.25***	-0.27***	-0.26***	-0.33***	-0.12	-0.63***	0.54***	0.90***	1.00

*P<0.05
**P<0.01
***P<0.001

Table 5.6. Correlation coefficients for the BP025 population grown under field conditions in 2019 between the mean values of the traits days to heading (DTH), plant height (PHT), spikelets per spike (SPS), kernels per spike (KPS), grain weight per spike (GWS), thousand kernel weight (TKW), kernel area (KA), kernel width (KW), kernel length (KL), kernel circularity (KC), and kernel length:width ratio (KLW).

	SPSavg	KPSavg	GWSavg	TKWavg	DTHavg	PHTavg	KAavg	KWavg	KLavg	KCavg	KLWavg
SPSavg	1.00										
KPSavg	0.13	1.00									
GWSavg	0.06	0.62***	1.00								
TKWavg	-0.05	0.05	0.80***	1.00							
DTHavg	0.57***	-0.16*	-0.14	-0.09	1.00						
PHTavg	0.45***	-0.02	0.31***	0.39***	0.44***	1.00					
KAavg	0.06	-0.02	0.70***	0.91***	0.09	0.37***	1.00				
KWavg	0.15*	-0.01	0.69***	0.89***	0.15*	0.42***	0.90***	1.00			
KLavg	-0.02	-0.08	0.39***	0.55***	0.03	0.15*	0.76***	0.45***	1.00		
KCavg	-0.04	-0.08	-0.49***	-0.58***	0.01	-0.30***	-0.35***	-0.65***	0.32***	1.00	
KLWavg	-0.16*	-0.06	-0.44***	-0.53***	-0.12	-0.33***	-0.37***	-0.71***	0.30***	0.95***	1.00

*P<0.05
**P<0.01
***P<0.001

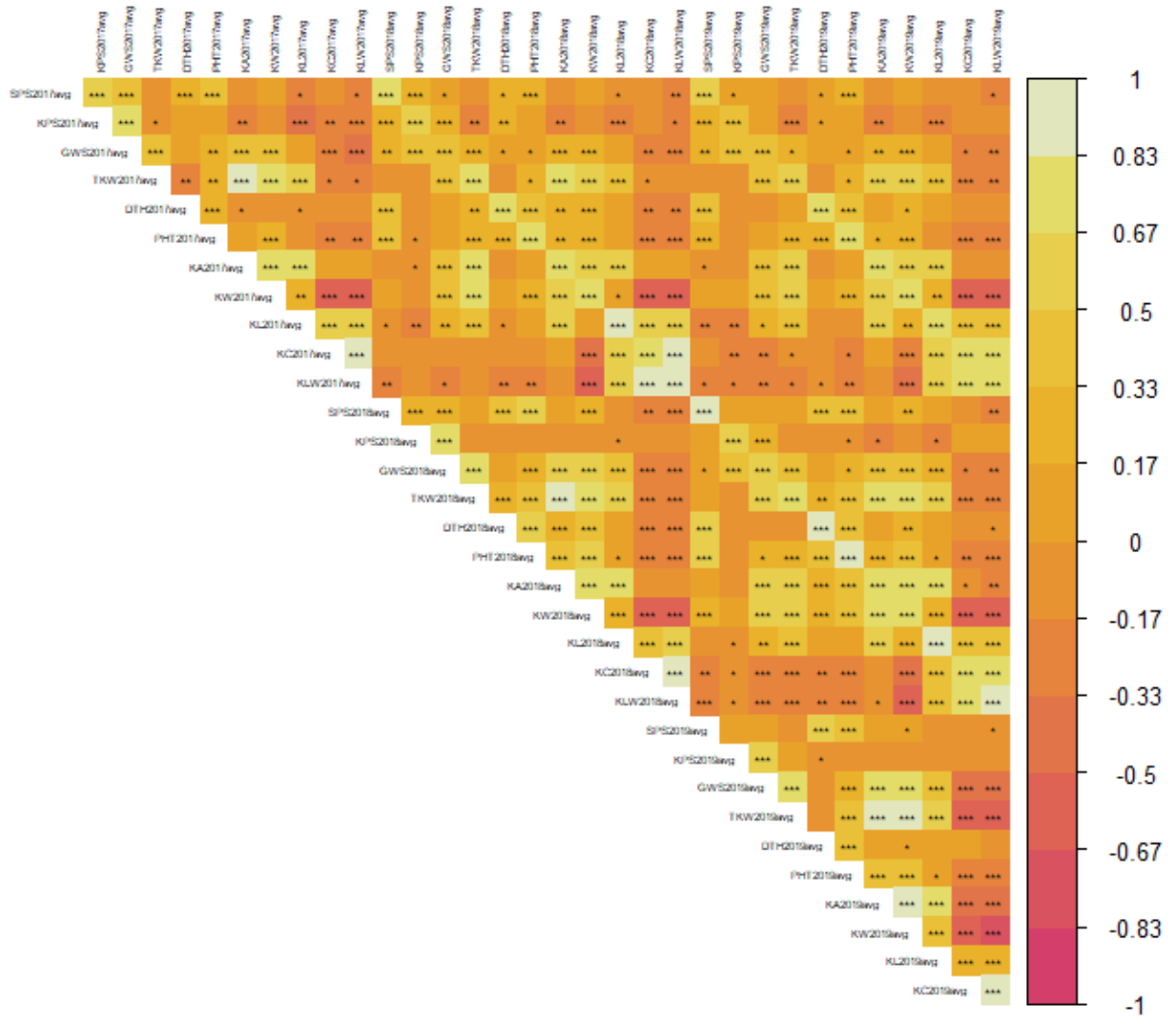

Figure 5.3. Pearson correlation coefficients between the 11 traits measured in the BP025 population grown under field conditions in 2017, 2018, and 2019. Trait abbreviations are: days to heading (DTH), plant height (PHT), spikelets per spike (SPS), kernels per spike (KPS), grain weight per spike (GWS), thousand kernel weight (TKW), kernel area (KA), kernel width (KW), kernel length (KL), kernel circularity (KC), and kernel leght:width ratio (KLW). Significance values are denoted as *P<0.05, **P<0.01, ***P<0.001. Along the right is a color scale for the correlation values. Blocks that are orange to pink have a negative correlation, with dark pink being a correlation close to -1. Blocks that are orange to light yellow have a positive correlation, with light yellow being a correlation close to 1. Significance values are denoted as *P<0.05, **P<0.01, ***P<0.001.

5.4.3. QTL Analysis in BP025

Among the three environments for the BP025 population, I identified 164 significant QTL and QTL×QTL interactions using forward/backward selection to identify the QTL model

with the highest LOD score. Within individual field seasons, 56, 59, and 49 QTL were identified in 2017, 2018, and 2019, respectively (Supplementary File 3).

For the purpose of this study, I was most interested in QTL that were significant across multiple environments. Twenty-six QTL were observed in two environments, and 18 were observed in all three years (Table 5.7, Figure 5.4, Supplementary File 3). A total of 15 genomic regions were associated with the 44 QTL that were observed in multiple environments. No QTL × QTL interactions were found to be consistent across environments.

Three QTL were associated with DTH in two or more environments. These QTL, *QEet.fcu-2B, QEet.fcu-5A*, *QEet.fcu-5B*, were mapped on chromosomes 2B, 5A, and 5B, and within the QTL regions are the known genes *Ppd-B1*, *Vrn-A1*, and *Vrn-B1*, respectively (Table 5.7, Figure 5.4). The QTL *QEet.fcu-2B* and *QEet.fcu-5B* were observed in all three environments. *QEet.fcu-2B, QEet.fcu-5A*, and *QEet.fcu-5B* had maximum LOD values of 13.11, 21.57, and 25.87 and explained up to 15.60, 25.74, and 32.61% of the variation in heading date, respectively. Ben contributed to increased DTH at the *QEet.fcu-5A* and *QEet.fcu-5B* QTL, whereas PI 41025 was at the *QEet.fcu-2B* QTL**.**

For PHT, five QTL were identified across two or more environments. These QTL were mapped to chromosomes 2A, 3A, 5A, and 5B and designated *QHt.fcu-2A*, *QHt.fcu-3A*, *QHt.fcu-5A.1*, *QHt.fcu-5A.2*, and *QHt.fcu-5B* (Table 5.7, Figure 5.4). The two QTL on 5A, *QHt.fcu-5A.1*, *QHt.fcu-5A.2*, were located approximately 70 cM apart, and *QHt.fcu-5A.2* was near the *Vrn-A1* locus. The only other PHT QTL near a known gene was *QHt.fcu-5B*, which was near the *Vrn-B1* locus. *QHt.fcu-3A, QHt.fcu-5A.1,* and *QHt.fcu-5B* were observed in all three environments. *QHt.fcu-2A*, *QHt.fcu-3A*, *QHt.fcu-5A.1*, *QHt.fcu-5A.2*, and *QHt.fcu-5B* had maximum LOD values of 16.56, 16.00, 7.60, 10.59, and 13.86 and explained up to 23.17, 19.37, 9.55, 11.99, and

16.34% of the variation in PHT. PI 41025 contributed to increased PHT at the *QHt.fcu-2A*, *QHt.fcu-3A*, and *QHt.fcu-5A.1* QTLs and Ben at the *QHt.fcu-5A.2* and *QHt.fcu-5B* QTLs.

Seven genomic regions had QTL associated with SPS across two or more environments, which was the most of the 11 traits evaluated in this population (Table 5.7, Figure 5.4). These QTL, designated *QSpn.fcu-1A, QSpn.fcu-2B, QSpn.fcu-3B, QSpn.fcu-5A.1, QSpn.fcu-5A.2, QSpn.fcu-5B,* and *QSpn.fcu-7A,* were located on chromosomes 1A, 2B, 3B, 5A, 5B, and 7A, respectively. *QSpn.fcu-2B*, *QSpn.fcu-5A.2, QSpn.fcu-5B,* and *QSpn.fcu-7A* were near the *Ppd-B1*, *Q*, *Vrn1-B1*, and *WAPO-A1* loci, respectively. Two of these QTL, *QSpn.fcu-5A.*2 and *QSpn.fcu-7A* were observed in all three environments. QSpn*.fcu-1A, QSpn.fcu-2B, QSpn.fcu-3B, QSpn.fcu-5A.1, QSpn.fcu-5A.2, QSpn.fcu-5B,* and *QSpn.fcu-7A* had maximum LOD values of 6.14, 7.87, 9.04, 4.11, 15.94, 5.67, and 14.14 and explained up to 7.05, 6.56, 11.24, 4.03, 14.59, 9.14, and 17.87% of the variation in SPS. PI 41025 alleles at the *QSpn.fcu-2B, QSpn.fcu-3B, QSpn.fcu-5A.1* and *QSpn.fcu-7A* QTL contributed to increased number of SPS, whereas Ben alleles contributed to increased SPS at *QSpn.fcu-2B, QSpn.fcu-5A.2,* and *QSpn.fcu-5B*.

Only one QTL was associated with KPS across multiple environments (Table 5.7, Figure 5.4). *QKps.fcu-2A*, located on chromosome 2A, was mapped near the *GNI1-A1* locus. This QTL had a maximum LOD of 6.22 and explained up to 12.39% of the variation in KPS. Ben contributed to increased KPS at *QKps.fcu-2A.*

Two QTL were identified for GWS across multiple environments (Table 5.7, Figure 5.4). These QTL, located on chromosomes 1A and 3B, are designated *QGws.fcu-1A* and *QGws.fcu-3B*, respectively, and had maximum LOD values of 6.10 and 10.26 and explained 8.84 and 16.61% of the variation in GWS. *QGws.fcu-3B* was observed in all three environments. Ben contributed the positive alleles for both QTL.

For TKW, a total of five stable QTL were identified (Table 5.7, Figure 5.4). These QTL, designated *QTkw.fcu-1A*, *QTkw.fcu-2A*, *QTkw.fcu-3B*, *QTkw.fcu-4A*, and *QTkw.fcu-5B*, mapped to chromosomes 1A, 2A, 3B, 4A, and 5B, respectively. Within the genetic regions of *QTkw.fcu-2A* and *QTkw.fcu-5B* are the known genes *GNI1-A1* and *Vrn1-B1*, respectively. *QTkw.fcu-3B* was observed in all three environments. The TKW QTL *QTkw.fcu-1A*, *QTkw.fcu-2A*, *QTkw.fcu-3B*, *QTkw.fcu-4A*, and *QTkw.fcu-5B* had maximum LOD values of 6.51, 6.82, 12.27, 4.94, and 9.56 and explained up to 9.73, 9.00, 17.28, 7.11, and 13.02% of the variation in TKW, respectively. PI 41025 was the contributor of increased TKW at *QTkw.fcu-2A*, whereas Ben was at the other four TKW QTL.

Four stable QTL were significantly associated with KA in the BP025 population. These four QTL, *QKa.fcu-1A, QKa.fcu-3B, QKa.fcu-4A*, and *QKa.fcu-5B*, were mapped to chromosomes 1A, 3B, 4A, and 5B (Table 5.7, Figure 5.4). Only one QTL, *QKa.fcu-5B*, was within the genomic region of a known gene (*Vrn1-B1*). *QKa.fcu-3B* was the only QTL observed in all three environments. *QKa.fcu-1A, QKa.fcu-3B, QKa.fcu-4A*, and *QKa.fcu-5B* had maximum LOD scores of 7.47, 9.45, 4.81, and 9.28 and explained up to 10.73, 14.28, 7.39, and 13.78% of the variation in KA, respectively. Ben was the contributor of increased KA at all four QTL.

For the kernel dimension trait KW, six stable QTL were identified. These QTL were mapped to chromosomes 1A, 3B, 4A, 5A, 5B, and 7A and were designated *QKw.fcu-1A*, *QKw.fcu-3B*, *QKw.fcu-4A*, *QKw.fcu-5A*, *QKw.fcu-5B*, and *QKw.fcu-7A* (Table 5.7, Figure 5.4). *Q* and *Vrn1-B1* are within the genetic regions of *QKw.fcu-5A* and *QKw.fcu-5B*. The QTL *QKw.fcu-3B*, *QKw.fcu-4A*, *QKw.fcu-5A,* and *QKw.fcu-7A* were observed in all three environments. *QKw.fcu-1A*, *QKw.fcu-3B*, *QKw.fcu-4A*, *QKw.fcu-5A*, *QKw.fcu-5B*, and *QKw.fcu-7A* had maximum LOD values of 8.72, 10.38, 13.98, 8.26, 13.89, and 17.12 and explained up

11.37, 9.97, 11.65, 7.93, 16.44, and 17.49% of the variation in KW. As with KA, Ben was the contributor of increased KW at all six QTL.

For KL, four QTL were identified in the BP025 population across two or more environments. These QTL, *QKl.fcu-1A*, *QKl.fcu-2A*, *QKl.fcu-3A*, and *QKl.fcu-3B* mapped to chromosomes 1A, 2A, 3A, and 3B, had maximum LOD values of 6.48, 9.71, 4.00, and 8.16 and explained up to 9.99, 15.47, 5.95, and 12.83% of the variation in KL, respectively (Table 5.7, Figure 5.4). Only *QKl.fcu-3B* was observed under all three environments. *QKl.fcu-1A* and *QKl.fcu-2A* are within the genomic regions of *ELF3* and *GNI1-A1*, respectively. At *QKl.fcu-1A*, *QKl.fcu-2A* and *QKl.fcu-3A*, PI 41025 was the contributor to increased KL, whereas at *QKl.fcu-3B* Ben was.

In the BP025 population, three stable QTL were identified for KC and were designated *QKc.fcu-1A, QKc.fcu-5B,* and *QKc.fcu-7A* and mapped to chromosomes 1A, 5B, and 7A, respectively (Table 5.7, Figure 5.4). Within the mapped genomic regions of *QKc.fcu-1A* and *QKc.fcu-5B* are the genes *ELF3* and *Vrn1-B1*. *QKc.fcu-1A* and *QKc.fcu-7A* were observed under all three environments. *QKc.fcu-1A, QKc.fcu-5B,* and *QKc.fcu-7A* had maximum LOD values of 8.35, 3.73, and 11.57 and explained up to 11.02, 5.53, and 15.87% of the variation in KC, respectively. PI 41025 was the donor parent at all three QTL for increased KC.

Lastly, within the BP025 population I identified four stable QTL which were associated with KLW. These QTL were mapped to chromosomes 1A, 2A, 5A, and 7A and were designated *QKlw.fcu-1A*, *QKlw.fcu-2A*, *QKlw.fcu-5A*, and *QKlw.fcu-7A* (Table 5.7, Figure 5.4). *ELF3*, *GNI1-A1*, and *Q* are within the genomic regions of *QKlw.fcu-1A*, *QKlw.fcu-2A*, and *QKlw.fcu-5A*, respectively. *QKlw.fcu-7A* is the only QTL which was identified in all three environments for KLW. *QKlw.fcu-1A*, *QKlw.fcu-2A*, *QKlw.fcu-5A*, and *QKlw.fcu-7A* had maximum LOD

values of 6.49, 6.17, 5.28, and 12.50 and explained up to 9.87, 9.35, 7.23, and 21.83% of the variation in KLW, respectively. PI 41025 was the donor parent at all four QTL associated with KLW.

Table 5.7. Quantitative trait loci associated with the traits evaluated in the Ben × PI 41025 (BP025) recombinant inbred population grown under field conditions and were present in two or more environments.

Trait	QTL	Chromosome	Position (cM)	Marker interval	LOD	$R^2 \times 100$	Donor parent	Putative gene
SPS	*QSpn.fcu-1A*	1A	47.31-48.86	*IWA2981-IWA2319*	5.83-6.14	4.72-7.05	Ben	
SPS	*QSpn.fcu-2B*	2B	55.99	*IWA1359-IWA6474*	5.74-7.87	6.53-6.56	PI 41025	*Ppd-B1*
SPS	*QSpn.fcu-3B*	3B	96.18-101.68	*IWA2661-IWA81*	6.87-9.04	7.61-11.24	PI 41025	
SPS	*QSpn.fcu-5A.1*	5A	38.21-44.69	*IWA8155-IWA8582*	3.62-4.11	3.26-4.03	PI 41025	
SPS	*QSpn.fcu-5A.2*	5A	159.26-187.03	*Xwmc110-IWA1670*	4.77-15.94	7.60-14.59	Ben	*Q*
SPS	*QSpn.fcu-5B*	5B	110.34-117.03	*IWA4774-Xwmc75*	3.73-5.67	2.95-9.14	Ben	*Vrn1-B1*
SPS	*QSpn.fcu-7A*	7A	128.27-132.97	*IWA5791-IWA5912*	8.63-14.14	7.34-17.87	PI 41025	*WAPO-A1*
KPS	*QKps.fcu-2A*	2A	108.70	*IWA241*	4.75-6.22	9.50-12.39	Ben	*GNI1-A1*
GWS	*QGws.fcu-1A*	1A	45.27-48.86	*IWA4649-IWA2319*	5.57-6.10	8.53-8.84	Ben	
GWS	*QGws.fcu-3B*	3B	63.58-73.73	*Xwmc612-IWA3997*	5.19-10.26	7.44-16.61	Ben	
TKW	*QTkw.fcu-1A*	1A	42.97-44.76	*IWA3884-IWA492*	4.50-6.51	7.43-9.73	Ben	
TKW	*QTkw.fcu-2A*	2A	92.08	*IWA549*	4.54-6.82	6.62-9.00	PI 41025	*GNI1-A1*
TKW	*QTkw.fcu-3B*	3B	63.58-75.57	*Xwmc612-Xwmc1*	7.30-12.27	11.21-17.28	Ben	
TKW	*QTkw.fcu-4A*	4A	12.53-13.32	*IWA7124-IWA8494*	4.85-4.94	6.37-7.11	Ben	
TKW	*QTkw.fcu-5B*	5B	120.80-128.03	*IWA7910-IWA3275*	4.99-9.56	8.28-13.02	Ben	*Vrn1-B1*
DTH	*QEet.fcu-2B*	2B	59.19-59.44	*IWA3868-IWA546*	7.18-13.11	10.31-15.60	PI 41025	*Ppd-B1*
DTH	*QEet.fcu-5A*	5A	126.09	*IWA4805*	10.38-21.57	15.50-25.74	Ben	*Vrn1-A1*
DTH	*QEet.fcu-5B*	5B	116.48-117.03	*IWA6718-Xwmc75*	10.08-25.87	11.49-32.61	Ben	*Vrn1-B1*
PHT	*QHt.fcu-2A*	2A	88.27-90.15	*Xgwm372-IWA2948*	7.50-16.56	8.17-23.17	PI 41025	
PHT	*QHt.fcu-3A*	3A	78.83-79.59	*IWA7541-IWA6914*	8.05-16.00	10.16-19.37	PI 41025	
PHT	*QHt.fcu-5A.1*	5A	47.60-55.04	*IWA1630-IWA300*	4.70-7.60	5.18-9.55	PI 41025	
PHT	*QHt.fcu-5A.2*	5A	125.84	*IWA4276*	3.66-10.59	4.39-11.99	Ben	*Vrn1-A1*
PHT	*QHt.fcu-5B*	5B	117.03-120.80	*Xwmc75-IWA7910*	5.01-13.86	6.11-16.34	Ben	*Vrn1-B1*
KA	*QKa.fcu-1A*	1A	42.97-45.27	*IWA492-IWA4649*	4.40-7.47	6.73-10.73	Ben	
KA	*QKa.fcu-3B*	3B	62.30-64.98	*IWA6201-IWA6017*	8.85-9.45	13.80-14.28	Ben	
KA	*QKa.fcu-4A*	4A	12.53	*IWA7124*	4.65-4.81	6.53-7.39	Ben	
KA	*QKa.fcu-5B*	5B	128.03	*IWA3275*	5.14-9.28	7.92-13.78	Ben	*Vrn1-B1*
KW	*QKw.fcu-1A*	1A	44.01-44.76	*IWA3338-IWA5956*	8.64-8.72	6.82-11.37	Ben	
KW	*QKw.fcu-3B*	3B	70.11-82.91	*IWA8480-IWA1703*	6.22-10.38	7.95-9.97	Ben	
KW	*QKw.fcu-4A*	4A	2.38	*IWA4321*	4.76-13.98	5.98-11.65	Ben	
KW	*QKw.fcu-5A*	5A	153.44-159.26	*Xcfa2155-Xwmc110*	5.13-8.26	6.42-7.93	Ben	*Q*
KW	*QKw.fcu-5B*	5B	120.80-128.03	*IWA7989-IWA3275*	10.47-13.89	8.36-16.44	Ben	*Vrn1-B1*
KW	*QKw.fcu-7A*	7A	92.99	*IWA1456-IWA4584*	8.20-17.12	9.06-17.49	Ben	
KL	*QKl.fcu-1A*	1A	142.80	*IWA3378*	5.10-6.48	7.69-9.99	PI 41025	*ELF3*
KL	*QKl.fcu-2A*	2A	108.70	*IWA240*	5.15-9.71	7.81-15.47	PI 41025	*GNI1-A1*

Table 5.7. Quantitative trait loci associated with the traits evaluated in the Ben × PI 41025 (BP025) recombinant inbred population grown under field conditions and were present in two or more environments (continued).

Trait	QTL	Chromosome	Position (cM)	Marker interval	LOD	$R^2 \times 100$	Donor parent	Putative gene
KL	*QKl.fcu-3A*	3A	172.89	*IWA7099*	3.47-4.00	5.16-5.95	PI 41025	
KL	*QKl.fcu-3B*	3B	94.42-111.28	*IWA2399-IWA3332*	3.83-8.16	7.57-12.83	Ben	
KC	*QKc.fcu-1A*	1A	143.57	*IWA1559-IWA2035*	3.85-8.35	5.72-11.02	PI 41025	*ELF3*
KC	*QKc.fcu-5B*	5B	120.80-128.03	*IWA7989-IWA3275*	3.56-3.73	4.67-5.53	PI 41025	*Vrn1-B1*
KC	*QKc.fcu-7A*	7A	90.92-92.99	*IWA305-IWA4584*	8.17-11.57	11.33-15.87	PI 41025	
KLW	*QKlw.fcu-1A*	1A	142.80-143.57	*IWA3378-IWA2035*	4.56-6.49	6.18-9.87	PI 41025	*ELF3*
KLW	*QKlw.fcu-2A*	2A	108.70	*IWA240*	3.25-6.17	5.09-9.35	PI 41025	*GNI1-A1*
KLW	*QKlw.fcu-5A*	5A	148.22-161.83	*Xbarc319-Xfcp650*	4.33-5.28	6.86-7.23	PI 41025	*Q*
KLW	*QKlw.fcu-7A*	7A	92.74-93.50	*IWA2496-IWA5895*	7.93-12.50	11.20-21.83	PI 41025	

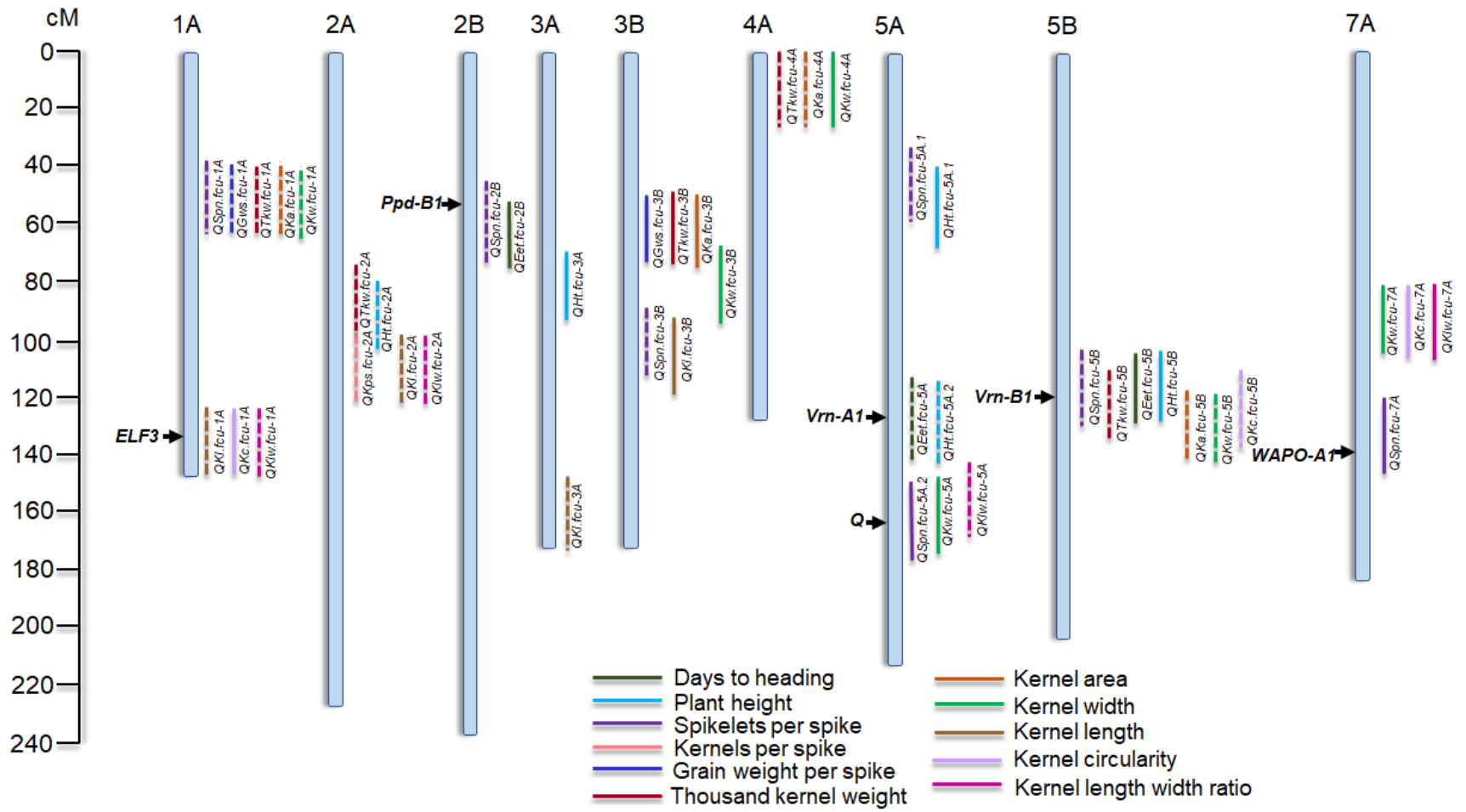

Figure 5.4. Illustration of the chromosomal locations of the 44 quantitative trait loci (QTL) associated with the eleven traits evaluated in the Ben × PI 41025 (BP025) recombinant inbred line population under field conditions. Only those QTL which were identified in two or more environments are illustrated. QTL observed in two environments are illustrated with dashed lines and those in three environments with solid lines. The known positions of the *ELF3*, *Ppd-B1*, *Vrn-A1*, *Q*, *Vrn-B1*, and *WAPO-A1* loci are indicated in black. Chromosomes 1B, 4B, 6A, 6B, and 7B are not shown because not stable QTL were detected on them in this research.

5.4.4. Trait Evaluations in RP883

For the RP883 population, the data for TKW 2018, KW 2018, and PHT 2020 were not homogeneous (Table 5.2) and therefore each replicate were evaluated separately in correlation and QTL analysis; however, I used the overall means for these trait/year combinations to determine the population mean and range (Table 5.8). For DTH, Rusty headed on average 65.56 days post planting whereas PI 193883 headed 46.89 days. The RP883 population mean was 52.54 DTH, with a population range of 46.33 to 67.33 days, 47.00 to 67.67 days, and 44.33 to 59.67 days in 2018, 2019, and 2020, respectively (Table 5.8, Figure 5.5a). Rusty had a higher number of DTH in 2019 than the population maximum, along with a value close to the population maximum in 2018 and 2020. The value for PI 193883 was lower than the population min in 2019, along with being close to the population minimum in 2018 and 2020. These values and ranges indicate that the Rusty is the sole contributor of genetic factors conferring increased number of DTH for the RP883 population.

For PHT, PI 193883 had an average height of 77.39 cm whereas Rusty had an average height that was 113.67 cm, which was 36.28 cm taller than PI 193883 (Table 5.8). The RP883 population mean was 100.13 cm, 104.96 cm, and 84.45 cm in 2018, 2019, and 2020, respectively. The population ranged from 77.00 to 123.00 cm in 2018, 82.00 to 132.00 cm in 2019, and 62.33 to 112.33 cm in 2020 (Table 5.8, Figure 5.5b). This data suggests that both parents are contributing genetic factors leading to increased height within this population.

Mature spikes and seed of Rusty and PI 193883 are presented in Figure 5.6. Rusty had on average 2.32 more SPS than PI 193883, however the only year the two parents were significantly different was 2019 (Table 5.8). The RP883 population had a mean of 18.87 SPS and a range of 15.63 to 23.00 SPS in 2018, a mean of 19.23 and a range of 15.54 to 23.04 SPS in 2019, and a

mean of 18.85 and a range of 15.46 to 29.17 SPS in 2020 (Table 8, Figure 5.5c). This data suggests that Rusty and PI 193883 possess different genes for increased number of spikelets per spike. Mean KPS values for Rusty, PI 193883, and the RP883 population were 32.34, 19.31, and 27.45, respectively (Table 5.8). For all three field seasons, the two parental lines significantly differed for the number of KPS, along with the population range falling below and above the parental values (Table 5.8, Figure 5.5d). This suggests that both Rusty and PI 193883 contribute genetic factors to increased KPS.

For GWS, Rusty had a higher weight than PI 193883 in all three years, however, the difference was not significant in 2019 (Table 5.8). GWS for Rusty widely varied across years, with values of 1.20 g, 0.57 g, and 0.94 g in 2018, 2019, and 2020, respectively. PI 193883 had more consistent values, with means of 0.62 g, 0.44 g, and 0.53 g in 2018, 2019, and 2020, respectively. The RP883 population averaged 0.82 g per spike. The population mean coupled with the population range suggest both Rusty and PI 193883 are contributing to genetic factors for increased spike weight (Table 5.8, Figure 5.5e). Unlike most of the other traits observed for the RP883 population, for TKW Rusty had a greater value than PI 193883 in 2018 with 41.30 g compared to 28.40; however, in 2019 Rusty had a TKW of 16.51 g and 27.91 g in 2020 whereas PI 193883 had a TKW of 22.89 g in 2019 and 30.79 g in 2020 (Table 5.8). The RP883 population mean was 35.49, 23.55, and 29.97 g in 2018, 2019, and 2020, respectively, which was close to or above the highest parental value. The population range fell far below and above the parental values (Table 5.8, Figure 5.5f), indicating that Rusty and PI 193883 possess different genes for kernel weight that results in increased TKW in a subset of the RILs.

For kernel size and shape, Rusty and PI 193883 did not significantly differ for KA 2019, KA 2020, and KL 2019 (Table 5.8). For KA, mean values for Rusty, PI 193883, and the RP883

population were 17.90, 15.93, and 17.83 mm^2 in 2018, 15.15, 14.43, and 15.15 mm^2 in 2019, and 15.90, 16.47, and 16.43 mm^2 in 2020, respectively. The RP883 population ranged from 12.50 to 22.70 mm^2 in 2018, 11.98 to 19.60 mm^2 in 2019, and 13.11 to 21.41 mm^2 in 2020 (Table 5.8, Figure 5.5g). The population range coupled with the parental means suggesting that the two parents both contribute to increased KA. Rusty had wider kernels with a mean of 3.04 mm for KW than PI 193883, which was 2.66 mm (Table 5.8). The RP883 population mean across all three years was 2.89 mm, with a range below and above the parental values (Table 5.8, Figure 5.5h), suggesting both parents contribute to increased KW in this population. For KL, KC, and KLW, PI 193883 had a higher value than Rusty for each of these traits (Table 5.8), with values of 7.34 mm, 1.60 mm, 2.44 mm for Rusty and values of 8.03 mm, 1.83 mm, and 3.01 mm for PI 193883 for KL, KC, and KLW, respectively. The RP883 population mean fell between the two parental lines with values of 7.79 mm, 1.71 mm, and 2.74 mm for KL, KC, and KLW, respectively, with transgressive segregation observed based on the population range (Table 84., Figure 5.5i, j, k). These results suggest that although PI 193883 had a higher value for KL, KC, and KLW, both PI 193883 and Rusty contribute genetic factors controlling these traits in the RP883 population.

Table 5.8. Parental and population means, ranges, and least significant differences (LSD) at the 0.05 level of probability (P<0.05) for the RP883 population grown under field conditions.

Trait[A]	Year[B]	Mean			RP883 population	LSD
		Rusty	PI 193883	RP883 population	range	(0.05)
DTH	2018	66.00	48.33	54.45	46.33-67.33	2.57
DTH	2019	74.00	46.67	53.77	47.00-67.67	4.47
DTH	2020	56.67	45.67	49.41	44.33-59.67	2.06
PHT	2018	116.00	76.50	100.13	77.00-123.00	8.03
PHT	2019	115.33	84.33	104.96	82.00-132.00	11.51
PHT	2020	109.67	71.33	84.45	62.33-112.33	12.16
SPS	2018	18.08	17.71	18.87	15.63-23.00	0.94
SPS	2019	19.50	16.25	19.23	15.54-23.04	1.04
SPS	2020	20.67	17.33	18.85	15.46-29.17	4.08
KPS	2018	29.17	21.96	28.38	11.67-42.44	5.46
KPS	2019	34.38	18.92	28.55	16.63-41.25	7.13
KPS	2020	33.46	17.04	25.41	12.08-38.71	5.75
GWS	2018	1.20	0.62	1.01	0.41-1.93	0.32
GWS	2019	0.57	0.44	0.68	0.30-1.21	0.28
GWS	2020	0.94	0.53	0.76	0.32-1.25	0.28
TKW	2018	41.30	28.40	35.49	18.81-54.14	8.30
TKW	2019	16.51	22.89	23.55	12.16-42.11	6.42
TKW	2020	27.91	30.79	29.97	18.29-49.41	7.14
KA	2018	17.90	15.93	17.38	12.50-22.70	1.79
KA	2019	15.15	14.43	15.15	11.98-19.60	2.19
KA	2020	15.90	16.47	16.43	13.11-21.41	1.79
KW	2018	3.27	2.73	3.01	2.46-3.51	0.20
KW	2019	2.85	2.57	2.78	2.35-3.33	0.27
KW	2020	3.00	2.67	2.87	2.37-3.35	0.20
KL	2018	7.43	8.00	7.97	6.80-9.10	0.37
KL	2019	7.35	7.80	7.56	6.62-8.49	0.52
KL	2020	7.23	8.30	7.83	6.61-9.08	0.37
KC	2018	1.50	1.80	1.67	1.40-1.90	0.07
KC	2019	1.70	1.87	1.74	1.55-1.94	0.12
KC	2020	1.60	1.83	1.71	1.51-1.97	0.07
KLW	2018	2.30	2.90	2.69	2.20-3.20	0.13
KLW	2019	2.60	3.07	2.76	2.37-3.22	0.24
KLW	2020	2.43	3.07	2.76	2.30-3.31	0.14

[A]Trait abbreviations are: days to heading (DTH), plant height (PHT), spikelets per spike (SPS), kernels per spike (KPS), grain weight per spike (GWS), thousand kernel weight (TKW), kernel area (KA), kernel width (KW), kernel length (KL), kernel circularity (KC), and kernel length:width ratio (KLW).
[B]Each field environment was analyzed separately.

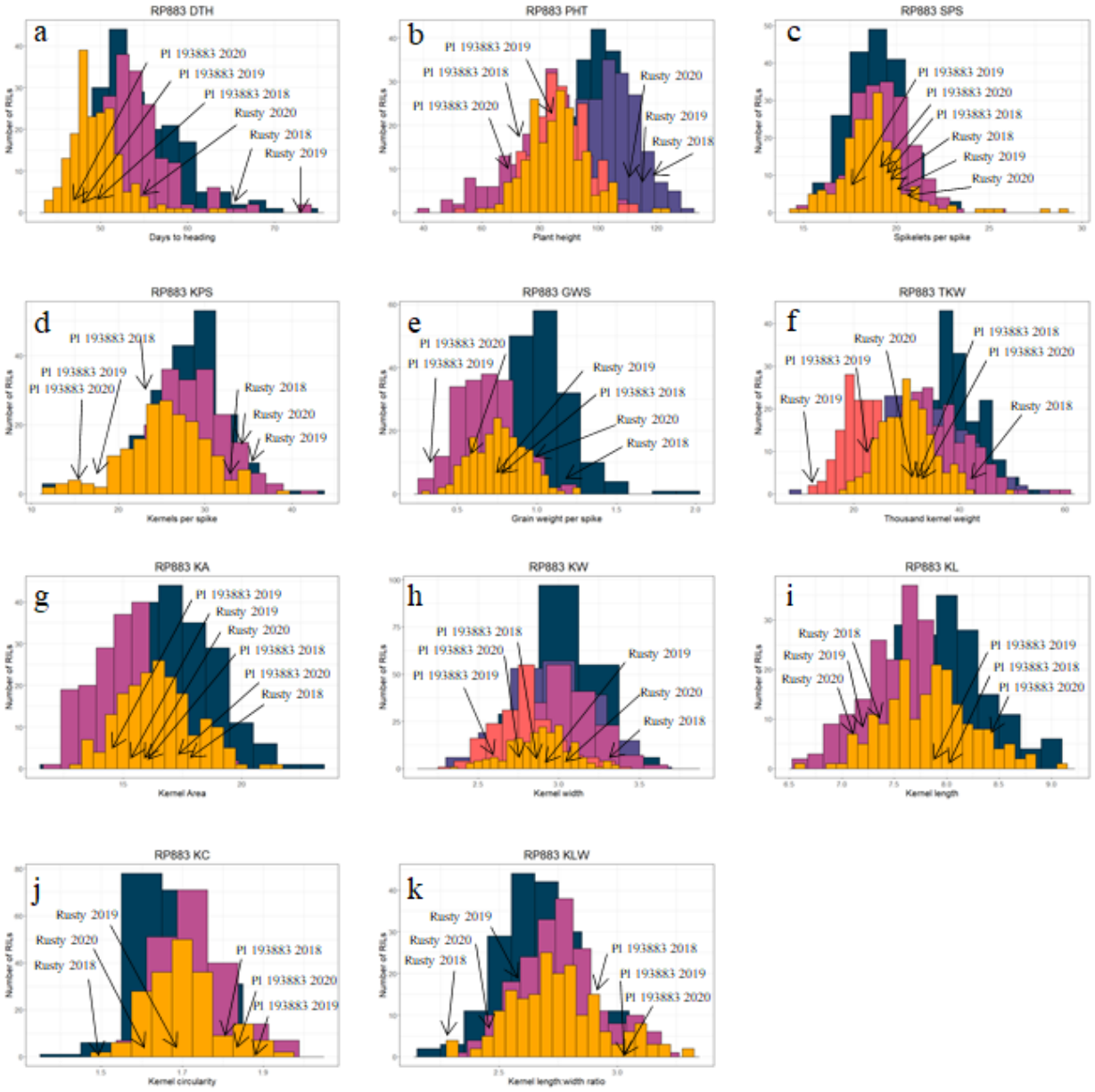

Figure 5.5. Histograms of the RP883 population for the traits a) days to heading (DTH), b) plant height (PHT), c) spikelets per spike (SPS), d) kernels per spike (KPS), e) grain weight per spike (GWS), f) thousand kernel weight (TKW), g) kernel area (KA), h) kernel weight (KW), i) kernel length (KL), j) kernel circularity (KC), k) kernel length:width ratio (KLW). For panels a, b, c, e, g, i, j, and k, values in blue are from the 2018 environment, pink from 2019, and yellow from 2020. For TKW, PHT, and KW, not all replicates were homogenous and therefor the data was not combined. For panel d, the three 2018 TKW replicates were dark blue, purple, and dark pink, with 2019 in coral and 2020 in yellow. For panel f, 2018 was dark blue, purple was 2019, and three 2020 replicates were dark pink, coral and yellow. For panel h, the three 2018 KW replicates were dark blue, purple, and dark pink, with 2019 in coral and 2020 in yellow.

Figure 5.6. Spike and seed morphology of Rusty and PI 193883, the two parental lines of the RP883 population. (a) Mature spikes of Rusty (left) and PI 193883 (right). (b) seed of the durum variety Rusty (top) and the cultivated emmer wheat accession PI 193883 (bottom).

5.4.5. Correlations in RP883

Correlations for the RP883 population between all the traits are shown in Figure 5.7, along with the correlation coefficient values given in Tables 5.9, 5.10, and 5.11. For each trait, there was a strong positive correlation across years (Figure 5.7), suggesting that these traits are consistent across environments. SPS had a strong, consistent positive correlation with KPS and DTH across all three years (Tables 5.9, 5.10, 5.11, Figure 5.7), with a strong correlation with GWS in 2018 (Table 5.9, Figure 5.7) and a weaker positive correlation with GWS in 2019 and 2020 (Tables 5.10, 5.11, Figure 5.7). KPS had a strong positive correlation with GWS across all three environments (Tables 5.9, 5.10, 5.11, Figure 5.7), along with a significant positive correlation with KLW. KPS also was significantly correlated with other traits, however these correlations were not consistent across environments.

In all three environments, GWS had a strong positive correlation with TKW, PHT, KA, KW, and KL (Tables 5.9, 5.10, 5.11, Figure 5.7). In 2019, GWS had a strong negative correlation with KC and KLW (Table 5.10, Figure 5.7). Interestingly, TKW also had a strong negative correlation with KC and KLW in 2019, along with 2018 (TKWrep2 and TKWrep3) and 2020 (Tables 5.9, 5.11, Figure 5.7). TKW had a strong positive correlation with PHT, KA, KW, and KL in 2018, 2019, and 2020 (Tables 5.9, 5.10, 5.11, Figure 5.7). DTH only had consistent significant correlations with PHT and KW, which ranged from weakly positive to strong. However, DTH had a significant negative correlation with KC in 2018 and 2020 and KLW in 2018, 2019, and 2020. As for PHT, weak to strong positive correlations were observed with KA, KW, and KL across all three environments.

For the kernel dimension traits, strong significant correlations were observed across all three environments between traits except for KA with KC and KLW in 2018 (Tables 5.9, 5.10,

5.11, Figure 5.7). KA was positively correlated with KW and KL all three environments and was negatively correlated with KC and KLW in 2019 and 2020. KW reps were analyzed separately in 2018 and consistent correlations were observed for the three replicates (Table 5.9, Figure 5.7). KW had a strong positive correlation with KL, and a strong negative correlation with KC and KLW. Across all three environments, KL, KC, and KLW all had strong positive correlations with one another (Tables 5.9, 5.10, 5.11, Figure 5.7).

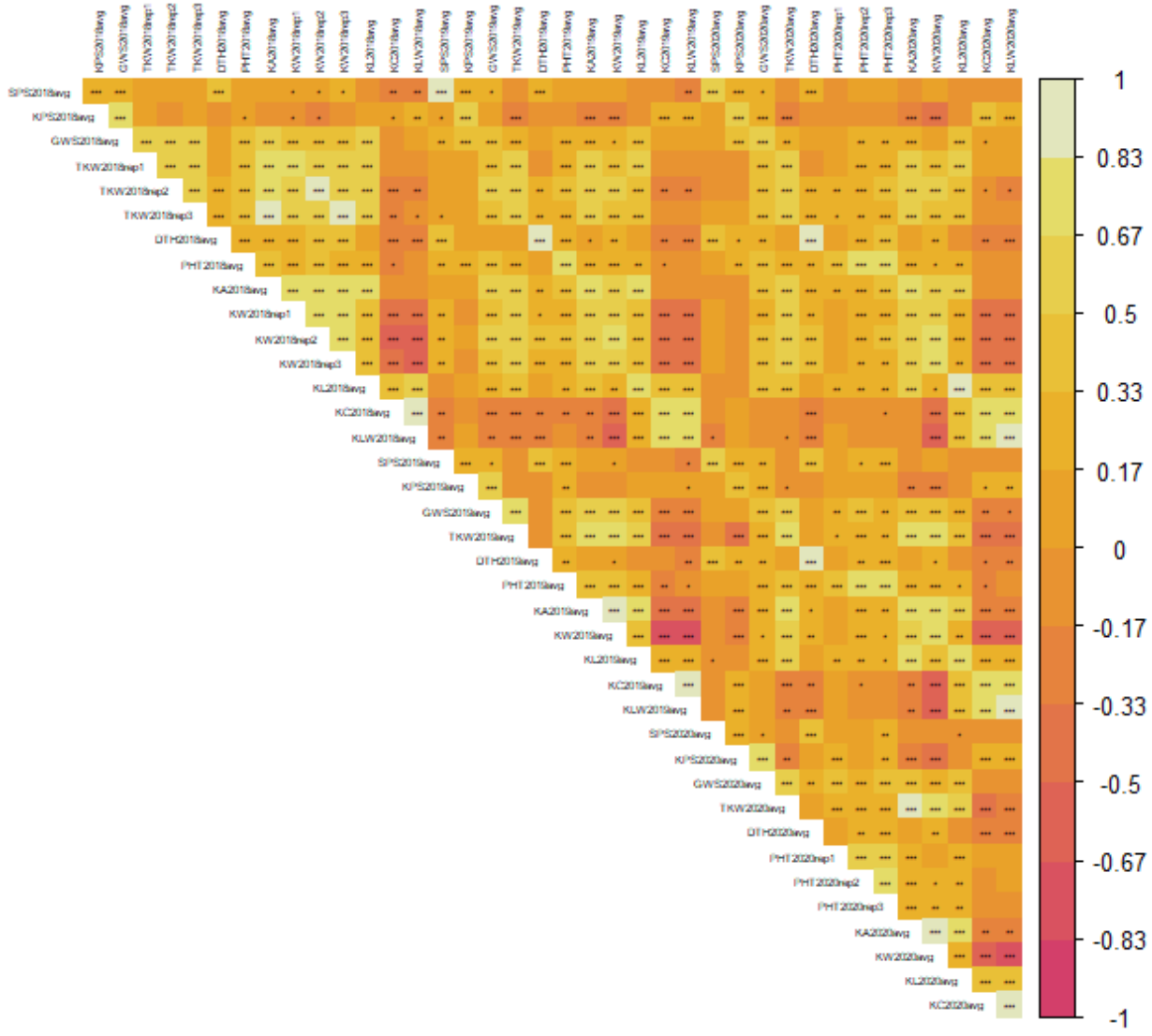

Figure 5.7. Pearson correlation coefficients between the 11 traits measured in the RP883 population grown under field conditions in 2018, 2019, and 2020. Trait abbreviations are: days to heading (DTH), plant height (PHT), spikelets per spike (SPS), kernels per spike (KPS), grain weight per spike (GWS), thousand kernel weight (TKW), kernel area (KA), kernel width (KW), kernel length (KL), kernel circularity (KC), and kernel leght:width ratio (KLW). For TKW and KW in 2018, and PHT in 2020 the replicates were not combined because they were not statistically homogeneous. Significance values are denoted as *P<0.05, **P<0.01, ***P<0.001. Along the right is a color scale for the correlation values. Blocks that are orange to pink have a negative correlation, with dark pink being a correlation close to -1. Blocks that are orange to light yellow have a positive correlation, with light yellow being a correlation close to 1. Significance values are denoted as *P<0.05, **P<0.01, ***P<0.001.

Table 5.9. Correlation coefficients for the RP883 population grown under field conditions in 2018 between the mean values of the traits days to heading (DTH), plant height (PHT), spikelets per spike (SPS), kernels per spike (KPS), grain weight per spike (GWS), thousand kernel weight (TKW), kernel area (KA), kernel width (KW), kernel length (KL), kernel circularity (KC), and kernel length:width ratio (KLW).

	SPSavg	KPSavg	GWSavg	TKWrep1	TKWrep2	TKWrep3	DTHavg	PHTavg	KAavg	KWrep1	KWrep2	KWrep3	KLavg	KCavg	KLWavg
SPSavg	1.00														
KPSavg	0.25***	1.00													
GWSavg	0.24***	0.69***	1.00												
TKWrep1	0.04	0.03	0.59***	1.00											
TKWrep2	0.07	-0.05	0.58***	0.55***	1.00										
TKWrep3	0.10	0.03	0.66***	0.61***	0.62***	1.00									
DTHavg	0.36***	-0.14	0.10	0.04	0.30***	0.31***	1.00								
PHTavg	0.11	0.15*	0.41***	0.35***	0.39***	0.34***	0.24***	1.00							
KAavg	0.05	-0.06	0.63***	0.80***	0.79***	0.83***	0.28***	0.41***	1.00						
KWrep1	0.15*	-0.15*	0.42***	0.82***	0.54***	0.55***	0.24***	0.31***	0.73***	1.00					
KWrep2	0.16*	-0.17*	0.46***	0.51***	0.90***	0.61***	0.42***	0.36***	0.77***	0.69***	1.00				
KWrep3	0.18*	-0.13	0.49***	0.54***	0.61***	0.87***	0.40***	0.30***	0.78***	0.71***	0.75***	1.00			
KLavg	-0.07	0.06	0.53***	0.64***	0.52***	0.62***	0.07	0.28***	0.81***	0.33***	0.35***	0.37***	1.00		
KCavg	-0.20**	0.16*	-0.07	-0.09	-0.28***	-0.21**	-0.27***	-0.17*	-0.10	-0.47***	-0.51***	-0.49***	0.45***	1.00	
KLWavg	-0.24**	0.21**	0.01	-0.05	-0.24**	-0.14*	-0.31***	-0.07	-0.05	-0.50***	-0.52***	-0.50***	0.52***	0.89***	1.00

*P<0.05
**P<0.01
***P<0.001

Table 5.10. Correlation coefficients for the RP883 population grown under field conditions in 2019 between the mean values of the traits days to heading (DTH), plant height (PHT), spikelets per spike (SPS), kernels per spike (KPS), grain weight per spike (GWS), thousand kernel weight (TKW), kernel area (KA), kernel width (KW), kernel length (KL), kernel circularity (KC), and kernel length:width ratio (KLW).

	SPSavg	KPSavg	GWSavg	TKWavg	DTHavg	PHTavg	KAavg	KWavg	KLavg	KCavg	KLWavg
SPSavg	1.00										
KPSavg	0.31***	1.00									
GWSavg	0.18*	0.54***	1.00								
TKWavg	-0.01	-0.01	0.83***	1.00							
DTHavg	0.45***	-0.04	-0.02	-0.03	1.00						
PHTavg	0.25***	0.23**	0.44***	0.38***	0.19**	1.00					
KAavg	0.07	-0.08	0.63***	0.81***	0.09	0.40***	1.00				
KWavg	0.15*	-0.13	0.57***	0.76***	0.16*	0.36***	0.91***	1.00			
KLavg	-0.02	0.01	0.48***	0.58***	-0.02	0.29***	0.78***	0.47***	1.00		
KCavg	-0.10	0.14	-0.29***	-0.43***	-0.14	-0.22**	-0.40***	-0.70***	0.25***	1.00	
KLWavg	-0.18*	0.15*	-0.24***	-0.37***	-0.20**	-0.17*	-0.38***	-0.72***	0.27***	0.97***	1.00

*P<0.05
**P<0.01
***P<0.001

Table 5.11. Correlation coefficients for the RP883 population grown under field conditions in 2020 between the mean values of the traits days to heading (DTH), plant height (PHT), spikelets per spike (SPS), kernels per spike (KPS), grain weight per spike (GWS), thousand kernel weight (TKW), kernel area (KA), kernel width (KW), kernel length (KL), kernel circularity (KC), and kernel length:width ratio (KLW).

	SPSavg	KPSavg	GWSavg	TKWavg	DTHavg	PHTrep1[A]	PHTrep2[A]	PHTrep3[A]	KAavg	KWavg	KLavg	KCavg	KLWavg
SPSavg	1.00												
KPSavg	0.24***	1.00											
GWSavg	0.14*	0.70***	1.00										
TKWavg	-0.10	-0.23**	0.52***	1.00									
DTHavg	0.35***	0.13	0.19**	0.07	1.00								
PHTrep1[A]	0.10	0.31***	0.46***	0.28***	0.11	1.00							
PHTrep2[A]	0.11	0.11	0.31***	0.30***	0.24**	0.57***	1.00						
PHTrep3[A]	0.21**	0.20**	0.42***	0.32***	0.30***	0.53***	0.75***	1.00					
KAavg	-0.10	-0.29***	0.42***	0.93***	0.08	0.25***	0.27***	0.29***	1.00				
KWavg	-0.01	-0.33***	0.31***	0.83***	0.22**	0.12	0.18*	0.21**	0.85***	1.00			
KLavg	-0.14*	-0.07	0.39***	0.62***	-0.10	0.27***	0.23***	0.22**	0.75***	0.32***	1.00		
KCavg	-0.05	0.24***	-0.05	-0.35***	-0.24***	0.03	-0.07	-0.10	-0.21**	-0.65***	0.47***	1.00	
KLWavg	-0.10	0.24***	-0.02	-0.31***	-0.29***	0.09	0.00	-0.03	-0.22**	-0.69***	0.46***	0.97***	1.00

*P<0.05
**P<0.01
***P<0.001
[A]For PHT, replicates were not statistically homogeneous and therefore were analyzed separately.

5.4.6. QTL Analysis in RP883

Between the three field seasons for the RP883 population, I identified 149 significant QTL and QTL×QTL interactions using forward/backward selection to identify the QTL model with the highest LOD score (Supplementary File 3). Within individual environments, 64, 38, and 47 QTL were identified in 2018, 2019, and 2020, respectively.

A total of 17 QTL were observed to be present in two environments, and 17 QTL were observed in all three environments (Table 5.12, Figure 5.8, Supplementary File 3). A total of 14 genomic regions were associated with these 34 QTL. No QTL × QTL interactions were found to be consistent across environments.

Two QTL were associated with SPS in two or more environments. These QTL, *QSpn.fcu-5A* and *QSpn.fcu-6B*, were mapped to chromosome 5A and 6B (Table 5.12, Figure 5.8). The peak marker for *QSpn.fcu-5A* was *Xfcp650*, the diagnostic marker for *Q,* and *QSpn.fcu-5A* was the only QTL for SPS observed in all three environments. *QSpn.fcu-5A* and *QSpn.fcu-6B* had maximum LOD values of 12.99 and 12.73 and explained up to 16.28 and 15.91% of the variation in SPS, respectively. Rusty contributed the alleles to increased SPS at both QTL.

Only one QTL was significantly associated with KPS in three environments (Table 5.12, Figure 5.8). This QTL, *QKps.fcu-2B*, was mapped on chromosome 2B and had a maximum LOD of 5.22 and explained as much as 11.88% of the variation in KPS. Rusty contributed the positive allele at this QTL.

As with KPS, only one stable QTL for GWS was identified in the RP883 population in two environments. *QGws.fcu-1B* was mapped on chromosome 1B (Table 5.12, Figure 5.8), and had a maximum LOD of 5.63 and explained as much as 12.03% of the variation in GWS. As with the KPS QTL, Rusty contributed the positive allele at *QGws.fcu-1B*.

For TKW, four QTL were identified in two or more environments. These QTL were mapped on chromosomes 3A, 4A, and 5A and designated *QTkw.fcu-3A*, *QTkw.fcu-4A*, *QTkw.fcu-5A.1*, and *QTkw.fcu-5A.2* (Table 5.12, Figure 5.8). Only *QTkw.fcu-3A* was identified in all three environments. The two QTL on chromosome 5A, *QTkw.fcu-5A.1* and *QTkw.fcu-5A.2*, were within the genomic regions of *Vrn1-A1* and *Vrn2*. *QTkw.fcu-3A*, *QTkw.fcu-4A*, *QTkw.fcu-5A.1*, and *QTkw.fcu-5A.2* had maximum LOD values of 6.54, 5.51, 10.55, and 8.69 and explained up to 9.89, 6.99, 10.55, and 8.69% of the variation in TKW, respectively. PI 193883 alleles contributed to increased TKW at *QTkw.fcu-3A* and *QTkw.fcu-5A.2*, whereas Rusty was the donor parent at *QTkw.fcu-4A* and *QTkw.fcu-5A.1*.

Six stable QTL were associated with DTH in the RP883 population. These QTL mapped to chromosomes 1A, 4B, 5A, and 7B and were designated *QEet.fcu-1A*, *QEet.fcu-4B*, *QEet.fcu-5A.1*, *QEet.fcu-5A.2*, *QEet.fcu-5A.3*, and *QEet.fcu-7B* (Table 5.12, Figure 5.8). All but *QEet.fcu-4B* were within the genomic regions of known genes, along with *QEet.fcu-4B* was the only QTL listed that was observed under two, rather than three, environments. *QEet.fcu-1A, QEet.fcu-5A.1*, *QEet.fcu-5A.2*, *QEet.fcu-5A.3*, and *QEet.fcu-7B* were near *ELF3*, *Vrn1-A1*, *Q*, *Vrn2*, and *FT-1*, respectively. *QEet.fcu-1A*, *QEet.fcu-4B*, *QEet.fcu-5A.1*, *QEet.fcu-5A.2*, *QEet.fcu-5A.3*, and *QEet.fcu-7B* had maximum LOD values of 20.39, 7.97, 34.55, 9.50, 12.61, and 24.58 and explained up to 14.31, 4.51, 27.72, 9.50, 7.56, and 17.23% of the variation in DTH, respectively. Rusty was the donor of alleles for increased DTH at each QTL except *QEet.fcu-5A.3*.

For PHT, three stable QTL were identified and mapped on chromosomes 1B, 4A, and 7B in the RP883 population. These QTL, *QHt.fcu-1B*, *QHt.fcu-4A*, and *QHt.fcu-7B*, had maximum LOD values of 10.78, 8.64, and 4.33 and explained up to 15.04, 16.96, and 6.59% of the variation in PHT, respectively (Table 5.12, Figure 5.8). *QHt.fcu-1B* and *QHt.fcu-4A* were both

observed in all three environments. Only *QHt.fcu-7B* was associated with a known gene (*FT-1*). Rusty contributed the alleles at all three QTL for increased PHT.

A total of four stable QTL were identified for KA in the RP883 population. These QTL, designated *QKa.fcu-1B*, *QKa.fcu-3A*, *QKa.fcu-4A*, and *QKa.fcu-5A* were mapped on chromosomes 1B, 3A, 4A, and 5A (Table 5.12, Figure 5.8). *QKa.fcu-5A* was within the *Vrn1-A1* gene region. *QKa.fcu-1B*, *QKa.fcu-3A*, *QKa.fcu-4A*, and *QKa.fcu-5A* had maximum LOD values of 13.38, 9.49, 5.33, and 8.41 and explained as much as 13.28, 12.28, 6.86, and 10.60% of the variation in KA, respectively. Rusty contributed the alleles at all the QTL except *QKa.fcu-3A*, in which PI 193883 was the donor.

For KW, the RP883 population had four QTL significant in two or more environments. These QTL were mapped on chromosomes 2B, 4B, and 5A and were designated *QKw.fcu-2B*, *QKw.fcu-4B*, *QKw.fcu-5A.1*, and *QKw.fcu-5A.2* (Table 5.12, Figure 5.8). Both QTL on chromosome 5A were identified in all three environments. *QKw.fcu-5A.1* was within the *Vrn1-A1* region on 5A. *QKw.fcu-2B*, *QKw.fcu-4B*, *QKw.fcu-5A.1*, and *QKw.fcu-5A.2* had maximum LOD values of 11.93, 5.32, 8.10, and 12.15 and explained up to 14.93, 7.36, 16.19, and 15.24% of the variation in KW, respectively. PI 193883 contributed the increased KW effects at *QKw.fcu-2B*, whereas Rusty was the donor parent at the other three QTL.

Three stable QTL were identified to be associated with KL. *QKl.fcu-2A*, *QKl.fcu-3A.1*, and *QKl.fcu-3A.2* mapped to chromosomes 2A and 3A (Table 5.12, Figure 5.8). *QKl.fcu-2A* and *QKl.fcu-3A.1* were identified in all three environments. *QKl.fcu-2A*, *QKl.fcu-3A.1*, and *QKl.fcu-3A.2* had maximum LOD values of 7.20, 10.03, and 5.66 and explained as much as 11.24, 16.21, and 8.66% of the variation in KL, respectively. PI 193883 was the donor parent of increased effects at all three QTL.

For KC, three stable QTL were identified in the RP883 population. These QTL were present on chromosomes 2B, 5A, and 6B and were designated *QKc.fcu-2B*, *QKc.fcu-5A*, and *QKc.fcu-6B* (Table 5.12, Figure 5.8). Only *QKc.fcu-5A* was observed in all three environments and was mapped near the *Q* region. *QKc.fcu-2B*, *QKc.fcu-5A*, and *QKc.fcu-6B* had maximum LOD values of 6.61, 7.06, and 8.52 and explained as much as 11.27, 11.15, and 15.31% of the variation in KC, respectively. Rusty contributed the increased effects for *QKc.fcu-2B*, whereas PI 193883 did for *QKc.fcu-5A* and *QKc.fcu-6B*.

Lastly, three QTL were also identified for KLW in the RP883 population. These QTL were present on chromosomes 2B, 5A, and 6B, like for KC, and were designated *QKlw.fcu-2B*, *QKlw.fcu-5A*, and *QKlw.fcu-6B* (Table 5.12, Figure 5.8). Of these QTL, only *QKlw.fcu-2B* was not observed in all three environments. *QKlw.fcu-5A* mapped near the *Q* region. *QKlw.fcu-2B*, *QKlw.fcu-5A*, and *QKlw.fcu-6B* had maximum LOD values of 6.19, 9.33, and 10.24 and explained as much as 9.83, 17.51, and 15.03% of the variation in KLW, respectively. Rusty contributed the increased effects for *QKlw.fcu-2B*, whereas PI 193883 did for *QKlw.fcu-5A* and *QKlw.fcu-6B*.

Table 5.12. Quantitative trait loci associated with the traits evaluated in the Rusty × PI 193883 (RP883) recombinant inbred population grown under field conditions and were present in two or more environments.

Trait	QTL	Chromosome	Position (cM)	Peak marker	LOD	$R^2 \times 100$	Donor parent	Putative gene
SPS	*QSpn.fcu-5A*	5A	169.50	*Xfcp650*	3.35-12.99	7.06-16.28	Rusty	*Q*
SPS	*QSpn.fcu-6B*	6B	65.96	*Xwmc756*	8.72-12.73	14.87-15.91	Rusty	
KPS	*QKps.fcu-2B*	2B	68.62-78.11	*IWB8102-IWB55767*	5.13-5.22	10.50-11.88	Rusty	
GWS	*QGws.fcu-1B*	1B	46.44-51.35	*IWB60559-IWB80169*	5.29-5.63	11.71-12.03	Rusty	
TKW	*QTkw.fcu-3A*	3A	72.52-89.40	*IWB79897-IWB69427*	4.24-6.54	5.29-9.89	PI 193883	
TKW	*QTkw.fcu-4A*	4A	60.60-87.24	*IWB32896-IWB35060*	4.49-5.51	6.63-6.99	Rusty	
TKW	*QTkw.fcu-5A.1*	5A	140.98-152.41	*IWB38320-IWB77935*	4.60-5.65	7.28-10.55	Rusty	*Vrn1-A1*
TKW	*QTkw.fcu-5A.2*	5A	205.19-206.08	*Xgwm291-IWB60850*	4.53-6.75	6.68-8.69	PI 193883	*Vrn2*
DTH	*QEet.fcu-1A*	1A	154.06	*IWB35476*	7.21-20.39	10.23-14.31	Rusty	*ELF3*
DTH	*QEet.fcu-4B*	4B	28.85	*IWB62043*	4.58-7.97	4.32-4.51	Rusty	
DTH	*QEet.fcu-5A.1*	5A	133.26	*IWB56489*	7.00-34.55	7.89-27.72	Rusty	*Vrn1-A1*
DTH	*QEet.fcu-5A.2*	5A	169.50-173.78	*Xfcp650-IWB34731*	6.17-9.50	4.35-9.50	Rusty	*Q*
DTH	*QEet.fcu-5A.3*	5A	204.06-205.19	*IWB65661-Xgwm291*	3.57-12.61	4.85-7.56	PI 193883	*Vrn2*
DTH	*QEet.fcu-7B*	7B	8.47	*IWB3164*	6.45-24.58	8.60-17.23	Rusty	*FT-1*
PHT	*QHt.fcu-1B*	1B	54.66	*IWB79935*	3.73-10.78	7.57-15.04	Rusty	
PHT	*QHt.fcu-4A*	4A	63.29-65.71	*IWB57309-IWB77157*	5.15-8.64	6.70-16.96	Rusty	
PHT	*QHt.fcu-7B*	7B	0.00-0.27	*IWB54418-IWB46416*	3.90-4.33	5.57-6.59	Rusty	*FT-1*
KA	*QKa.fcu-1B*	1B	51.08-52.73	*IWB12387-IWB58936*	3.58-13.38	4.51-13.28	Rusty	
KA	*QKa.fcu-3A*	3A	67.23-68.32	*IWB67595-IWB68071*	9.10-9.49	8.96-12.28	PI 193883	
KA	*QKa.fcu-4A*	4A	62.22-63.29	*IWB47489-IWB57309*	3.61-5.33	6.58-6.86	Rusty	
KA	*QKa.fcu-5A*	5A	132.99-140.98	*IWB36340-IWB38320*	5.67-8.41	7.84-10.60	Rusty	*Vrn1-A1*
KW	*QKw.fcu-2B*	2B	73.49-78.11	*IWB65409-IWB55767*	6.95-11.93	10.96-14.93	PI 193883	
KW	*QKw.fcu-4B*	4B	97.81	*IWB76600*	4.70-5.32	7.21-7.36	Rusty	
KW	*QKw.fcu-5A.1*	5A	132.99-136.80	*IWB36340-IWB76977*	3.43-8.10	8.01-16.19	Rusty	*Vrn1-A1*
KW	*QKw.fcu-5A.2*	5A	151.59-152.41	*IWB10765-IWB77935*	4.73-12.15	6.50-15.24	Rusty	
KL	*QKl.fcu-2A*	2A	132.920135.67	*IWB32430-IWB81441*	4.14-7.20	7.86-11.24	PI 193883	
KL	*QKl.fcu-3A.1*	3A	68.32-69.72	*IWB68071-IWB72601*	6.24-10.03	11.76-16.21	PI 193883	
KL	*QKl.fcu-3A.2*	3A	168.14-172.45	*IWB52090-IWB11837*	3.62-5.66	6.83-8.66	PI 193883	
KC	*QKc.fcu-2B*	2B	74.30-81.27	*IWB65533-IWB73000*	4.82-6.61	8.42-11.27	Rusty	
KC	*QKc.fcu-5A*	5A	152.41-159.64	*IWB77935-IWB73761*	4.28-7.06	7.42-11.15	PI 193883	
KC	*QKc.fcu-6B*	6B	63.45-67.89	*IWB6601-IWB79198*	8.39-8.52	14.86-15.31	PI 193883	
KLW	*QKlw.fcu-2B*	2B	74.30-81.27	*IWB65533-IWB73000*	4.42-6.19	6.04-9.83	Rusty	
KLW	*QKlw.fcu-5A*	5A	152.41-183.50	*IWB77935-IWB10029*	4.24-9.33	5.78-17.51	PI 193883	*Q*
KLW	*QKlw.fcu-6B*	6B	63.45-67.89	*IWB6601-IWB79198*	7.95-10.24	14.51-15.03	PI 193883	

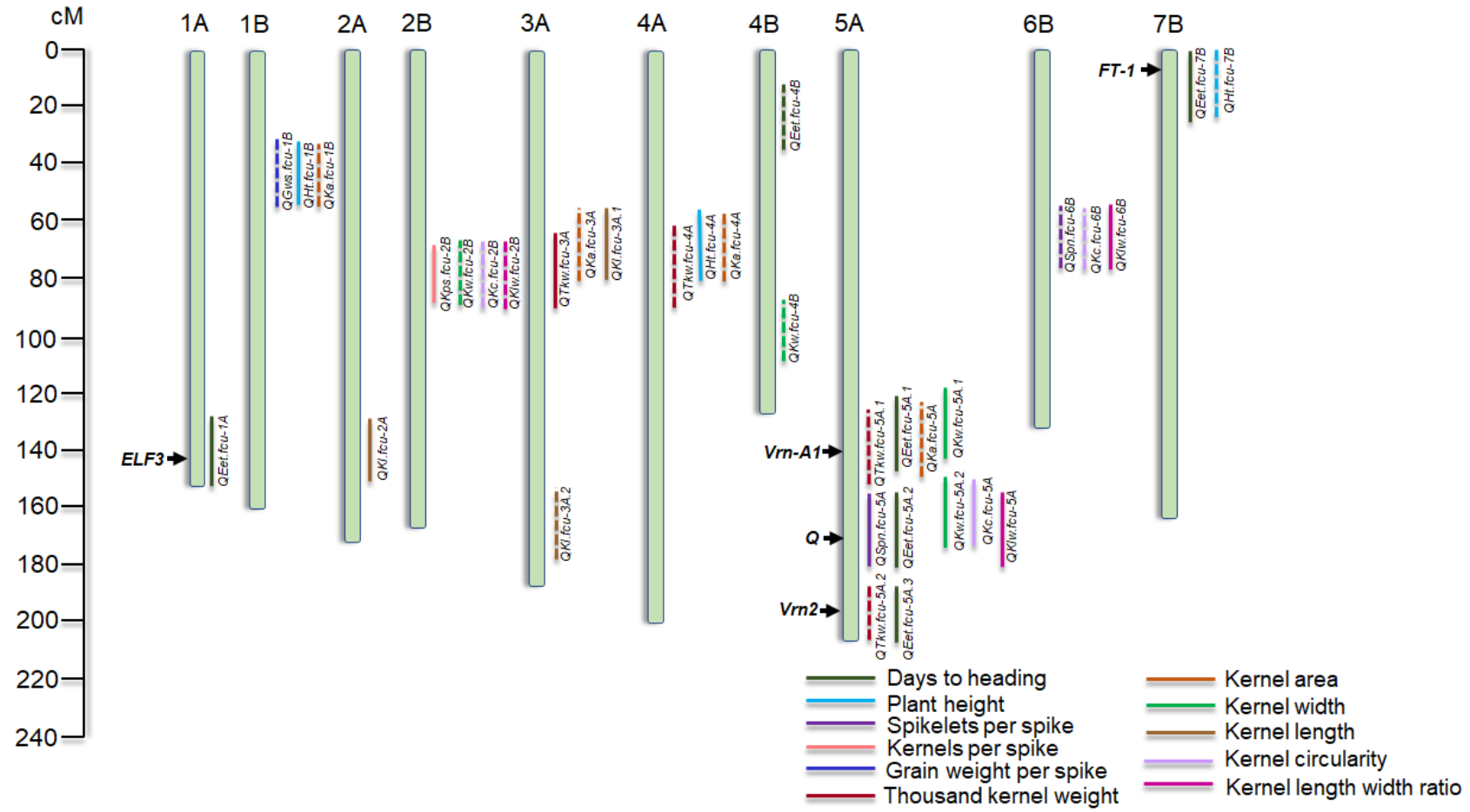

Figure 5.8. Illustration of the chromosomal locations of the 34 quantitative trait loci (QTL) associated with the eleven traits evaluated in the Rusty × PI 193883 (RP883) recombinant inbred line population under field conditions. Only those QTL which were identified in two or more environments are illustrated. QTL observed in two environments are illustrated with dashed lines and those in three environments with solid lines. The known positions of the *ELF3*, *Vrn-A1*, *Q*, *Vrn2*, and *FT-1* loci are indicated in black. Chromosomes 3B, 5B, 6A, and 7A are not shown because not stable QTL were detected on them in this research.

5.5. Discussion

5.5.1. Trade-offs Between Yield Component Traits

In this study, I calculated the correlations between the eleven traits measured. For the sake of our interest, although PHT and DTH are correlated with multiple yield component traits, it has already extensively shown that there are correlations between DTH and PHT with these traits (Cao et al. 2020). In all but one environment/population combination, the number of SPS was positively correlated with the number of KPS and overall GWS. This was consistent with the findings for the BP025 population when grown under greenhouse conditions (Faris et al. 2014), whereas Sharma et al. (2019a) did not measure grain weight and KPS for the RP883 population in the greenhouse. Consistently, I observed in both populations when the number of KPS increased, overall GWS increased but individual kernel weight, measured as TKW, had no correlation or a negative correlation with the number of KPS. These findings have been previously observed in other studies (as reviewed by Brinton and Uauy 2018; Cao et al. 2020), along with my findings in the DP527 paper, as discussed in chapter 4. As the number of KPS increases, source limitations often cause the plant to reduce kernel size and weight, therefore decreasing TKW. This has been an obstacle when breeding for increased yield when balancing the trade-offs that occur under source limited situations (Brinton and Uauy 2018).

A large focus of this study was identifying regions of the genome associated with kernel size traits, along with how kernel size is correlated with different yield component traits. To my knowledge, relatively few studies have evaluated the relationship between kernel number and size, with most focusing on kernel number and weight. In this study, I observed either no correlation or a negative correlation between the number of KPS and KA, KW, and KL under field conditions in both populations. However, in the RP883 population, a positive correlation

was observed between KPS and KC and KLW. Corsi et al. (2021) observed a negative to no correlation between KPS and kernel size traits, implying that as the spike produces more kernels, resources are limited, and kernel size is reduced (Brinton and Uauy 2018). Additionally, these results are consistent with the findings in the DP527 population, as discussed in Chapter 4.

In general, I observed that there was a positive correlation between the kernel size components KA, KW, and KL with kernel weight (both GWS and TKW). However, I observed a negative to no correlation between kernel weight with KC and KLW. These findings are consisted with those of Sun et al. (2020), Corsi et al. (2021) and the DP527 population (Chapter 4). As reviewed by Brinton and Uauy (2018), there are mechanical and physical forces and constraints that influence final kernel size, along with complex interactions occurring during the development phase. Based on our observations, I suggest that when selecting for increased kernel weight, the kernel size traits KA and KW are useful physical markers to use when selecting lines for increased kernel weight, especially when the sample size is too small to obtain accurate TKW values.

Lastly, my findings for relationships between the various kernel size components were consistent with those by Sun et al. (2020), Corsi et al. (2021), and in the DP527 population discussed in Chapter 4. KA and KW are described as kernel size traits, whereas KL, KC, and KLW are grain shape traits (Gegas et al. 2010). In each population/environment combinations in this study, KA was always positively correlated with KW and KL, but had no to a negative correlation with KC and KLW. Therefore, measuring just KW or KL may be useful for indicating KA in situations that KA cannot be measured. Interestingly, I found, along with the other two studies, that KL, KC, and KLW were always positively correlated, and KW and KL were positively correlated, but KW was not correlated with KLW. Therefore, the KL must have a

larger influence on the KLW ratio than KW. Brinton and Uauy (2018) illustrate that KL reaches its max before the grain filling period, whereas KW does not reach its max until the maturation and desiccation period of grain development. Gegas et al. (2010) found that kernel shape and size are independent traits and are most likely under the influence of different pathways and genes. Potentially, the physiological mechanisms underlying this, along with the developmental difference, may play a factor in the differences among the grain size components and their interactions with one another.

5.5.2. QTL Associated with Multiple Traits in Multiple Environments in the BP025 and RP883 Populations

5.5.2.1. Chromosome 1A

Two multi-trait QTL were identified on chromosome 1A. One was specific to the BP025 population and associated with SPS, GWS, TKW, KA, and KW. Typically, an increase in the number of SPS is associated with an increase in the number of kernels per spike and decreased kernel weight. However, a KPS QTL was not observed at this multi-trait QTL. Faris et al. (2014) reported QTL within this genomic region of the BP025 population under greenhouse conditions for GWS and TKW, but not SPS. Perhaps the underlying genetic and/or physiological mechanisms underlying the SPS phenotype associated with this region is more influenced by environmental factors than GWS and TKW. Cao et al. (2020) reported a region slightly distal to this region as being QTL rich for multiple yield component traits. Although I did not observe a KPS QTL within this region, Hai et al. (2008) reported one, along with Li et al. (2018) reported a QTL for SPS within this region. Gegas et al. (2010) reported a meta-QTL for kernel shape within this region. Although there is a good probability that this genomic region is fixed within the North Dakota Durum breeding germplasm, introgressing this region into other North American

durum lines may be beneficial for increasing yield. Because of the lack of the negative trade-off between the number of SPS and kernel weight/size observed in this region, potentially breeders could use this region to increase SPS without affecting yield. However, although the number of SPS may be increased, the fertility of these spikelets may not increase and therefor may not result in more kernels. Further elucidation is needed to untangle the relationships between these different phenotypes and their usefulness in breeding endeavors.

The second multi-trait QTL observed was on the long arm of chromosome 1A and physically located near the circadian clock regulator gene *ELF3* (Alvarez et al. 2016). *ELF3* is involved in controlling flowering time and an interaction between *ELF3* and temperature has been documented (Ochagavía et al. 2019). In the RP883 population, only one QTL was observed at this locus and was associated with DTH. A DTH QTL was also present under GH conditions at this genetic location (Sharma et al. 2019a). Interestingly, in the BP025 population, a QTL for DTH was not associated with *ELF3*; however, QTL for KL, KC, and KLW were. The presence of these QTL could be due to differences in the number of days to grain filling, with lines having the PI 41025 allele at the *ELF3* locus having an increased number of days for grain filling, resulting in increased kernel shape due to increases in KL, KC, and KLW. The parental lines in both the BP025 and RP883 populations will need to be sequenced to determine if 1) *ELF3* is polymorphic and indeed the gene underlying these QTL and 2) if not, whether there is another gene within this region controlling these traits. Introgressing this QTL region from PI 41025 may not be beneficial to breeders if it significantly increases the number of DTH. However, in the RP883 population, lines with PI 193883 alleles in this region had decreased number of DTH than lines with Rusty alleles, and PI 193883 may be a source for slightly decreasing the number of DTH.

5.5.2.2. Chromosome 1B

A region spanning from 56.67 Mb to 334.67 Mb was associated with QTL for GWS, KA, and PHT in the RP883 population. Based on previous research, PHT is not often associated with increases in GWS and KA, especially when a DTH or SPS QTL is not observed, but major genes controlling PHT have often been reported in close linkage with yield component QTL (Cao et al. 2020). Therefore, I hypothesize that two different loci are within this region, one controlling PHT and the other controlling GWS and KA. To determine if this hypothesis is true, further mapping is needed with a larger population size and additional markers within this region.

5.5.2.3. Chromosome 2A

Within the BP025 population, a region spanning 16.62 cM and 85.18 Mb on chromosome 2A had QTL associated with TKW, KPS, PHT, KL, and KLW. *GNI-A1*, which encodes an HD-Zip I transcription factor, is located within this physical region based on the Svevo reference sequence (Sakuma et al. 2019). Sakuma et al. (2019) found that the level of *GNI1* expression has decreased over the course of wheat domestication, resulting in increased number of fertile florets per spike. Golan et al. (2019) found the GNI-A1 protein to be a transcriptional activator and a reduction in kernel number resulted in enlarged and heavier kernels. In the BP025 population within this region, increased number of KPS was conferred by the Ben alleles, whereas increases in TKW, KL, and KLW were conferred by PI 41025 alleles. These findings are consistent with the relationship between grain number and grain weight at *GNI-A1* reported by Golan et al. (2019) and Sakuma et al. (2019); where a reduction in *GNI-A1* expression, common in domesticated wheat, results in an increase in the fertile number of florets per spike and increased number of KPS but smaller kernel weight/size. The PI 41025 allele of *GNI-A1* may be a strong candidate for introgression into durum germplasm for breeders interested in increasing grain

size/weight; however, further field studies and validation are needed to determine the effects of these QTL and their interactions with one another.

5.5.2.4. Chromosome 2B

Two multi-trait QTL regions were identified on chromosome 2B. The first multi-trait QTL region was in the BP025 population, was associated with SPS and DTH, and the peak markers for each was within 10 Mb of *Ppd-B1*. This QTL was also associated with DTH under greenhouse conditions in this population (Faris et al. 2014). *Ppd* is a component in the photoperiod regulatory flowering pathway (Beales et al. 2007; Nishida et al. 2013) and differences in DTH due to *Ppd-B1* is from copy number variation, with two copies of the gene resulting in earlier DTH (Würschum et al. 2019). Boden et al. (2015) found *Ppd* to be a regulator of *FT*, with increased number of DTH at the *Ppd* locus resulting in a modification of the number and arrangement of spikelets. Surprisingly, I only observed a QTL at *FT* for SPS in Field 2018 within the BP025 population (suppl material). Analysis of copy number between the Ben and PI 41025 is needed to validate if *Ppd-B1* is influencing the number of SPS and DTH within the BP025. However, although PI 41025 alleles within this region led to an increase in the number of SPS, this also resulted in increased number of DTH, which may not be desirable in most durum breeding programs.

The second mulit-trait QTL region on chromosome 2B was observed in the RP883 population and was associated with KPS, KW, KC, and KLW. QTL associated with kernel dimension traits were identified near this physical region by Corsi et al. (2021) and Sun et al. (2020). Surprisingly, there was not any QTL for increased kernel weight (GWS or TKW) in this region, although there was QTL for kernel number and size/shape traits. Within this region, lines with PI 193883 alleles had wider kernels, but lower KPS, KC, and KLW. As has been previously

stated, the number of KPS and kernel size/weight are typically negatively correlated (Brinton and Uauy 2018; Cao et al. 2020). I hypothesis that at the physiological level, having 193883 alleles within this region results in plants with wider grains but does not affect KC and KLW because kernel shape is controlled by a different pathway (Golan et al. 2010). This results in these lines having fewer KPS, which is the reason behind Rusty being the positive parent for KPS at this QTL. From a breeding perspective, lines with certain parental alleles within this region could be used to fine tune the number of KPS or kernel size, depending on what the breeder is interested in.

5.5.2.5. Chromosome 3A

A multi-trait QTL was identified on chromosome 3A to be associated with TKW, KA, and KL in the RP883 population. Under these same field studies, I observed QTL for TKW, PHT, KA, and KL within this physical region in another durum × cultivated emmer population, DP527 (Chapter 4). Sun et al. (2020) also observed QTL within this region for TKW and kernel size. kernel size and weight are normally positively correlated, therefore breeding for one often results in an increase in the other (Brinton and Uauy 2018). The QTL at this locus for TKW and KL were present in all three environments, indicating that these were stable QTL in our experiment and would be good candidates to develop lines with the PI 193883 alleles within this region for germplasm improvement.

5.5.2.6. Chromosome 3B

Two multi-trait QTL associated with five QTL were observed on chromosome 3B in the BP025 population, along with a QTL for KW that spanned between the two multi-trait regions. The first region spanned from 127 Mb to 518 Mb, however the peak markers for most environments were localized within 50 Mb of 150 Mb. The second region spanned form 374 Mb

to 747 Mb, however the genetic distance was less than 10 cM. These two QTL regions could potentially belong to one large, multi-trait QTL; however, further analysis is needed under GH and field conditions to determine this. Interestingly, Faris et al. (2014) observed under greenhouse conditions a QTL for SPS on chromosome 3B near the first multi-trait QTL and QTL for TKW near our second multi-trait QTL in the BP025 population, which is the opposite from what I observed. Peak markers may have shifted due to environmental influences, differences in our QTL analysis methods, along with differences in how the traits were measured. Further work will be needed to untangle if one locus is responsible for all these traits, or if this is a yield component gene rich region. Russo et al. (2014), Sun et al. (2020), and Corsi et al. (2021) all identified QTL for grain size traits near this region on chromosome 3B, suggesting the later may be the more likely scenario.

5.5.2.7. Chromosome 4A

In this study, I identified two multi-trait QTL on chromosome 4A, with one in each population. These two regions, which are located ~55 Mb apart, both had QTL for TKW and KW, whereas the BP025 population also had a QTL for KW and the RP883 population a QTL for PHT. None of these QTL were observed under greenhouse conditions (Faris et al. 2014; Sharma et al. 2019a). For both multi-trait QTL, lines with the durum parent alleles saw an increase in the phenotype, implying that these QTL may already be present and potentially fixed in the NDSU durum breeding program. However, they may be beneficial for other breeding programs for increasing kernel size and weight. It would be interesting to cross Ben and Rusty with one another to see the effects the combination would have on kernel size and weight and if a germplasm line could be developed with significantly higher kernel weight. Numerous QTL for

kernel weight have been identified on chromosome 4A (Cao et al. 2020), with some identified in tetraploid wheat (Arriagada et al. 2020).

5.5.2.8. Chromosome 5A

Among the BP025 and RP883 populations, a total of five multi-trait QTL were identified on chromosome 5A, with two regions overlapping between the two populations. In both populations, the physical regions of *Q* and *Vrn-A1* were associated with multiple traits, which were also observed under greenhouse conditions (Faris et al. 2014; Sharma et al. 2019a). For the BP025 population, QTL for SPS, KW, and KLW were associated with *Q*, whereas in the RP883 population, QTL for SPS, DTH, KW, KC, and KLW were present. It has been previously shown that *Q* influences numerous yield component traits in these two populations (Faris et al. 2014; Sharma et al. 2019a), along with durum and cultivated emmer having different alleles of *Q* (Simons et al. 2006). Recently, Zhang et al. (2020) showed using near isogenic lines that *Q* is involved in the regulation of over 3000 genes and numerous pathways. Therefore, it was not a surprise to see numerous yield component traits associated with *Q* in the BP025 and RP883 populations.

Vrn-A1 was associated with QTL in both populations. In the BP025 population, a QTL for DTH and PHT was observed in this region, and QTL for TKW, DTH, KA, and KLW in the RP883 population. *Vrn-A1* is involved in vernalization-mediated flowering in wheat and is therefore influences DTH (Yan et al. 2003; Yan et al. 2004). *Vrn-A1* was associated with a QTL for DTH for both populations under field and greenhouse conditions (Faris et al. 2014; Sharma et al. 2019a). Additionally, changes in PHT may be associated with the increased number of DTH at this locus within the BP025 population. In the RP883 population, *Vrn-A1* was shown to be associated with numerous yield related QTL under greenhouse conditions (Sharma et al. 2019a).

Interestingly, Sharma et al. (2019a) sequenced Rusty and PI 193883 at the *Vrn-A1* locus and did not find any polymorphisms, along with no differences in expression. Further investigation is needed to determine if *Vrn-A1* is truly underlying this multi-trait QTL.

Under field conditions, QTL for TKW and DTH are hypothesized to be associated with *Vrn2* but a DTH QTL was not observed at this locus under greenhouse conditions (Sharma et al. 2019a). *VRN2* interacts with *VRN1*, including *Vrn-A1*, and plays a role in flowering repression during the vernalization process (Yan et al. 2004; Distelfeld et al. 2009; Kippes et al. 2016). It was not surprising to identify a DTH QTL within this region, but the presence of a TKW QTL was not expected. Lines with PI 193883 alleles within this region had an increase in the number of DTH, along with TKW. Further work is needed to unravel the relationship between these two traits.

Lastly, a region on the short arm of chromosome 5A in the BP025 population was associated with SPS and PHT. An increase in both traits was observed in lines with PI 41025 alleles in this region, with this QTL having a small effect on SPS and PHT. Therefore, this QTL may not be worth breeding into durum breeding programs due to the small effect on SPS, increase in PHT associated with it, and potential linkage drag from the cultivated emmer background.

5.5.2.9. Chromosome 5B

QTL for SPS, TKW, DTH, PHT, KA, KW, and KC were associated with the physical region near the *Vrn-B1* locus on chromosome 5B in the BP025 population. When this population was grown under greenhouse conditions, Faris et al. (2014) also observed QTL for DTH, KPS and GWS in this region but not SPS and TKW. In my study, a QTL was observed for GWS in the 2019 environment, implying a strong environmental influence of the genetic factors for the

phenotypes associated with this region. *Vrn-B1* is homoeologous to *Vrn-A1* (Yan et al. 2004), with both these genes having an effect on DTH, PHT, kernel weight and kernel size in both of the populations I studied. At both *Vrn-A1* and *Vrn-B1* loci, the durum parent, Ben and Rusty, were the donor of the allele which resulted in increased number of DTH, PHT, and kernel size/weight. Recently, Royo et al. (2020) found that *Vrn-1* and *Ppd-1* genes influence numerous agronomic traits through differences in days to anthesis and a prolonged grain filling period. Although lines with Ben alleles within this region result in increased number of DTH, these lines also had increased SPS, TKW, KA, KW, and KC. The Ben allele at *Vrn-B1* should already be fixed in local durum germplasm but may be beneficial for durum breeders outside of North America.

5.5.2.10. Chromosome 6B

In the RP883 population, a multi-trait QTL was identified on chromosome 6B for SPS, KC, and KLW. A trade-off between the number of SPS and kernel size was observed at this locus, where lines with Rusty alleles had increased number of SPS but decreased kernel size, which has been previously reported in the literature (Brinton and Uauy 2018; Cao et al. 2020). Relatively few QTL have been identified for yield component traits on chromosome 6B (Brinton and Uauy 2018; Cao et al. 2020, Arriagada et al. 2020); however, located near this QTL region is the grain protein content gene *Gpc-B1* (Uauy et al. 2006; Distelfeld et al. 2007). Although I did not measure grain protein content in this study, it has been proposed that because spike development and grain yield formation are tightly linked, a gene controlling one may influence the other (Cao et al. 2020).

5.5.2.11. Chromosome 7A

A multi-trait QTL was identified on chromosome 7A associated with KW, KC, and KLW near 92.5 cM in the BP025 population. Interestingly, lines with Ben alleles in this region had increased KW, but lines with PI 41025 had higher KC and KLW values. Potentially, in cases when KL is not lengthened, this may influence the overall KLW ratio. This interplay between the two different parental allele types and kernel size may be the reason a kernel weight QTL is not observed consistently within this region. QTL for kernel size traits have been observed on chromosome 7A near this region by Corsi et al. (2021), Sun et al. (2020), and Russo et al. (2014).

Additionally, a QTL was identified on the long arm of chromosome 7A associated with the number of SPS. Previously, the 2017 and 2018 field data for the BP025 population was used validate the candidate region for *WAPO-A1* (Kuzay et al. 2019). *WAPO-A1* encodes an F-box protein and regulates floral organ identity (Muqaddasi et al. 2019; Kuzay et al. 2019; Voss-Fels et al. 2019). Kuzay et al. (2019) found that in the BP025 population, PI 41025 contained the favorable haplotype for increased number of SPS. Further analysis of a diverse panel of diploid, tetraploid, and hexaploid wheat identified the *WAPO-A1b* allele, which PI 41025 has, to be less frequent in modern cultivars than the other two *WAPO-A1* alleles. Almost all durum lines sequenced by Kuzay et al. (2019) had the *WAPO-A1a* allele, including Ben, which has on average a fewer number of SPS than the *WAPO-A1b* allele. The results from our study, along with Kuzay et al. (2019), indicate that *WAPO-A1* can be used for increasing the number of SPS in durum wheat. I have already begun the backcrossing process to introgress the PI 41025 allele at *WAPO-A1* into a more suitable background for use in germplasm improvement.

5.5.2.12. Chromosome 7B

A multi-trait QTL was identified on the distal end of the short arm of chromosome 7B in the RP883 population. QTL for DTH and PHT co-segregated at this locus, with the wheat gene *FT1* within this region. *FT1* was cloned by Yan et al. (2006) and is involved in flowering time regulation and the transition from vegetative to reproductive growth (reviewed by Gauley and Boden 2018). Surprisingly, a QTL for SPS was not observed at this locus. *FT1* is known to play a role in promoting inflorescence development and regulate the number of SPS (Dixon et al. 2018). In the DP527 population, *FT1* was found to be associated with a SPS QTL, along with DTH and PHT (Peters Haugrud et al. unpublished). Potentially, the effects of the other SPS QTL may play a strong enough role in determining the final number of SPS that *FT1* had no effect on this phenotype. The two parental lines still need to be sequenced and polymorphisms identified in order to determine if *FT1* is indeed the gene underlying these two QTL. Having Rusty alleles within this region resulted in an increased in PHT and DTH.

5.5.3. Beneficial Traits from PI 41025

A focus of this study was not only identifying yield component traits and their relationships, but useful genes that may be introduced into the local germplasm from the cultivated emmer parents. In the PI 41025 population, PI 41025 had consistently a greater number of SPS than Ben. Three QTL, *QSpn.fcu-2B*, *QSpn.fcu-3B*, and *QSpn.fcu-5A.1* were consistently responsible for an increase in the number of SPS in lines that had PI 41025 alleles under these QTL. Additionally, an increase in lines with PI 41025 alleles at the TKW QTL *QTkw.fcu-2A* may be beneficial in breeding endeavors. If *GNI1-A1* is indeed the gene underlying this QTL, introgressing the cultivated emmer allele of *GNI1-A1* into the durum germplasm pool may provide benefits for increasing kernel weight and yield (Golan et al. 2019).

5.5.4. Beneficial Traits from PI 193883 and Rusty

PI 193883 had many more desirable traits in the RP883 population than Rusty, the durum parent. Rusty was initially developed as a genetic stock for stem rust resistance (Klindworth et al. 20016). Therefore, it has not been released as a durum cultivar and selections were not made for yield and quality. Compared to the other two populations grown, BP025 and DP527 (Peters Haugrud et al. unpublished), PI 193883 headed very early and may be useful in breeding for decreased heading data if desired. Overall, none of the other yield component traits studied performed much superior for either parent compared to the BP025 population. Individual QTL/mulit-trait QTL, such as those discussed above, may be useful in durum breeding programs.

5.5.5. Future Directions/Conclusions

Now that multiple genetic regions have been identified in the BP025 and RP883 populations to be associated with various yield component traits, the next steps include 1) verifying those with known genes within the genetic regions whether these are the underlying genes for these traits, 2) identify candidate genes within QTL regions, and 3) develop breeder friendly markers for these QTL regions. Recently, more breeding programs and implementing the use of large effect SNP as fixed markers in their genomic selection models in wheat (Lozada et al. 2019; Sarinelli et al. 2019). Markers associated with stable QTL identified in this study may be beneficial to local breeding programs who implement genomic selection. Additionally, the use of the BP025 population to validate the *WAPO-A1* (Kuzay et al. 2019) illustrates the usefulness of these types of populations in the gene validation process. Lastly, identifying yield component genes is critical in not only gene cloning, but unraveling the genetic mechanisms that determine final grain yield and providing knowledge to increase overall yield and feed future generations.

5.6. Literature Cited

Alvarez MA, Tranquilli G, Lewis S, Kippes N, Dubcovsky J (2016) Genetic and physical mapping of the earliness per se locus *Eps-A^{m}1* in *Triticum monococcum* identifies *EARLY FLOWERING 3 (ELF3)* as a candidate gene. Fuct Integr Genomics 16:365-382

Arriagada O, Marcotuli I, Gadaleta A, Schwember AR (2020) Molecular mapping and genomics of grain yield in durum wheat: a review. Int J Mol Sci 21:7021

Beales J, Turner A, Griffiths S, Snape JW, Laurie DA (2007) A *Pseudo-Response Regulator* is misexpressed in the photoperiod insensitive *Ppd-D1a* mutant of wheat (*Triticum aestivum* L.). Theor Apple Genet 115:721-733

Boden SA, Cavanagh C, Cullis BR, Ramm K, Greenwood J, Finnegan EJ, Trevaskis B, Swain SM (2015) *Ppd-1* is a key regulator of inflorescence architecture and paired spikelet development in wheat. Nat Plants 1:14016

Borrill P, Harrington SA, Uauy C (2018) Applying the latest advances in genomics and phenomics for trait discovery in polyploid wheat. Plant J 97:56-72

Brinton J and Uauy C (2018) A reductionist approach to dissecting grain weight and yield in wheat. J Integr Plant Biol 61:337-358

Broman KW, Wu H, Sen S, Churchill GA (2003) R/qtl: QTL mapping in experimental crosses. Bioinformatics 19:889-890

Cao S, Xu D, Hanif M, Xia X, He Z (2020) Genetic architecture underpinning yield component traits in wheat. Theor Appl Genet 133:1811-1823

Cavanagh CR, Chao S, Wang S, Huang BE, Stephen S, Kiani S, Forrest K, Saintenac C, Brown-Guedira GL, Akhunova A, See D, Bai G, et al. (2013) Genome-wide comparative

diversity uncovers multiple targets of selection for improvement in hexaploid wheat landraces and cultivars. Proc Natl Acad Sci 110:8057-8062

Corsi B, Obinu L, Zanella CM, Cutrupi S, Day R, Geyer M, Lillemo M, Lin M, Mazza L, Percival-Alwyn L, Stadlmeier M, Mohler V, Hartl L, Cockram J (2021) Identification of eight QTL controlling multiple yield components in a German multi-parental wheat population, including *Rht24*, *WAPO-A1*, *WAPO-B1* and genetic loci on chromosomes 5A and 6A. Theor Appl Genet 134L1435-1454

Distelfeld A, Cakmak I, Peleg Z, Ozturk L, Yazici AM, Budak H, Saranga Y, Fahima T (2007) Multiple QTL-effects of wheat *Gpc-B1* locus on grain protein and micronutrient concentrations. Physiol Plantarum 129:635-643

Distelfeld A, Tranquilli G, Li C, Yan L, Dubcovsky J (2009) Genetic and molecular characterization of the *VRN2* loci in tetraploid wheat. Plant Physiol 149:245-257

Elias EM and Miller JD (1998) Registration of 'Ben' durum wheat. Crop Sci 38:895

Faris JD (2014) Wheat domestication: key to agricultural revolutions past and future. Genomics and Plant Genetic Resources Volume 1. Managing, sequencing and mining genetic resources (pp. 439-464). Springer Netherlands.

Faris JD, Zhang Q, Chao S, Zhang Z, Xu SS (2014) Analysis of agronomic and domestication traits in a durum × cultivated emmer wheat populations using a high-density single nucleotide polymorphism-based linkage map. Theor Appl Genet 127:2333-2348

Gegas VC, Nazari A, Griffiths S, Simmonds J, Fish L, Orford S, Sayers L, Doonan JH, Snape JW (2010) A genetic framework for grain size and shape variation in wheat. Plant Cell 22:1046-1056

Golan G, Ayalon I, Perry A, Zimran G, Ade-Ajayi T, Mosquna A, Distelfeld A, Peleg Z (2019) *GNI-A1* mediated trade-offs between grain number and grain weight in tetraploid wheat. Theor Appl Genet 132:2353-2365

Guo J, Shi G, Kalil A, Friskop A, Elias E, Xu SS, Faris JD, Liu Z (2020) *Pyrenophora tritici-repentis* Race 4 isolates cause disease on tetraploid wheat. Fungal Biol Genet 111:1781-1790

Hai L, Guo H, Wagner C, Xiao S, Friedt W (2008) Genomic regions for yield and yield parameters in Chinese winter wheat (*Triticum aestivum* L.) genotypes tested under varying environments correspond to QTL in widely different wheat materials. Plant Sci 175:226-232

Haley CS and Knott SA (1992) A simple regression method for mapping quantitative trait loci in line crosses using flanking markers. Heredity 69:315-324

Hao M, Zhang L, Ning S, Huang L, Yuan Z, Wu B, Yan Z, Dai S, Jiang B, Zheng Y, Liu D (2020) The resurgence of introgression breeding, as exemplified in wheat improvement. Front Plant Sci 11:252

Kippes N, Chen A, Zhang X, Lukaszewski A, Dubcovsky J (2016) Development and characterization of a spring hexaploid wheat line with no functional *VRN2* genes. Theor Appl Genet 129:1417-1428

Klindworth DL, Miller JD, Xu SS (2006) Registration of Rusty durum wheat. Crop Sci 46:1012-1014

Kuzay S, Xu Y, Zhang J, Katz A, Pearce S, Su Z, Fraser M, Anderson JA, Brown-Guedira G, DeWitt N, Peters Haugrud A, Faris JD, Akhunov E, Bai G, Dubcovsky J (2019) Identification of a candidate gene for a QTL for spikelet number per spike on wheat

chromosome arm 7AL by high-resolution genetic mapping. Theor Appl Genet 132:2689-2705

Levene H (1960) Robust tests for equality of variances. In: Olkin I, Hotelling H et al (eds) Contributions to probability and statistics: essays in honor of harold hoteling. Stanford University Press, Stanford, CA, pp 278-292

Li F, Wen W, He Z, Liu J, Jin H, Cao S, Geng H, Yan J, Zhang P, Wan Y and Xia X (2018) Genome-wide linkage mapping of yield-related traits in three Chinese bread wheat populations using high-density SNP markers. Theor Appl Genet 131:1903-1924

Liu Y, Salsman E, Wang R, Galagedara N, Zhang Q, Fiedler JD, Liu Z, Xu S, Faris JD, Li X (2020) Meta-QTL analysis of tan spot resistance in wheat. Theor Appl Genet 133:2363-2375

Lozada D, Mason RE, Sarinelli JM, Brown-Guedira G (2019) Accuracy of genomic selection for grain yield and agronomic traits in soft red winter wheat. BMC Genet 20:82

Manichaikul A, Moon JY, Sen Ś, Yandell BS and Broman KW (2009) A model selection approach for the identification of quantitative trait loci in experimental crosses, allowing epistasis. Genetics 181:1077–1086.

Muqaddasi QH, Brassac J, Kppolu R, Plieske J, Ganal MW, Röder MS (2019) *TaAPO-A1*, an ortholog of rice *ABERRANT PANICLE ORGANIZATION 1*, is associated with total spikelet number per spike in elite European hexaploid winter wheat (*Triticum aestivum* L.) varieties. Sci Rep-UK 9:13853

Nishida H, Yoshida T, Kawakami K, Fujita M, Long B, Akashi Y, Laurie DA, Kato K (2013) Structural variation in the 5’ upstream region of photoperiod-insensitive alleles *Ppd-A1a*

and *Ppd-B1a* identified in hexaploid wheat (*Triticum aestivum* L.), and their effect on heading time. Mol Breeding 31:27-37

Royo C, Dreisigacker S, Ammar K, Villegas D (2020) Agronomic performance of durum wheat landraces and modern cultivars and its association with genotypic variation in vernalization response (*Vrn-1*) and photoperiod sensitivity (*Ppd-1*) genes. Eur J Agron 120:126129

Russo MA, Ficco DBM, Laidò G, Marone D, Papa R, Blanco A, Gadaleta A, De Vita P, Mastrangelo AM (2014) A dense durum wheat × *T. dicoccum* linkage map based on SNP markers for the study of seed morphology. Mol Breeding 34:1579-1597

Sakuma S, Golan G, Guo Z, Ogawa T, Tagiri A, Sugimoto K, Bernhardt N, Brassac J, Mascher M, Hensel G, et al. (2019) Unleashing floret fertility in wheat through the mutation of a homeobox gene. Proc Natl Acad Sci 116:5182-5187

Salsman E, Liu Y, Hosseinirad SA, Kumar A, Manthey F, Elias E, Li X (2021) Assessment of genetic diversity and agronomic traits of durum wheat germplasm under drought environment of the northern Great Plains. Crop Sci 61:1194-1206

Sarinelli JM, Murphy JP, Tyagi P, Holland JB, Johnson JW, Mergoum M, Mason RE, Babar A, Harrison S, Sutton R, Griffey CA, Brown-Guedira G (2019) Training population selection and use of fixed effects to optimize genomic predictions in a historical USA winter wheat panel. Theor Appl Genet 132:1247-1261

Sen Ś and Churchill GA (2001) A statistical framework for quantitative trait mapping. Genetics 159:371-387

Sharma JS, Running KLD, Xu SS, Zhang Q, Peters Haugrud AR, Sharma S, McClean PE, Faris JD (2019a) Genetic analysis of threshability and other spike traits in the evolution of cultivated emmer to fully domesticated durum wheat. Mol Genet Genomics 294:757-771

Sharma JS, Zhang Q, Rouse MN, Klindworth DL, Friesen TL, Long Y, Olivera PD, Jin Y, McClean PE, Xu SS, Faris JD (2019b) Mapping and characterization of two stem rust resistance genes derived from cultivated emmer wheat accession PI 193883. Theor Appl Genet 132:3177-3189

Simons KJ, Fellers JP, Trick HN, Zhang Z, Tai YS, Gill BS, Faris JD (2006) Molecular characterization of the major wheat domestication gene *Q*. Genetics 172:547-555

Snedecor GW and Cochran WG (1989) Statistical methods, Eighth Edition. Iowa State University Press, Ames

Sun L, Huang S, Sun G, Zhang Y, Hu X, Nevo E, Peng J, Sun D (2020) SNP-based association study of kernel architecture in a worldwide collection of durum wheat germplasm. PLoS ONE 15:e0229159

Uauy C, Brevis JC, Dubcovsky J (2006) The high grain protein content gene *Gpc-B1* accelerates senescence and has pleiotropic effects on protein content in wheat. J Exp Biol 57:2785-2794

Voss-Fels KP, Keeble-Gagnère G, Hickey LT, Tibbits J, Nagornyy S, Hayden MJ, Pasam RK, Kant S, Friedt W, Snowdon RJ, Appels R, Wittkop B (2019) High-resolution mapping of rachi nodes per rachis, a critical determinant of grain yield components in wheat. Theor Appl Genet 132:2707-2719

Wang S, Wong D, Forrest K, Allen A, Chao S, Huang BE, Maccaferri M, Salvi S, Milner SG, Cattivelli L, et al. (2014) Characterization of polyploidy wheat genomic diversity using a

high-density 90,000 single nucleotide polymorphism array. Plant Biotechnol J 12:787-796

Würschem T, Rapp M, Miedaner T, Longin CFH, Leiser WL (2019) Copy number variation of *Ppd-B1* is the major determinant of heading time in durum wheat. BMC Genet 20:64

Yan L, Fu D, Li C, Blechl A, Tranquilli G, Bonafede M, Sanchez A, Valarik M, Yasuda S, Dubcovsky J (2006) The wheat and barley vernalization gene *VRN3* is an orthologue of *FT*. Proc Natl Acad Sci 103:19581-19586

Yan L, Helguera M, Kato K, Fukuyama S, Sherman J, Dubcovsky J (2004) Allelic variation at the *VRN-1* promoter region in polyploid wheat. Theor Appl Genet 109:1677-1686

Yan L, Loukoianov A, Tranquilli G, Helguera M, Fahima T, Dubcovsky J (2003) Positional cloning of the wheat vernalization gene *VRN1*. Proc Natl Acad Sci 100:6263-6268

Yan L, Loukoianov A, Blechl A, Tranquilli G, Ramakrishna W, SanMiguel P, Bennetzen JL, Echenique V, Dubcovksy J (2004) The wheat *VRN2* gene is a flowering repressor downregulated by vernalization. Science 303:1640-1644

Zhang Q, Axtman JE, Faris JD, Chao S, Zhang Z, Friesen TL, Zhong S, Cai X, Elias EM, Xu SS (2014) Identification and molecular mapping of quantitative trait loci for Fusarium head blight resistance in emmer and durum wheat using a single nucleotide polymorphism-based linkage map. Mol Breeding 34:1677-1687

Zhang Z, Li A, Song G, Geng S, Gill BS, Faris JD, Mao L (2020) Comprehensive analysis of *Q* gene near-isogenic lines reveals key molecular pathways for wheat domestication and improvement. Plant J 102:299-310

CHAPTER 6. MARKER DEVELOPMENT AND FINE-MAPPING OF A KERNELS PER SPIKE QTL ON CHROMOSOME 2B IN TETRAPLOID WHEAT

6.1. Abstract

Compared to other major food crops, relatively few yield genes have been cloned in characterized in wheat (*Triticum* ssp.) partially due to the large genome size and complexity of being an allopolyploid. Previously, a QTL on chromosome 2B associated with kernels per spike was identified in the tetraploid wheat population BP025, derived from crossing the North Dakota durum variety Ben with the cultivated emmer accession PI 41025. In this study, I developed a backcross population to 'mendelize' this QTL region for fine mapping using recombinant inbred lines from the BP025 population as donor parents and Ben as the recurrent parent. Here, I report the use of a BC_3F_2 population to fine map this region, along with the results of screening BC_3F_2 plants twice to narrow down this region, and greenhouse results from one replicated yield trial using BC_3F_4 plants. Additionally, I report the development of additional STARP and KASP markers in this target region. Findings from this study provides a base for future work in cloning the kernels per spike gene within this region, along with closely linked markers that may be used by breeders who are interested in introgressing this trait into their germplasm.

6.2. Introduction

Durum wheat (*Triticum turgidum* L. ssp. *durum*) is a major world food crop and is used to make pasta and other semolina-based products. Although the FAOSTAT does not report separate values for durum and bread, or common, wheat (*Triticum aestivum* L.), durum wheat is grown on approximately 16 million hectares annually (Arriagada et al. 2020). Within the United States, North Dakota produces over half of the 75 million bushels grown per year (https://www.ndwheat.com/buyers/NorthDakotaWheatClasses/Durum/). As with other crops,

durum yield will need to significantly increase to feed the growing global population by 2050, while adapting to climate change and extreme weather (Cao et al. 2020).

One approach to increase grain yield is to map, clone, and characterize yield component traits to better understand the genetic mechanisms that control yield (Kuzay et al. 2019). Grain yield can be broken up into three main parts: the number of spikes per unit area, the number or kernels per spike, and grain weight/size; with each part being comprised of multiple additional subunits (Brinton and Uauy 2018; Cao et al. 2020). Compared to other major cereal crops, such as rice (*Oryza sativa*) and maize (*Zea mays*), relatively few yield-related genes have been cloned in wheat (Cao et al. 2020; Arriagada et al. 2020; Colasuonno et al. 2021). This is partially due to the complexity of the wheat genome, with durum wheat having two subgenomes and bread wheat having three (Borrill et al. 2015). Additionally, the first reference sequences were not publsihed until 2018 and 2019 for common and durum wheat, respectively (IWGSC et al. 2018; Maccaferri et al. 2019).

To overcome this lag in cloning and characterizing wheat yield genes, multiple initiatives have been formed over the last 10 years to not only address this issue but to form larger collaborations and networks. These groups include the International Wheat Yield Partnership, Designing Future Wheat, and the Wheat Coordinated Agriculture Project (WheatCAP). The goal of the current WheatCAP project is the "validation, characterization and deployment of QTL for grain yield components in wheat and the training of a new generation of plant breeders" (https://www.triticeaecap.org/about/). The project discussed in this chapter is part of this group.

A QTL governing kernels per spike (KPS) was identified in a tetraploid recombinant inbred line (RIL) population developed from crossing Ben, a North Dakota durum variety (Elias and Miller 1998) by PI 41025, a cultivated emmer wheat (*T. turgidum* ssp. *dicoccum* (Schrank)

Schübl) accession collected near Samara, Russia. The population, referred to as BP025, consisted of 200 RILs. A KPS QTL was mapped to chromosome 2B under greenhouse conditions with a LOD score of 17.7 and explained 15.2% of the phenotypic variation in the number of kernels per spike (Faris et al. 2014). Peters Haugrud et al. (unpublished) evaluated the BP025 population under field conditions and observed a significant QTL in this region in summer 2017. This QTL region was also associated with increased grain weight per spike under greenhouse conditions but not field conditions, indicating that the increase in weight is due to increased kernel number. The durum parent, Ben, contributed to the increase in KPS due to this QTL region (Faris et al. 2014).

As part of the WheatCAP project, my goal was to perform fine mapping of this 2BL KPS QTL region to eventually identify the gene underlying this trait. My objectives were to develop a mapping population for fine mapping and to add additional markers within this region using a variety of resources. This work provides a solid base for further fine and high-resolution mapping within this region, along with markers for breeders who are interested in introgressing this trait into their breeding program.

6.3. Material and Methods

6.3.1. Initial Greenhouse Trials to Determine RILs for Crossing

The BP025 population was previously evaluated for kernels per spike under greenhouse conditions by Faris et al. (2014) and in the field (Chapter 5). To determine which RILs to use for population development, a replicated greenhouse trial was planted in Fall 2016 in 15 cm pots with 16-h photoperiod and a temperature around 21 °C. The two parental lines, Ben and PI 41025, along with three RILs, BP025-26, BP025-28, and BP025-83, were grown with 10 replicates of each. The three RILs had PI 41025 alleles in the 2BL KPS region, spanning form

IWA8599 to *IWA6076* on chromosome 2B on the map published by Faris et al. (2014), and Ben alleles in the other KPS QTL regions identified by Faris et al. (2014). Four spikes per plant were harvested and the number of kernels per spike was manually counted. The two RILs with the lowest number of kernels per spike were used for population development (Table 6.1).

Table 6.1. Results of the replicated greenhouse trial to determine which RILs to use for population development.

	Kernels per spike	
Line	Mean[a]	Range
PI 41025	26.33a	7.50-36.75
Ben	23.42ab	18.75-26.50
BP025-83	22.85ab	15.75-27.00
BP025-28	20.68bc	13.50-28.00
BP025-26	16.63c	9.00-21.75

[a]LSD=4.75, numbers followed by the same number are not significantly different at the 0.05 level of probability.

6.3.2. Population Development and Selection of F_1 Plants

The BP025 population was developed by Steven Xu at the USDA-ARS in Fargo, ND from crossing Ben (PI 596557), a North Dakota hard amber durum variety (Elias and Miller 1998), with PI 41025, a cultivated emmer accession collected near Samara, Russia. The BP025 RIL population consists of 200 lines and was developed using the single seed descent method.

Two RILs in the BP025 population, BP025-26 and BP025-28, were selected as donor parents for backcrossing to Ben for high-resolution mapping population development. The two RILs, BP025-26 and BP025-28, were used as the donor parents and Ben was the recurrent parent, and a total of three backcrosses were performed (Figure 6.1). For each backcross, plants were screened with the SSR marker *Xwmc245* and the STARP marker *IWA427* to select plants which were heterozygous in the target region. BC_3F_1 plants were screened with the same two markers to select plants which were heterozygous in my target region, which were selfed to produce BC_3F_2 plants.

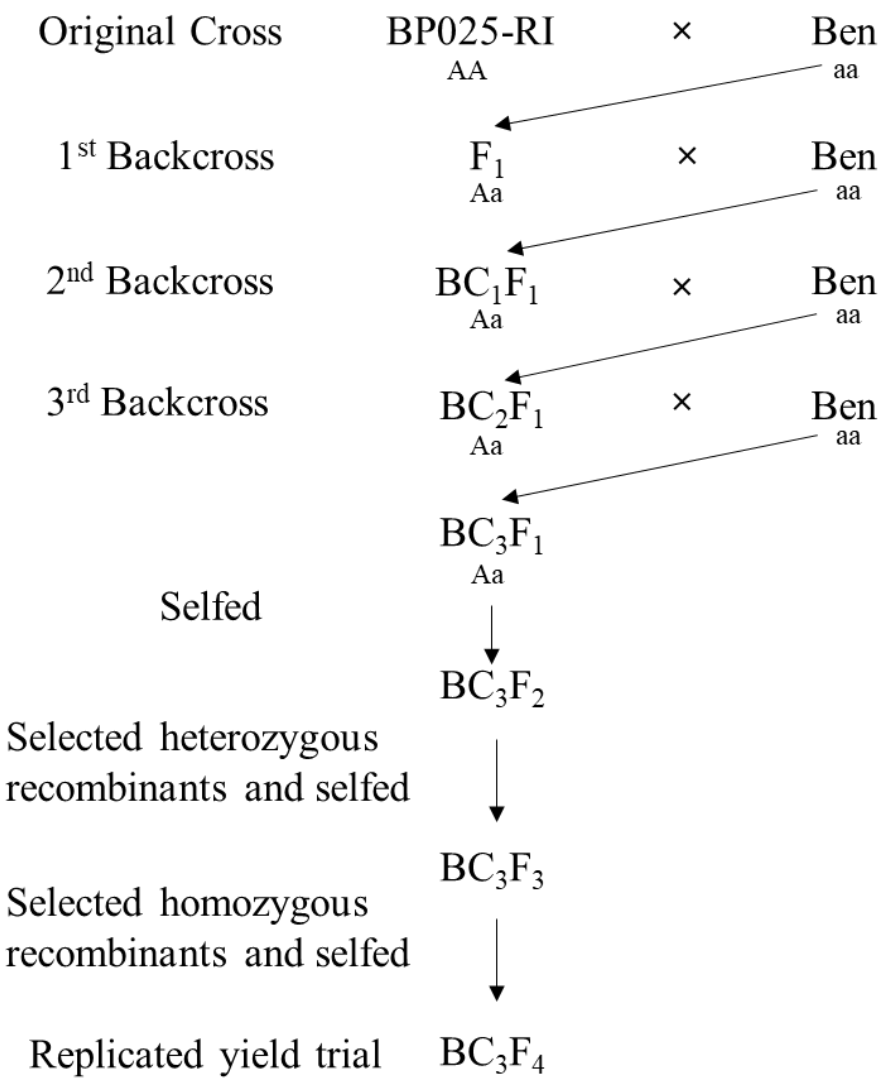

Figure 6.1. Crossing scheme used for population development for saturation mapping. BP025-RI stands for either BP025-26 or BP025-28. Ben was the recurrent parent. A total of three backcrosses were done. For selections, genetic markers were used to select desired plants.

6.3.3. Marker Development

Markers were developed using a combination of the 9K SNP array data (Cavanagh et al. 2013) from the Faris et al. (2014) genetic map, 90K SNP array data (Wang et al. 2014), and exome capture data. Bulk segregate analysis was used to genotype with the 90K SNP array. The 90K iSelect SNP array was genotyped at the small grains genotyping laboratory in Fargo, ND by Dr. Jason Fiedler. Clustering data was analyzed using Genome Studio from Illumina, Inc (2013).

Both the parental lines, Ben and PI 41025, were genotyped along with two unique sets of the two different bulk groups. One bulk group consisted of 10 lines with PI 41025 alleles in the region between *Xwmc245* and *IWA427* and the other bulk was 10 lines with Ben alleles in this same region. Markers that were polymorphic within each bulk where discarded, and only markers that were monomorphic within each bulk but polymorphic between the two were converted into semi-thermal asymmetric reverse PCR (STARP) (Long et al. 2016) and competitive allele-specific PCR (KASP) (https://www.biosearchtech.com) markers.

Exome capture was performed on the two parents, Ben and PI 41025, in Spring 2018 by Dr. Eduard Akhunov (Department of Plant Pathology, Kansas State University, Manhattan, KS). The exome capture array developed by Jordan et al. (2015) was used. The Akhunov Lab used GATK software to do variant calling. Data was filtered to remove multiallelic SNPs, heterozygous sites, and singletons with less than 10x coverage. The data was aligned to the IWGSC WGA v1.0. Polymorphic SNPs between the two parents were converted into STARP and KASP markers when used during genotyping.

6.3.4. PCR Amplification and Electrophoresis

DNA was extracted from young leaf tissue as described by Faris et al. (2000) for tube extractions and the ammonium acetate method as described by Pallota et al. (2003) for plate extractions. DNA for plate extractions was used for the initial screening process, and then tube extractions of leaf tissue of homozygous recombinant BC_3F_3 plants. DNA fragments were amplified using a GeneAmp^{TM}PCR system 97000 for PCR. For SSR markers, the 10 µl PCR reaction consisted of 100 ng of template DNA, 1X PCR buffer, 2 mM $MgCl_2$, 0.2 mM dNTPs, 4 pmol of each primer, and 0.5 unit of *Taq* DNA polymerase, with diluted water added to a final volume of 10 µL. The PCR conditions were: 94°C for 5 minutes, 35 cycles consisting of 30 sec

94°C, 30 sec 65-56°C, 90 sec 72°C; finishing with one cycle for 7 min at 72°C and cooling to 4°C. For STARP markers, the 10 µl PCR reaction consisted of 100 ng of template DNA, 0.9 µL × NH4 + buffer, 1.5 mM MgCl2, 50 µM dNTPs, 0.8 M betaine, 0.04% (w/v) bovine serum albumin (BSA), 200 nM common reverse primer, 200 nM of each priming element-adjustable primer (PEA-primer 1 and PEA-primer 2), 40 nM of each asymmetrically modified allele-specific primer (AMAS forward primer 1 and AMAS forward primer 2), and 1.5 units of *Taq* DNA polymerase. The PCR conditions were: 94°C for 5 minutes; cycle 6 times through: 30 sec 94°C, 2 minutes 56°C; cycle 40 times through 20 sec 94°C, 30 sec 62°C, 90 sec 72°C; finishing with one cycle for 7 min at 72°C and cooling to 4°C. PCR products from both SSR and STARP makers were separated on 6% polyacrylamide gels, stained with GelRed nucleic acid gel stain, and scanned on a Typhoon FLA 9500 variable mode laser scanner (GE Healthcare Life Sciences, Piscataway, NJ). KASP markers were ran by the USDA-ARS small grains genotyping laboratory in Fargo, ND.

6.3.5. Fine Mapping

For each round of fine mapping, BC_3F_2 plants were genotyped to identify heterozygous recombinants. Plants were grown in 2 inch 98 well plug flats (Greenhouse Megastore, Danville, IL) and genotyped using markers listed in Table 6.2 and Table 6.3. Heterozygous recombinants were transplanted to pots, grown, selfed, and harvested. Each BC_3F_3 family was screened using the same markers and method to identify one homozygous recombinant BC_3F_3 individual. BC_3F_3 plants were also genotyped with internal markers (Tables 6.2, 6.3) and self-pollinated to obtain BC_3F_4 seed, which was homozygous for the selected recombination event. The BC_3F_4 plants were grown for replicated greenhouse trials to delineate the location of the target QTL.

Table 6.2. Primers used in the first round of saturation mapping. Those in red font were used as the flanking primers when selecting heterozygous recombinants in the BC_3F_2 and homozygous recombinants in the BC_3F_3.

Marker designation	Marker Type	Forward primer 1	Forward primer 2*	Reverse primer	SNP source*
Xbarc230	SSR	CCCCTCCTCCTTCTCCCTCCTCCT		GGCTCATGCGGGCGTGTTTGG	
Xwmc245	SSR	GCTCAGATCATCCACCAACTTC		AGATGCTCTGGGAGAGTCCTTA	
Xbarc18	SSR	CGCTTCCCATAACGCCGATAGTAA		CGCCCGCATCATGAGCAATTCTATCC	
Xwmc272	SSR	TCAGGCCATGTATTATGCAGTA		ACGACCAGGATAGCCAATTCAA	
Xgwm319	SSR	GGTTGCTGTACAAGTGTTCACG		CGGGTGCTGTGTGTAATGAC	
IWB74647	STARP	1-TGTCCGGTGAAGGACGAT	2-TGTCCGGTGAAGGAAAAC	AGTGCAAACATAGTCCTGCGA	90K array
IWB77487	STARP	1-CAAACATAGTCCTGCAACCA	2-CAAACATAGTCCTGCGATCG	CGCCGACATCCTTGAGTTCT	90K array
Chr2B426480198	STARP	1-CCCATACATCTTAAAATGCAAGAT	2-CCCATACATCTTAAAATGCAGAAG	ATCTTACCTGCACACAAGGCA	Exome capture
IWB75857	STARP	2-GAGACTTATCTGGAACCACTAC	1-GAGACTTATCTGGAACCATCAT	CCTGATCGCAGAATCTTGGC	90K array
Xwmc265	SSR	GTGGATAACATCATGGTCAAC		TACTTCGCACTAGATGAGCCT	
IWA7524	STARP	2-TTCCCAGGCTCAAGAATG	1-TTCCCAGGCTCAAGGCTA	CATCAAATGACGAATGCCGC	9K array
Chr2B432555726	STARP	1-CTTTGTCAATGCATGTTTAAGCAA	2-CTTTGTCAATGCATGTTTAAAAAG	TGCATCAACCACAGCTACCA	Exome capture
Chr2B433542242	STARP	1-CTCGATGACCTGTATGTCCTA	2-CTCGATGACCTGTATGTTTTG	CGATCATGTATTGGATGGGCA	Exome capture
Chr2B434695029	STARP	2-CGAGGATGGCAAGTTTAATTG	1-CGAGGATGGCAAGTTTAGCTT	GCAACAAGTAGCACAGAGGC	Exome capture
Xgwm630	SSR	GTGCCTGTGCCATCGTC		CGAAAGTAACAGCGCAGTGA	
Chr2B443160586	STARP	1-CCTGCTGTTTTCTTCTACCGA	2-CCTGCTGTTTTCTTCTATTGC	AGGTTGTTTTCATTGGCAAGC	Exome capture
Chr2B446082351	STARP	1-AGTTTTTTGGTTACTACGTACCCT	2-AGTTTTTTGGTTACTACGTATACC	CCAAGACGTTCTACGACCCG	Exome capture
Chr2B446116612	STARP	2-CACCTTTTTATTTAACGGACTCG	1-CACCTTTTTATTTAACGGAACCT	AACGGACAAGGACATTTGGC	Exome capture
Chr2B448579361	STARP	1-GTCGAGATCGGGAGCAGA	2-GTCGAGATCGGGAAAAGG	CCGGAGGGTTCCTAGTTCCT	Exome capture
IWB77429	STARP	2-CACAAAGATTTAATGCAGATTGG	1-CACAAAGATTTAATGCAGGCTGA	AGCGTGCCAATAACGATGAA	90K array
IWB42378	STARP	1-GCACAAAGATTTAATGCAGGTCGA	2-GCACAAAGATTTAATGCAGATTGG	AGCGTGCCAATAACGATGAA	90K array
Chr2B450759236	STARP	1-GATCGGTTTTATATACACTGCGAT	2-GATCGGTTTTATATACACTGTAAC	TGGCGTTTAGGGGGCAAAAT	Exome capture
IWB9833	STARP	1-CAGCACAGCATGACCACA	2-CAGCACAGCATGATAACG	TGGTGCGCTCAAGCACTG	90K array
IWA1215	STARP	1-ACGGACGACTACAGCAGA	2-ACGGACGACTACAATAGC	TCAAGCCGCCAGTGAAATTG	9K array
IWB29666	STARP	1-ATTATCGACCATCTCCATCGA	2-ATTATCGACCATCTCCACTGC	AGCACCGCCTAAAGACGAC	90K array
Chr2B459250101	STARP	1-ATGTCCATGTATCGACTACGT	2-ATGTCCATGTATCGACTCTGC	CTGAAATCGCTGGAGGTGGA	Exome capture
Chr2B465653389	STARP	2-CTCCTCCCAATTCCCTACG	1-CTCCTCCCAATTCCTCACA	TTTCCTGTGCCCGAAGTTGA	Exome capture
Xgwm55	SSR	GCATCTGGTACACTAGCTGCC		TCATGGATGCATCACATCCT	
Chr2B486953078	STARP	1-GGTACTCACCAGAGTAGCA	2-GGTACTCACCAGAGCAACG	TGCAGGCACGAAAACCATCA	Exome capture
Chr2B501009984	STARP	1-TCTCAGCCATACGACTCCTT	2-TCTCAGCCATACGACTTTTC	CGGCACCCTGAACATAGGTAA	Exome capture
Chr2B504323864	STARP	1-CACATCCCCATTGCTCTT	2-CACATCCCCATTGCCTTC	TCATGGTGTCCCTTCCAAGA	Exome capture
Chr2B523086763	STARP	2-TCACGTAAACCTGGACCATC	1-TCACGTAAACCTGGACTGTA	GGTAGCACACATCAGTCACCA	Exome capture
Chr2B528794281	STARP	1-TACTGCCTGAACGTACTCT	2-TACTGCCTGAACGTGTTCC	ACAGGTCGTTGATGAGGTCG	Exome capture
IWA1690	STARP	1-GATCCAAATGATCTGAATAACGGT	2-GATCCAAATGATCTGAATAAAAGC	CGCGCTCATTCAAATACGCC	9K array
Chr2B538239714	STARP	2-GATACCAACAGCGAAGACG	1-GATACCAACAGCGAAAGCA	AGTCCAACAAGGAGCTGCAA	Exome capture
IWA6969	STARP	1-GCCCTGGAGAAAGTACAGT	2-GCCCTGGAGAAAGTGTAGC	TCTAAAACTACACACGCAGAAGC	9K array
IWA7019	STARP	1-CGAACCTCCGTTAGATGCT	2-CGAACCTCCGTTAGGTACC	TCTCAACATCCTTCCGCAGC	9K array
IWB50897	STARP	1-GGTTCAACTACCTTGCTGAT	2-GGTTCAACTACCTTGCCAAC	ATATCCCTTCGCCTCCGGG	90K array

*not applicable for SSR primers.

1=[Tail 2] = 5′-GACGCAAGTGAGCAGTATGAC-3′

2=[Tail 1] = 5′-GCAACAGGAACCAGCTATGAC-3′

Table 6.3. Primers used in the second round of saturation mapping. Those in red font were used as the flanking primers when selecting heterozygous recombinants in the BC_3F_2 and homozygous recombinants in the BC_3F_3. All primers listed are KASP markers.

Marker designation	Forward primer 1	Forward primer 2	Reverse primer	SNP source
Chr2B446082351	FAMAGTTTTTTGGTTACTACGTACCCT	HEXAGTTTTTTGGTTACTACGTATACC	CCAAGACGTTCTACGACCCG	Exome capture
Chr2B446116612	FAMCACCTTTTTATTTAACGGAATCG	HEXCACCTTTTTATTTAACGGAATCT	AACGGACAAGGACATTTGGC	Exome capture
Chr2B447741566	FAMCATCATCTGGTAATAATGGGTTGAGG	HEXCATCATCTGGTAATAATGGGTTGAGC	TGAAGATCCAATCCGCACAC	Exome capture
Chr2B447822409	FAMCCGCTTCTCCCGGCTCCGC	HEXCCGCTTCTCCCGGCTCCGT	TGGCTCTGCCCTCTTTCCT	Exome capture
Chr2B448080365	FAMCTGATGACGAGGAACCTGGAG	HEXCTGATGACGAGGAACCTGGAA	GCAACTCACACGCCGATGTA	Exome capture
Chr2B448905051	FAMCTGGATTCGGTATTTGTTTTTGCCAT	HEXCTGGATTCGGTATTTGTTTTTGCCAC	GCGGCAGGTCGTACTGTG	Exome capture
Chr2B449166206	FAMGTGAGCTGTGATGTTTGGTGC	HEXGTGAGCTGTGATGTTTGGTGT	CGGTTCCTGAGACTCTTTGTT	Exome capture
IWB77429	FAMGCACAAAGATTTAATGCAGGTTGA	HEXGCACAAAGATTTAATGCAGGTTGG	AGCTAGCGTGCCAATAACGA	90K array
IWB42378	FAMGCACAAAGATTTAATGCAGGTTGA	HEXGCACAAAGATTTAATGCAGGTTGG	AGCTAGCGTGCCAATAACGA	90K array
Chr2B450183215	FAMTGTTCAGCGGTTGCCTTTTGT	HEXTGTTCAGCGGTTGCCTTTTGC	AGCAAAAACTACCTCAGCTAAAAC	Exome capture
Chr2B450739111	FAMGCACTACCACCAGCACCAC	HEXGCACTACCACCAGCACCAG	ATAAGCAGGAGGCGGCAAG	Exome capture
Chr2B451890281	FAMGTAAGGTCTAAGGAGCATGGGGA	HEXGTAAGGTCTAAGGAGCATGGGGG	AAGATGAACTCCACCACCACC	Exome capture
Chr2B451923155	FAMCCATAGCCATAAACATCAACTTTTGT	HEXCCATAGCCATAAACATCAACTTTTGC	CAGCAAGAGGAACCGTAGGA	Exome capture
Chr2B453751477	FAMGCATTCCGAAGGACACCATTCC	HEXGCATTCCGAAGGACACCATTCT	GGTATGCGCTACATTGCTGT	Exome capture
Chr2B454482299	FAMTAATGGGTGCTATGGCCGACA	HEXTAATGGGTGCTATGGCCGACG	GAAAGGGCGGGTACCAATC	Exome capture
Chr2B455466692	FAMAGCTCACCAAAACAAGATCAGCAA	HEXAGCTCACCAAAACAAGATCAGCAG	AAGATGTCGATGATGCAGCCG	Exome capture
IWB9833	FAMGCAGCACAGCATGACAACA	HEXGCAGCACAGCATGACAACG	CTCTGGGTGGTGCGCTCA	90K array
IWB76099	FAMCTTGTTGTAGCCGCCACTT	HEXCTTGTTGTAGCCGCCACTG	GGTGGGTACAGGAACACCG	90K array
IWA1215	FAMACGGACGACTACAGTAGA	HEXACGGACGACTACAGTAGC	TCAAGCCGCCAGTGAAATTG	9K array
IWB29666	FAMGAGATTATCGACCATCTCCATTGA	HEXGAGATTATCGACCATCTCCATTGC	ACCGCCTAAAGACGACCG	90K array
IWB51413	FAMAAAGGGGAAGAACTTGGACAA	HEXAAAGGGGAAGAACTTGGACAG	CTGCTGATTTTGCGCCTCT	90K array
Chr2B456024533	FAMGGACCGGCGAGCAAGTGC	HEXGGACCGGCGAGCAAGTGT	TTGATGTCGGTCTCTCCCCA	Exome capture
Chr2B456304658	FAMCCGAGAAAGGCTAACAGCTA	HEXCCGAGAAAGGCTAACAATTG	AGGCAGCAAAGTAGCAAAACGA	Exome capture
Chr2B456019275	FAMCGGCAAAGTACAGCGTGTCGG	HEXCGGCAAAGTACAGCGTGTCGT	GCCTTTGCCTCCAAAGGACA	Exome capture
Chr2B459800224	FAMCAGCCAAGACTGGAGTTTCAT	HEXCAGCCAAGACTGGAGTTTCAC	CCAGGATCACCACATTTGTCA	Exome capture
Chr2B463768947	FAMCTCCAGCCTACTGAGGTCAAT	HEXCTCCAGCCTACTGAGGTCAAC	GAAGCTCCAAACAAGGATCGC	Exome capture
Chr2B464291292	FAMCCGATAATGTTATAATCAGGACAAG	HEXCCGATAATGTTATAATCAGGAACAA	TGCAGAGAAGGCTCAACAGT	Exome capture
Chr2B466193574	FAMAGCTCTACATTGACCACGCTA	HEXAGCTCTACATTGACCACGCTA	CAGCAGCTTGACCAGTACCT	Exome capture
Chr2B467477266	FAMCTGACTCTCCATGTTGACTAC	HEXCTGACTCTCCATGTTGCATAT	GTGTACGGAGTTATAGTCATTTGGC	Exome capture
Chr2B476407551	FAMATGGTTTTAATAGCTTTGTTAATGTA	HEXATGGTTTTAATAGCTTTGTTAACATC	ATCCGCGCTGGCTATTGAAA	Exome capture
Chr2B465653389	FAMCTCCTCCCAATTCCCCACG	HEXCTCCTCCCAATTCCCCACA	TTTCCTGTGCCCGAAGTTGA	Exome capture
Chr2B470913679	FAMATCCCGGCATTGTTAGCTATTA	HEXATCCCGGCATTGTTAGCTATTT	CCATGTTCAGATTGGTGCTG	Exome capture
Chr2B477564181	FAMGCTCTTGATGAAGCTATGAAGTCC	HEXGCTCTTGATGAAGCTATGAAGTCT	GTTAATTGTGGTGGTGCTGCAT	Exome capture
Chr2B478107531	FAMTTTGTTGTTTGTGCCCATTGTAA	HEXTTTGTTGTTTGTGCCCATTGTAG	TCTTCTGGACTGGGTTCATCT	Exome capture
Chr2B486194062	FAMTAGAAACATTCCAACAAGCAGGGT	HEXTAGAAACATTCCAACAAGCAGGGC	TGTGTAGTTCTTTTCTTGTGGCT	Exome capture
Chr2B491023492	FAMCAGGAAGTAGCATTTCTCCCACTG	HEXCAGGAAGTAGCATTTCTCCCACTA	TGAACTGCAGGCATTTACAGA	Exome capture
Chr2B491054244	FAMAAGTGGCTTGTGAGTTCCAT	HEXAAGTGGCTTGTGAGTTTTAC	ATATTCTTGTGGCGAAGCACG	Exome capture
Chr2B494278866	FAMGTGGTGGGTCGGCGAGA	HEXGTGGTGGGTCGGCGAGC	GATGGGTTCAGGCGACGA	Exome capture
Chr2B494860481	FAMCCGGCAGCATGTGGTTGG	HEXCCGGCAGCATGTGGTTGA	CGCATCTCCACCGTCCTAAC	Exome capture
Chr2B494880740	FAMGTCATAAGAAACATCCTCAACCT	HEXGTCATAAGAAACATCCTCACTCC	GACGGTGAACCTGAAAGGGA	Exome capture
Chr2B494273758	FAMAACACACCCCAAAGTTGTTACGT	HEXAACACACCCCAAAGTTGTTACGC	TGTGCGCACGATCGGTAGAT	Exome capture
Chr2B500593313	FAMATGGTCAGGTAAGGCGACTGG	HEXATGGTCAGGTAAGGCGACTGA	CAGGCCAGAGCTGGGTTC	Exome capture
Chr2B501009984	FAMGTTTCTCAGCCATACGACTTCTT	HEXGTTTCTCAGCCATACGACTTCTC	TGATCAACCCATCCACTCCG	Exome capture
Chr2B504323864	FAMTGCCACATCCCCATTGCTTTT	HEXTGCCACATCCCCATTGCTTTC	ACATGAGCAGAGTGGTCTTTCT	Exome capture
Chr2B506507689	FAMCAGGTCAAGAGGAAACGGT	HEXCAGGTCAAGAGGAAAAAGC	CACTATCTGGCACGGACGAA	Exome capture

Table 6.3. Primers used in the second round of saturation mapping (continued). Those in red font were used as the flanking primers when selecting heterozygous recombinants in the BC3F2 and homozygous recombinants in the BC3F3. All primers listed are KASP markers.

Marker designation	Forward primer 1	Forward primer 2	Reverse primer	SNP source
Chr2B507911105	FAMGATTCCCATGATACCCAATCAC	HEXGATTCCCATGATACCCAACTAT	TGAGACCCCTTCCCTGTCAT	Exome capture
Chr2B509713066	FAMCTCCGCACCATCGCTCTTCG	HEXCTCCGCACCATCGCTCTTCA	TCCCTAGTTTTGGTGCGTCG	Exome capture
Chr2B511136108	FAMGGGATCAAGGGAGCCATCGA	HEXGGGATCAAGGGAGCCATCGG	CGAGCACCGTCACCTCCG	Exome capture
Chr2B513480840	FAMGCAGACCTTGCGCATCTGGC	HEXGCAGACCTTGCGCATCTGGT	ACCGAGCTGCAGGAGATCA	Exome capture
Chr2B513499035	FAMTGTCCTCTCATTGAACTGTAGAAGCA	HEXTGTCCTCTCATTGAACTGTAGAAGCG	CGTCATGTGTCCGCTTTTGT	Exome capture
Chr2B517599131	FAMTTTGTTCTGGTTATGTCAATCTCC	HEXTTTGTTCTGGTTATGTCAATACCT	ATCAGTAGCAGCAAGCCAGC	Exome capture
Chr2B523086763	FAMATCACGTAAACCTGGACCGTA	HEXATCACGTAAACCTGGACCGTC	TGTGACTGCATTGCATTGGT	Exome capture
Chr2B525074970	FAMTTTAATCCAGTCTCCAGTGCCC	HEXTTTAATCCAGTCTCCAGTGCCT	TGCTGCGTTTCCTCTGACAT	Exome capture
Chr2B526776450	FAMGCTGGGCACGGAATCCTCG	HEXGCTGGGCACGGAATCCTCC	CGCGCTGAAGGTGATGGAAT	Exome capture
Chr2B526886014	FAMCCCTAGAAGATGCGAGTGCTC	HEXCCCTAGAAGATGCGAGTGCTT	GTACATCTTCCGGGACACGC	Exome capture
Chr2B527877066	FAMGTAGATTACAAAACTCGACACTCATC	HEXGTAGATTACAAAACTCGACACTCATG	ACAGATGCATATTGTTACTACACTG	Exome capture
Chr2B528794281	FAMTACTGCCTGAACGTGCTCT	HEXTACTGCCTGAACGTGCTCC	ACAGGTCGTTGATGAGGTCG	Exome capture
Chr2B529290113	FAMCCCTAGAGCAAGATGAGGCAAAC	HEXCCCTAGAGCAAGATGAGGCAAAT	AACTGCTGCACCACAAGCAA	Exome capture
Chr2B530731940	FAMTGAATAGGATGCGAAACAGAAGGA	HEXTGAATAGGATGCGAAACAGAAGGG	ATCTGCGCGTGATGTAGGTT	Exome capture
Chr2B532010814	FAMGGGGCTCGCCAAGGAGG	HEXGGGGCTCGCCAAGGAGA	CCACTGGTGCAGAGGTTGTA	Exome capture
Chr2B534398278	FAMCGTCATTATTATTTTGCCTGGTTTCG	HEXCGTCATTATTATTTTGCCTGGTTTCC	GGCTAAAAGGGCCGCATCT	Exome capture
Chr2B534843854	FAMCGCTCAGGGACGGGAGAAC	HEXCGCTCAGGGACGGGAGAAT	GCCCTCTTTCCGCATTCAATTT	Exome capture
IWB35321	FAMTTCTCTGGCAGAGGCGGA	HEXTTCTCTGGCAGAGGCGGC	CAATAGGACACCATAATAACCAAGC	90K array
IWB75883	FAMTTCTCTGGCAGAGGCGGA	HEXTTCTCTGGCAGAGGCGGC	CAATAGGACACCATAATAACCAAGC	90K array
IWA1690	FAMGATCCAAATGATCTGAATAAAGGT	HEXGATCCAAATGATCTGAATAAAGGC	CGCGCTCATTCAAATACGCC	9K array
Chr2B538239714	FAMGATACCAACAGCGAAGACG	HEXGATACCAACAGCGAAAGCA	AGTCCAACAAGGAGCTGCAA	Exome capture

FAM:GAAGGTGACCAAGTTCATGCT
HEX:GAAGGTCGGAGTCAACGGATT

6.3.6. Phenotyping for Fine Mapping

Replicated yield trials of BC_3F_4 plants were grown under greenhouse conditions in 15 cm pots with 16-h photoperiod and a temperature around 21 °C. In this first round of fine mapping, the yield trial consisted of five replicates from each $BC_3F_{3:4}$ family along with Ben, PI 41025, BP025-26, and BP025-28. Four spikes per plant were evaluated for the number of kernels per spike, with the plant average representing the score for mapping. Kernels per spike were counted manually for each spike, along with the total number of kernels per plant were counted using a MARVIN seed analyzer (GAT Sensorik GMBH, Neubrandenburg, Germany). Each family mean was calculated and used for determining which internal markers were most significantly associated with the kernel per spike trait. A one-tailed t-test was performed comparing the mean of families with Ben alleles at each marker with the mean of families with PI 41025 alleles at that same marker.

6.4. Results

6.4.1. RILs Used for Population Development

A replicated experiment was done to determine which RILs to use for backcrossing and population development. BP025-83, BP025-28, and BP025-26 averaged 22.85, 20.68, and 16.63 KPS, respectively (Table 6.1). My aim was to identify two RILs with PI 41025 alleles in this region and Ben alleles in the other KPS QTL regions and had lower number of KPS than Ben, which I backcrossed to. Although BP025-83 had lower number of KPS than Ben, it was not significantly different than either parent. BP025-26 had significant lower number of KPS than Ben and PI 41025. BP025-28 had fewer KPS than both parents but was only significantly lower than PI 41025. Therefore, I used BP025-26 and BP025-28 for my backcrosses.

6.4.2. Fine Mapping: Round One

All markers used for mapping were tested for polymorphism between Ben and PI 41025, along with the ability to distinguish heterozygous individuals. In the results published by Faris et al. (2014), the markers *IWA1217* and *IWA652* flanked the KPS QTL peak on chromosome 2B using CIM (Figure 6.2). The physical location of *IWA1217* and *IWA652* in the Svevo R1.0 was 445,441,818 and 483,022,545 bp, respectively, which were 37.58 Mb apart. For the first round of fine mapping, I screened outside of this region due to the complexity of the KPS trait, along with moving out towards a drop LOD score of 1.5 from the peak marker in SIM. I screened 1,072 BC_3F_2 gametes with the SSR marker *Xbarc230* and the STARP marker *IWB50897* (Table 6.2). *Xbarc230* was on the original BP025 map and *IWB50897* was developed from the 90K bulk segregate analysis and converted to a STARP marker. On the Svevo reference, *Xbarc230* was physically located at 213,613,003 bp and was on the short arm. *IWB50897* was located at 536,078,652 bp on the long arm, making the physical size of this region 322,465,649 bp in Svevo and spanning the centromere.

I identified 87 recombinants between *Xbarc230* and *IWB50897* (Table 6.4). Forty-four of these were from BP025-28/3*Ben BC_3F_2 plants and 43 from BP025-26/3*Ben BC_3F_2 plants. These same two markers were used to screen each BC_3F_2 family to identify BC_3F_3 homozygous recombinants. Homozygous recombinants were genotyped with an additional 36 markers, consisting of 7 SSR markers and 36 STARP markers (5 designed from 9k, 7 from 90k, and 17 from exome capture). These markers, listed in Table 6.2, consisted of the SSR markers on the original map, along with newly developed STARP markers. The newly developed markers were mapped using the first 94 lines of the BP025 population to validate that they mapped between the flanking markers (data not shown) before genotyping homozygous recombinants.

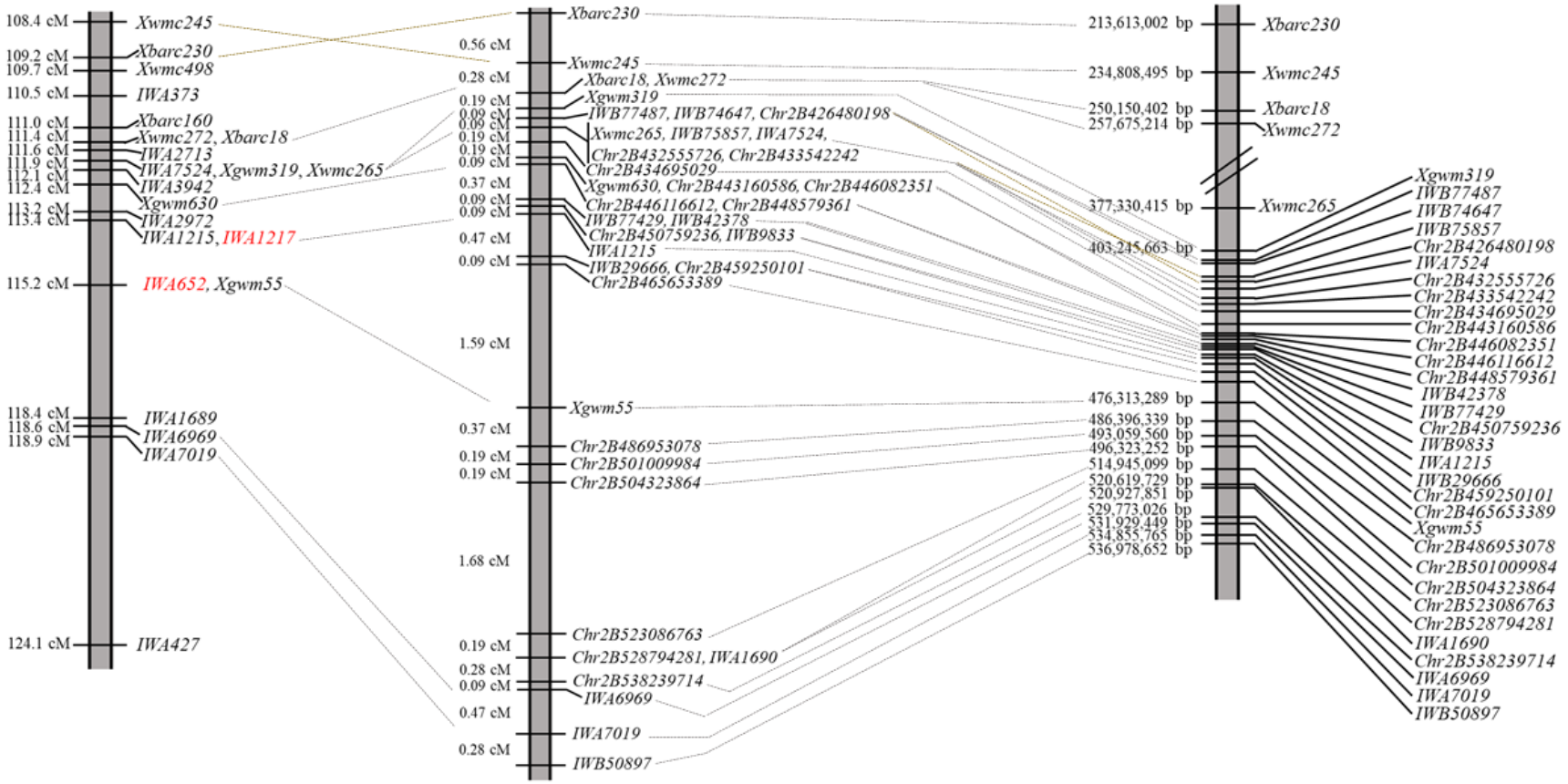

Figure 6.2. Map-based analysis of the KPS QTL region on chromosome 2B in the BP025 population. Left: The original BP025 map construction from 200 RILs as publsihed by Faris et al. (2014). Loci which had multiple-cosegregating markers are represented by one marker, unless multiple markers at that locus were used for saturation mapping. Markers highlighted in red were the original flanking markers in Faris et al. (2014). Center: Saturation map constructed from 1,072 BC_3F_2 gametes from the BP025-26/3*Ben BP025-28/3*Ben populations. Right: Physical map constructed using the Svevo Re. 1.0 pseudomolecules. The dashed lines between each map connect the same markers. The golden dashed lines indicate markers in which inversions were observed between the two maps.

Table 6.4. Results from replicated $BC_3F_{3:4}$ greenhouse yield trial and recombination region in BC_3F_3. For each BC_3F_3, the markers that flank the recombination event are listed.

		KPS			Recombination region			
Line	Donor RIL	Mean	Range	St. dev	Left marker[1]	Allele[2]	Right marker[1]	Allele[2]
Ben	NA	28.50	18.25-36.50	6.69	NA	NA	NA	NA
PI 41025	NA	33.95	23.75-39.00	6.03	NA	NA	NA	NA
BP025-26	NA	20.13	15.25-23.00	3.45	NA	NA	NA	NA
BP025-28	NA	26.55	9.50-33.75	10.16	NA	NA	NA	NA
J19P1275	BP025-26	32.95	29.00-40.75	4.98	*Xbarc230*	B	*Xwmc245*	A
J19P1371	BP025-26	32.85	25.00-41.00	7.88	*Xbarc230*	B	*Xwmc245*	A
J19P1409	BP025-26	16.50	13.75-20.75	3.35	*Xwmc245*	A	*Xbarc18*[a]	B
J19P1283	BP025-26	24.55	20.50-27.50	2.81	*Xgwm319*	A	*IWB77487*[b]	B
J19P962	BP025-26	31.58	28.00-36.75	4.58	*IWB77487*[b]	A	*Xwmc265*[c]	B
J19P1368	BP025-26	31.30	25.75-37.25	4.45	*Xwmc265*[c]	B	*Chr2B434695029*	A
J19P1015	BP025-26	27.00	25.25-29.50	1.66	*Xwmc265*[c]	B	*Chr2B434695029*	A
J19P1373	BP025-26	32.31	27.75-36.25	3.56	*Chr2B434695029*	B	*Xgwm630*[d]	A
J19P1853	BP025-26	24.56	22.50-26.00	1.56	*Xgwm630*[d]	A	*Chr2B446116612*[e]	B
J19P1292	BP025-26	20.30	12.50-28.25	7.34	*Chr2B446116612*[e]	B	*IWB77429*[f]	A
J19P1406	BP025-26	25.60	22.50-29.75	2.63	*Chr2B446116612*[e]	B	*IWB77429*[f]	A
J19P1360	BP025-26	30.06	26.50-34.50	3.56	*IWA1215*	B	*IWB29666*[h]	A
J19P1376	BP025-26	17.85	10.25-20.75	4.35	*IWA1215*	A	*IWB29666*[h]	B
J19P965	BP025-26	31.45	28.25-33.50	2.12	*IWB29666*[h]	A	*Chr2B465653389*	B
J19P1022	BP025-26	20.83	18.75-23.25	2.27	*Chr2B465653389*	B	*Xgwm55*	A
J19P1003	BP025-26	27.90	23.75-30.50	2.64	*Chr2B465653389*	B	*Xgwm55*	A
J19P1279	BP025-26	20.87	16.50-24.00	2.73	*Chr2B465653389*	B	*Xgwm55*	A
J19P1282	BP025-26	23.20	20.75-24.5	1.44	*Chr2B465653389*	B	*Xgwm55*	A
J19P1858	BP025-26	19.88	6.25-22.50	3.10	*Chr2B465653389*	B	*Xgwm55*	A
J19P1413	BP025-26	21.72	18.33-24.50	2.27	*Chr2B465653389*	B	*Xgwm55*	A
J19P1005	BP025-26	31.25	22.00-41.00	9.51	*Chr2B465653389*	A	*Xgwm55*	B
J19P1277	BP025-26	25.38	21.75-31.50	4.38	*Chr2B465653389*	A	*Xgwm55*	B
J19P1852	BP025-26	34.58	30.75-39.25	3.63	*Chr2B465653389*	A	*Xgwm55*	B
J19P1288	BP025-26	20.40	16.00-23.50	2.75	*Xgwm55*	B	*Chr2B486953078*	A
J19P1358	BP025-26	35.20	23.75-47.25	9.47	*Xgwm55*	A	*Chr2B486953078*	B
J19P1013	BP025-26	28.56	25.00-32.00	2.88	*Xgwm55*	A	*Chr2B486953078*	B
J19P1293	BP025-26	26.05	22.50-33.25	4.28	*Chr2B486953078*	A	*Chr2B501009984*	B
J19P1017	BP025-26	26.95	25.25-29.00	1.52	*Chr2B501009984*	B	*Chr2B504323864*	A
J19P1290	BP025-26	22.25	18.00-27.50	3.48	*Chr2B504323864*	B	*Chr2B523086763*	A
J19P1012	BP025-26	25.00	19.00-29.25	4.32	*Chr2B504323864*	B	*Chr2B523086763*	A
J19P1286	BP025-26	27.94	25.00-30.25	2.18	*Chr2B504323864*	A	*Chr2B523086763*	B

Table 6.4. Results from replicated $BC_3F_{3:4}$ greenhouse yield trial and recombination region in BC_3F_3 (continued). For each BC_3F_3, the markers that flank the recombination event are listed.

		KPS			Recombination region			
Line	Donor RIL	Mean	Range	St. dev	Left marker[1]	Allele[2]	Right marker[1]	Allele[2]
J19P1273	BP025-26	40.25	37.75-42.33	2.32	*Chr2B504323864*	A	*Chr2B523086763*	B
J19P1361	BP025-26	29.83	26.75-33.00	3.13	*Chr2B504323864*	A	*Chr2B523086763*	B
J19P1357	BP025-26	28.30	26.00-29.75	1.51	*Chr2B504323864*	A	*Chr2B523086763*	B
J19P1364	BP025-26	21.73	16.50-27.75	4.32	*Chr2B504323864*	A	*Chr2B523086763*	B
J19P1369	BP025-26	28.08	26.25-30.00	1.88	*Chr2B504323864*	A	*Chr2B523086763*	B
J19P1407	BP025-26	33.13	29.50-36.50	2.93	*Chr2B528794281*[i]	A	*Chr2B538239714*	B
J19P961	BP025-26	18.75	17.50-19.50	0.79	*IWA6969*	B	*IWA7019*	A
J19P956	BP025-26	19.45	13.25-26.00	5.80	*IWA6969*	B	*IWA7019*	A
J19P972	BP025-26	34.13	31.75-38.75	3.24	*IWA6969*	A	*IWA7019*	B
J19P963	BP025-26	29.30	26.25-33.50	2.90	*IWA6969*	A	*IWA7019*	B
J19P1265	BP025-26	14.65	12.25-18.00	2.21	*IWA7019*	B	*IWB50897*	A
J19P958	BP025-26	29.33	27.25-33.33	2.74	*IWA7019*	B	*IWB50897*	A
J19P983	BP025-28	20.63	16.75-24.75	3.27	*Xbarc230*	B	*Xwmc245*	A
J19P1384	BP025-28	23.61	21.50-26.67	2.71	*Xbarc230*	B	*Xwmc245*	A
J19P1385	BP025-28	26.30	21.25-29.25	3.11	*Xbarc230*	B	*Xwmc245*	A
J19P1388	BP025-28	29.83	28.50-30.75	1.18	*Xbarc230*	B	*Xwmc245*	A
J19P993	BP025-28	17.75	14.25-19.25	2.35	*Xwmc245*	A	*Xbarc18*[a]	B
J19P1396	BP025-28	21.83	21.50-22.25	0.38	*Xwmc245*	A	*Xbarc18*[a]	B
J19P998	BP025-28	19.83	16.75-22.00	2.74	*Xbarc18*[a]	B	*Xgwm319*	A
J19P1270	BP025-28	19.19	14.50-26.50	5.35	*Xbarc18*[a]	A	*Xgwm319*	B
J19P951	BP025-28	23.63	21.25-29.75	4.10	*Chr2B434695029*	B	*Xgwm630*[d]	A
J19P1379	BP025-28	25.52	21.33-29.00	2.93	*Chr2B446116612*[e]	B	*IWB77429*[f]	A
J19P974	BP025-28	31.50	26.25-36.00	4.92	*Chr2B446116612*[e]	B	*IWB77429*[f]	A
J19P1394	BP025-28	24.81	24.00-26.00	0.99	*IWB77429*[f]	A	*Chr2B450759236*[g]	B
J19P1027	BP025-28	23.50	18.50-30.00	5.12	*Chr2B450759236*[g]	A	*IWA1215*	B
J19P969	BP025-28	29.83	26.50-36.25	5.56	*IWA1215*	B	*IWB29666*[h]	A
J19P1001	BP025-28	25.30	20.50-28.00	3.46	*IWA1215*	B	*IWB29666*[h]	A
J19P954	BP025-28	14.13	1.25-38.33	14.96	*IWA1215*	A	*IWB29666*[h]	B
J19P1393	BP025-28	12.69	4.25-21.25	6.95	*Chr2B465653389*	B	*Xgwm55*	A
J19P1404	BP025-28	16.75	14.25-18.75	2.98	*Chr2B465653389*	B	*Xgwm55*	A
J19P994	BP025-28	27.88	24.50-31.25	2.98	*Chr2B465653389*	A	*Xgwm55*	B
J19P990	BP025-28	29.25	23.25-33.50	4.32	*Chr2B465653389*	A	*Xgwm55*	B
J19P1025	BP025-28	20.03	6.67-34.75	12.06	*Chr2B465653389*	A	*Xgwm55*	B
J19P1023	BP025-28	28.80	24.25-31.75	2.79	*Chr2B465653389*	A	*Xgwm55*	B
J19P1268	BP025-28	26.29	22.25-29.50	3.00	*Chr2B465653389*	A	*Xgwm55*	B

Table 6.4. Results from replicated $BC_3F_{3:4}$ greenhouse yield trial and recombination region in BC_3F_3 (continued). For each BC_3F_3, the markers that flank the recombination event are listed.

		KPS			Recombination region			
Line	Donor RIL	Mean	Range	St. dev	Left marker[1]	Allele[2]	Right marker[1]	Allele[2]
J19P1400	BP025-28	25.17	23.75-26.75	1.51	*Chr2B465653389*	A	*Xgwm55*	B
J19P1264	BP025-28	28.50	21.75-35.50	5.62	*Xgwm55*	A	*Chr2B486953078*	B
J19P1381	BP025-28	20.15	19.00-21.00	0.89	*Chr2B486953078*	B	*Chr2B501009984*	A
J19P1390	BP025-28	24.83	17.75-31.75	7.00	*Chr2B501009984*	A	*Chr2B504323864*	B
J19P981	BP025-28	23.15	21.25-26.50	2.00	*Chr2B504323864*	B	*Chr2B523086763*	A
J19P975	BP025-28	20.06	18.25-21.75	1.70	*Chr2B504323864*	B	*Chr2B523086763*	A
J19P1410	BP025-28	25.42	24.50-26.25	0.88	*Chr2B504323864*	B	*Chr2B523086763*	A
J19P1391	BP025-28	21.92	17.75-24.75	3.69	*Chr2B504323864*	B	*Chr2B523086763*	A
J19P1855	BP025-28	22.92	19.33-28.50	3.49	*Chr2B504323864*	B	*Chr2B523086763*	A
J19P1398	BP025-28	21.13	17.00-25.25	3.49	*Chr2B504323864*	B	*Chr2B523086763*	A
J19P953	BP025-28	25.55	17.00-35.00	6.70	*Chr2B504323864*	A	*Chr2B523086763*	B
J19P992	BP025-28	29.85	24.25-31.75	4.07	*Chr2B504323864*	A	*Chr2B523086763*	B
J19P1008	BP025-28	19.31	10.50-27.75	7.95	*Chr2B504323864*	A	*Chr2B523086763*	B
J19P1401	BP025-28	22.04	17.67-24.75	3.05	*Chr2B504323864*	A	*Chr2B523086763*	B
J19P985	BP025-28	10.40	3.25-17.25	6.62	*Chr2B523086763*	B	*Chr2B528794281*[i]	A
J19P966	BP025-28	15.92	12.50-18.75	3.17	*Chr2B523086763*	A	*Chr2B528794281*[i]	B
J19P977	BP025-28	30.58	27.25-32.75	2.93	*Chr2B528794281*[i]	A	*Chr2B538239714*	B
J19P1000	BP025-28	29.06	27.50-31.00	1.71	*Chr2B528794281*[i]	A	*Chr2B538239714*	B
J19P1378	BP025-28	20.30	15.25-26.00	4.98	*Chr2B538239714*	B	*IWA6969*	A
J19P1009	BP025-28	28.21	25.33-32.75	3.22	*IWA6969*	A	*IWA7019*	B
J19P971	BP025-28	19.12	7.33-30.25	8.69	*IWA7019*	A	*IWB50897*	B

[1]List of markers that co-segregate:

[a]*Xbarc18*, *Xwmc272*

[b]*IWB77487*, *IWB74647*, *Chr2B426480198*

[c]*Xwmc265*, *IWB75857*, *IWA7524*, *Chr2B432555726*, *Chr2B433542242*

[d]*Xgwm630*, *Chr2B443160586*, *Chr2B446082351*

[e]*Chr2B446116612*, *Chr2B448579361*

[f]*IWB77429*, *IWB42378*

[g]*Chr2B450759236*, *IWB9833*

[h]*IWB29666*, *Chr2B459250101*

[i]*Chr2B528794281*, *IWA1690*

[2]Ben allele=A, PI 41025 allele=B

A total of three markers were added that mapped between the original flanking markers (Figure 6.2). *IWB29666* was designed from the 90K SNP array and *Chr2B459250101* and *Chr2B465653389* were from the exome capture results. The region was expanded from 1.8 cM in the original BP025 genetic map to 2.15 cM in the fine map. Compared to the original map, the fine map showed an inversion between *Xwmc245* and *Xbarc230*. Comparing the fine map to the physical location, the markers *Chr2B426480198* and *IWB75857* were inverted between the two maps.

$BC_3F_{3:4}$ plants were phenotyped with five replicates per family under greenhouse conditions. Five replicates were used because this filled an entire greenhouse room. The results of this trial are shown in Table 6.4. Due to the complexity of the KPS trait, along with a few discrepancies in values for a handful of lines, the candidate region was delineated by markers *Chr2B446082351* and *Chr2B538239714* by comparing the mean values for each allele type for each internal marker (Table 6.5). Based on the Svevo reference sequence, *Chr2B446082351* was at 439,345,516 bp and *Chr2B538239714* was at 529,773,026 bp. The physical size of this delineated region was 90,427,510 bp and no longer spanned the centromere.

Table 6.5. Comparison of means and t-test for the different markers. The markers highlighted in red are on the outer edge of the QTL region associated with KPS.

	Allele KPS average		
Marker	Ben	PI 41025	T-test *P*-value
Xbarc230	26.18	23.59	0.015459092
Xwmc245	26.36	22.93	0.001573134
Xbarc18	26.85	22.61	0.000150597
Xwmc272	26.85	22.61	0.000150597
Xgwm319	26.86	22.59	0.000135347
IWB74647	26.91	22.64	0.000130887
IWB77487	26.91	22.64	0.000130887
Chr2B426480198	26.91	22.64	0.000130887
IWB75857	26.81	22.85	0.00038427
Xwmc265	26.81	22.85	0.00038427
IWA7524	26.81	22.85	0.00038427
Chr2B432555726	26.81	22.85	0.00038427
Chr2B433542242	26.81	22.85	0.00038427
Chr2B434695029	26.91	22.54	9.3967E-05
Xgwm630	26.95	22.25	2.88122E-05
Chr2B443160586	26.95	22.25	2.88122E-05
Chr2B446082351	26.95	22.25	2.88122E-05
Chr2B446116612	27.00	22.31	2.84552E-05
Chr2B448579361	27.00	22.31	2.84552E-05
IWB77429	26.90	21.92	1.12797E-05
IWB42378	26.90	21.92	1.12797E-05
Chr2B450759236	26.94	22.00	1.21493E-05
IWB9833	26.94	22.00	1.21493E-05
IWA1215	27.01	22.04	9.93909E-06
IWB29666	27.53	21.18	8.4298E-09
Chr2B459250101	27.53	21.18	8.4298E-09
Chr2B465653389	27.45	21.45	6.17462E-08
Xgwm55	26.28	23.12	0.004247403
Chr2B486953078	25.87	23.76	0.040551293
Chr2B501009984	25.74	23.91	0.064886613
Chr2B504323864	25.79	23.86	0.055122224
Chr2B523086763	24.91	24.89	0.492436734
Chr2B528794281	24.79	25.02	0.424684836
IWA1690	24.79	25.02	0.424684836
Chr2B538239714	24.35	25.41	0.1904714
IWA6969	24.26	25.53	0.146590889
IWA7019	23.56	26.15	0.015463157
IWB50897	23.59	26.18	0.015459092

6.4.3. Fine Mapping: Round Two

New BC_3F_2 plants were screened for the reduced region using the STARP markers *Chr2B446082351* and *Chr2B538239714*. A total of 73 heterozygous recombinants were identified from 1,556 gametes. Forty-six of these were from BC_3F_2 plants derived from BP025-28 and 27 were from BC_3F_2 plants derived from BP025-26. These same two markers were used to screen each BC_3F_2 family to identify BC_3F_3 homozygous recombinants; however, the markers were converted to KASP markers for genotyping BC_3F_3 plants to speed up the process (Table 6.3). The BC_3F_3 homozygous recombinants were genotyped with 64 internal markers using KASP assays for the development of the new genetic linkage map.

The genetic linkage map developed using the BC_3F_3 homozygous recombinants was 4.65 cM and spanned a physical distance from 439,345,516 bp to 529,773,026 bp on the Svevo reference (Figure 6.3). No inversions or translocations were observed when comparing the marker order in the genetic map with the physical map (Figure 6.3). The markers in which a recombination occurred for each BC_3F_2 family are listed in Table 6.6. A total of 18 new markers were added between the original flanking markers of *IWA1215* and *XGwm55* from Faris et al. (2014). Based on the Svevo reference, a total of 576 high confidence genes are within this region.

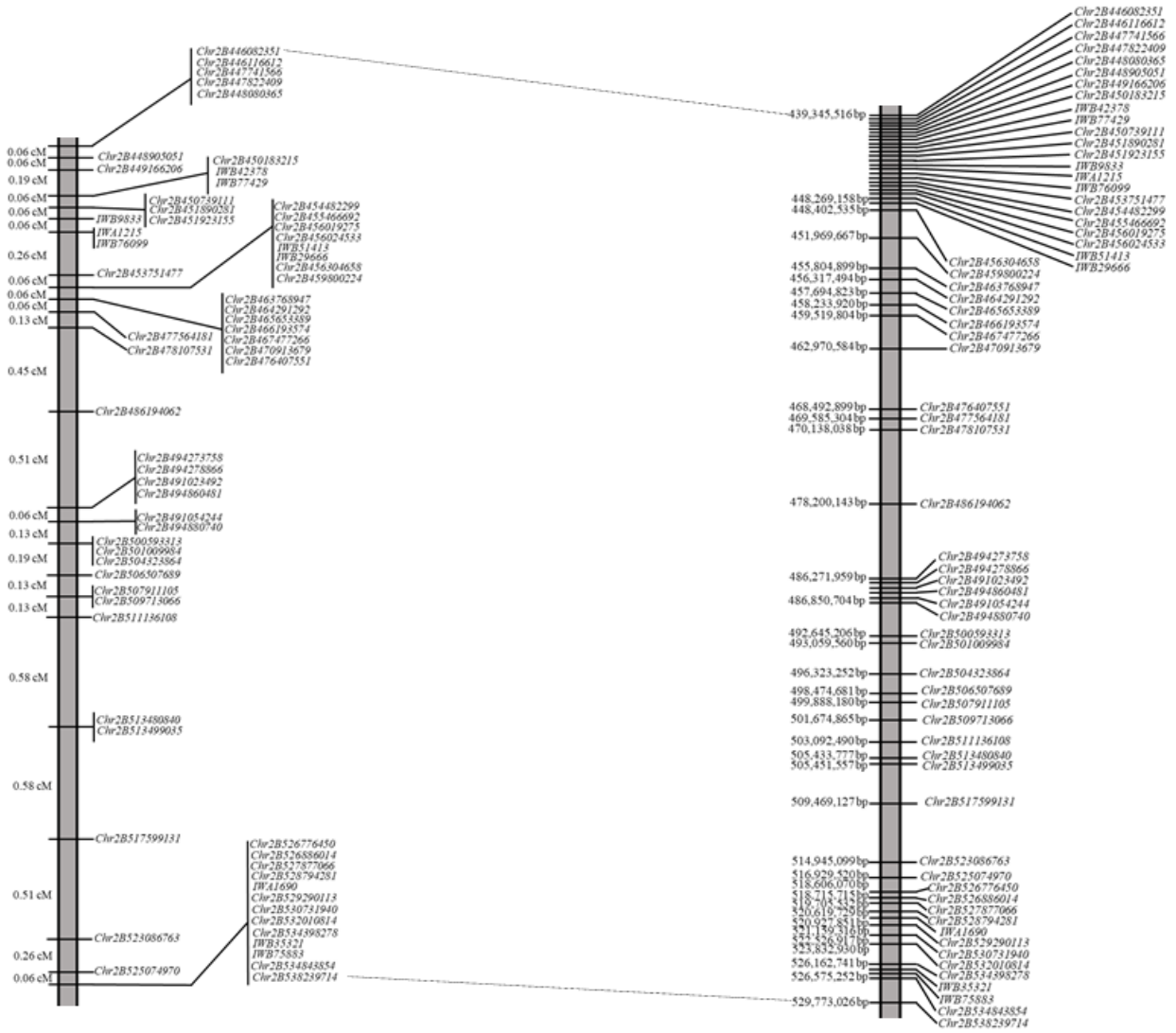

Figure 6.3. Map-based analysis of the KPS QTL region on chromosome 2B in the BP025 population. Left: Saturation map constructed from 1,556 BC_3F_2 gametes from the BP025-26/3*Ben BP025-28/3*Ben populations. Right: Physical map constructed using the Svevo Re. 1.0 pseudomolecules. The dashed lines connect the flanking markers between the two maps.

Table 6.6. Genetic linkage results from the second round of fine-mapping and the markers in which a recombination occurred in the BC_3F_3 plants.

		Recombination region			
Line	Donor RIL	Left marker[1]	Allele[2]	Right marker[1]	Allele[2]
J21P21	BP025-26	*Chr2B446082351*[a]	A	*Chr2B448905051*	B
J21P115	BP025-28	*Chr2B448905051*	B	*Chr2B449166206*	A
J21P1	BP025-26	*Chr2B449166206*	B	*Chr2B450183215*[b]	A
J21P24	BP025-26	*Chr2B449166206*	A	*Chr2B450183215*[b]	B
J21P56	BP025-28	*Chr2B449166206*	A	*Chr2B450183215*[b]	B
J21P145	BP025-28	*Chr2B450183215*[b]	A	*Chr2B450739111*[c]	B
J21P91	BP025-28	*Chr2B450739111*[c]	B	*IWB9833*	A
J21P78	BP025-28	*IWB9833*	B	*IWA1215*[d]	A
J21P98	BP025-28	*IWA1215*[d]	B	*Chr2B453751477*	A
J21P108	BP025-28	*IWA1215*[d]	A	*Chr2B453751477*	B
J21P69	BP025-28	*IWA1215*[d]	A	*Chr2B453751477*	B
J21P88	BP025-28	*IWA1215*[d]	A	*Chr2B453751477*	B
J21P101	BP025-28	*Chr2B453751477*	B	*Chr2B454482299*[e]	A
J21P137	BP025-26	*Chr2B454482299*[e]	B	*Chr2B463768947*[f]	A
J21P161	BP025-28	*Chr2B463768947*[f]	B	*Chr2B477564181*	A
J21P40	BP025-26	*Chr2B477564181*	B	*Chr2B478107531*	A
J21P123	BP025-28	*Chr2B477564181*	A	*Chr2B478107531*	B
J21P99	BP025-28	*Chr2B478107531*	B	*Chr2B486194062*	A
J21P157	BP025-28	*Chr2B478107531*	B	*Chr2B486194062*	A
J21P28	BP025-26	*Chr2B478107531*	B	*Chr2B486194062*	A
J21P158	BP025-28	*Chr2B478107531*	B	*Chr2B486194062*	A
J21P116	BP025-28	*Chr2B478107531*	A	*Chr2B486194062*	B
J21P26	BP025-26	*Chr2B478107531*	A	*Chr2B486194062*	B
J21P3	BP025-26	*Chr2B478107531*	A	*Chr2B486194062*	B
J21P120	BP025-28	*Chr2B486194062*	B	*Chr2B494273758*[g]	A
J21P142	BP025-28	*Chr2B486194062*	B	*Chr2B494273758*[g]	A
J21P73	BP025-28	*Chr2B486194062*	B	*Chr2B494273758*[g]	A
J21P94	BP025-28	*Chr2B486194062*	A	*Chr2B494273758*[g]	B
J21P105	BP025-28	*Chr2B486194062*	A	*Chr2B494273758*[g]	B
J21P81	BP025-28	*Chr2B486194062*	A	*Chr2B494273758*[g]	B
J21P23	BP025-26	*Chr2B486194062*	A	*Chr2B494273758*[g]	B
J21P7	BP025-26	*Chr2B486194062*	A	*Chr2B494273758*[g]	B
J21P93	BP025-28	*Chr2B494273758*[g]	A	*Chr2B491054244*[h]	B
J21P85	BP025-28	*Chr2B491054244*[h]	B	*Chr2B500593313*[i]	A
J21P31	BP025-26	*Chr2B491054244*[h]	B	*Chr2B500593313*[i]	A
J21P154	BP025-28	*Chr2B500593313*[i]	B	*Chr2B506507689*	A
J21P14	BP025-26	*Chr2B500593313*[i]	A	*Chr2B506507689*	B
J21P55	BP025-28	*Chr2B500593313*[i]	A	*Chr2B506507689*	B
J21P58	BP025-28	*Chr2B506507689*	B	*Chr2B507911105*[j]	A
J21P59	BP025-28	*Chr2B506507689*	A	*Chr2B507911105*[j]	B
J21P19	BP025-26	*Chr2B507911105*[j]	B	*Chr2B511136108*	A
J21P113	BP025-28	*Chr2B507911105*[j]	A	*Chr2B511136108*	B
J21P30	BP025-26	*Chr2B511136108*	B	*Chr2B513480840*[k]	A
J21P36	BP025-26	*Chr2B511136108*	B	*Chr2B513480840*[k]	A
J21P37	BP025-26	*Chr2B511136108*	B	*Chr2B513480840*[k]	A
J21P42	BP025-26	*Chr2B511136108*	B	*Chr2B513480840*[k]	A
J21P44	BP025-26	*Chr2B511136108*	B	*Chr2B513480840*[k]	A
J21P46	BP025-26	*Chr2B511136108*	B	*Chr2B513480840*[k]	A
J21P48	BP025-26	*Chr2B511136108*	B	*Chr2B513480840*[k]	A
J21P52	BP025-26	*Chr2B511136108*	B	*Chr2B513480840*[k]	A

Table 6.6. Genetic linkage results from the second round of fine-mapping and the markers in which a recombination occurred in the BC_3F_3 plants (continued).

		Recombination region			
Line	Donor RIL	Left marker[1]	Allele[2]	Right marker[1]	Allele[2]
J21P71	BP025-28	*Chr2B511136108*	B	*Chr2B513480840*[k]	A
J21P68	BP025-28	*Chr2B513480840*[k]	B	*Chr2B517599131*	A
J21P65	BP025-28	*Chr2B513480840*[k]	B	*Chr2B517599131*	A
J21P15	BP025-26	*Chr2B513480840*[k]	B	*Chr2B517599131*	A
J21P130	BP025-28	*Chr2B513480840*[k]	B	*Chr2B517599131*	A
J21P97	BP025-28	*Chr2B513480840*[k]	A	*Chr2B517599131*	B
J21P103	BP025-28	*Chr2B513480840*[k]	A	*Chr2B517599131*	B
J21P33	BP025-26	*Chr2B513480840*[k]	A	*Chr2B517599131*	B
J21P119	BP025-28	*Chr2B513480840*[k]	A	*Chr2B517599131*	B
J21P109	BP025-28	*Chr2B513480840*[k]	A	*Chr2B517599131*	B
J21P112	BP025-28	*Chr2B517599131*	B	*Chr2B523086763*	A
J21P89	BP025-28	*Chr2B517599131*	B	*Chr2B523086763*	A
J21P16	BP025-26	*Chr2B517599131*	B	*Chr2B523086763*	A
J21P136	BP025-26	*Chr2B517599131*	B	*Chr2B523086763*	A
J21P5	BP025-26	*Chr2B517599131*	A	*Chr2B523086763*	B
J21P76	BP025-28	*Chr2B517599131*	A	*Chr2B523086763*	B
J21P127	BP025-28	*Chr2B517599131*	A	*Chr2B523086763*	B
J21P125	BP025-28	*Chr2B517599131*	A	*Chr2B523086763*	B
J21P9	BP025-26	*Chr2B523086763*	B	*Chr2B525074970*	A
J21P174	BP025-28	*Chr2B523086763*	B	*Chr2B525074970*	A
J21P75	BP025-28	*Chr2B523086763*	A	*Chr2B525074970*	B
J21P63	BP025-28	*Chr2B523086763*	A	*Chr2B525074970*	B
J21P61	BP025-28	*Chr2B525074970*	A	*Chr2B526776450*[l]	B

[1]List of markers that co-segregate:

[a]*Chr2B446082351, Chr2B446116612, Chr2B447741566, Chr2B447822409, Chr2B448080365*

[b]*Chr2B450183215, IWB42378, IWB77429*

[c]*Chr2B450739111, Chr2B451890281, Chr2B451923155*

[d]*IWA1215*, *IWB76099*

[e]*Chr2B454482299, Chr2B455466692, Chr2B456019275, Chr2B456024533, IWB51413, IWB29666, Chr2B456304658, Chr2B459800224*

[f]*Chr2B463768947, Chr2B464291292, Chr2B465653389, Chr2B46619357, Chr2B467477266, Chr2B470913679, Chr2B476407551*

[g]*Chr2B494273758, Chr2B494278866, Chr2B491023492, Chr2B494860481*

[h]*Chr2B491054244, Chr2B494880740*

[i]*Chr2B500593313, Chr2B501009984, Chr2B504323864*

[j]*Chr2B507911105, Chr2B509713066*

[k]*Chr2B513480840, Chr2B513499035*

[l]*Chr2B526776450, Chr2B526886014, Chr2B527877066, Chr2B528794281, IWA1690, Chr2B529290113, Chr2B530731940, Chr2B532010814, Chr2B534398278, IWB35321, IWB75883, Chr2B534843854, Chr2B538239714*

[2]Ben allele=A, PI 41025 allele=B

6.5. Discussion

Relatively few yield related genes have been cloned in wheat compared to the other two major cereal crop species, rice and maize (Nadolska-Orczyk et al. 2017). This is partially due to the large genome size of wheat, the complexity with multiple subgenomes, and the difficulty of phenotyping yield and yield components (Borrill et al. 2015). It is important to clone yield components genes to understand the underlying pathways involved in determining final yield, along with using this information for breeding purposes (Cao et al. 2020). Previously, a QTL for increased kernels per spike was identified by Faris et al. (2014) under greenhouse conditions and later under field conditions (Chapter 5) in the BP025 population. Here, I reported the development of a fine map around the genetic region of a kernels per spike QTL on chromosome 2B in tetraploid wheat.

One issue with map-based cloning of yield related traits is the small effect of these genes and effects from homoeologous genes. One method to overcome this is the use of heterogenous inbred families (Taagen et al. 2021). However, the use of these type of lines also presents challenges. In this study, I developed near-isogenic lines to 'Mendelize' the trait. To develop these lines, I performed a series of backcrosses to develop lines that contained high percentage of the Ben background throughout the genome but were heterozygous for both Ben and PI 41025 alleles in the target region. Ben was chosen as the recurrent parent due to having more favorable traits for greenhouse work, such as shorter height and days to heading, than PI 41025 (Faris et al. 2014).

One hurdle I have observed, along with others, was the presence of many yield related traits near the centromeric region (Chapters 4, 5; Arriagada et al. 2020; Colasuonno et al. 2021; Cao et al. 2020). Maccaferri et al. (2019) demonstrated using the sequence of Zavitan, a wild

emmer wheat line, and Svevo, a durum wheat cultivar, that QTL in tetraploid wheat for numerous traits have been mapped to the pericentromeric region. In Svevo, the pericentromeric, low recombinogenic region spans from 209.7 to 441.5 Mb. The initial region included in the first round of the fine mapping in this study included this region. Few recombinants were observed between the markers which were physically located within this region, although the physical size of this region is quite large (Figure 6.2, Table 6.4). Fortunately, I was able to delineate the region for the second round of fine mapping to be on the edge of this region and outwards, from 439.3 to 529.8 Mb.

An initial aim of this project was to develop and map markers between the original flanking markers of *IWA1217* and *IWA652* (Faris et al. 2014). I was not able to convert these SNP markers to STARP markers for my initial fine mapping. Therefore, I used the SSR marker *Xgwm55* and converted the SNP marker *IWA1215* into a STARP marker. For this first round, I only added three markers which mapped between the original flanking markers, *IWB29666*, *Chr2B459250101*, and *Chr2B465653389* (Figure 6.2). More markers could have been developed from the exome capture data; however, for this first round I was visualizing markers using polyacrylamide gels. Due to the time commitment of running these gels, it was not feasible possible to run a large number of markers within this region. Additionally, I added markers around these flanking markers outside of my region in case the initial peak QTL region identified by Faris et al. (2014) did not contain the target gene for KPS.

The second round of fine mapping added 18 markers between the original flanking markers of *IWA1215* and *XGwm55* reported by Faris et al. (2014). A larger number of markers was used for genotyping in this round due to converting my markers to KASP based and using a non-gel based visualization method. Currently, we are growing BC_3F_4 plants representing each

BC_3F_3 family in the greenhouse in a replicated yield trial to delineate this region further using the newly developed genetic linkage map of this region.

Once I have identified a narrower target region, I will use reference sequence data to look for candidate genes within this region. Recently, the wheat gene *WAPO-A1* was cloned and is an ortholog of the rice gene *ABERRANT PANICLE ORGANIZATION 1* (Muqaddasi et al. 2019; Voss-Fels et al. 2019; Kuzay et al. 2019). Additional wheat yield related genes which have been identified and have orthologs in rice include *TaGW2*, *TaTGW6-A1*, *TaFlo2-A1*, *TaTPP-6AL1*, *TaTGW-7A*, *TaCwi-A1*, *Tabas1-B1*, *TaCWI*, and *TaCYP78A3* (Wang et al. 2018; Hanif et al. 2015; Sajjad et al. 2017; Zhang et al. 2017; Hu et al. 2016; Ma et al. 2012; Zhu et al. 2016; Jiang et al. 2015; Ma et al. 2015); however, many of these have not been validated. Many yield related genes have been cloned and characterized in rice (Huang et al. 2018), therefore I will use BLAST analysis to evaluate genes within the region in comparison to genes in rice and other cereal genomes as needed. Once strong candidates are identified, I will utilize reverse genetic methods, such as the Kronos and Cadenza Targeting Induced Local Lesions in Genomes (TILLING) populations (Krasileva et al. 2016) and multiplex gene editing via CRISPR-Cas9 (Wang et al. 2018), to determine if any candidate genes have an effect on kernel number per spike.

In conclusion, I am currently working on fine mapping a region on chromosome 2B that is associated with kernels per spike in tetraploid wheat. To overcome many of the obstacles due to the complexity of the wheat genome, I developed near-isogenic lines using the backcross method to "Mendelize" the trait, along with the use of replicated yield trials. If I succeed in identifying, cloning, and characterizing my target gene, this knowledge will contribute to the understanding of the genes or pathways are involved in determining the final number of kernels

per spike. The cloning of yield related genes may prove useful for the future of plant breeding, giving breeders the knowledge and power to fine-tune wheat yield to feed future generations.

6.6. Literature Cited

Arriagada O, Marcotuli I, Gadaleta A, Schwember AR (2020) Molecular mapping and genomics of grain yield in durum wheat: a review. Int J Mol Sci 21:7021

Borrill P, Adamski N, Uauy C (2015) Genomics as the key to unlocking the polyploid potential of wheat. New Phytol 208:1008-1022

Brinton J and Uauy C (2018) A reductionist approach to dissecting grain weight and yield in wheat. J Integr Plant Biol 61:337-358

Cao S, Xu D, Hanif M, Xia X, He Z (2020) Genetic architecture underpinning yield component traits in wheat. Theor Appl Genet 133:1811-1823

Cavanagh CR, Chao S, Wang S, Huang BE, Stephan S, Kiani S, Forrest K, Saintenac C, Brown-Guedira GL, Akhunova A, et al. (2013) Genome-wide comparative diversity uncovers multiple targets of selection for improvement in hexaploid wheat landraces and cultivars. Proc Natl Aced Sci 110:8057-8062

Colasuonno P, Marcotuli I, Gadaleta A, Soriano JM (2021) From genetic maps to QTL cloning: an overview for durum wheat. Plants 10:315

Elias EM, Miller JD (1998) Registration of 'Ben' durum wheat. Crop Sci 38:895

Faris JD, Haen KM, Gill BS (2000) Saturation mapping of a gene-rich recombination hot spot region in wheat. Genetics 154:823-835

Faris JD, Zhang Q, Chao S, Zhang Z, Xu SS (2014) Analysis of agronomic and domestication traits in a durum × cultivated emmer wheat population using a high-density single nucleotide polymorphism-based linkage map. Theor Appl Genet 127:2333-2348

Hanif M, Gao F, Liu J, Wen W, Zhang Y, Rasheed A, Xia X, He Z, Cao S (2016) *TaTGW6-A1*, an artholog of rice *TGW6*, is associated with grain weight and yield in bread wheat. Mol Breeding 36:1

Huang J, Li J, Zhou J, Wang L, Yang S, Hurst LD, Li WH, Tian D (2018) Identifying a large number of high-yield genes in rice by pedigree analysis, whole-genome sequencing, and CRIPSR-Cas9 gene knockout. Proc Natl Acad Sci 115:E7559-E7567

Hu MJ, Zhang HP, Liu K, Cao JJ, Wang SX, Jiang H, Wu ZY, Lu J, Zhu XF, Xia XC, Sun GL, Ma CX, Chang C (2016) Cloning and characterization of *TaTGW-7A* gene associated with grain weight in wheat via SLAF-seq-BSA. Front Plant Sci 7:1902

IWGSC, Appels R, Eversole K, Stein N, Feuillet C, Keller B, Rogers J, Pozniak CJ, Choulet F, Distelfeld A, et al. (2018) Shifting the limits in wheat research and breeding using a fully annotated reference genome. Science 361:6403

Jiang Y, Jiang Q, Hao C, Hou J, Wang L, Zhang H, Zhang S, Chen X, Zhang X (2015) A yield-associated gene *TaCWI*, in wheat: its function, selection and evolution in global breeding revealed by haplotype analysis. Theor Appl Genet 128:131-143

Krasileva KV, Vasquez-Gross HA, Howell T, Bailey P, Paraiso F, Clissold L, Simmonds J, Ramirez-Gonzalez RH, Wang X, Borrill P, Fosker C, Ayling S, Phillips AL, Uauy C, Dubcovsky J (2016) Uncovering hidden variation in polyploid wheat. Proc Natl Acad Sci 114:E913-E921

Kuzay S, Xu Y, Zhang J, Katz A, Pearce S, Su Z, Fraser M, Anderson JA, Brown-Guedira G, DeWitt N, Peters Haugrud A, Faris JD, Akhunoc E, Bai G, Dubcovsky J (2019) Identification of a candidate gene for a QTL for spikelet number per spike on wheat chromosome arm 7AL by high-resolution mapping. Theor Appl Genet 132:2689-2705

Long YM, Chao WS, Ma GJ, Xu SS, Qi LL (2017) An inoovative SNP genotyping method adapting to multiple platforms and throughputs. Theor Appl Genet 130:597-607

Ma D, Yan J, He Z, Wu L, Xia X (2012) Characterization of a cell wall invertase gene *TaCwi-A1* on common wheat chromosome 2A and development of functional markers. Mol Breeding 29:43-52

Ma M, Wang Q, Li Z, Cheng H, Li Z, Liu X, Song W, Appels R, Zhao H (2015) Expression of *TaCYP78A3*, a gene encoding cytochrome P450 CYP78A3 protein in wheat (*Triticum aestivum* L.) affects seed size. Plant J 83:312-325

Maccaferri M, Harris NS, Twardziok SO, Pasam RK, Gundlach H, Spannagl M, Ormanbekova D, Lux T, Prade VM, Milner SG, et al. (2019) Durum wheat genome highlights past domestication signatures and future improvement targets. Nat Genet 51:885-895

Muqaddasi QH, Brassac J, Koppolu R, Plieske J, Ganal MW, Röder MS (2019) *TAPO-A1*, an otholog of rice *ABERRANT PANICLE ORGANIZATION 1*, is associated with total spikelet number per spike in elite European hexaploid winter wheat (*Triticum aestivum* L.) varieties. Sci Rep-UK 9:13853

Nadolska-Orczyk A, Rajchel IK, Orczyk W, Gasparis S (2017) Major genes determining yield-related traits in wheat and barley. Theor Appl Genet 130:1081-1098

Pallotta MA, Warner P, Fox RL, Kuchel H, Jefferies SJ, Langridge P (2003) Marker assisted wheat breeding in the southern region of Australia. In: Pogna NE, Romano M, Pogna EA, Galterio Z (eds) Proceedings of the 10th international wheat genetics symposium, Paestum, Italy, 1–6 September, 2003. Instituto Sperimentale per la Cerealicoltura, Sant'Angelo Lodigiano, pp 789–791

Sajjad M, Xiaoling M, Khan SH, Shoaib M, Song Y, Yang W, Zhang A, Liu D (2017) *TaFlo2-A1*, an ortholog of rice *Flo2*, is associated with thousand grain weight in bread wheat (*Triticum aestivum* L.). BMC Plant Biol 17:164

Taagen E, Tanaka J, Gul A, Sorrells ME (2021) Positional-based cloning 'fail-safe' approach is overpowered by wheat chromosome structural variation. Plant Genome-US 14:e20106

Voss-Fels KP, Keeble-Gagnère G, Hickey LT, Tibbits J, Nagornyy S, Hayden MJ, Pasam RK, Kant S, Friedt W, Snowdon RJ, Appels R, Wittkop B (2019) High-resolution mapping of rachis nodes per rachis, a critical determinant of grain yield components in wheat. Theor Appl Genet 132:2707-2719

Wang S, Wong D, Forrest K, Allen A, Chao S, Huang BE, Maccaferri M, Salvi S, Milner SG, Cattivelli L, et al. (2014) Characterization of polyploid wheat genomic diversity using a high-density 90,000 single nucleotide polymorphism array. Plant Biotechnol J https://doi.org/10.1111/pbi.12183

Wang W, Pan Q, He F, Akhunova A, Chao S, Trick H, Akhunov E (2018) Transgenerational CRIPSR-Cas9 activity facilitates multiplex gene editing in allopolyploid wheat. The CRISPR Journal 1:65-74

Wang W, Simmonds J, Pan Q, Davidson D, He F, Battal A, Akhunova A, Trick HN, Uauy C, Akhunov E (2018) Gene editing and mutagenesis reveal inter-cultivar differences and additivity in the contribution of *TaGW2* homoeologous to grain size and weight in wheat. Theor Appl Genet 131:2463-2475

Zhang P, He Z, Tian X, Gao F, Xu D, Liu J, Wen W, Fu L, Li G, Sui X, Xia X, Wang C, Cao S (2017) Cloning of *TaTPP-6AL1* associated with grain weight in bread wheat and development of functional marker. Mol Breeding 37:78

Zhu XF, Zhang HP, Hu MJ, Wu ZY, Jiang H, Cao JJ, Xia XC, Ma CX, Chang C (2016) Cloning and characterization of *Tabas1-B1* gene associated with flag leaf chlorophyll content and thousand-grain weight and development of a gene-specific marker in wheat. Mol Breeding 36:142

CHAPTER 7. GENOME-WIDE ASSOCIATION MAPPING FOR SUSCEPTIBILITY TO *PARASTAGONOSPORA NODORUM* AND ASSESSING NECROTROPHIC EFFECTOR SENSTIVITIES IN A GLOBAL WINTER WHEAT PANEL

7.1. Abstract

A major pathogen in wheat (*Triticum aesitivum* L.) is *Parastagonospora nodorum*, a necrotroph which causes septoria nodorum blotch (SNB). Wheat and *P. nodorum* interact in an inverse gene-for-gene manner, with a total of nine interactions characterized to date. Here, I report the evaluation of a global winter wheat panel for SNB susceptibility and the first report of the prevalence of sensitivity in a wheat panel to the necrotrophic effectors (NEs) SnTox5 and SnTox267. Infiltrations with the NEs SnToxA, SnTox1, SnTox267, SnTox3 and SnTox5 found 38.64, 36.74, 53.03, 48.86, and 42.42% of the lines were sensitive, respectively. Significant QTL associated with SNB susceptibility were identified above the previously characterized sensitivity genes *Tsn1* and *Snn3-B1* on chromosome 5B when the panel was inoculated with *P. nodorum* isolates Sn2000 and Sn4, respectively. Therefore, I did not identify any new genomic regions associated with SNB disease in this panel. Future research is needed using additional isolates collected from Iran and Europe, which many of the lines in this panel originate from, to determine whether there are truly no new regions associated with SNB in this panel. However, the screening results with purified NEs will be useful for cloning and validation of the sensitivity genes *Snn3-B1*, *Snn2, Snn5*, *Snn6*, and *Snn7*, along with marker development.

7.2. Introduction

Bread, or common, wheat (*Triticum aestivum* L.) is a major world food crop and is grown on over 200 million hectares worldwide (www.wheatinitiative.org). There are two growth habits of bread wheat: spring type, which is planted in the spring and harvested in the summer/fall, and

winter type, which is planted in the fall and overwinters to reach a vernalization requirement for flowering and is harvested mid-summer. Within the United States, winter wheat production accounts for 70-80 % of the total wheat production (https://www.ers.usda.gov/topics/crops/wheat/wheat-sector-at-a-glance/#classes) and therefore has major economic importance. Like other crop species, wheat yield can be reduced due to abiotic stresses (drought, soil degradation, floods, temperature increases, increased CO_2) and biotic stresses, such as pathogens (Singh and Upadhyaya 2016).

A major pathogen on wheat is the necrotrophic pathogen *Parastagonospora nodorum* (Berk.) Quaedvleig, Verkley, & Crous. *P. nodorum* is the causal agent of septoria nodorum blotch (SNB), which results in chlorotic and necrotic lens-shaped lesions on wheat leaves and can decrease wheat quality and yield by up to 50% (Eyal 1987). Wheat and *P. nodorum* interact in an inverse gene-for-gene manner (reviewed by Friesen and Faris 2010, 2021; Faris and Friesen 2020), with host sensitivity genes recognizing *P. nodorum* necrotrophic effectors (NEs). Once a compatible interaction occurs where the host recognizes the pathogen, a host defense response occurs, resulting in programmed cell death of the leaf tissue surrounding the pathogen. Due to *P. nodorum* being a necrotroph, this recognition results in *P. nodorum* gaining nutrients from the dying and dead tissue and disease progressing further.

A total of nine interactions have been characterized in the wheat-*P. nodorum* pathosystem, and they involved the wheat genes *Tsn1, Snn1, Snn2, Snn3-B1, Snn3-D1, Snn4, Snn5, Snn6*, and *Snn7* along with the NEs SnToxA, SnTox1, SnTox267, SnTox3, SnTox4, and SnTox5 (see Chapter 3). Additional host genes associated with SNB have been identified on almost every chromosome except 1D, 3D, 4D, and 6D (see Chapter 3). To date, the host genes *Tsn1* (Faris et al. 2010), *Snn1* (Shi et al. 2016b), and *Snn3-D1* (Zhang et al. 2021) have been

cloned. In *P. nodorum*, the NE genes *SnToxA* (Friesen et al. 2006), *SnTox3* (Liu et al. 2009), *SnTox1* (Liu et al. 2012), *SnTox5* (Kariyawasam et al. 2021), and *SnTox267* (Richards et al. 2021) have been cloned.

Discovery and validation of all the characterized interactions, along with much of the early work on this pathosystem, involved the use of bi-parental mapping populations (see Chapter 3 for review). However, QTL mapping in biparental populations has drawbacks. Identification of new genomic regions is limited by whether the two parents have those genes, and if so, they must be polymorphic, along with low mapping resolution due to fewer recombination events, and bi-parental populations are tedious to develop (Xu et al. 2017). Using genome-wide association studies (GWAS), some of the disadvantages of bi-parental mapping can be overcome. For example, the laborious process of biparental population development is circumvented and large panels of unrelated lines allows for the sampling of much greater diversity compared to a single biparental population (Korte and Farlow 2013). In the last decade, multiple GWAS studies in wheat have been published evaluating genomic regions associated with resistance/susceptibility to SNB (Adhikari et al. 2011; Gurung et al. 2014; Liu et al. 2015; Downie et al. 2018; Phan et al. 2018; Halder et al. 2019; Ruud et al. 2019; Cowger et al. 2020; Ballini et al. 2020; Francki et al. 2020; Phan et al. 2021; AlTameemi et al. 2021). These studies have been able to identify new genomic regions associated with SNB that were not detected in bi-parental mapping populations.

Previously, a winter wheat collection from the National Small Grains Collection was evaluated for stripe and stem rust resistance (Bulli et al. 2016; Muleta et al. 2020; Mihalyov et al. 2017). In this study, I investigated a subset of this collection consisting of 264 lines for prevalence of sensitivity to the known NEs SnToxA, SnTox1, SnTox267, SnTox3, and SnTox5.

I also inoculated the panel with three *P. nodorum* isolates to identify genomic regions associated with SNB. Findings from this study will provide beneficial knowledge for breeders on the prevalence of NE sensitivity genes in winter wheat, which interactions contribute to disease for particular isolates, and useful information for marker development and gene cloning projects.

7.3. Materials and Methods

7.3.1. Association Mapping Panel

A subset of the National Small Grains Collection core global hexaploid winter wheat (*Triticum aestivum* ssp. *aestivum*) germplasm collection was used in this study. The original set consisted of 300 lines representing most of the diversity of the panel used by Bulli et al. (2016), Mihalyoy et al. (2017); and Muleta et al. (2020). After two rounds of seed increase, 264 lines were selected and used for disease evaluations based on the number of seed available (100+ seeds). Of the 264 lines used in this study, 46 countries from six continents were represented (0.4% Africa, 34.47% Asia, 55.3% Europe, 8.0% North America, 0.4% Oceania, 1.5% South America), and the panel consisted of 35 breeding lines (13.3%), 84 cultivars (31.8%), 32 uncertain improvement status (12.1%), 1 genetic line (0.4%), and 112 landraces (42.4%) (Appendix A).

7.3.2. Phenotyping

The *P. nodorum* genes *SnTox1*, *SnToxA*, *SnTox3*, *SnTox267*, and *SnTox5* were previously cloned (Liu et al 2012; Friesen et al. 2006; Liu et al. 2009, Richards et al. 2021; Kariyawasam et al. 2021). *SnTox1*, *SnToxA*, *SnTox3*, and *SnTox267* were expressed separately in the yeast *Pichia pastoris* as described by Friesen and Faris (2012), which was used to make culture filtrate for infiltrations with these NEs. *SnTox5* has not been cloned into *Pichia pastoris*, therefore culture filtrates of Sn79+Tox5-4 were used as described by Kariyawasam et al. (2021).

For both infiltrations and inoculations, plants were grown in plastic cones that were 3.8 cm in diameters and 21 cm deep (Stuewe and Sons, Inc., Corvallis, OR, USA), with 3 plants per cone. For inoculations, lines were arranged in a completely randomized design (CRD) with Alsen, a susceptible wheat variety, planted as the border to reduce any edge effect. Infiltrations and inoculations of *P. nodorum* on seedlings was as described by Friesen and Faris (2012). *P. nodorum* isolates Sn4, Sn2000, and AR2-1 were used for inoculations (Table 7.1).

For infiltrations with NE-encoding genes expressed in *P. pastoris*, cultures for each were obtained from Dr. Tim Friesen at the USDA-ARS Cereal Crop Unit in Fargo, ND. The tip of a toothpick was inserted into the frozen culture, then dropped into 2 ml YPD (10 g yeast extract, 20 g peptone, 900 mL distilled H_2O, autoclaved, then 100 mL 10 X dextrose) and incubated at 30 °C with vigorous shaking for 48 hours. Samples were diluted to 1:1000 in a new tube with YPD. Another incubation period of 30 °C for 48 hours with vigorous shaking followed. Culture filtrate was harvested by centrifuging at 1250 rpm/rcf for 10 minutes, and then filtered through a 0.45 µm bottle top filter. The harvested culture filtrate was stored at -20 °C until plants were infiltrated.

Plants were infiltrated when the second leaf was fully expanded. Two plants per cone were infiltrated on the second leaf using a 1-mL needleless syringe. The infiltration boundaries were marked using a permanent marker. Plants were placed in a growth chamber at 21 °C with a 12-h photoperiod. For culture filtrates, reactions were scored at 5 days post infiltration, SnToxA, SnTox1, SnTox3, and SnTox5 were scored at 5 days post infiltration, and SnTox267 was scored at 7 days post infiltration. The scoring system was as follows: 0 = no visible necrosis or chlorosis, 1 = mottled chlorosis or necrosis extending to boundaries of the infiltrated area, 2 = highly visible necrosis or chlorosis with little mottling extending to the boundaries of the

infiltrated area without complete tissue collapse and little or no shriveling or narrowing of the leaf within the infiltrated region, 3 = necrosis throughout the entire infiltrated area with complete tissue collapse and shriveling or narrowing of the leaf within the infiltrated region (Zhang et al. 2011). Reaction types of 2 and 3 were considered sensitive and 0 and 1 were insensitive.

For inoculations, *P. nodorum* fungal plugs were grown on V-8-potato dextrose agar under 24 hour fluorescent light for 7 days until the pycnidium released spores, The agar plate was rinsed with sterile-distilled water, after which 200 µL of spore suspension was streaked onto a new V8 plate. Spores were collected after 7 days and diluted to a concentration of 10^6 spores/mL and one drop of Tween 20 was added to the inoculum for every 50 mL of spore suspension. Plants were inoculated when the second leaf was fully expanded for all plants with an airflow of 17 psi until runoff was observed. After inoculation, plants were placed in a 100% humidity growth chamber at 21 °C for 24 hours under constant light, then moved to a controlled growth chamber at 21 °C with a 12 h photoperiod. Plants were scored at 7 days post inoculation using the scale described by Liu et al. (2004) (Table 7.2).

Table 7.1. Isolates used in this study, along with the collection information and when the genome sequence was published.

Isolate	Location	Year	Wheat type	Sequenced	NEs
Sn2000	North Dakota	2000	Durum	Richards et al. (2018)	SnToxA, SnTox1, SnTox5
Sn4	North Dakota	2003	Spring wheat	Richards et al. (2018)	SnToxA, SnTox1, SnTox267, SnTox3
AR2-1	Arkansas	1995	Winter wheat	Richards et al. (2019)	SnTox1, SnTox267

Table 7.2. Inoculation scoring scale to be used on wheat leaves inoculated with *P. nodorum* isolates.

Scale	Phenotype	Disease Level
0	Absence of visible lesions	Highly resistant
1	Few penetration points with lesions consisting of flecking or small dark spots	Resistant
2	Lesions consisting of dark spots with surrounding necrosis or chlorosis	Moderately resistant
3	Dark lesions completely surrounded by necrosis or chlorosis, lesions 2-3 mm	Moderately susceptible
4	Larger necrotic or chlorotic lesions 4 mm or greater, little coalescence	Susceptible
5	Large coalescent lesions with very little green tissue remaining	Highly susceptible

7.3.3. SNP Genotyping

The panel was previously genotyped with the Illumina 9K SNP array (data available on T3 and Bulli et al. 2016). Here, I genotyped the 264 lines in my subset using the Illumina 90K SNP array (Wang et al. 2014). DNA was extracted using the ammonium acetate method (Pallota et al. 2003) and diluted to 40 ng/ul for running the SNP array. A BeadStation and iScan instrument from Illumina were used for the assay, which was performed at the small grains genotyping laboratory in Fargo, ND, USA. Clustering data was analyzed using GenomeStudio 2.0.5 from Illumina, Inc. (2020). SNPs were ordered based on their physical position in the Chinese Spring IWGSC RefSeq v2.0. In TASSEL v5.2 (Bradbury et al. 2007), SNP markers were filtered with a minor allele frequency greater than 0.01 and missing data less than 50%. For the remaining markers, missing values were imputed using the LD-KNNi method (Money et al. 2015).

7.3.4. Population Structure and Linkage Disequilibrium

The principal component analysis (PCA) was performed using TASSEL v5.2. Linkage disequilibrium (LD) was estimated using a Fischer's Exact test as r^2 between pairs of SNPs in TASSEL v5.2. Heterozygous SNP markers were converted to missing, and markers were again filtered for missing data less than 50%. LD decay plots were generated in R v4.0.3. The half-decay distance was calculated using the estimated maximum value of LD and the Remington model was used to fit a nonlinear model for the relationship between LD decay and distance (Remington et al. 2001).

7.3.5. Statistical Analysis

Statistical analysis was performed using SAS 9.4 (SAS Institute). The PROC GLM procedure was used because my dataset contained missing entries. The data were analyzed for

homogeneity of variances between replicates using Bartlett's Chi squared test for homogeneity of error variances (Snedecor and Cochran 1989) to determine if replicates could be combined (Table 7.3). Pearson's correlation coefficients were calculated in R v4.0.3 using the R command *cor* (R Development Core Team).

Table 7.3. Bartlett's Chi squared test for homogeneity of error variances.

Trait	χ^2	*p*-value
SnToxA	0.03	0.99
SnTox1	1.07	0.59
SnTox267	0.16	0.92
SnTox3	0.42	0.81
SnTox5	0.88	0.65
Sn4	2.58	0.28
Sn2000	3.90	0.14
AR2-1	0.62	0.74

7.3.6. Genome-wide Association Analyses

Association mapping was conducted using TASSEL and the R package GAPIT v.3 (Lipka et al. 2012; Wang and Zhang 2020). The naïve model was run in TASSEL and the other models in GAPIT. Based on the eigenplots, the first four principal components (PCs) were used for analysis. A kinship matrix (K) was calculated using the Emma algorithm in GAPIT. The four models evaluated were: (i) a naïve model, (ii) a general linear model (GLM) with four PCs included as mixed effects (Patterson et al. 2006); (iii) a mixed linear model (MLM) with four mixed-effect PCs and a random-effect kinship matrix (K matrix) (Zhao et al. 2007); and (iv) FarmCPU, a fixed and random model Circulating Probability Unification model, which fits associated markers as cofactors to control false positives (Liu et al. 2016).

Models naïve, GLM, MLM, and FarmCPU were run and the most robust model was chosen based off of visualization of the Q-Q plots (which show the observed vs expected unadjusted *P*-values) and the lowest mean of the squared difference (MSD) values. The MSD values were calculated with the R package hydroGOF (Zambrano-Bigiarini 2020) using the mse

function which returns the difference between the observed and expected *P* values for that model. Marker *P*-values were adjusted using a false discovery rate (FDR) and markers with an FDR adjusted *P*-value of 0.001 or less were deemed significant for infiltrations, and a *P*-value of 0.05 or less was significant for inoculations. Manhattan plots were developed using the R package qqman (Turner 2018).

7.4. Results

7.4.1. Population Structure and Linkage Disequilibrium

The final SNP marker set used for association mapping consisted of 42,022 markers after filtering for a minor allele frequency greater than 1%, missing values less than 50%, and removing minor SNP states. The first four PCs were used for GWAS analysis and explained 13.91, 9.18, 4.41, and 2.01% of the total variation, respectively. For linkage disequilibrium, the data set was further filtered for markers with a high percentage of heterozygous calls. The estimated r^2 for half decay ranged from 0.2290 on chromosome 7D to 0.2347 on chromosome 5B. The physical distance for LD decay to reach 50% ranged from 323,535 bp on chromosome 6D to 2,601,754 bp on chromosome 5B (Figures 7.1, 7.2, 7.3). For both values, chromosome 4D was the outlier, with an estimated r^2 for half decay of 0.6453 and a physical distance of 6,425 bp (Figure 7.3).

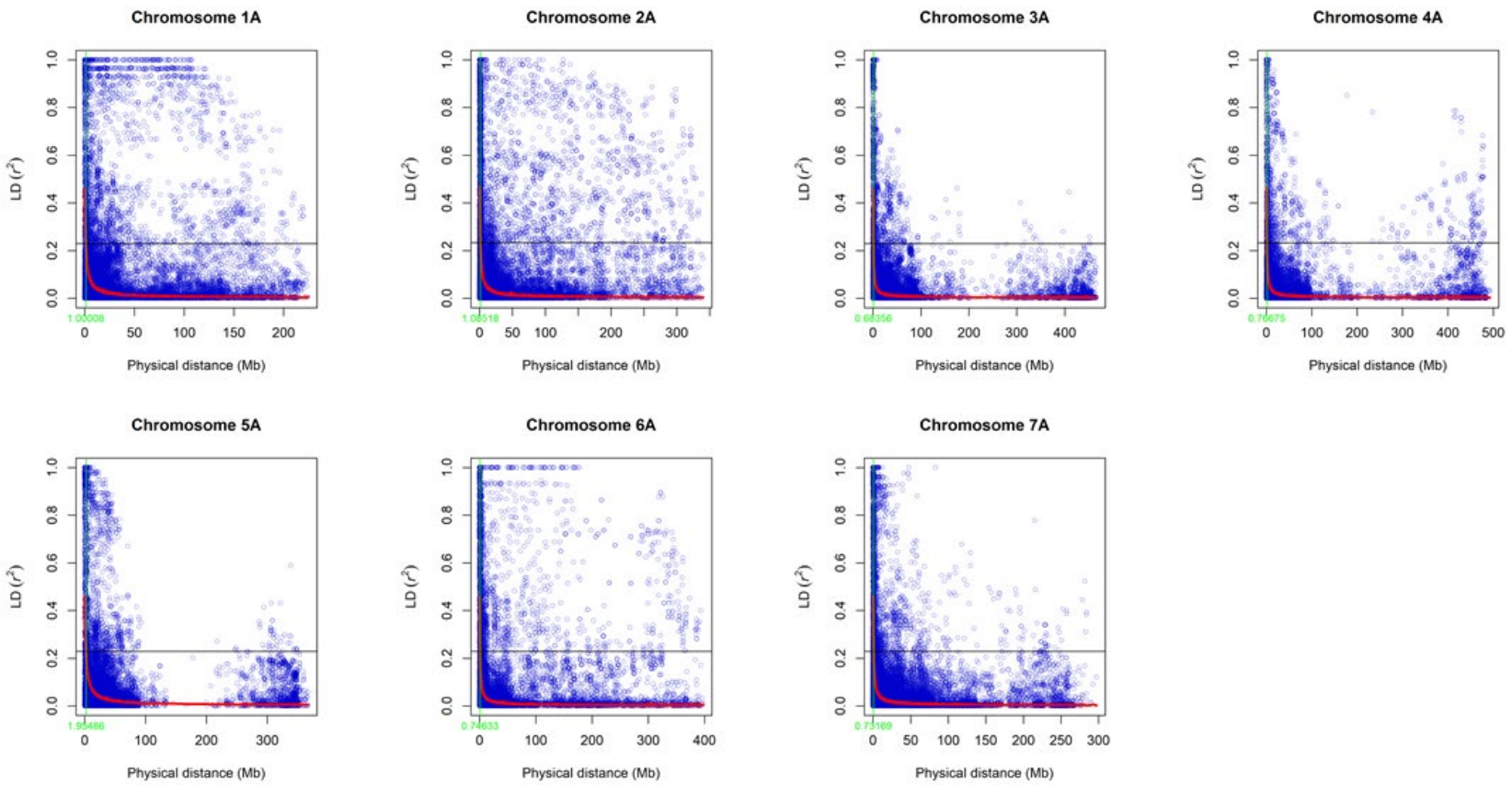

Figure 7.1. LD decay plots based on pairwise comparisons of loci for the A genome chromosomes. The red line is the estimated LD points. The horizontal line is the LD significance based on the estimated LD value for half decay. The green line shows the distance in Mb for half decay, with the half decay distnace shown in green along the bottom of each plot. These values were calculated as described by Remington et al. (2001).

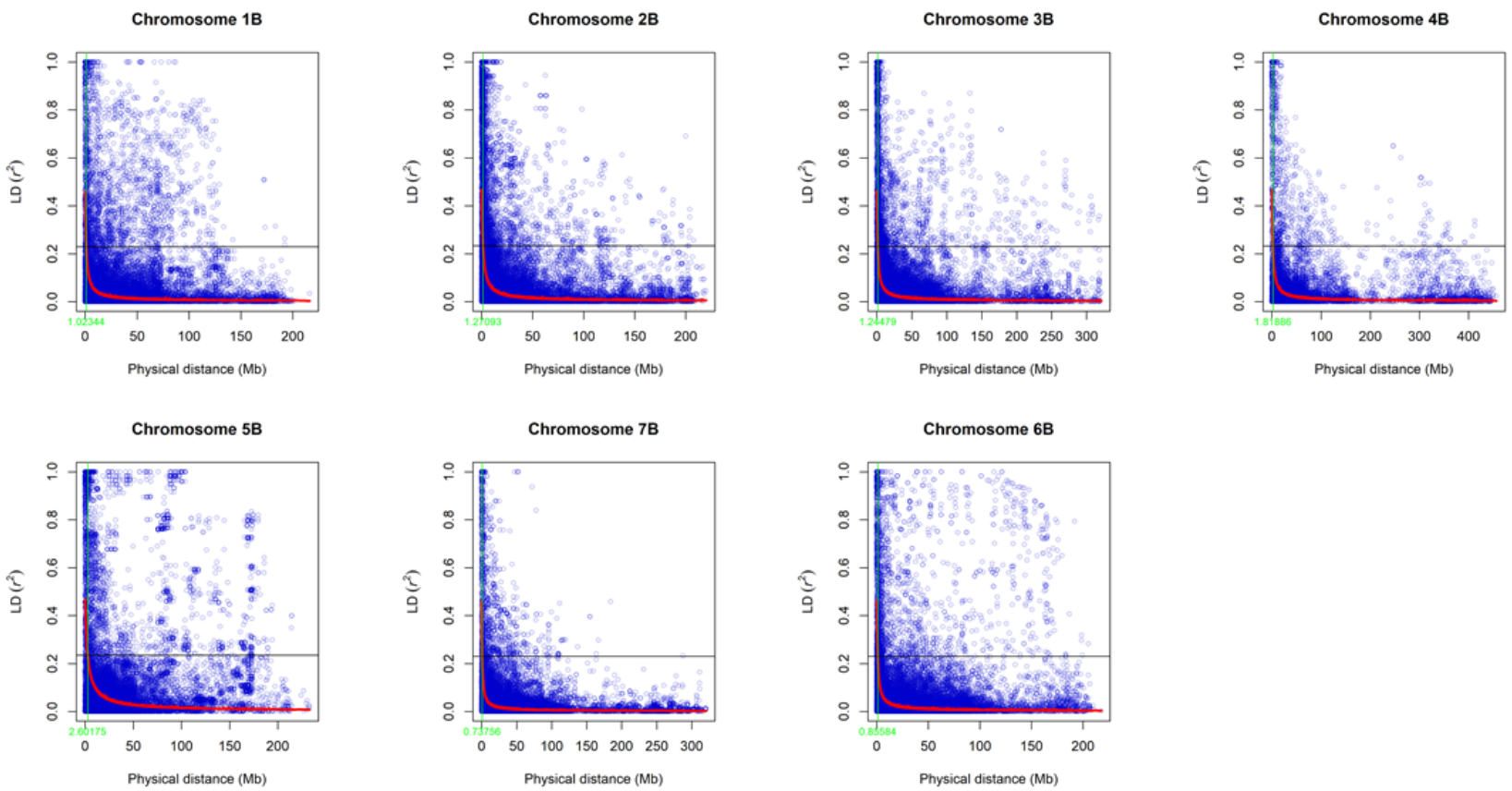

Figure 7.2. LD decay plots based on pairwise comparisons of loci for the B genome chromosomes. The red line is the estimated LD points. The horizontal line is the LD significance based on the estimated LD value for half decay. The green line shows the distance in Mb for half decay, with the half decay distnace shown in green along the bottom of each plot. These values were calculated as described by Remington et al. (2001).

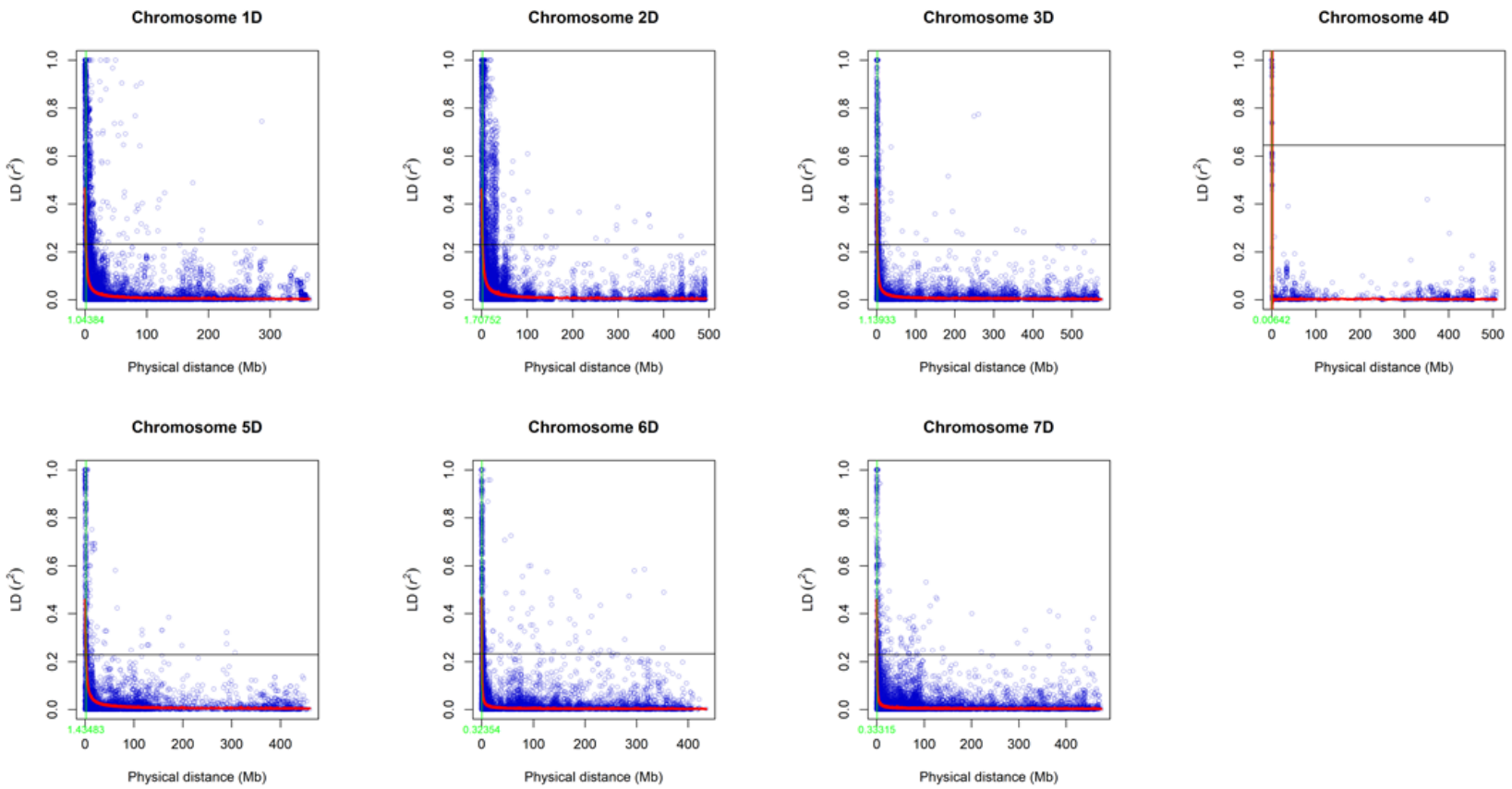

Figure 7.3. LD decay plots based on pairwise comparisons of loci for the D genome chromosomes. The red line is the estimated LD points. The horizontal line is the LD significance based on the estimated LD value for half decay. The green line shows the distance in Mb for half decay, with the half decay distnace shown in green along the bottom of each plot. These values were calculated as described by Remington et al. (2001).

7.4.2. Sensitivity to Known NEs

Sensitivity to the known *P. nodorum* NEs SnToxA, SnTox1, SnTox267, SnTox3 and SnTox5 were evaluated in this global winter wheat panel (Table 7.4). For GWAS analysis, I chose to use the MLM model for all five NEs based on MSD values (Table 7.5) and visualization of Q-Q plots.

In this panel, 38.64% of lines were sensitive to SnToxA (Table 7.4). Sensitivity among the different geographic origins varied, with the three main groups, North America, European, and Asian lines having 42.86, 13.01, and 78.02% SnToxA sensitivity, respectively (Appendix A). GWAS data on SnToxA infiltrations yielded 14 SNP markers with FDR adjusted *P*-values below 0.001 (Table 7.6, Figure 7.4). These SNPs ranged in physical position from 549,788,309 (*IACX9261*) to 549,933,008 bp (*Excalibur_rep_c105815_305*) on chromosome 5B and were within the *Tsn1* region. The most significant SNP, *Tdurum_contig25513_123*, explained 22.95% of the total variation.

For SnTox1, 36.74% of the panel was sensitive (Table 7.4). As with SnToxA, a high percentage of Asian lines were sensitive (62.64%). Only two SNP markers, *RAC875_rep_c97766_145* and *BS00064465_51*, were significantly associated with SnTox1 sensitivity in the MLM model based on FDR adjusted *P*-values (Table 7.6, Figure 7.5). *RAC875_rep_c97766_145* and *BS00064465_51* were positioned at 2,381,165 and 2,358,687 bp on chromosome 1B, respectively, and the *Snn1* gene is positioned at 2,383,732 bp in the CS ref v2, indicating the region associated with SnTox1 sensitivity in this panel is the *Snn1* region. *RAC875_rep_c97766_145* and *BS00064465_51* explained 15.92 and 11.86% of the total variation, respectively.

Sensitivity to SnTox3 had a slightly different pattern than SnTox1 and SnToxA. Overall, a higher percent, 48.86%, was sensitive to SnTox3, with 45.21 and 59.34% of the European and Asian lines being sensitive, respectively (Table 7.4). Only one North American line out of 21 lines was sensitive. A total of 11 SNP markers had *P*-values below 0.001 with FDR adjustment (Table 7.6, Figure 7.6). The genomic region ranged from 6,704,549 (*GENE-3324_338*) to 7,091,681 bp (*Kukri_c912_1423*) on chromosome 5B. BLAST searches of *Snn3-D1* sequence (Zhang et al. 2021) against the CS Ref v2 yielded a high identity hit on chromosome 5B at 7,041,691, suggesting this is the *Snn3-B1* region. The most significant marker, *Excalibur_c47452_183*, explained 35.36% of the total variation. Two additional markers, *wsnp_Ku_c439_913400* and *Ex_c1846_1818*, were located slightly more proximal at 65,759,133 and 65,759,716 bp, respectively.

SnTox267 sensitivity was the most prevalent for the five NEs screened on this panel, with 53.03% of lines being sensitive (Table 7.4). Both North America and European lines had approximately the same percent of sensitive lines, with 42.86 and 44.52%, respectively, whereas 70.32% of Asian lines were sensitive to SnTox267. No markers were significant after the FDR-adjustment (Figure 7.7). The markers with the lowest *P*-values were located on chromosomes 2B, 2D, and 3B.

Lastly, 42.42% of lines in this panel were sensitive to SnTox5 (Table 7.4). Major differences were observed in the percent per geographic origins, with only 21.23% of European lines having sensitivity, whereas 81.32% of Asian lines were sensitive. For the GWAS results, no markers were significant after the FDR-adjustment (Figure 7.8). The three markers with the lowest *P*-values, *BS00023035_51*, *Excalibur_c1706_1413*, and *BS00102481_51*, were

positioned from 635,842,996 to 635,844,327 bp on chromosome 4B and within the proposed *Snn5* gene region (Sharma 2019).

As for individual lines, 35 lines in this panel were insensitive to SnToxA, SnTox1, SnTox267, SnTox3, and SnTox5 (Table 7.4, Figure 7.9). The majority of these lines originated from European countries (Appendix A). Interestingly, of these 35 lines, 10 had disease scores of 2.5 or higher to one or more of the isolates and were considered susceptible. On the contrary, 19 lines were sensitive to all five NEs, and all but one of these lines originated from Asian countries. The majority of these were landraces from Iran. Six of these 19 lines had disease scores of 2.5 or lower to one or more isolates and were considered resistant.

Table 7.4. Infiltration results using purified NEs.

	Score							
NE	0-0.49	0.5-0.99	1-1.49	1.5-1.99	2-2.49	2.5-3	% insensitive	% sensitive
SnToxA	161	1	0	0	1	101	61.36	38.64
SnTox1	153	6	8	1	26	70	63.26	36.74
SnTox267	79	24	21	7	39	94	46.97	53.03
SnTox3	128	4	3	2	7	120	51.14	48.86
SnTox5	135	5	12	3	22	87	57.58	42.42

Table 7.5. MSD values for the naïve, GLM, MLM, and FarmCPU models for infiltrations.

	naïve	GLM	MLM	FarmCPU
SnToxA	0.097428	0.002606	0.000328	0.000252
SnTox1	0.103818	0.001099	0.000062	0.000058
SnTox3	0.019960	0.002236	0.000075	0.000017
SnTox5	0.194716	0.000019	0.000239	0.001058
SnTox267	0.029853	0.000083	0.000067	0.000079

Table 7.6. Significant associations between single nucleotide polymorphism (SNP) markers and *Parastagonospora nodorum* necrotrophic effectors. The MLM model was used for each trait to identify significant marker trait associations. Markers with a *P*-value less than 0.001 after the FDR adjustment were considered significant.

NE	SNP[a]	Allele	Chromosome	Position (bp)[b]	*P*-value	FDR adjusted *P*-value	-Log$_{10}$(*P*)	R^2 × 100	Effect
SnToxA	*Tdurum_contig25513_123*	A/G	5B	549,910,986	1.93E-17	8.12E-13	16.71	22.95	2.01
SnToxA	*BobWhite_c48435_165*	T/C	5B	549,911,221	6.78E-17	9.49E-13	16.17	22.03	2.01
SnToxA	*Tdurum_contig12066_126*	T/G	5B	549,910,391	6.78E-17	9.49E-13	16.17	22.03	2.01
SnToxA	*wsnp_Ku_c40334_48581010*	A/G	5B	549,932,605	3.19E-16	3.35E-12	15.50	20.91	1.90
SnToxA	*tplb0027f13_1346*	A/G	5B	549,911,640	4.65E-16	3.91E-12	15.33	20.64	1.90
SnToxA	*Tdurum_contig12066_247*	G/A	5B	549,910,462	1.17E-15	8.18E-12	14.93	19.98	-1.89
SnToxA	*tplb0027f13_1493*	C/T	5B	549,911,493	1.68E-14	9.04E-11	13.78	18.12	-1.77
SnToxA	*Tdurum_contig25513_195*	C/T	5B	549,911,058	1.72E-14	9.04E-11	13.76	18.10	-1.66
SnToxA	*Excalibur_rep_c105815_305*	C/T	5B	549,933,008	5.61E-13	2.62E-09	12.25	15.73	-1.43
SnToxA	*GENE-3198_56*	C/T	5B	549,911,389	5.79E-10	2.43E-06	9.24	11.25	0.90
SnToxA	*IACX9261*	A/C	5B	549,788,309	1.68E-09	6.42E-06	8.77	10.59	-1.56
SnToxA	*tplb0027f13_452*	A/G	5B	549,914,572	7.58E-09	2.66E-05	8.12	9.67	1.09
SnToxA	*CAP8_c7929_203*	G/T	5B	549,788,353	2.88E-08	9.31E-05	7.54	8.86	1.42
SnToxA	*BS00010590_51*	T/G	5B	549,788,359	7.27E-08	2.20E-04	7.14	8.31	1.20
SnTox1	*RAC875_rep_c97766_145*	C/A	1B	2,381,165	3.15E-11	1.32E-06	10.50	15.92	-0.75
SnTox1	*BS00064465_51*	T/C	1B	2,358,687	6.52E-09	1.40E-04	8.19	11.86	-1.02
SnTox3	*Excalibur_c47452_183*	T/C	5B	6,710,705	2.19E-16	9.20E-12	15.66	35.36	-1.77
SnTox3	*GENE-3324_338*	A/G	5B	6,704,549	6.69E-16	1.40E-11	15.17	34.02	1.77
SnTox3	*BS00091519_51*	A/G	5B	6,705,156	2.11E-15	2.96E-11	14.68	32.66	-1.72
SnTox3	*BobWhite_c4838_58*	T/C	5B	6,710,620	1.59E-14	1.67E-10	13.80	30.31	1.65
SnTox3	*wsnp_Ku_c439_913400*	G/A	5B	65,759,133	3.10E-12	2.61E-08	11.51	24.37	-1.05
SnTox3	*BS00091518_51*	T/C	5B	6,705,136	5.36E-12	3.75E-08	11.27	23.78	1.35
SnTox3	*RAC875_c39204_91*	C/T	5B	6,909,035	2.03E-11	1.22E-07	10.69	22.33	-1.59
SnTox3	*BS00064298_51*	G/A	5B	7,031,414	4.05E-11	2.13E-07	10.39	21.59	0.93
SnTox3	*Kukri_c912_1423*	T/C	5B	7,091,681	1.36E-10	6.33E-07	9.87	20.31	1.25
SnTox3	*BS00064297_51*	C/T	5B	7,031,396	1.92E-10	8.07E-07	9.72	19.94	-0.89
SnTox3	*Ex_c1846_1818*	G/A	5B	65,759,716	9.39E-10	3.59E-06	9.03	18.28	-1.05

[a]SNP markers are from the Infinium SNP 90K array (Wang et al. 2014)

[b]Physical location is based on the IWGSC RefSeq v2

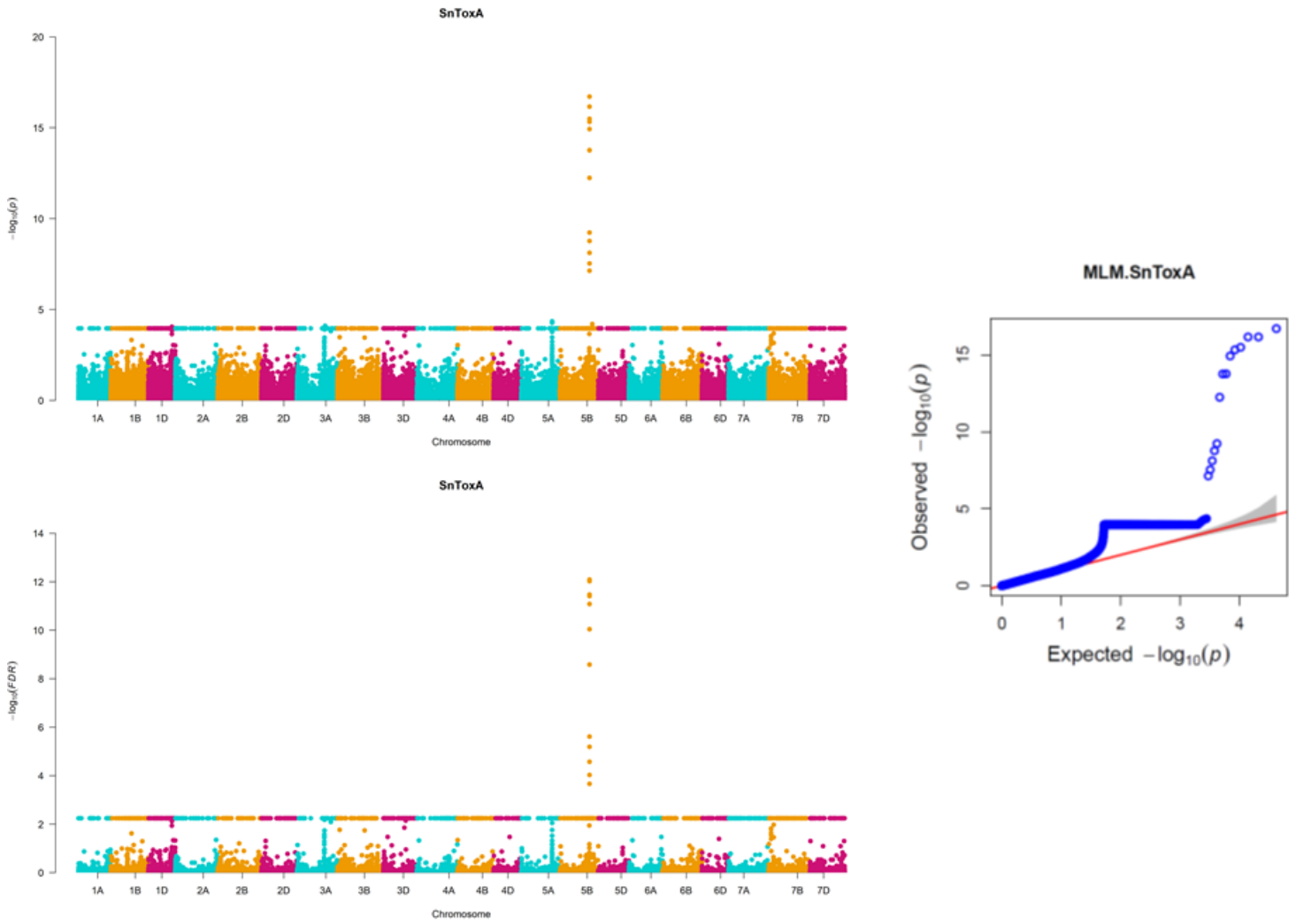

Figure 7.4. Manhattan plots for the association mapping using the MLM model for sensitivity to SnToxA. For the top Manhattan plot, the y-axis indicated –log10(*p*) for SNP markers whereas for the bottom Manhattan plot, the y-axis indicated –log10(FDR) for SNP markers. The x-axis for both is the physical distribution of all the SNP markers on the 21 common wheat chromosomes based on the alignment to the IWGSC Chinese Spring Ref Seq v2. On the right is the QQ plot output for the MLM model from GAPIT.

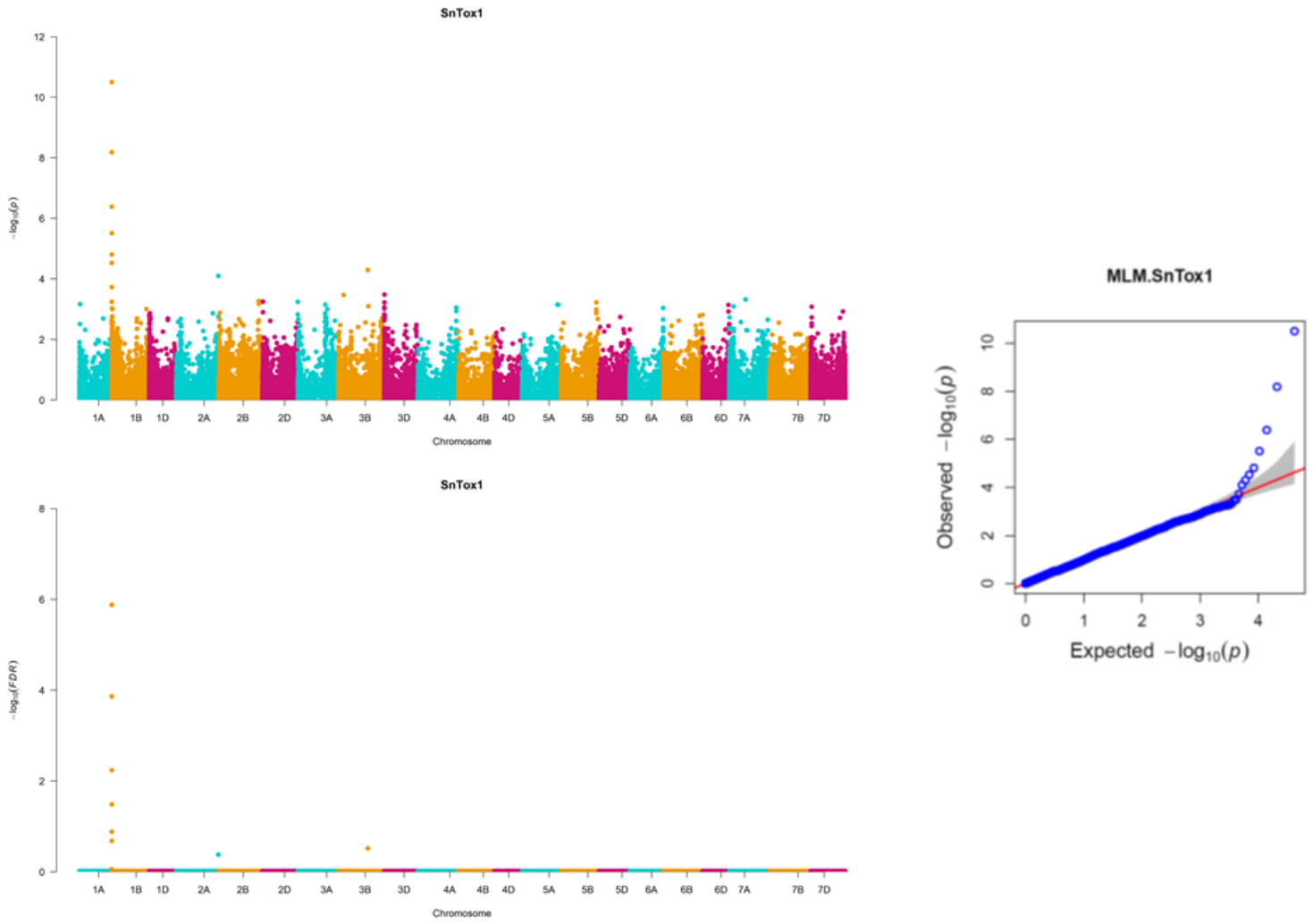

Figure 7.5. Manhattan plots for the association mapping using the MLM model for sensitivity to SnTox1. For the top Manhattan plot, the y-axis indicated –log10(*p*) for SNP markers whereas for the bottom Manhattan plot, the y-axis indicated –log10(FDR) for SNP markers. The x-axis for both is the physical distribution of all the SNP markers on the 21 common wheat chromosomes based on the alignment to the IWGSC Chinese Spring Ref Seq v2. On the right is the QQ plot output for the MLM model from GAPIT.

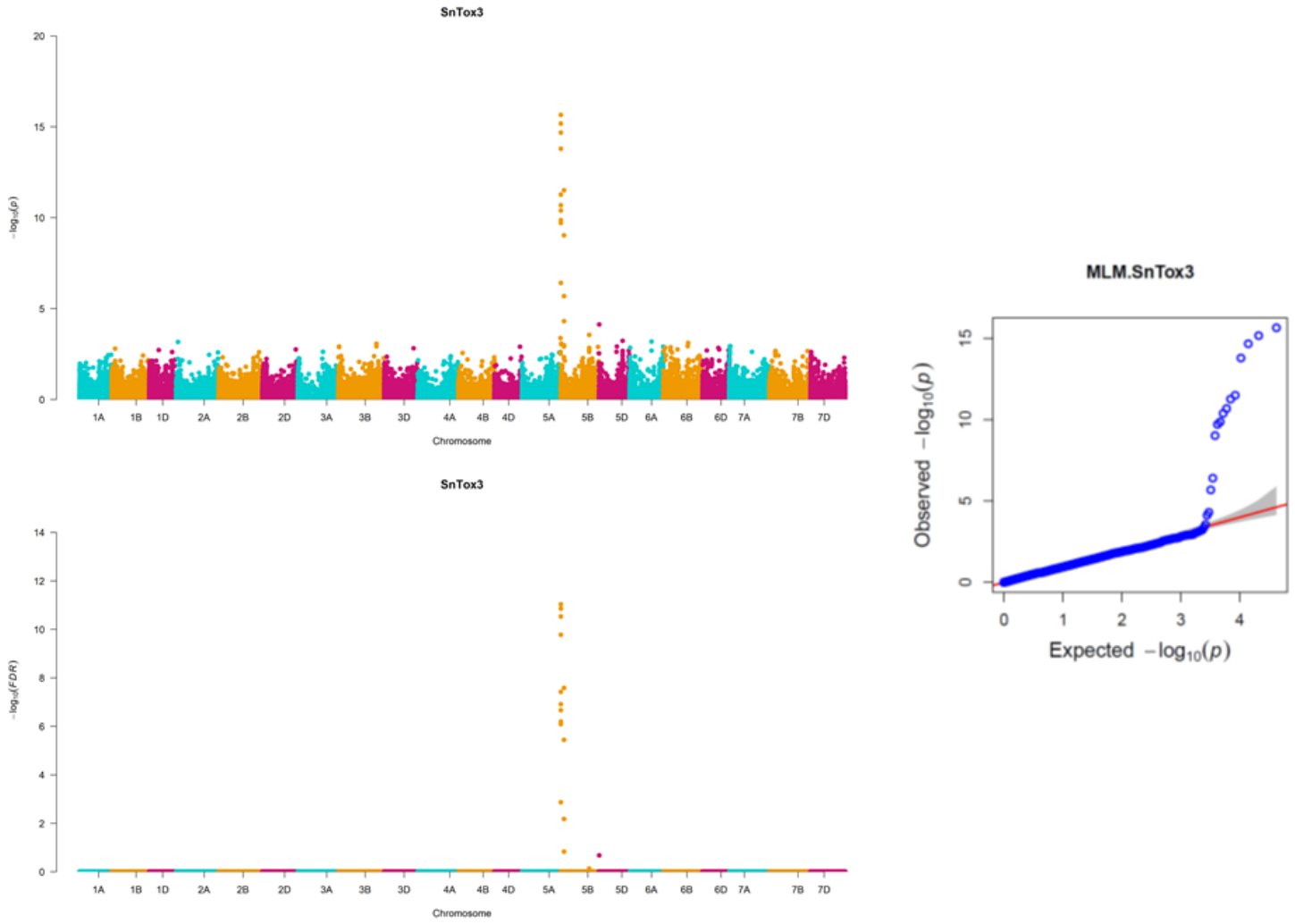

Figure 7.6. Manhattan plots for the association mapping using the MLM model for sensitivity to SnTox3. For the top Manhattan plot, the y-axis indicated –log10(*p*) for SNP markers whereas for the bottom Manhattan plot, the y-axis indicated –log10(FDR) for SNP markers. The x-axis for both is the physical distribution of all the SNP markers on the 21 common wheat chromosomes based on the alignment to the IWGSC Chinese Spring Ref Seq v2. On the right is the QQ plot output for the MLM model from GAPIT.

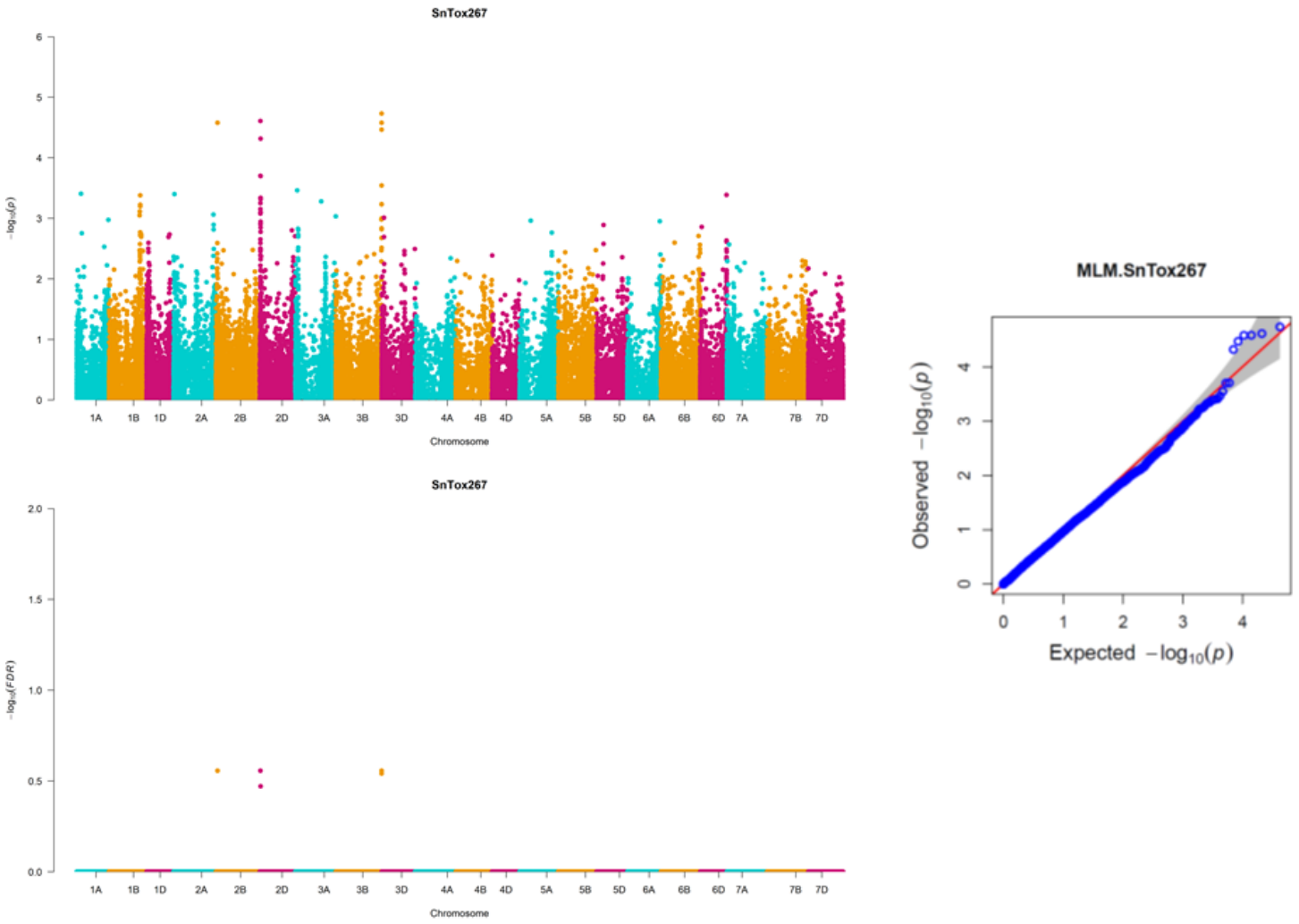

Figure 7.7. Manhattan plots for the association mapping using the MLM model for sensitivity to SnTox267. For the top Manhattan plot, the y-axis indicated –log10(*p*) for SNP markers whereas for the bottom Manhattan plot, the y-axis indicated –log10(FDR) for SNP markers. The x-axis for both is the physical distribution of all the SNP markers on the 21 common wheat chromosomes based on the alignment to the IWGSC Chinese Spring Ref Seq v2. On the right is the QQ plot output for the MLM model from GAPIT.

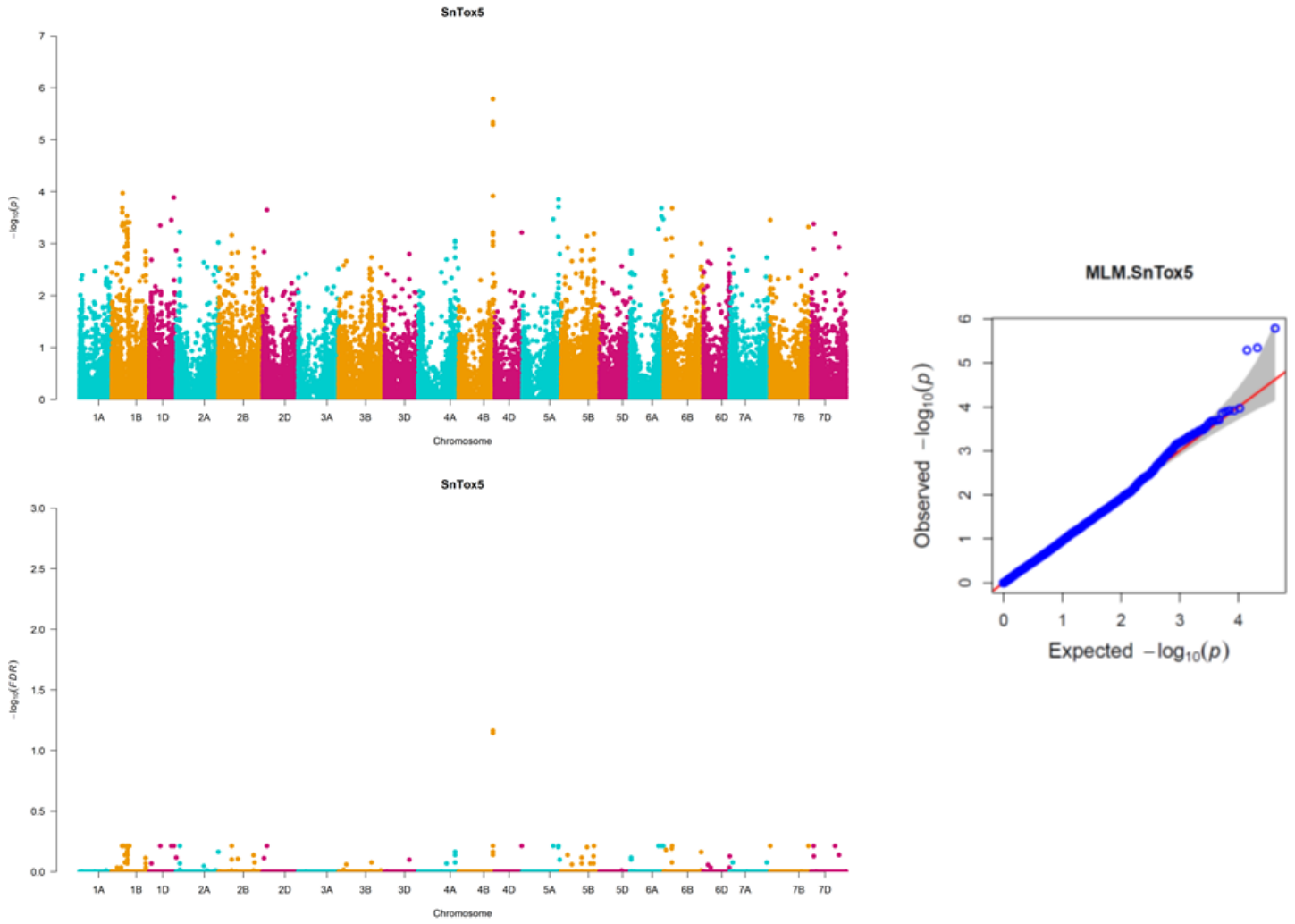

Figure 7.8. Manhattan plots for the association mapping using the MLM model for sensitivity to SnTox5. For the top Manhattan plot, the y-axis indicated –log10(*p*) for SNP markers whereas for the bottom Manhattan plot, the y-axis indicated –log10(FDR) for SNP markers. The x-axis for both is the physical distribution of all the SNP markers on the 21 common wheat chromosomes based on the alignment to the IWGSC Chinese Spring Ref Seq v2. On the right is the QQ plot output for the MLM model from GAPIT.

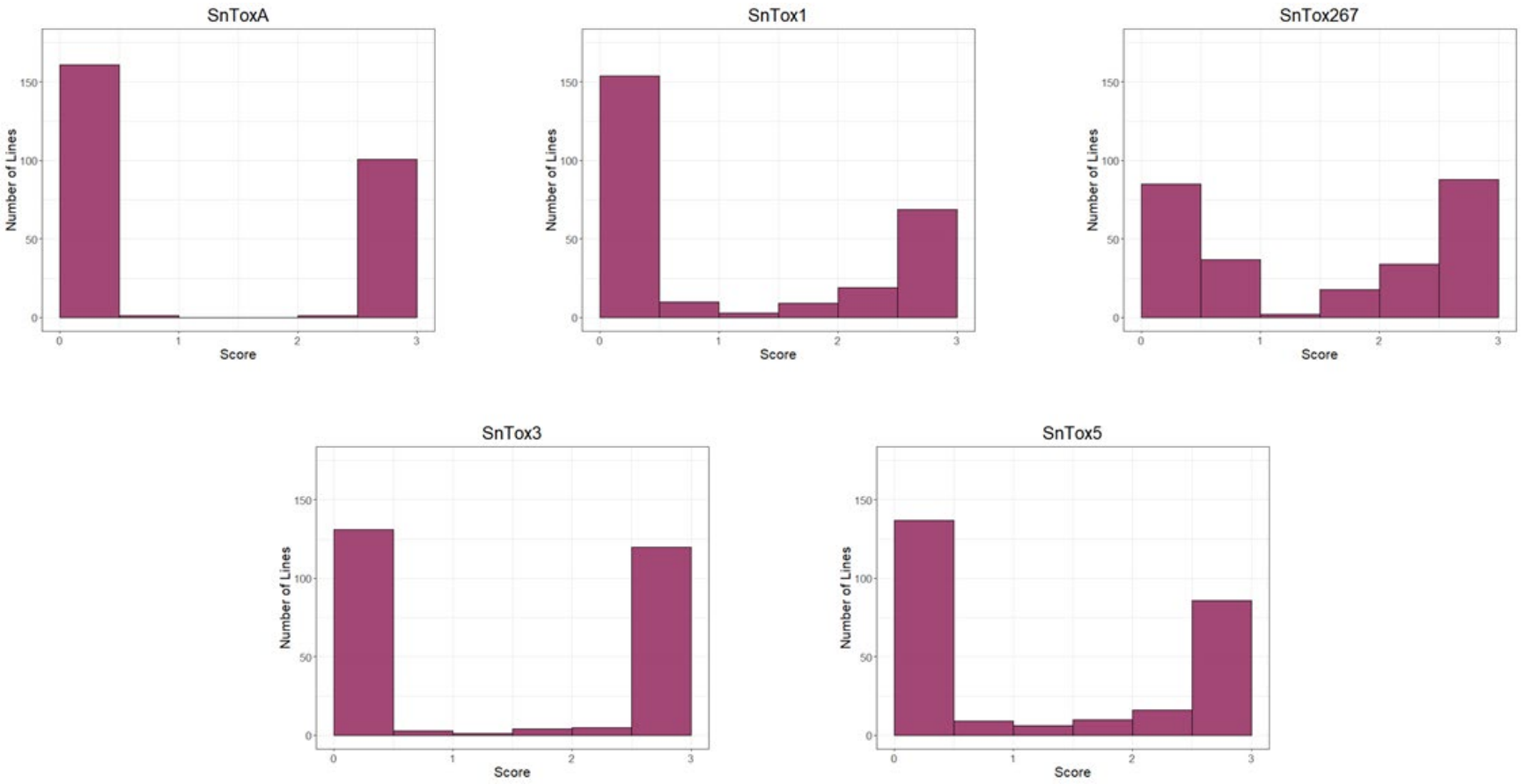

Figure 7.9. Histograms displaying the distribution of infiltration scores in the winter wheat panel to the NEs SnToxA, SnTox1, SnTox267, SnTox3, and SnTox5.

7.4.3. Inoculations

For inoculations, there were three homogenous replicates for each isolate (Table 7.3), therefore, the averages for each isolate was used for analysis. For all three isolates, the model with the lowest MSD value was MLM (Table 7.7). For AR2-1, no significant markers associated with disease were detected (Figure 7.10), therefore the AR2-1 GWAS results are not discussed below.

Table 7.7. MSD values for the naïve, GLM, MLM, and FarmCPU models for inoculations

	naïve	GLM	MLM	FarmCPU
Sn4-avg	0.062862	0.003281	0.000050	0.001938
AR2avg	0.001171	0.004656	0.000041	0.000101
Sn2000avg	0.165204	0.000193	0.000013	0.000180

The winter wheat lines in this panel ranged from highly resistant to highly susceptible in their reaction to SNB caused by the isolates Sn4, Sn2000, and AR2-1. The overall average disease scores were 3.35, 2.52, and 2.19 for Sn4, AR2-1, and Sn2000, respectively (Figure 7.11). For disease caused by Sn4, a total of 10 lines were considered highly resistant (score of 0.5 or lower) and 58 lines were highly susceptible (score of 4.5 or higher). As shown in the GWAS inoculation results (discussed below), the *Snn3*-SnTox3 interaction was the most significant contributor to disease for Sn4 inoculations; however, no significant associations were identified to be associated with the *Tsn1*-SnToxA, *Snn1*-SnTox1, *Snn2*-SnTox267, *Snn6*-SnTox267, and *Snn7*-SnTox267 interactions. Interestingly, some lines that were highly susceptible were not sensitive to SnTox3 based on the infiltration data. However, all the highly resistant lines were insensitive to SnTox3.

For disease caused by Sn2000, the panel had 72 lines that were resistant and 19 lines that were susceptible. Sn2000 is known to produce SnToxA, and GWAS results showed that the *Tsn1*-SnToxA interaction was the largest contributor of disease severity from Sn2000 in this

panel. No significant associations were observed at the *Snn1* or *Snn5* loci, although Sn2000 has been shown to produce SnTox1 and SnTox5 (Table 7.1). All of the highly susceptible lines were sensitive to SnToxA, whereas all of the highly resistant were not, which is consistent with the GWAS results. Lastly, 15 lines were highly resistant to AR2-1, whereas 17 lines were highly susceptible. No known interactions were found to be significantly associated with disease, although AR2-1 has been shown to contain the SnTox1 and SnTox267 genes; therefore, we had expected the *Snn1*-SnTox1, *Snn2*-SnTox267, *Snn6*-SnTox267, and *Snn7*-SnTox267 interactions to present but there were instead absent.

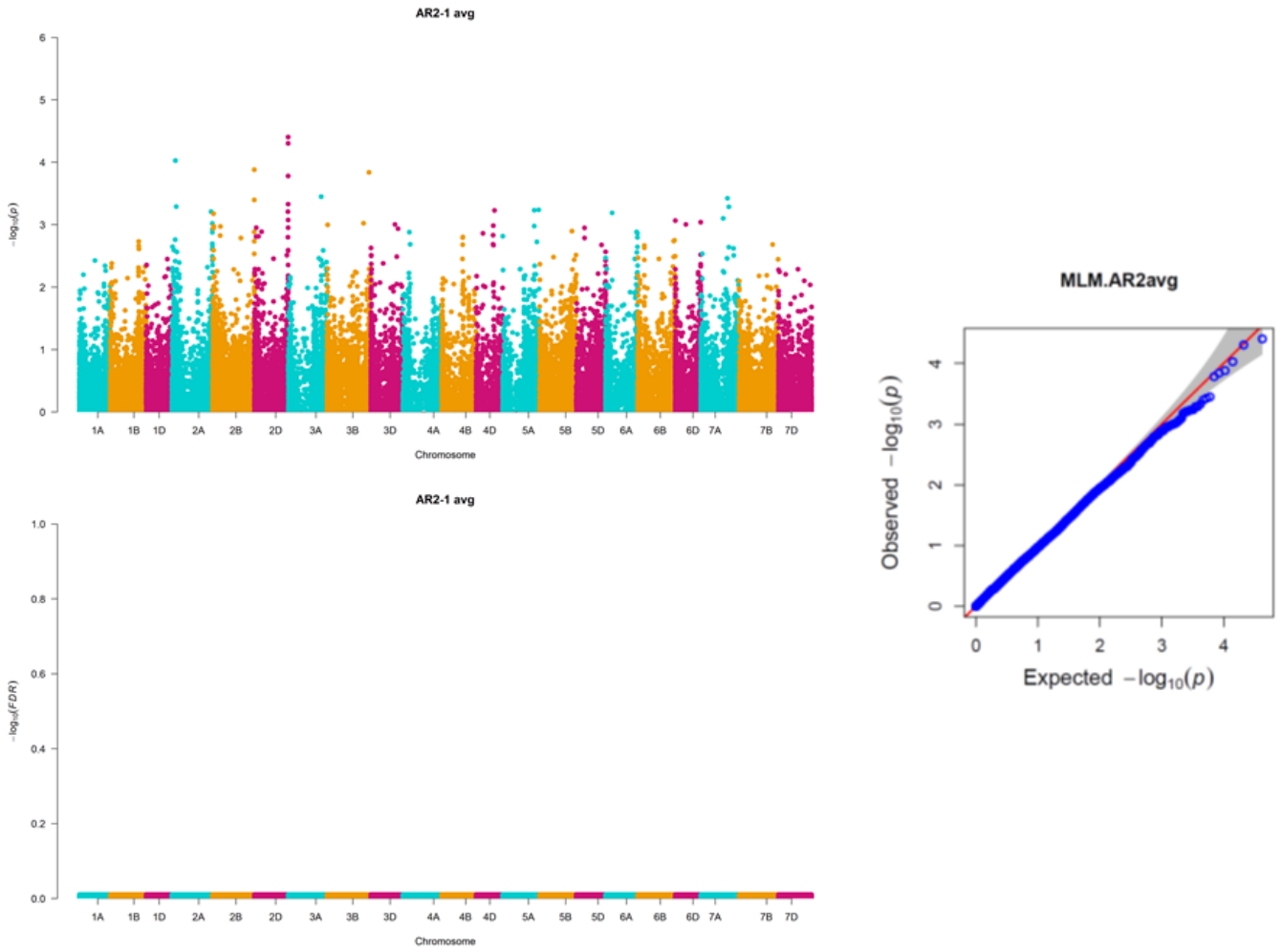

Figure 7.10. Manhattan plots for the association mapping using the MLM model for reaction to septoria nodorum blotch caused by the *P. nodorum* isolate AR2-1. For the top Manhattan plot, the y-axis indicated –log10(*p*) for SNP markers whereas for the bottom Manhattan plot, the y-axis indicated –log10(FDR) for SNP markers. The x-axis for both is the physical distribution of all the SNP markers on the 21 common wheat chromosomes based on the alignment to the IWGSC Chinese Spring Ref Seq v2. On the right is the QQ plot output for the MLM model from GAPIT.

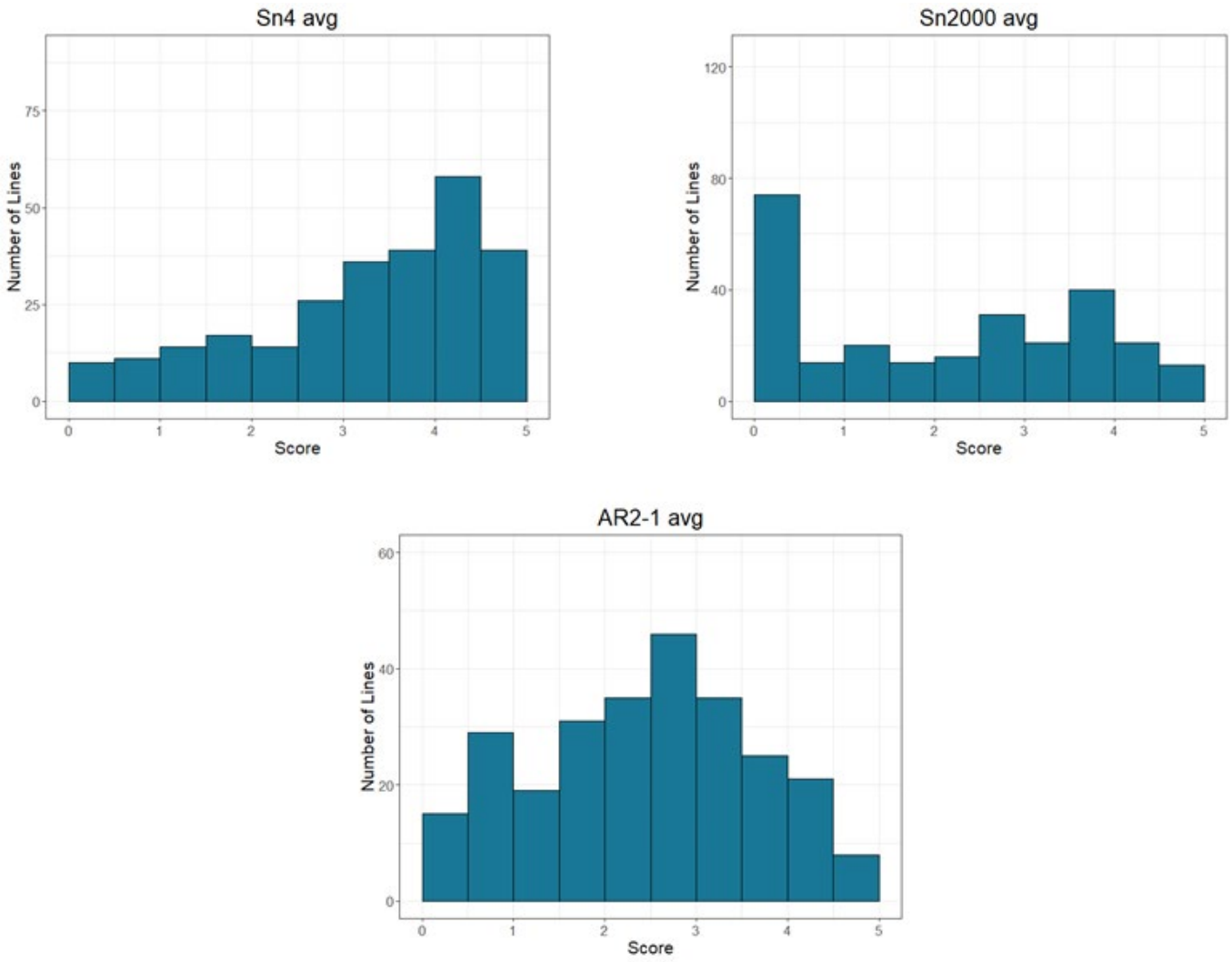

Figure 7.11. Histograms displaying the distribution of the disease reaction to the *P. nodorum* isolate Sn4, Sn2000, and AR2-1. Replicates of each were statistically homogeneous and therefore were combined.

7.4.4. Sn4

GWAS for SNB response to *P. nodorum* isolate Sn4 identified four significant marker-trait associations (Table 7.8, Figure 7.12). These four markers, *BS00091519_51*, *GENE-3324_338*, *Excalibur_c47452_183* and *BS00064298_51* were within the *Snn3-B1* region on chromosome 5BS. *BS00064298_51* was the most significant marker and explained 0.94% of the disease variation. These significant SNPs spanned from 6,704,549 bp (*GENE-3324_338*) to 7,031,414 bp (*BS00064298_51*).

7.4.5. Sn2000

For response to Sn2000, a total of 14 SNPs were significantly associated with disease in the GWAS analysis (Table 7.8, Figure 7.13). These 14 SNPs were within the *Tsn1* region on chromosome 5BL. The first 13 most significant SNPs spanned from 549,788,309 bp (*IACX9261*) to 549,933,008 bp (*Excalibur_rep_c105815_305*). The significant SNP *wsnp_Ex_c63909_62932437* was at 784,753,007 bp. *BobWhite_c48435_165* and *Tdurum_contig12066_126* were the most significant markers, each explaining 10.83% of the disease variation.

Table 7.8. Significant associations between single nucleotide polymorphism (SNP) markers and Septoria nodorum blotch disease after inoculating with multiple *Parastagonospora nodorum* isolates. The MLM model was used for each trait to identify significant marker trait associations. Markers with a *P*-value less than 0.05 after the FDR adjustment were considered significant.

Isolate	SNP[a]	Allele	Chromosome	Position[b]	*P*-value	FDR adjusted *P*-value	-Log$_{10}$(*P*)	R^2 × 100	Effect
Sn4 avg	*BS00091519_51*	A/G	5B	6,705,156	8.38E-07	0.03236	6.08	9.04	-0.83
Sn4 avg	*GENE-3324_338*	A/G	5B	6,704,549	1.54E-06	0.03236	5.82	8.58	0.82
Sn4 avg	*Excalibur_c47452_183*	T/C	5B	6,710,705	2.42E-06	0.03387	5.62	8.25	-0.79
Sn4 avg	*BS00064298_51*	G/A	5B	7,031,414	3.61E-06	0.03789	5.44	7.95	0.51
Sn2000 avg	*BobWhite_c48435_165*	C/T	5B	549,911,221	4.51E-10	6.41E-06	9.35	10.83	1.54
Sn2000 avg	*Tdurum_contig12066_126*	G/T	5B	549,910,391	4.51E-10	6.41E-06	9.35	10.83	1.54
Sn2000 avg	*Tdurum_contig25513_123*	G/A	5B	549,910,986	4.58E-10	6.41E-06	9.34	10.82	1.50
Sn2000 avg	*tplb0027f13_1346*	A/G	5B	549,911,640	5.58E-09	4.17E-05	8.25	9.37	1.40
Sn2000 avg	*wsnp_Ku_c40334_48581010*	G/A	5B	549,932,605	5.66E-09	4.17E-05	8.25	9.36	1.39
Sn2000 avg	*Tdurum_contig12066_247*	G/A	5B	549,910,462	5.95E-09	4.17E-05	8.23	9.34	-1.42
Sn2000 avg	*Tdurum_contig25513_195*	C/T	5B	549,911,058	7.27E-09	4.37E-05	8.14	9.22	-1.29
Sn2000 avg	*tplb0027f13_1493*	C/T	5B	549,911,493	4.43E-08	0.00023	7.35	8.20	-1.30
Sn2000 avg	*Excalibur_rep_c105815_305*	C/T	5B	549,933,008	2.17E-07	0.00101	6.66	7.31	-1.03
Sn2000 avg	*IACX9261*	A/C	5B	549,788,309	3.15E-07	0.00132	6.50	7.10	-1.30
Sn2000 avg	*CAP8_c7929_203*	G/T	5B	549,788,353	3.90E-07	0.00149	6.41	6.99	1.30
Sn2000 avg	*BS00010590_51*	T/G	5B	549,788,359	3.92E-06	0.01372	5.41	5.73	1.05
Sn2000 avg	*GENE-3198_56*	C/T	5B	549,911,389	8.34E-06	0.02696	5.08	5.33	0.69
Sn2000 avg	*wsnp_Ex_c63909_62932437*	C/T	2A	784,753,007	1.62E-05	0.04877	4.79	4.97	0.83

[a]SNP markers are from the Infinium SNP 90K array (Wang et al. 2014)

[b]Physical location is based on the IWGSC RefSeq v2

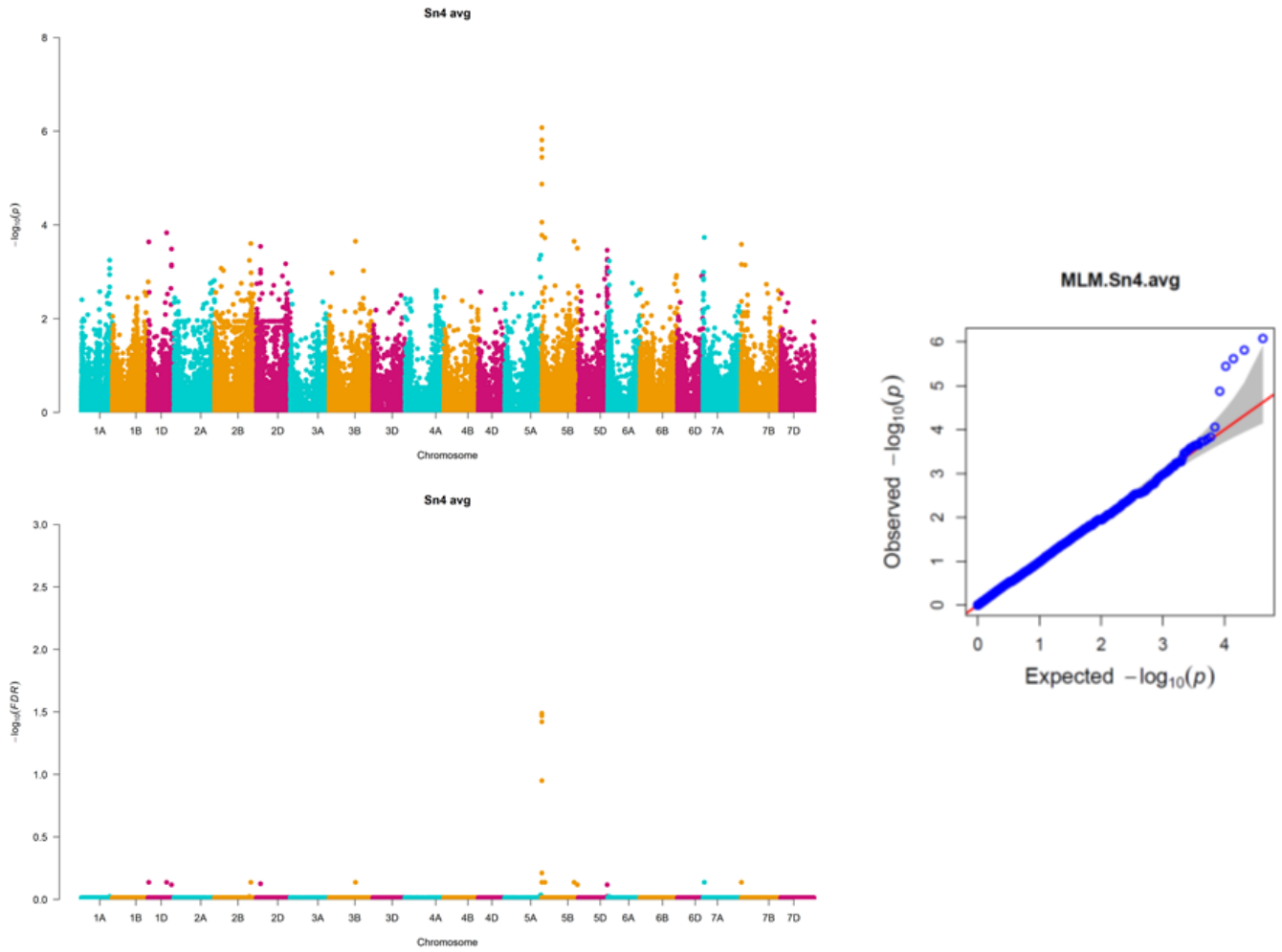

Figure 7.12. Manhattan plots for the association mapping using the MLM model for reaction to septoria nodorum blotch caused by the *P. nodorum* isolate Sn4. For the top Manhattan plot, the y-axis indicated –log10(*p*) for SNP markers whereas for the bottom Manhattan plot, the y-axis indicated –log10(FDR) for SNP markers. The x-axis for both is the physical distribution of all the SNP markers on the 21 common wheat chromosomes based on the alignment to the IWGSC Chinese Spring Ref Seq v2. On the right is the QQ plot output for the MLM model from GAPIT.

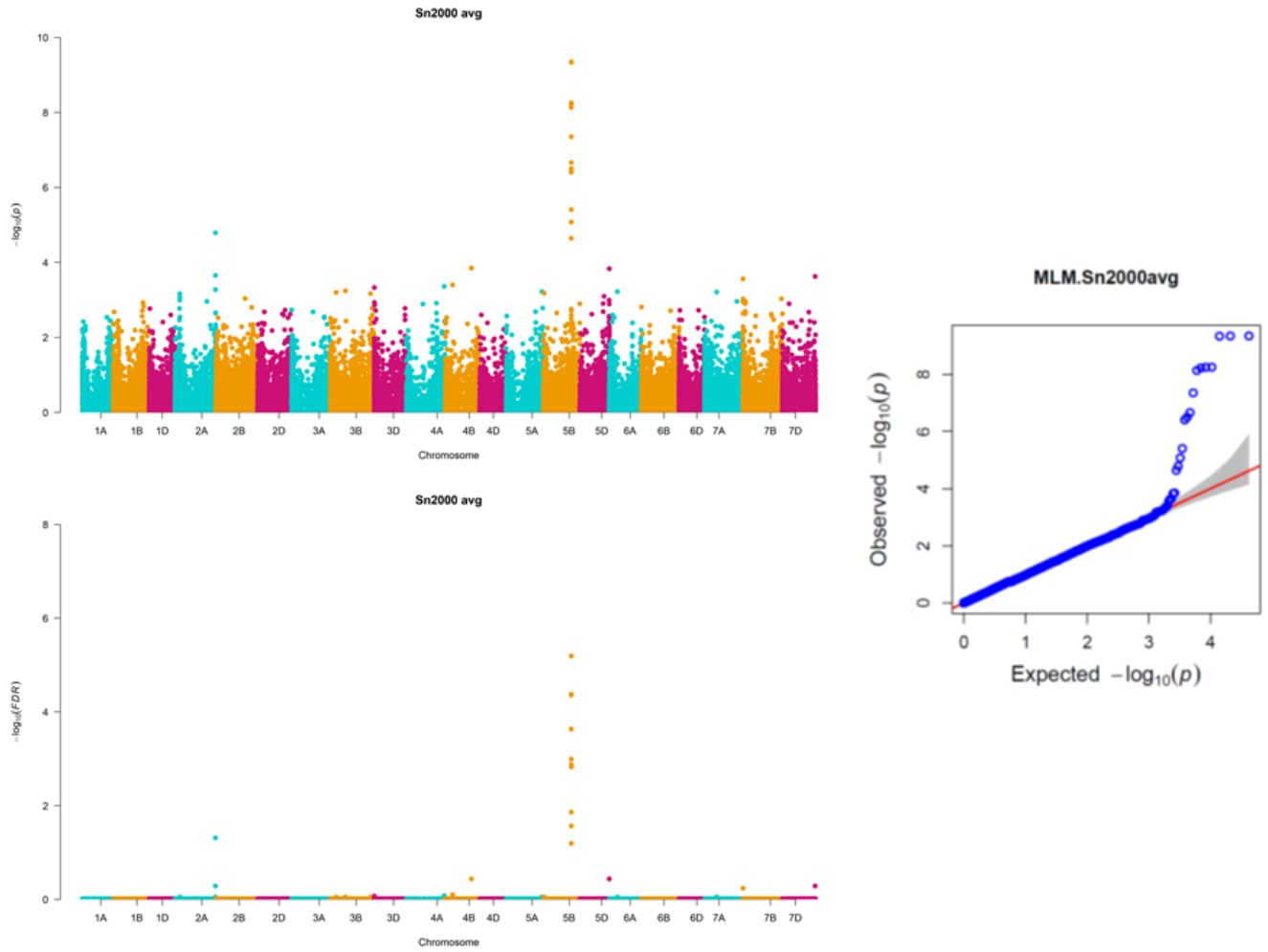

Figure 7.13. Manhattan plots for the association mapping using the MLM model for reaction to septoria nodorum blotch caused by the *P. nodorum* isolate Sn2000. For the top Manhattan plot, the y-axis indicated –log10(*p*) for SNP markers whereas for the bottom Manhattan plot, the y-axis indicated –log10(FDR) for SNP markers. The x-axis for both is the physical distribution of all the SNP markers on the 21 common wheat chromosomes based on the alignment to the IWGSC Chinese Spring Ref Seq v2. On the right is the QQ plot output for the MLM model from GAPIT.

7.4.6. Correlation Between Sensitivity and Disease Reactions

Using Pearson's correlation coefficients, I determined whether there were correlations between the disease scores from inoculations and the NE sensitivity scores (Table 7.9). Sn4 average disease scores had strong significant correlations with scores for infiltrations of SnToxA, SnTox1, SnTox267, and SnTox3. Sn4 is known to produce SnToxA, SnTox1, SnTox3, SnTox267. Sn2000 average disease scores had strong significant correlations with SnToxA, SnTox1, and SnTox5. Sn2000 is known to produce these three NEs. Interestingly, a significant positive correlation between Sn2000 with SnTox267 and SnTox3 was also observed. This may be due to a high percentage of lines being sensitive to two or more NEs. Lastly, AR2-1 average disease scores had strong significant correlations with SnTox1 and SnTox267. A slight correlation was observed between AR2-1 and SnTox5.

Table 7.9. Correlations among the NEs and the inoculation results.

	SnToxA	SnTox1	SnTox267	SnTox3	SnTox5
Sn4 avg	0.35***	0.23***	0.39***	0.47***	0.13*
Sn2000 avg	0.76***	0.61***	0.20**	0.17**	0.49***
AR2-1 avg	0.09	0.24***	0.55***	0.11	0.15*

*P<0.05
**P<0.01
***P<0.001

7.5. Discussion

SNB is an economically damaging foliar disease on wheat and is part of the fungal leaf disease complex. The wheat-*P. nodorum* pathosystem has been studied extensively over the last three decades as a model system for the inverse gene-for-gene interaction (Liu et al. 2004; Friesen and Faris 2010, 2021; Faris and Friesen 2020; Oliver et al. 2012). Previously, nine host sensitivity gene-pathogen NE interactions have been characterized and shown to play an important role in contributing to disease severity. Multiple winter wheat panels have previously been evaluated for SNB resistance/susceptibility using GWAS (AlTameemi et al. 2021; Downie

et al. 2018; Cowger et al. 2020; Liu et al. 2015; Phan et al. 2018; Halder et al. 2019). However, to my knowledge, these panels have consisted of only regional germplasm or the global sets include both winter and spring type common wheat.

In this study, my goal was to evaluate a diverse global panel to evaluate SNB disease and identify genomic regions associated with SNB resistance/susceptibility. Although I found genomic regions significantly associated with SNB disease caused by the *P. nodorum* isolates Sn4 and Sn2000, these regions corresponded to the known NE sensitivity genes *Snn3-B1* and *Tsn1*, respectively. Potential reasons I may not have identified new genomic regions associated with SNB disease include a) GWAS is not powerful enough to detect rare variants and small effect alleles, b) my population size was not large enough, c) population structure and relatedness confounded my results, and d) the number of markers I observed in high LD may influence my observed results (Korte and Farlow 2013; Cortes et al. 2021).

It is possible the large effect of the *Tsn1*-SnToxA and *Snn3-B1*-SnTox3 interactions may mask interactions with minor effects. Previously, Phan et al. (2021) performed GWAS analysis on a wheat panel that lacked lines with SnTox1 and SnToxA sensitivity to reduce disease complexity and increase their chances of detecting minor interactions. I tried this method with my analysis by removing SnToxA-sensitive lines and SnTox3-sensitive lines (not at the same time) and rerunning GWAS. For Sn4, the *Snn3-B1*-SnTox3 peak disappeared when analyzing lines that were SnTox3-insensitive, but no new significant marker-trait associations were detected. The same occurred when re-analyzing disease caused by Sn2000 where the *Tsn1*-SnToxA peaked disappeared when only SnToxA insensitive lines were used (results not shown). Therefore, it appears the effects of the *Tsn1*-SnToxA and *Snn3-B1*-SnTox3 interactions did not hinder the detection of other interactions.

Recently, AlTameemi et al. (2021) published a study evaluating a US hard red winter wheat panel for SNB caused by *P. nodorum* isolate Sn2000. In their model, the SNP *tplb0027f13_1346* on chromosome 5B associated with the *Tsn1* locus was the most significant. *tplb0027f13_1346* was also significantly associated with SNB caused by Sn2000 in the panel I evaluated. However, AlTameemi et al. (2021) also identified six other genomic regions associated with SNB caused by Sn2000 on chromosomes 1B, 2A, 2D, 4A, 6B, and 7A. The model they used in their analysis was the FarmCPU model. I also ran the FarmCPU model and had SNPs on chromosomes 2A and 7A (results not shown) which were significant and in the same region as significant SNPs in AlTameemi et al. (2021). However, whether these regions were associated with disease or were introduced due to the model needs to be validated.

Additionally, the *P. nodorum* isolate Sn2000 was used for disease evaluations by Halder et al. (2019) on a subset of the Watkins wheat landrace collection. Halder et al. (2019) found using MLM, the same model I used in this study, that the *Tsn1*-SnToxA interaction was significantly associated with disease. Consistent with my findings, they did not identify the *Snn1*-SnTox1 and *Snn5*-SnTox5 interactions to be significantly associated with disease. However, they identified markers on chromosome 2B, 5A, and 7A to be associated with disease that are not associated with any previously characterized interactions. Therefore, based on the findings in this study, along with Halder et al. (2019) and AlTameemi et al. (2021), I think it is reasonable to conclude that the *Tsn1*-SnToxA interaction plays a significant role in determining disease in the panel I evaluated.

The rate of LD decay I observed and the number of SNPs with high LD was partially skewed by a large proportion of heterozygous calls in this panel at SNP markers. Another round of filtering was recommended for LD analysis by Dr. Jason Fiedler, to remove heterozygous

markers. This was most likely caused by using seed that was not completely homozygous and this panel may have benefited from additional single seed descent increases. The panel I used is a subset of a larger panel. Research on the whole panel by Bulli et al. (2016) and two subsets by Muleta et al. (2020) and Mihalyov et al. (2017) found that the rate of LD decay within this panel is slower than that in spring wheat collections, which may also skew or influence my marker trait association results.

I decided to run a correlation between the infiltration results with the disease scores to determine if sensitivity to a NE was correlated with disease even though a marker-trait association was not detected in the GWAS analysis. Previously, Ruud et al. (2018) did something similar with the wheat-*P. nodorum* pathosystem. From my correlation results, SnTox1, SnTox5, and SnToxA infiltration results were highly correlated with Sn2000 disease scores. This is consistent with genome sequencing results, with the Sn2000 genome containing SnToxA, SnTox1, and SnTox5, but not SnTox3 or SnTox267 (Richards et al. 2018, Kariyawasam et al. 2021; Richards et al. 2021). Although we observed a correlation between Sn2000 scores with SnTox3 and SnTox267, it was not as significant as the other three interactions. Additionally, many of the lines that were sensitive to SnToxA, SnTox1, and/or SnTox5 were sensitive to SnTox3 and/or SnTox267, which may inflate the correlation between the latter two NEs and Sn2000 disease. Previous research showed that the *Tsn1*-SnToxA interaction can have an antagonistic effect on the *Snn1*-SnTox1 and *Snn5*-SnTox5 interactions in Sn2000 in a biparental population (Peters Haugrud et al. 2019). The white flecking phenotype associated with a compatible *Snn1*-SnTox1 interaction does not always fit into the published scoring scale (Liu et al. 2004), which may influence the lack of a significant marker trait association at the *Snn1* locus (Liu et al. 2016; Peters Haugrud et al. 2019).

As for Sn4 disease reaction, only the *Snn3-B1*-SnTox3 interaction was significant. It has been previously shown that Sn4 produces SnTox3, SnToxA, SnTox1, SnTox267 (Richards et al. 2018; Richards et al. 2021). For these four NEs, the correlation results were significantly correlated with SNB disease caused by Sn4. Surprisingly, I did not observe any marker trait associations at the *Tsn1*, *Snn1*, *Snn2*, *Snn6*, and *Snn7* loci. Previous work has illustrated variable expression of NE genes within *P. nodorum*, which directly influences the disease severity contributed to a host gene-NE interaction (Faris et al. 2011; Phan et al. 2016; Peters Haugrud et al. 2019; Jones et al. 2019; John et al. 2021). It is possible that *SnTox3* had higher expression than the other NE genes in Sn4, which could have masked the effects of other interactions in disease severity.

For the isolate AR2-1, I observed no significant marker trait associations. AR2-1 is an isolate first collected in Arkansas. Only 8% of the panel is North American lines and none of these lines originate from the southern part of the United States. Disease severity caused by AR2-1 was significantly correlated with SnTox1 and SnTox267 infiltration results. AR2-1 has the NE genes *SnTox267* (Richards et al. 2021) and *SnTox1* (Dr. Timothy Friesen, personal communication), and the differentials for SnTox267 and SnTox1 were susceptible in my inoculations (data not shown). In my GWAS results for infiltrations with SnTox267, I did not identify any marker-trait associations. This may be due to the NE SnTox267 interacting with multiple host target genes. In my AR2-1 GWAS results, the marker with the highest association was on the long arm of chromosome 2D, which could potentially be *Snn7* (Shi et al. 2015). Another observation I made was that the percent of leaf area affected by AR2-1 was lower than when the panel was infected with Sn4 and Sn2000. Richards et al. (2019) found AR2-1 to be less virulent than Sn4 and Sn2000 on six wheat lines tested. Therefore, the lower virulence and the

interaction of SnTox267 with multiple host genes most likely contributed to the lack of any significant marker trait associations for SNB disease caused by AR2-1 on this panel.

Lastly, a large portion of this project was to determine the prevalence of sensitivity to the different NEs in a global winter wheat panel. To my knowledge, this is the first panel that has been screened for sensitivity to SnTox5 and SnTox267. My results show that a little over half (53.03%) of the lines were sensitive to SnTox267, whereas only 42.42% of lines were sensitive to SnTox5. This difference may be due to SnTox267 interacting with *Snn2*, *Snn6*, and *Snn7* (Richards et al. 2021; Friesen et al. 2007; Gao et al. 2015; Shi et al. 2015). As for prevalence of SnToxA, SnTox1, and SnTox3 sensitivity, my results fall approximately in the middle of the range reported for other panels (Chapter 3). The knowledge gained from testing for sensitivity using infiltrations is being applied in marker development and for future cloning projects and validation. Currently, new markers are being developed with more accurate genotyping for *Tsn1* and *Snn1*, and this panel was used as part of the validation. Additionally, *Snn3-B1* and *Snn5* are in the final cloning validation steps and this panel will be used to validate markers developed from those projects.

Although no new genomic regions associated with SNB disease were identified in this study, I have shown the importance of the known interactions *Snn3-B1*-SnTox3 and *Tsn1*-SnToxA in contributing to disease. Additionally, I have evaluated the first global winter wheat panel, to my knowledge, for prevalence of sensitivity to five NEs. Lastly, this project has been a steppingstone for the future direction with this panel. I plan to evaluate the panel for SNB disease severity using isolates from Iran and Europe. A large portion of this panel is Iranian landraces and lines from Europe, therefore using isolates from those geographic regions may provide beneficial for identifying new genomic regions associated with SNB. I also plan to

inoculate this panel with *Pyrenophora tritici-repentis*, the causal agent of tan spot. I hope that future findings will provide us with new avenues to explore in the wheat-*P. nodorum* pathosystem, along with aiding in the cloning of host NE sensitivity genes and marker development.

7.6. Literature Cited

Abeysekara NS, Faris JD, Chao S, McClean PE, Friesen TL (2012) Whole-genome analysis of Stagonospora nodorum blotch resistance and validation of the SnTox4-*Snn4* interaction in hexaploid wheat. Phytopathology 102:94-104

Abeysekara NS, Friesen TL, Keller B, Faris JD (2009) Identification and characterization of a novel host-toxin interaction in the wheat-*Stagonospora nodorum* pathosystem. Theor Appl Genet 120:117-126

Adhikari TB, Jackson EW, Gurung S, Hansen JM, Bonman JM (2011) Association mapping of quantitative resistance to *Phaeosphaeria nodorum* in spring wheat landraces from the USDA National Small Grains Collection. Phytopathology 101:1301-1310

AlTameemi R, Gill HS, Ali S, Ayana G, Halder J, Sidhu JS, Gill US, Turnipseed B, Gonzalez Hernandez JL, Sehgal SK (2021) Genome-wide association analysis permits characterization of Stagonospora nodorum blotch (SNB) resistance in hard winter wheat. Sci Rep-UK 11:12570

Ballini E, Tavaud M, Ducasse A, Sanchez D, Paux E, Kitt J, Charmet G, Audigeos D, Roumet P, David J, Morel J (2020) Genome wide association mapping for resistance to multiple fungal pathogens in a panel issued from a broad composite cross-population of tetraploid wheat *Triticum turgidum*. Euphytica 216:92

Bradbury PJ, Zhang Z, Kroon DE, Casstevens TM, Ramdoss Y, Buckler ES (2007) TASSEL: software for association mapping of complex traits in diverse samples. Bioinformatics 23:2633-2635

Bulli P, Zhang J, Chao S, Chen X, Pumphrey M (2016) Genetic architecture of resistance to stripe rust in a global winter wheat germplasm collection. G3-Genes Genom Genet doi:10.1534/g3.116.028407

Cortes LT, Zhang Z, Yu J (2021) Status and prospects of genome-wide association studies in plants. Plant Genome-US 14:e20077

Cowger C, Ward B, Brown-Guedira G, Brown JKM (2020) Role of effector-sensitivity gene interactions and durability of quantitative resistance to septoria nodorum blotch in Eastern U.S. wheat. Front Plant Sci https://doi.org/10.3389/fpls.2020.00155

Downie RC, Bouvet L, Furuki E, Gosman N, Gardner KA, Mackay IJ, Campos Mantello C, Mellers G, Phan HTT, Rose GA, Tan KC, Oliver RP, Cockram J (2018) Assessing European Wheat Sensitivities to *Parastagonospora nodorum* necrotrophic effectors and fine-mapping the *Snn3-B1* locus conferring sensitivity to the effector SnTox3. Front Plant Sci https://doi.org/10.3389/fpls.2018.00881

Eyal Z (1987) The Septoria diseases of wheat: concepts and methods of disease management. CIMMYT, Mexico

Faris JD and Friesen TL (2009) Reevaluation of a tetraploid wheat population indicates that the *Tsn1*-ToxA interaction is the only factor governing Stagonospora nodorum blotch susceptibility. Phytopathology 99:906-912

Faris JD and Friesen TL (2020) Plant genes hijacked by necrotrophic fungal pathogens. Curr Opin Plant Biol 56:74-80

Faris JD, Zhang Z, Lu H, Lu Z, Reddy L, Cloutier S, Fellers JP, Meinhardt SW, Rasmussen JB, Xu SS, Oliver RP, Simons KJ, Friesen TL (2010) A unique wheat disease resistance-like gene governs effector-triggered susceptibility to necrotrophic pathogens. Proc Natl Acad Sci 107:13544-13549

Faris JD, Zhang Z, Rasmussen JB, Friesen TL (2011) Variable expression of the *Stagonospora nodorum* effector SnToxA among isolates is correlated with levels of disease in wheat. Mol Plant Microbe In 24:1419-1426

Francki MG, Walker E, McMullan CJ, Morris WG (2020) Multi-location evaluation of global wheat lines reveal multiple QTL for adult plant resistance to Septoria nodorum blotch (SNB) detected in specific environments and in response to different isolates. Front Plant Sci 11:771

Friesen TL, Chu CG, Liu ZH, Xu SS, Halley S, Faris JD (2009) Host-selective toxins produced by *Stagonospora nodorum* confer disease susceptibility in adult wheat plants under field conditions. Theor Appl Genet 118:1489-1497

Friesen TL, Chu C, Xu SS, Faris JD (2012) SnTox5-*Snn5*: a novel *Stagonospora nodorum* effector-wheat gene interaction and its relationship with the SnToxA-*Tsn1* and SnTox3-*Snn3-B1* interactions. Mol Plant Pathol 13:1101-1109

Friesen TL and Faris JD (2010) Characterization of the wheat-*Stagonospora nodorum* system: what is the molecular basis of this quantitative necrotrophic disease interaction? Can J Plant Pathol 32:20-28

Friesen TL and Faris JD (2012) Characterization of plant-fungal interactions involving necrotrophic effector-producing plant pathogens. In: Bolton M, Thomma B (eds) Plant

Fungal Pathogens. Methods in Molecular Biology (Methods and Protocols), vol 835. Humana Press. https:doi.org/10.1007/978-1-61779-501_12

Friesen TL and Faris JD (2021) Characterization of effector-target interactions in necrotrophic pathosystems reveals trends and variation in host manipulation. Ann Rev Phytopathol https://doi.org/10.1146/annurev-phyto-120320-012807

Friesen TL, Meinhardt SW, Faris JD (2007) The *Stagonospora nodorum*-wheat pathosystem involves multiple proteinaceous host-selective toxins and corresponding host sensitivity genes that interact in an inverse gene-for-gene manner. Plant J 51:681-692

Friesen TL, Stukenbrock EH, Liu Z, Meinhardt S, Ling H, Faris JD, Rasmussen JB, Solomon PS, McDonald BA, Oliver RP (2006) Emergence of a new disease as a result of interspecific virulence gene transfer. Nat Genet 38:953-956

Friesen TL, Zhang Z, Solomon PS, Oliver RP, Faris JD (2008) Characterization of the interaction of a novel *Stagonospora nodorum* host-selective toxin with a wheat susceptibility gene. Plant Physiol 146:682-693

Gao Y, Faris JD, Liu Z, Kim M, Syme RA, Oliver RP, Xu SS, Friesen TL (2015) Identification and characterization of the SnTox6-*Snn6* interaction in the Parastagonospora nodorum-wheat pathosystem. Mol Plant Microbe In 28:615-625

Gurung S, Mamidi S, Bonman JM, Xiong M, Brown-Guedira G, Adhikari TB (2014) Genome-wide association study reveals novel quantitative loci associated with resistance to multiple leaf spot diseases of spring wheat. PLoS ONE 9:e108179

Halder J, Zhang J, Ali S, Sidhu JS, Gill HS, Talukder SK, Kleinjan J, Turnipseed B, Sehgal SK (2019) Mining and genomic characterization of resistance to tan spot, Stagonospora

ndoroum blotch (SNB), and Fusarium head blight in Watkins core collection of wheat landraces. BMC Plant Biol 19:480

Jones DAB, John E, Rybak K, Phan HTT, Singh KB, Lin SY, Solomon PS, Oliver RP, Tan KC (2019) A specific fungal transcription factor controls effector gene expression and orchestrates the establishment of the necrotrophic pathogen lifestyle on wheat. Sci Rep-UK 9:15884

John E, Jacques S, Phan HTT, Liu L, Pererira D, Croll D, Singh KB, Oliver RP, Tan KC (2021) Variability in an effector gene promoter of a necrotrophic fungal pathogen dictates epistasis and effector-triggered susceptibility in wheat. bioRxiv https://doi.org/10.1101/2021.07.28.454099

Kariyawasam GK, Richards JK, Wyatt NA, Running KLD, Xu SS, Liu Z, Borowicz P, Faris JD, Friesen TL (2021) The *Parastagonospora nodorum* necrotrophic effector SnTox5 targets the wheat gene *Snn5* and facilitates entry into the leaf mesophyll. New Phytol https://doi.org/10.1111/nph.17602

Korte A and Farlow A (2013) The advantages and limitations of trait analysis with GWAS: a review. Plant Methods 9:29

Lipka AE, Tian F, Wang Q, Peiffer J, Li M, Bradbury PJ, Gore MA, Buckler ES, Zhang Z (2012) GAPIT: genome association and prediction integrated tool. Bioinformatics 28:2397-2399

Liu X, Huang M, Fan B, Buckler ES, Zhang Z (2016) Iterative usage of fixed and random effect models for powerful and efficient genome-wide association studies. PLoS Genet 12:e1005767

Liu Z, El-Basyoni I, Kariyawasam G, Zhang G, Fritz A, Hansen J, Marais F, Friskop A, Chao S, Akhunov E, Baenziger PS (2015) Evaluation and association mapping of resistance to tan spot and stagonospora nodorum blotch in adapted winter wheat germplasm. Plant Dis 99:1333-1341

Liu Z, Faris JD, Oliver RP, Tan KC, Solomon PS, McDonald MC, McDonald BA, Nunez A, Lu S, Rasmussen JB, Friesen TL (2009) SnTox3 acts in effector triggered susceptibility to induce disease on wheat carrying the *Snn3* gene. PLoS Pathog 5:e1000581

Liu ZH, Faris JD, Meinhardt SW, Ali S, Rasmussen JB, Friesen TL (2004a) Genetic and physical mapping of a gene conditioning sensitivity in wheat to a partially purified host-selective toxin produced by *Stagonospora nodorum*. Phytopathology 94:1056-1060

Liu ZH, Friesen TL, Rasmussen JB, Ali S, Meinhardt SW, Faris JD (2004b) Quantitative trait loci analysis and mapping of seedling resistance to Stagonospora nodorum leaf blotch in wheat. Phytopathology 94:1061-1067

Liu Z, Friesen TL, Ling H, Meinhardt SW, Oliver RP, Rasmussen JB, Faris JD (2006) The *Tsn1*-ToxA interaction in the wheat-*Stagonospora nodorum* pathosystem parallels that of the wheat-tan spot system. Genome 49:1265-1273

Liu Z, Gao Y, Kim YM, Faris JD, Shelver WL, de Wit PJGM, Xu SS, Friesen TL (2016) SnTox1, a *Parastagonospora nodorum* necrotrophic effector, is a dual-function protein that facilitates infection while protecting from wheat-produced chitinases. New Phytol 211:1052-1064

Liu Z, Zhang Z, Faris JD, Oliver RP, Syme R, McDonald MC, McDonald BA, Solomon PS, Lu S, Shelver WL, Xu S, Friesen TL (2012) The cysteine rich necrotrophic effector SnTox1

produced by *Stagonospora nodorum* triggers susceptibility of wheat lines harboring *Snn1*. PLoS Pathog 8:e1002467

Mauricio Zambrano-Bigiarini (2020). hydroGOF: Goodness-of-fit functions for comparison of simulated and observed hydrological time series. doi:10.5281/zenodo.839854, R package version 0.4-0, https://github.com/hzambran/hydroGOF.

Mihalyov PD, Nichols VA, Bulli P, Rouse MN, Pumphrey MO (2017) Multi-locus mixed model analysis of stem rust resistance in winter wheat. Plant Genome-US https://doi.org/10.3835/plantgenome2017.01.0001

Money D, Gardner KM, Migicovsky Z, Schwaninger H, Zhong GY, Myles S (2015) LinkImpute-fast and accurate genotype imputation for non-model organisms. G3-Genes Genomes Genet 5:2383

Muleta KT, Chen X, Pumphrey M (2020) Genome-wide mapping of resistance to stripe rust caused by *Puccinia striiformis* f. sp. *tritici* in hexaploid wheat. Crop Sci 60:115-131

Patterson N, Price AL, Reich D (2006) Population structure and eigenanalysis. PLoS Genetics 12:e190

Peters Haugrud AR, Zhang Z, Richards JK, Friesen TL, Faris JD (2019) Genetics of variable disease expression conferred by inverse gene-for-gene interactions in the wheat-*Parastagonospora nodorum* pathosystem. Plant Physiol 180:420-434

Phan HTT, Furuki E, Hunziker L, Ryback K, Tan KC (2021) GWAS analysis reveals distinct pathogenicity profiles of Australian *Parastagonospora nodorum* isolates and identification of marker-trait-associations to septoria nodorum blotch. Sci Rep-UK 11:10085

Phan HTT, Rybak K, Bertazzoni S, Furuki E, Dinglasan E, Hickey LT, Oliver RP, Tan KC (2018) Novel sources of resistance to Septoria nodorum blotch in the Vavilov wheat collection identified by genome-wide association studies. Theor Appl Genet 131:1223-1238

Phan HTT, Rybak K, Furuki E, Breen S, Solomon PS, Oliver RP, Tan KC (2016) Differential effector gene expression underpins epistasis in a plant fungal disease. Plant J 87:343-354

Oliver RP, Friesen TL, Faris JD, Solomon PS (2012) *Stagonospora nodorum*: from pathology to genomics and host resistance. Ann Rev Phytopathol 50:23-43

Reddy L, Friesen TL, Meinhardt SW, Chao S, Faris JD (2008) Genomic analysis of the *Snn1* locus on wheat chromosome arm 1BS and the identification of candidate genes. Plant Genome 1:55-66

Remington DL, Thornsberry JM, Matsuoka Y, Wilson LM, Whitt SR, Doebley J, Kresovich S, Goodman MM, Buckler IV ES (2001) Structure of linkage disequilibrium and phenotypic associations in the maize genome. Proc Natl Acad Sci 98:11479-11484

Richards JK, Kariyawasam GK, Seneviratne S, Wyatt NA, Xu SS, Liu Z, Faris JD, Friesen TL (2021) A triple threat: the *Parastagonospora nodorum* SnTox267 effector exploits three distinct host genetic factors to cause disease in wheat. New Phytol https://doi.org/10.1111/nph.17601

Richards JK, Stukenbrock EH, Carpenter J, Liu Z, Cowger C, Faris JD, Friesen TL (2019) Local adaptation drives the diversification of effectors in the fungal wheat pathogen *Paratagonospora nodorum* in the United States. PLoS Genetics 15:e1008223

Richards JK, Wyatt NA, Liu Z, Faris JD, Friesen TL (2018) Reference quality genome assemblies of three *Parastagonospora nodorum* isolates differing in virulence on wheat. G3-Genes Genome Genet 8:393-399

Ruud AK, Dieseth JA, Ficke A, Furuki E, Phan HTT, Oliver RP, Tan KC, Lilemo M (2019) Genome-wide association mapping of resistance to Septoria nodorum leaf blotch in a Nordic spring wheat collection. Plant Genome-US 12:180105

Segura V, Vilhjálmsson BJ, Platt A, Korte A, Seren Ü, Long Q, Nordborg M (2012) An efficient multi-locus mixed-model approach for genome-wide association studies in structured populations. Nat Genet 44:825-830

Sharma S (2019) Genetics of wheat domestication and Septoria nodorum blotch susceptibility in wheat. Masters thesis, North Dakota State University

Shi G, Friesen TL, Saini J, Xu SS, Rasmussen JB, Faris JD (2015) The wheat *Snn7* gene confers susceptibility on recognition of the *Parastagonospora nodorum* necrotrophic effector SnTox7. Plant Genome-US plantgenome2015.02.0007

Shi G, Zhang Z, Friesen TL, Bansal U, Cloutier S, Wicker T, Rasmussen JB, Faris JD (2016a) Marker development, saturation mapping, and high-resolution mapping of the Septoria nodorum blotch susceptibility gene *Snn3-B1* in wheat. Molecular Genet Genomics 291:107-119

Shi G, Zhang Z, Friesen TL, Raats D, Fahima T, Brueggeman RS, Lu S, Trick HN, Liu Z, Chao W, Frenkel Z, Xu SS, Rasmussen JB, Faris JD (2016b) The hijacking of a receptor kinase-driven pathway by a wheat fungal pathogen leads to disease. Science Adv 2:e1600822

Singh M and Upadhyaya HD (2015) *Genetic and Genomic Resources for Grain Cereals Improvement.* Academic Press.

Snedecor GW and Cochran WG (1989) Statistical methods, Eighth Edition. Iowa State University Press, Ames

Turner SD (2018) qqman: an R package for visualizing GWAS results using the Q-Q and manhattan plots. The Journal of Open Source Software DOI:10.21105/joss.00731

Wang J and Zhang Z (2020) GAPITVersion 3: Boosting power and accuracy for genomic association and prediction. Genomics Proteomics Bioinformatics https://doi.org/10.1016/j.gpb.2021.08.005

Wang S, Wong D, Forrest K, Allen A, Chao S, Huang BE, Maccaferri M, Salvi S, Milner SG, Cattivelli L, et al. (2014) Characterization of polyploidy wheat genomic diversity using a high-density 90,000 single nucleotide polymorphism array. Plant Biotechnol J 12:787-796

Xu Y, Li P, Yang Z, Xu C (2017) Genetic mapping of quantitative trait loci in crops. The Crop Journal 5:175-184

Zhang Z, Friesen TL, Simons KJ, Xu SS, Faris JD (2009) Development, identification, and validation of markers for marker-assisted selection against the *Stagonospora nodorum* toxin sensitivity genes *Tsn1* and *Snn2* in wheat. Mol Breeding 23:35-49

Zhang Z, Friesen TL, Xu SS, Shi G, Liu Z, Rasmussen JB, Faris JD (2011) Two putatively homoeologous wheat genes mediate recognition of SnTox3 to confer effector-triggered susceptibility to *Stagnonospora nodorum*. Plant J 65:27-38

Zhang Z, Running KLD, Seneviratne S, Peters Haugrud AR, Szabo-Hever A, Shi G, Brueggeman R, Xu SS, Friesen TL, Faris JD (2021) A protein kinase-major sperm

protein gene hijacked by a necrotrophic fungal pathogen triggers disease susceptibility in wheat. Plant J doi:10.1111/tpj.15194

Zhao K, Aranzana MJ, Kim S, Lister C, Shindo C, Tang C, Toomajian C, Zheng H, Dean C, Marjoram P, Nordborg M (2007) An *Arabidopsis* example of association mapping in structured samples. PLoS Genetics https://doi.org/10.1371/journal.pgen.003000

APPENDIX A. LIST OF LINES IN THE GLOBAL WINTER WHEAT PANEL OBTAINED FROM THE USDA NATIONAL SMALL GRAINS COLLECTION

The average results for each line for infiltration with the necrotrophic effectors SnToxA, SnTox1, SnTox3, SnTox5, and SnTox267 are listed, along with the average disease score to inoculations with the *Parastagonospora nodorum* isolates Sn4, AR2-1, and Sn2000.

Accession	Line	ACIMPT	Country	Continent	SnToxA	SnTox1	SnTox3	SnTox5	SnTox267	Sn4 avg	AR2-1 avg	Sn2000 avg
PI238406	358-R.3.C	Breeding	Kenya	Africa	3.00	0.67	0.00	2.00	3.00	4.33	4.17	3.83
PI269407	322	Landrace	Afghanistan	Asia	3.00	1.00	0.00	3.00	3.00	4.17	1.50	3.00
PI347180	Sirhosha	Landrace	Afghanistan	Asia	0.00	0.33	0.00	0.00	1.00	1.33	2.83	0.17
PI367025	1566	Landrace	Afghanistan	Asia	0.00	3.00	3.00	3.00	0.67	3.17	3.00	2.67
PI68236	413	Cultivated	Azerbaijan	Asia	0.33	0.00	0.00	3.00	3.00	2.50	1.67	1.17
PI73338	2908	Landrace	Azerbaijan	Asia	3.00	0.00	0.00	0.00	0.67	4.50	0.67	4.67
PI262603	Hydri Bugda	Landrace	Azerbaijan	Asia	3.00	2.33	0.00	0.33	0.00	2.83	1.17	2.50
PI68265	64	Cultivated	Azerbaijan	Asia	0.00	0.33	0.00	3.00	3.00	4.50	4.50	1.50
PI615323	Ker Yi 26	Cultivar	China	Asia	3.00	3.00	3.00	2.00	3.00	4.17	3.33	4.33
PI414568	Feng Chan 3	Cultivar	China	Asia	0.33	3.00	3.00	0.33	1.67	3.33	2.33	3.17
PI57164	CI 7111	Landrace	Georgia	Asia	3.00	0.33	0.00	3.00	2.50	4.33	2.50	4.00
PI591870	HW 6554/86	Landrace	Georgia	Asia	0.00	0.33	0.00	0.33	0.67	2.33	2.00	0.00
PI221699	3	Cultivated	Indonesia	Asia	3.00	2.67	0.00	3.00	2.00	4.67	1.25	3.75
PI210371		Landrace	Iran	Asia	3.00	2.67	2.67	2.33	0.67	4.50	2.33	4.25
PI222650	1620	Landrace	Iran	Asia	0.33	0.33	3.00	3.00	2.50	5.00	2.00	2.00
PI243674	5396	Landrace	Iran	Asia	3.00	2.67	3.00	2.67	2.67	4.50	3.00	4.67
PI243777	5520	Landrace	Iran	Asia	3.00	2.33	3.00	2.33	3.00	4.50	1.67	4.17
PI621168	IWA8607008	Landrace	Iran	Asia	3.00	0.00	3.00	3.00	3.00	4.33	3.00	3.17
PI621178	IWA8607024	Landrace	Iran	Asia	3.00	0.17	3.00	3.00	2.33	3.17	3.17	3.50
PI621205	IWA8607058	Landrace	Iran	Asia	0.00	3.00	3.00	3.00	2.67	3.33	3.17	4.00
PI621237	IWA8607130	Landrace	Iran	Asia	3.00	3.00	0.33	3.00	0.00	3.17	2.50	3.67
PI621404	IWA8607810	Landrace	Iran	Asia	3.00	3.00	3.00	3.00	0.67	5.00	2.33	4.75
PI621434	IWA8607941	Landrace	Iran	Asia	3.00	3.00	3.00	2.17	2.67	5.00	3.67	3.83
PI621449	IWA8608044	Landrace	Iran	Asia	3.00	0.00	2.67	2.33	2.00	4.17	2.00	3.83
PI621480	IWA8608194	Landrace	Iran	Asia	3.00	3.00	3.00	2.00	0.33	4.83	1.00	3.67
PI621550	IWA8608626	Landrace	Iran	Asia	3.00	0.00	2.67	3.00	2.33	5.00	3.50	5.00
PI621642	IWA8609149	Landrace	Iran	Asia	3.00	0.00	0.50	2.33	3.00	4.17	2.83	3.67
PI621645	IWA8609160	Landrace	Iran	Asia	0.00	0.00	3.00	2.83	3.00	2.83	3.33	0.33
PI621654	IWA8609181	Landrace	Iran	Asia	3.00	3.00	3.00	0.83	3.00	3.00	4.00	3.50
PI621655	IWA8609182	Landrace	Iran	Asia	3.00	3.00	0.00	3.00	1.00	3.17	4.00	3.83
PI621657	IWA8609184	Landrace	Iran	Asia	3.00	2.67	0.33	2.67	2.67	3.83	3.67	4.83
PI621710	IWA8609329	Landrace	Iran	Asia	3.00	3.00	3.00	2.67	2.67	4.33	2.67	3.83
PI621720	IWA8609352	Landrace	Iran	Asia	3.00	0.00	3.00	3.00	2.67	3.83	4.17	4.83
PI621846	IWA8609690	Landrace	Iran	Asia	2.67	3.00	3.00	3.00	0.00	3.00	2.00	3.67
PI621874	IWA8609910	Landrace	Iran	Asia	3.00	0.00	0.00	2.67	0.00	2.33	2.00	3.00
PI621900	IWA8609948	Landrace	Iran	Asia	3.00	3.00	3.00	3.00	2.67	4.17	3.50	3.67
PI621939	IWA8610035	Landrace	Iran	Asia	3.00	3.00	0.50	3.00	2.67	3.50	1.83	3.50
PI621959	IWA8610093	Landrace	Iran	Asia	3.00	3.00	3.00	3.00	3.00	2.83	2.67	3.33

Accession	Line	ACIMPT	Country	Continent	SnToxA	SnTox1	SnTox3	SnTox5	SnTox267	Sn4 avg	AR2-1 avg	Sn2000 avg
PI621980	IWA8610164	Landrace	Iran	Asia	3.00	0.00	2.33	3.00	2.67	4.50	3.50	4.75
PI622004	IWA8610266	Landrace	Iran	Asia	3.00	3.00	3.00	3.00	3.00	3.67	3.83	3.83
PI622065	IWA8610508	Landrace	Iran	Asia	3.00	0.33	2.67	3.00	1.83	3.50	1.75	3.67
PI622558	IWA8611883	Landrace	Iran	Asia	3.00	3.00	0.00	2.67	2.00	2.75	2.50	3.50
PI622589	IWA8612001	Landrace	Iran	Asia	3.00	2.67	3.00	0.00	3.00	2.83	3.00	4.17
PI622609	IWA8612063	Landrace	Iran	Asia	3.00	3.00	2.67	3.00	2.67	5.00	3.50	4.50
PI622644	IWA8612218	Landrace	Iran	Asia	3.00	3.00	3.00	2.33	3.00	3.17	2.33	4.33
PI622719	IWA8612533	Landrace	Iran	Asia	0.00	3.00	0.00	2.67	0.33	3.67	2.50	2.67
PI622801	IWA8613087	Landrace	Iran	Asia	3.00	3.00	3.00	3.00	0.50	3.83	1.00	4.00
PI622884	IWA8613583	Landrace	Iran	Asia	3.00	2.67	0.33	3.00	2.17	3.83	3.33	4.67
PI622919	IWA8613811	Landrace	Iran	Asia	3.00	3.00	0.00	2.33	3.00	4.50	2.33	4.50
PI622926	IWA8613853	Landrace	Iran	Asia	3.00	3.00	0.00	2.67	0.67	4.00	1.83	4.17
PI622963	IWA8613954	Landrace	Iran	Asia	3.00	0.00	1.33	3.00	2.67	4.33	1.67	2.67
PI622972	IWA8613988	Landrace	Iran	Asia	3.00	0.00	3.00	3.00	2.67	4.17	2.33	4.50
PI623020	IWA8614108	Landrace	Iran	Asia	3.00	3.00	3.00	3.00	3.00	2.50	3.83	4.00
PI623036	IWA8614166	Landrace	Iran	Asia	3.00	3.00	3.00	3.00	2.67	4.83	2.17	4.33
PI625352	IWA8610928	Landrace	Iran	Asia	3.00	3.00	3.00	2.67	3.00	3.67	3.33	3.67
PI626716	IWA8600106	Landrace	Iran	Asia	0.00	3.00	3.00	3.00	0.67	4.50	3.00	2.83
PI626785	IWA8600215	Landrace	Iran	Asia	0.00	3.00	2.33	3.00	2.33	2.83	2.67	3.25
PI626830	IWA8600282	Landrace	Iran	Asia	3.00	0.00	1.00	3.00	0.00	3.33	1.17	4.33
PI626842	IWA8600299	Landrace	Iran	Asia	3.00	3.00	0.00	3.00	2.33	4.83	3.50	3.67
PI627071	IWA8600667	Landrace	Iran	Asia	3.00	1.33	2.67	3.00	0.33	4.00	4.17	4.17
PI627093	IWA8600702	Landrace	Iran	Asia	3.00	3.00	3.00	2.67	0.75	4.33	4.50	4.00
PI627122	IWA8600748	Landrace	Iran	Asia	3.00	3.00	0.00	3.00	2.67	3.50	3.33	4.17
PI627137	IWA8600773	Landrace	Iran	Asia	3.00	3.00	0.00	3.00	2.33	3.00	3.33	3.00
PI627236	IWA8600968	Landrace	Iran	Asia	3.00	3.00	3.00	3.00	3.00	4.33	2.83	4.50
PI627377	IWA8602246	Landrace	Iran	Asia	3.00	3.00	0.00	3.00	1.00	3.83	2.67	3.25
PI627480	IWA8602500	Landrace	Iran	Asia	3.00	0.00	3.00	2.33	2.67	4.67	2.83	3.83
PI627605	IWA8603012	Landrace	Iran	Asia	3.00	3.00	3.00	3.00	2.67	1.67	1.83	2.67
PI627629	IWA8603046	Landrace	Iran	Asia	3.00	0.00	3.00	0.33	2.33	4.33	3.33	3.00
PI627660	IWA8603087	Landrace	Iran	Asia	3.00	3.00	0.00	3.00	0.50	3.33	2.50	4.00
PI627662	IWA8603089	Landrace	Iran	Asia	3.00	0.00	3.00	3.00	2.33	5.00	1.00	4.00
PI627688	IWA8603128	Landrace	Iran	Asia	3.00	3.00	2.33	2.33	0.00	5.00	2.83	3.75
PI627780	IWA8603251	Landrace	Iran	Asia	3.00	3.00	2.67	3.00	2.00	2.67	2.00	3.67
PI627798	IWA8603271	Landrace	Iran	Asia	3.00	3.00	3.00	3.00	0.33	5.00	4.67	4.33
PI627861	IWA8604057	Landrace	Iran	Asia	0.00	3.00	0.00	0.67	1.00	2.33	3.33	3.50
PI627963	IWA8604293	Landrace	Iran	Asia	3.00	3.00	3.00	3.00	3.00	1.50	2.33	3.00
PI628233	IWA8604924	Landrace	Iran	Asia	0.33	2.67	3.00	2.67	2.67	4.00	2.83	3.33

Accession	Line	ACIMPT	Country	Continent	SnToxA	SnTox1	SnTox3	SnTox5	SnTox267	Sn4 avg	AR2-1 avg	Sn2000 avg
PI285896	Akakkowa Aka	Cultivated	Japan	Asia	0.00	0.00	3.00	0.00	3.00	2.83	2.83	0.25
PI383988	Furutsu Masari	Cultivar	Japan	Asia	0.00	0.00	3.00	0.00	3.00	5.00	1.83	0.00
PI420646	Krasnovodopadskaja 210	Cultivar	Kazakhstan	Asia	3.00	0.33	0.33	3.00	3.00	5.00	4.67	4.67
PI572648	Bogarnaja 56	Cultivar	Kazakhstan	Asia	3.00	0.00	0.00	0.33	0.00	4.00	0.83	2.83
PI94479	159	Landrace	Kazakhstan	Asia	0.00	0.00	0.00	0.00	2.00	4.33	3.00	0.33
PI362187	Won Kwang	Cultivar	Korea, South	Asia	0.00	0.00	3.00	1.00	2.67	4.17	3.83	2.00
PI157577	Nang Rim No. 17	Cultivated	Korea, South	Asia	0.00	0.00	0.00	3.00	2.67	3.17	4.50	2.50
PI362180	Seu Seun 7	Cultivar	Korea, South	Asia	0.00	0.00	2.67	0.33	1.83	4.83	4.33	1.00
PI362184	Seu Yuk 126	Cultivar	Korea, South	Asia	2.67	0.00	3.00	2.33	2.33	5.00	3.17	2.50
PI157608	Yuc Song 3	Cultivated	Korea, South	Asia	3.00	2.67	0.00	2.33	1.75	4.33	4.33	4.67
PI172582	8728	Landrace	Turkey	Asia	3.00	3.00	0.33	0.67	2.33	2.33	2.17	3.25
PI178184	Tir	Landrace	Turkey	Asia	3.00	2.67	0.33	3.00	0.17	4.50	2.00	4.00
PI560615	TU85-033-01-1	Landrace	Turkey	Asia	3.00	2.50	0.00	0.00	3.00	4.33	3.67	4.67
PI262605	Karagach	Landrace	Turkmenistan	Asia	3.00	3.00	0.00	3.00	1.00	3.17	1.69	3.67
PI278491	2447	Landrace	Uzbekistan	Asia	3.00	3.00	3.00	3.00	3.00	4.50	4.50	4.33
PI565358	Teremai Bugdai	Landrace	Uzbekistan	Asia	0.00	2.67	3.00	3.00	2.67	4.00	2.17	4.17
PI162002	Ritzelhofer I	Cultivar	Austria	Europe	3.00	2.67	0.67	3.00	0.00	2.83	2.17	4.00
PI195545	Hohenauer	Cultivar	Austria	Europe	0.00	2.33	2.67	0.00	0.00	3.00	2.83	2.83
PI195546	Korneuburger	Cultivar	Austria	Europe	0.00	2.67	0.00	0.00	1.67	2.17	3.50	2.75
PI278185	Immendorfer Kolben	Cultivar	Austria	Europe	0.00	0.00	3.00	3.00	0.00	4.00	3.33	2.83
PI519235	P 4821-80	Breeding	Austria	Europe	0.00	0.00	0.00	0.33	0.00	2.33	4.50	0.33
PI254844	Primus	Cultivar	Austria	Europe	0.00	0.00	0.00	0.00	3.00	3.17	4.17	0.00
PI193067	Directeur Journee	Cultivar	Belgium	Europe	0.00	0.00	0.00	0.00	0.00	1.00	0.67	1.33
PI284551	Leda	Cultivar	Belgium	Europe	0.00	0.00	0.00	3.00	0.00	2.00	3.33	0.00
PI338358	Cama	Cultivar	Belgium	Europe	0.00	0.00	3.00	2.33	1.00	4.67	1.33	0.33
PI338360	Mina	Cultivar	Belgium	Europe	0.00	3.00	3.00	1.00	1.00	3.83	3.83	3.33
PI340733	Panter	Cultivar	Belgium	Europe	3.00	0.00	0.00	0.00	0.00	4.67	1.25	4.00
PI278612	Sarajevo 18	Landrace	Bosnia and Herzegovina	Europe	0.00	0.00	0.00	0.00	0.00	1.00	2.67	1.00
PI345417	416-V/69	Landrace	Bosnia and Herzegovina	Europe	0.00	0.00	0.00	0.00	0.33	0.25	0.75	0.00
PI374678	216/71	Landrace	Bosnia and Herzegovina	Europe	0.00	0.67	3.00	0.00	0.50	4.67	0.50	0.50
PI350267	911-IX/4	Landrace	Bosnia and Herzegovina	Europe	0.00	0.00	2.67	0.00	3.00	1.33	2.50	0.83
PI520594	ID 779-11	Breeding	Bulgaria	Europe	0.00	0.00	0.50	3.00	0.00	0.00	0.83	0.83
PI564287	1037-24-5	Breeding	Bulgaria	Europe	0.00	0.00	0.00	0.33	2.33	3.83	4.50	0.50
PI564351	5989-1	Breeding	Bulgaria	Europe	0.00	0.00	0.00	0.00	0.00	0.17	0.83	0.00
PI564354	6063-5	Breeding	Bulgaria	Europe	0.00	0.00	0.00	0.00	2.33	4.50	4.00	0.00

Accession	Line	ACIMPT	Country	Continent	SnToxA	SnTox1	SnTox3	SnTox5	SnTox267	Sn4 avg	AR2-1 avg	Sn2000 avg
PI564363	622-24-65	Breeding	Bulgaria	Europe	0.00	0.00	1.83	0.00	3.00	2.50	2.17	0.00
PI294930	Titscha	Cultivated	Bulgaria	Europe	3.00	2.67	3.00	0.00	0.67	4.33	2.83	3.00
PI344545		Cultivated	Croatia	Europe	0.00	0.00	3.00	0.00	2.67	4.00	3.75	0.00
PI278614	Dalmatia 3	Landrace	Croatia	Europe	0.00	2.67	3.00	0.00	0.33	4.00	2.25	3.67
CItr15192	Dubrava	Cultivar	Croatia	Europe	0.00	0.00	3.00	0.33	1.00	4.00	4.17	0.00
PI574324	KM 803-92	Breeding	Czech Republic	Europe	0.00	0.00	0.00	0.00	0.00	1.00	1.00	0.00
PI574330	KM 669-92	Breeding	Czech Republic	Europe	0.00	0.00	0.00	2.00	0.00	3.00	0.00	1.33
PI330406	Lada	Cultivar	Czech Republic	Europe	0.00	0.00	0.00	0.00	3.00	2.83	3.00	0.25
PI428660	Slavia	Cultivar	Czech Republic	Europe	0.00	0.00	0.00	0.33	0.00	0.67	0.00	1.25
PI584795	Zdar	Cultivar	Czech Republic	Europe	0.00	0.00	0.00	0.00	0.67	1.33	1.33	0.00
PI428657	Draga	Cultivar	Czechoslovakia	Europe	0.00	0.00	3.00	0.00	2.33	4.83	2.83	0.17
PI351217	Nevodvorska Niva	Cultivated	Czechoslovakia	Europe	0.00	1.33	2.33	0.00	2.33	5.00	5.00	1.50
PI361855	Krim	Cultivated	Denmark	Europe	3.00	0.00	3.00	3.00	3.00	4.83	1.83	3.00
PI361783	Tystofte Stakket	Cultivar	Denmark	Europe	0.00	2.00	2.00	0.00	0.00	3.17	2.00	3.17
PI361749	Konrad	Cultivated	Denmark	Europe	3.00	0.00	0.00	2.67	3.00	4.17	3.50	4.00
PI340762	Trifolium	Cultivar	Denmark	Europe	0.00	2.67	3.00	0.00	0.83	4.33	5.00	4.50
PI361785	Varma Tammisto	Cultivar	Denmark	Europe	3.00	0.00	3.00	0.00	3.00	5.00	3.67	4.00
PI361713	XIII T.I	Cultivated	Denmark	Europe	0.00	0.00	3.00	0.00	2.33	3.00	2.17	0.17
PI361755	Paduvano	Cultivated	Denmark	Europe	0.00	2.33	3.00	0.00	0.00	3.67	2.17	1.00
PI361810	Blak. Fra. Prof. Tsckem.	Cultivated	Denmark	Europe	0.00	1.33	0.00	0.00	1.00	2.50	3.17	2.50
PI254046		Cultivated	Europe	Europe	0.00	0.00	3.00	0.33	1.67	4.33	1.83	0.00
PI254049		Cultivated	Europe	Europe	0.00	0.00	0.00	0.33	2.33	4.33	3.00	0.67
PI254080		Cultivated	Europe	Europe	0.67	0.00	0.33	2.67	2.00	2.00	3.50	0.00
PI265484	Varma	Cultivar	Finland	Europe	3.00	0.00	3.00	0.00	3.00	5.00	3.67	4.33
PI351207	Malakof	Cultivated	Former Soviet Union	Europe	3.00	0.00	0.00	0.00	0.67	2.33	0.83	2.67
PI368010	187-199-VI/8 A	Cultivated	Former Yugoslavia	Europe	0.00	0.00	0.00	0.00	0.00	1.83	1.33	1.50
PI346424	29/60	Cultivated	Former Yugoslavia	Europe	0.00	0.00	0.00	2.67	0.00	1.17	0.67	1.33
PI352032	Floress	Cultivar	France	Europe	0.00	2.00	3.00	0.00	0.00	3.67	1.17	0.17
PI174649	Hybride de Bonnance	Cultivar	France	Europe	0.00	2.00	3.00	0.33	0.00	4.17	2.50	2.67
PI174653	Hybride du Joncquois	Cultivar	France	Europe	0.00	0.00	3.00	0.00	2.00	4.17	2.33	0.17
PI298405	Druchamp 1940	Cultivar	France	Europe	0.00	0.00	0.00	0.33	0.00	0.83	0.50	1.83
PI315976	Chambord	Cultivar	France	Europe	0.00	2.67	0.33	0.00	0.50	4.83	3.83	3.00
PI315997	Moeres	Cultivar	France	Europe	0.00	0.00	0.00	1.33	1.00	2.67	4.00	1.75
PI351410	Lemaire 4	Cultivar	France	Europe	0.00	0.00	0.00	0.00	0.00	0.33	0.17	0.33
PI180610	Strain No. 1827/47	Breeding	Germany	Europe	0.33	0.33	3.00	0.00	0.00	5.00	1.00	0.00
PI180588	Rimpaus Bastard II	Cultivar	Germany	Europe	0.00	0.33	3.00	0.33	2.00	5.00	2.67	0.67
PI209794	Heines VII	Cultivar	Germany	Europe	0.00	0.00	0.33	2.67	0.50	1.83	3.00	2.25
PI285953	Heines VI	Cultivar	Germany	Europe	0.00	0.33	0.00	0.00	0.67	3.5	2.17	0.33

Accession	Line	ACIMPT	Country	Continent	SnToxA	SnTox1	SnTox3	SnTox5	SnTox267	Sn4 avg	AR2-1 avg	Sn2000 avg
PI300950	Hanno	Cultivar	Germany	Europe	0.00	0.00	0.00	1.17	0.00	1.83	0.33	0.00
PI351268	Graf Toerring II	Cultivar	Germany	Europe	0.00	0.33	0.00	1.33	1.00	1.33	0.83	2.17
PI351330	Siegerlander Neu	Cultivar	Germany	Europe	0.00	2.33	0.00	0.00	2.50	4.33	5.00	3.67
PI351333	Marquardt II	Cultivar	Germany	Europe	0.33	2.33	3.00	1.17	3.00	3.33	3.17	2.17
PI352152	Berthold	Cultivar	Germany	Europe	0.00	0.00	0.00	0.00	1.00	1.83	1.17	0.00
PI192030	Roemer	Cultivated	Germany	Europe	0.00	2.33	3.00	1.00	0.00	3.83	2.67	2.67
PI272351	Hezohegyesi 7286	Cultivar	Hungary	Europe	0.00	0.33	0.00	0.00	3.00	4.33	3.33	0.00
PI272384	Arpadhalmi 267	Cultivar	Hungary	Europe	0.00	0.00	3.00	0.33	0.00	3.33	0.50	0.00
PI272411	Eszterhazai Mindenes	Cultivar	Hungary	Europe	0.00	0.00	2.67	0.00	3.00	4.00	2.67	0.00
PI272433	Lovaszpatonai 157	Cultivar	Hungary	Europe	0.00	0.00	2.67	1.67	1.67	4.17	4.25	1.25
PI278315	Szekacs 267	Cultivar	Hungary	Europe	0.00	2.33	0.00	0.00	2.67	3.33	3.67	3.33
PI272374	Barabas-Fele	Landrace	Hungary	Europe	0.00	0.00	0.33	0.33	3.00	2.50	1.50	2.67
PI278318	Hungarian 3	Landrace	Hungary	Europe	0.00	0.00	0.00	0.33	0.00	1.17	2.17	1.33
PI107302	Galway Land Wheat	Landrace	Ireland	Europe	0.00	0.00	0.33	1.00	2.00	3.17	2.83	1.67
PI294570	Cologna Lunga	Cultivar	Italy	Europe	3.00	3.00	3.00	3.00	2.17	4.33	2.83	4.50
PI351461	T-1164	Breeding	Italy	Europe	0.00	0.00	3.00	0.33	0.00	4.17	1.83	0.50
PI259889	San Pastore	Cultivar	Italy	Europe	0.00	0.00	3.00	3.00	0.00	3.25	2.75	1.83
PI284531	Acciaio	Cultivar	Italy	Europe	0.00	2.00	0.00	0.00	0.00	2.50	2.33	3.50
PI192716	T de Lituania	Cultivated	Lithuania	Europe	0.00	2.67	3.00	0.00	2.33	4.00	3.33	3.17
PI378391	1666	Landrace	Macedonia	Europe	2.67	2.00	3.00	0.00	0.00	4.00	0.67	3.17
PI345244	243-VII/4	Landrace	Macedonia	Europe	0.00	2.33	2.67	0.00	1.00	3.50	0.83	2.83
PI362612	VII/8-B	Landrace	Macedonia	Europe	3.00	0.00	0.00	0.00	0.00	3.50	1.00	4.00
PI378519	1794	Landrace	Macedonia	Europe	0.00	3.00	3.00	0.00	0.83	4.50	2.83	2.83
PI390330	I/2	Landrace	Macedonia	Europe	0.33	2.33	3.00	0.33	0.00	2.00	2.67	3.67
PI390342	I/14	Landrace	Macedonia	Europe	0.00	0.00	0.00	3.00	3.00	4.00	5.00	1.33
PI405857	I/23	Landrace	Macedonia	Europe	0.00	0.00	0.00	0.00	0.00	1.33	1.00	1.50
PI572642	Mil'turum 1	Cultivar	Moldova	Europe	0.00	0.33	0.00	0.00	3.00	3.00	4.67	0.00
PI262653	Beltskaya Mestnaya	Landrace	Moldova	Europe	0.00	0.00	0.00	0.00	2.67	4.00	2.83	0.00
PI345355	354A-I/7	Landrace	Montenegro	Europe	0.00	1.00	3.00	3.00	3.00	1.33	3.00	1.17
PI197639	Elisabeth	Cultivar	Netherlands	Europe	0.00	0.00	3.00	0.00	0.33	4.83	1.33	0.50
PI197640	Juliana	Cultivar	Netherlands	Europe	0.00	0.00	3.00	0.50	2.50	4.17	3.00	0.00
PI315840	Apollo	Cultivar	Netherlands	Europe	0.00	0.00	0.00	0.00	1.00	2.00	2.83	0.00
PI342612	Vada	Cultivar	Netherlands	Europe	0.00	0.00	3.00	0.00	0.00	5.00	2.17	0.67
PI351580	Moystad 0944	Cultivar	Norway	Europe	3.00	0.00	3.00	0.00	0.33	3.33	1.33	2.00
PI542450	H82-710-1	Breeding	Poland	Europe	0.00	0.00	0.00	0.00	3.00	5.00	5.00	1.83
PI285773	Edel Epp Markowicka	Cultivated	Poland	Europe	0.00	0.67	3.00	3.00	2.33	4.50	4.00	1.83
PI285921	Stylowa	Cultivated	Poland	Europe	0.00	2.33	3.00	2.00	0.00	4.50	3.17	3.75
PI285999	Ruska	Cultivated	Poland	Europe	0.00	2.33	0.00	0.00	1.00	2.83	2.50	1.33

Accession	Line	ACIMPT	Country	Continent	SnToxA	SnTox1	SnTox3	SnTox5	SnTox267	Sn4 avg	AR2-1 avg	Sn2000 avg
PI286030	For East 32996	Cultivated	Poland	Europe	0.00	0.00	0.00	0.00	2.67	3.33	3.83	0.00
PI338387	C 48	Cultivar	Poland	Europe	0.00	0.00	0.00	0.00	0.00	1.33	1.67	0.00
PI338389	Dankowska Biala	Cultivar	Poland	Europe	0.00	0.00	3.00	0.50	2.00	4.33	4.50	0.33
PI338401	Szelejewska	Cultivar	Poland	Europe	0.00	0.00	0.00	0.00	0.00	1.17	1.50	0.17
PI304095	Cenad 512	Cultivar	Romania	Europe	0.00	0.00	0.00	3.00	3.00	2.50	3.33	2.00
PI304105	520B	Cultivated	Romania	Europe	3.00	0.00	3.00	1.00	3.00	4.67	3.33	1.83
PI306510	Tiganesti 906	Cultivated	Romania	Europe	0.00	0.00	0.00	2.33	2.67	3.50	2.00	0.00
PI306566	2878	Cultivated	Romania	Europe	0.00	2.33	0.00	2.50	2.67	4.33	3.50	3.67
PI282687	Bezostaja 1	Cultivar	Russian Federation	Europe	3.00	0.00	0.00	0.00	0.00	1.25	0.67	2.33
PI295349	Mil'turum 321	Cultivar	Russian Federation	Europe	0.00	2.00	0.00	0.00	2.33	3.00	3.00	0.50
PI361858	L'govskaja	Cultivar	Russian Federation	Europe	0.00	0.00	0.00	0.00	0.00	0.83	0.67	0.00
PI565427	Lutescens 321	Cultivar	Russian Federation	Europe	0.00	0.00	0.00	0.00	2.67	2.00	2.17	0.00
PI591858	Pirotriks 50	Cultivar	Russian Federation	Europe	0.00	0.00	0.33	0.33	3.00	3.50	3.33	0.33
PI591992	Yugtina	Cultivar	Russian Federation	Europe	0.00	0.00	0.00	0.00	2.33	3.17	2.83	0.00
PI278451	Blaue Dame	Cultivated	Russian Federation	Europe	0.00	0.00	3.00	3.00	2.33	4.00	3.67	0.67
PI350046	650-IV/6	Landrace	Serbia	Europe	0.00	0.00	0.00	0.00	0.00	1.00	0.00	0.17
PI350118	736-VII/1	Landrace	Serbia	Europe	0.00	0.00	3.00	0.00	0.50	1.67	0.50	0.50
PI362412	II/7-B	Landrace	Serbia	Europe	0.00	1.00	0.00	0.00	0.00	0.00	1.33	1.00
PI362443	III/15-X27	Landrace	Serbia	Europe	0.00	0.50	3.00	0.00	0.00	3.67	0.00	1.00
PI362486	IV/9-E	Landrace	Serbia	Europe	0.33	0.00	3.00	2.00	1.33	4.17	2.17	0.83
PI362526	V/2-A	Landrace	Serbia	Europe	0.00	0.00	0.00	2.67	0.00	1.75	2.50	1.17
PI362546	VI/3-A	Landrace	Serbia	Europe	2.33	0.00	0.00	0.00	0.00	3.67	0.67	3.00
PI378276	1548	Landrace	Serbia	Europe	0.00	0.00	0.00	0.00	2.00	2.00	1.67	0.00
PI378527	1802	Landrace	Serbia	Europe	3.00	0.00	3.00	2.67	2.67	3.00	2.33	2.50
PI434671	NS 18-99	Breeding	Serbia	Europe	0.00	0.00	0.00	3.00	3.00	3.17	4.50	2.00
CItr15203	Ebro	Cultivar	Spain	Europe	0.00	0.00	0.33	0.00	1.17	2.67	1.67	0.33
PI469020	MG 27174	Landrace	Spain	Europe	0.33	2.33	3.00	0.33	1.00	4.50	4.17	2.50
PI190985	Akagomugh Involcable Vilmorin	Cultivated	Spain	Europe	0.00	3.00	0.00	2.33	0.00	2.00	2.75	2.83
PI192416	Ankar II	Cultivar	Sweden	Europe	3.00	0.33	1.00	0.00	3.00	3.83	4.50	2.50
PI192701	Saxo	Cultivar	Sweden	Europe	3.00	2.67	3.00	0.00	2.33	4.50	3.33	3.00
PI192582	Plantahof 3	Cultivar	Switzerland	Europe	0.33	2.00	3.00	0.33	0.67	5.00	4.00	1.33
PI350885	69Z2.11/1147I	Landrace	Switzerland	Europe	0.00	0.00	3.00	0.00	0.00	3.50	0.17	0.00
PI350974	69Z2.104/672A	Landrace	Switzerland	Europe	0.00	1.83	3.00	0.00	2.67	4.17	3.17	1.17
PI351983	A 912	Breeding	Switzerland	Europe	0.00	0.00	0.00	1.67	0.00	0.83	1.17	2.17
PI351172	Rothenbrunnen 32	Cultivar	Switzerland	Europe	0.00	0.00	3.00	0.00	0.33	4.17	0.83	0.00
PI350905	69Z2.32/840C	Landrace	Switzerland	Europe	0.33	2.67	3.00	0.00	3.00	4.50	3.83	2.83
PI350959	69Z2.88/7B	Landrace	Switzerland	Europe	0.00	2.33	0.00	0.00	3.00	3.83	2.67	2.67
PI350972	69Z2.102/85A	Landrace	Switzerland	Europe	0.00	2.33	0.33	0.00	3.00	4.00	3.67	2.50

Accession	Line	ACIMPT	Country	Continent	SnToxA	SnTox1	SnTox3	SnTox5	SnTox267	Sn4 avg	AR2-1 avg	Sn2000 avg
PI293918	Michurinka	Cultivar	Ukraine	Europe	3.00	0.00	0.00	0.00	3.00	3.50	2.75	2.33
PI393980	Novostepniachka	Cultivar	Ukraine	Europe	0.33	0.00	1.67	1.33	3.00	4.17	3.83	0.00
PI572638	Saljut	Cultivar	Ukraine	Europe	3.00	0.00	0.00	0.00	2.67	4.00	4.17	5.00
PI94464	144	Landrace	Ukraine	Europe	0.00	0.00	3.00	0.33	2.33	5.00	2.50	0.17
PI94468	148	Landrace	Ukraine	Europe	0.00	0.00	0.00	1.67	2.33	1.50	2.00	0.00
PI94499	179	Landrace	Ukraine	Europe	0.00	0.00	3.00	0.00	2.33	4.50	1.67	0.25
PI292998	TP 114/78-79	Breeding	United Kingdom	Europe	0.00	0.00	0.00	3.00	0.00	0.17	0.25	1.75
CItr6316	Gold Drop	Cultivar	United Kingdom	Europe	0.00	0.00	3.00	0.00	0.00	4.00	0.83	0.33
CItr12569	Holdfast	Cultivar	United Kingdom	Europe	0.00	2.00	2.33	0.00	2.33	4.00	2.67	1.00
PI278595	Little Tich	Cultivar	United Kingdom	Europe	0.00	0.00	0.00	0.33	0.00	0.83	1.00	0.50
PI447429	Virtue	Cultivar	United Kingdom	Europe	0.33	0.00	0.00	0.33	0.00	0.50	2.50	0.17
PI547263	Colonel	Cultivar	United Kingdom	Europe	0.00	0.00	2.67	0.33	3.00	3.50	2.00	0.00
PI592129	Twyford 71	Cultivar	United Kingdom	Europe	0.00	2.67	0.00	0.00	1.00	4.50	4.33	2.50
CItr11731	Kansas No. 343273	Breeding	United States	North America	3.00	0.00	0.00	0.00	2.67	4.67	2.67	3.67
CItr12523	Nebr. Sel. 383134	Breeding	United States	North America	0.00	0.00	0.00	2.00	0.33	1.83	0.33	1.50
CItr17561	OH 106	Breeding	United States	North America	0.00	0.00	0.00	0.00	0.00	0.00	0.67	0.00
PI486211	NE 76706	Breeding	United States	North America	3.00	0.00	0.00	0.00	0.67	3.33	2.50	2.50
PI595379	KS95WGRC33	Breeding	United States	North America	2.67	0.83	3.00	1.00	2.67	4.83	2.00	3.33
PI620732	943075	Breeding	United States	North America	3.00	0.00	3.00	0.33	3.00	4.83	4.00	4.50
PI620751	910231	Breeding	United States	North America	3.00	1.00	3.00	0.00	3.00	3.00	2.00	3.50
PI631091	ARS92 303	Breeding	United States	North America	3.00	0.00	2.67	2.67	0.00	3.83	0.33	4.00
PI633777	N02Y4648	Breeding	United States	North America	0.00	0.00	0.00	0.00	2.33	2.67	2.83	0.00
PI633885	N02Y5057	Breeding	United States	North America	3.00	0.67	0.00	2.33	2.50	4.67	3.00	3.33
PI633901	N02Y5191	Breeding	United States	North America	3.00	0.00	0.00	0.00	3.00	3.83	3.33	2.83
PI638644	99CF 810	Breeding	United States	North America	0.00	0.00	2.00	3.00	2.67	1.83	3.17	0.50
CItr6471	Fulcaster	Cultivar	United States	North America	0.00	0.00	3.00	0.00	0.00	5.00	1.25	0.00
CItr11605	Hymar	Cultivar	United States	North America	0.00	0.00	0.00	3.00	2.50	2.83	3.50	1.33
PI583669	Iobred 73	Cultivar	United States	North America	0.00	0.00	0.00	0.00	1.00	1.33	2.00	0.00
PI599664	Ivory	Cultivar	United States	North America	3.00	2.33	0.00	0.00	0.67	4.33	3.00	4.00
CItr17774	REA 77-2	Breeding	United States	North America	0.00	0.00	0.00	0.00	0.00	0.67	0.67	0.00
PI620650	910102	Breeding	United States	North America	0.00	0.00	0.00	3.00	0.00	0.17	0.75	2.00
PI639107	KW981718h0024	Breeding	United States	North America	2.67	0.00	0.00	0.33	0.67	3.33	1.00	2.83
PI565371	Bearded Winter	Cultivated	United States	North America	0.00	0.00	0.00	0.00	0.17	4.33	4.17	0.50
CItr14121	Near Isogenic (Pm3b)	Genetic	United States	North America	0.00	1.00	3.00	0.00	0.00	3.17	1.33	1.00
PI198267		Breeding	Australia	Oceania	3.00	2.17	2.67	0.33	3.00	4.00	3.83	5.00
CItr15985	CAR 59	Breeding	Chile	South America	0.00	2.67	0.00	0.00	1.00	1.83	2.00	2.67
CItr16003	CAR 76	Breeding	Chile	South America	0.00	0.00	2.67	1.33	0.00	2.83	1.00	0.33
CItr16268	CAR 341	Breeding	Chile	South America	0.00	0.00	0.00	0.00	0.00	0.00	0.50	0.33

Accession	Line	ACIMPT	Country	Continent	SnToxA	SnTox1	SnTox3	SnTox5	SnTox267	Sn4 avg	AR2-1 avg	Sn2000 avg
CItr16343	CAR 416	Breeding	Chile	South America	0.00	0.00	0.00	3.00	0.00	1.00	1.17	1.50